THE FRACTURE OF FILLED EPOXY RESINS

by

J. Lilley, B.Sc. M.Inst.P.

Presented to the University of Keele for the Degree of Doctor of Philosophy.

1973

TEXT CUT OFF IN THE ORIGINAL

ACKNOWLEDGEMENTS

The author would like to express his thanks and gratitude to the following:

Professor D.J.E. Ingram for the use of laboratory and research facilities.

Dr. D.G. Holloway for many helpful discussions and for his encouragement.

Messrs. B.R. McQuillin, S.P. Gunasekera and G.W. Weidmann and other members of the Physics Department for their co-operation.

Messrs. J.W. Johnson and F.P. Mallinder of Rolls-Royce Limited, again for helpful discussions.

The technical staff of the Physics Department for their assistance during this programme of research and for help in the production of this thesis.

Rolls-Royce Limited and the University of Keele for the provision of funds.

Miss G. Watts and Mrs. E. Cook for their particular care and patience in typing this thesis.

ABSTRACT

The physical processes involved during the fracture of three epoxy resin systems and related particulate filled composites have been investigated. A mathematical model is also presented which accurately predicts some of the observed effects.

SYNOPSIS

The useful structural materials are those that are both strong and tough. The "toughness" of a given material is characterised by its fracture energy which is defined as the total work expended in propagating the crack so as to produce unit area of new fracture surface: the fracture energy is a characteristic property of the material and may be determined by direct experiment.

Earlier work had shown that the addition of particulate fillers to a "brittle" epoxy resin matrix produced composite materials having fracture energies somewhat greater than that of the base matrix. The main object of this work was to examine in detail the fracture characteristics of the above family of materials with a view to identifying the physical mechanisms responsible for this effect. Hence, a reasonably systematic examination of the effect on toughness of the size, shape, nature, concentration and adhesion of the matrix to the filler particles has been undertaken.

Estimates of the fracture energies of three epoxy resin systems, i.e. CT200/HT901, LY558/HT973 and EPON828/NMA/BDMA and related composites have been made by a double cantilever beam technique. Chapter I contains a detailed review of the mechanics of such a system: the basic experimental techniques and the specimen preparation procedures are described in Chapter II. It was considered that before any detailed conclusions could be drawn about the crack propagation processes in the composites, more detailed information than was at present available was required on the base matrices. These experiments are described in Chapter III and the results indicate that our cured epoxy resins exhibit a "jumping"mode of crack propagation and are therefore characterised by two fracture energies which correspond to conditions of

crack initiation and arrest. The effect of fillers on the fracture toughness of our epoxy resins is described in Chapter IV: these results are compared with the Charpy Impact Energies in Chapter V.

The possibility of interpreting the crack propagation behaviour in the base matrices in relation to variations in crack opening displacements and flow stresses seemed attractive and hence these parameters were determined and are presented in Chapter VI. Finally in Chapter VII the "jumping"mode of crack propagation is discussed in detail, and a simple mathematical model is developed which predicts correctly the type of changes in fracture energy that may be expected when particulate fillers are added to an epoxy resin matrix.

CONTENTS

		Page
CHAPTER 1	BASIC CONCEPTS OF STRENGTH AND FRACTURE TOUGHNESS	1
1.1	Introduction	1
1.2	Basic Energy Concepts of Strength and Toughness	2
1.3	The Determination of Fracture Energy	12
1.4	The Mechanics of the Double Cantilever Beam System	13
1.5	A More Detailed Analysis	17
1.5.1.	Gillis and Gillman	18
1.5.2.	Berry's Method	22
1.5.3.	Srawley and Gross	23
1.6	Grooved Specimens	24
1.7	Discussion	26
1.8	Summary	27
CHAPTER II	BASIC EXPERIMENTAL TECHNIQUES	28
2.1	Introduction	28
2.2	Basic Cure Mechanisms	28
2.2.1.	CT200/HT901	28
2.2.2.	LY558/HT973	31
2.2.3.	EPON828/NMA/BDMA	32
2.3	Specimen Preparation	32
2.3.1.	CT200/HT901	33
2.3.2.	LY558/HT973	34
2.3.3.	EPON828/NMA/BDMA	34

		Page
2.4	Description of Apparatus and Experimental Procedure Used for Determination of Fracture Energy	35
2.5	Processing of Observational Data	40
2.6	Summary	41
CHAPTER III	PRELIMINARY EXPERIMENTS WITH UNFILLED RESINS	45
3.1	Introduction	45
3.2	General Behaviour	45
3.3	The Role of Effective Crack Tip Extension Rate	48
3.4	The Effect of Temperature and Environment on Fracture Energy	53
3.4.1.	Experimental Procedure	53
3.5	Survey of Results	54
3.6	Preliminary Discussions	69
3.7	Summary	75
CHAPTER IV	THE EFFECT OF FILLERS ON THE FRACTURE TOUGHNESS OF EPOXY RESINS	76
4.1	Introduction	76
4.2	Experimental	76
4.3	Results	84
4.3.1.	The Fracture Energies of Glass Filled CT200/HT901	84
4.3.2.	The Fracture Energies of Aluminium Filled CT200/HT901	88
4.3.3.	The Fracture Energies of Alumina Filled CT200/HT901	88
4.3.4.	The Fracture Energies of Two Composites as a Function of Effective Extension Rate	92
4.3.5.	Other Fillers	92
4.3.6.	The Effect on Fracture Energy of Filler Surface Pre-Treatment	95

Page

4.3.7. The Effect of Temperature on the Fracture Energies of a CT200/Ballotini Composite 99

4.3.8. The Young's Modulus of Ballotini Filled CT200/HT901 102

4.3.9. The Young's Modulus of Aluminium Filled CT200/HT901 102

4.3.10. K_{Ic} for Ballotini Filled CT200/HT901 105

4.3.11. K_{Ic} for Aluminium Filled CT200/HT901 105

4.4 Preliminary Discussion 112

CHAPTER V THE CHARPY IMPACT ENERGY, "NOTCH TOUGHNESS PARAMETERS" AND MODULUS OF RUPTURE OF VARIOUS COMPOSITES 118

5.1 Introduction 118

5.2 The Charpy Impact Test 119

5.3 The Modulus of Rupture of Various Materials 121

5.4 The "Notch Toughness Parameters" of Some Arbitrarily Blunted Cracks 124

5.5 Results 124

5.6 Discussion 126

CHAPTER VI THE PLASTIC ZONE EXTENSION, VICKER'S HARDNESS NUMBERS AND FLOW STRESSES OF THE EPOXY MATRIX MATERIALS 135

6.1 Introduction 135

6.2 The Microhardness Test 136

6.3 Basic Apparatus 139

6.4 Specimen Preparation 146

6.5 Experimental Procedures 148

Page

6.5.1. Long Term Loading 148

6.5.2. Short Term Indentations 149

6.6 Results 150

6.7 The Plastic Zone Extension α 158

6.8 Results 162

6.9 Preliminary Discussion 162

CHAPTER VII THE FRACTURE OF EPOXY RESIN BASED COMPOSITE MATERIALS 168

7.1 Introduction 168

7.2 Base Matrices 169

7.3 The Composite Materials 177

7.4 Recommendations for Further Work 200

7.5 Final Summary 202

REFERENCES 204

LIST OF FIGURES

FIG.		Page
1.1	The three fundamental modes of crack surface displacement	6
1.2	The geometry of the region close to a crack tip	8
1.3	A double cantilever beam specimen	14
1.4	A grooved double cantilever beam specimen	25
2.1	Basic apparatus used for the determination of fracture energy	37
2.2	Diagrammatic representation of basic test apparatus	38
2.3	Typical crack front in cured CT200/HT901 (magnification x 75)	39
2.4	Typical corrected data used for the determination of the fracture energies ($1\gamma_{FS}$ and $A\gamma_{FS}$) of unfilled CT200/HT901	42
2.5	Typical corrected data used for the determination of the Young's modulus of CT200/HT901	43
3.1	The fracture energies of CT200/HT901 as a function of effective extension rate	50
3.2	The fracture energies of LY558/HT973 as a function of effective extension rate	51
3.3	The fracture energies of EPON828/NMA/BDMA as a function of effective extension rate	52
3.4	The fracture energies of CT200/HT901 in air as a function of temperature	55
3.5	The fracture energies of CT200/HT901 in dry silicone oil as a function of temperature	56
3.6	The fracture energies of CT200/HT901 in water as a function of temperature	57
3.7	Crazes around a crack tip in polystyrene (magnification x 100)	61
3.8	"Crazes" around a crack tip in cured CT200/HT901 (magnification x 800)	62

FIG.		Page
3.9	"Crazes" ahead of a crack tip in cured CT200/HT901 (magnification x 2000)	63
3.10	"Crazes" normal to the tensile surface of a simple cantilever beam of cured CT200/HT901 (magnification x 400)	64
3.11	Region close to a crack arrest position in cured CT200/HT901 (magnification x 400)	66
3.12	Region close to a crack arrest position in cured LY558/HT973 (magnification x 400)	68
3.13	The surface of CT200/HT901 having been etched in chromic acid (magnification x 40,000)	71
3.14	The surface of CT200/HT901 having been etched by argon ion bombardment in a radio frequency glow discharge (magnification x 40,000)	72
4.1	Typical particle size distribution for 75 to 105 μm ballotini	78
4.2	Typical specimens used to determine the adhesion between silane treated glass and cured CT200/HT901	82
4.3	The fracture energies of ballotini filled CT200/HT901 as a function of filler volume fraction	
4.4	The fracture energies of ballotini filled CT200/HT901 as a function of filler size	87
4.5	The fracture energies of aluminium filled CT200/HT901 as a function of filler volume fraction	89
4.6	The fracture energies of aluminium filled CT200/HT901 as a function of filler size	90

FIG.		Page
4.7	The fracture energies of aluminium filled CT200/HT901 as a function of effective extension rate	93
4.8	The fracture energies of ballotini filled CT200/HT901 as a function of effective extension rate	94
4.9	The fracture energies of talc filled CT200/HT901 as a function of filler volume fraction	96
4.10	The fracture energies of etched aluminium filled CT200/HT901 as a function of filler volume fraction	100
4.11	The fracture energies of ballotini filled CT200/HT901 as a function of temperature	101
4.12	The Young's modulus of ballotini filled CT200/HT901 as a function of filler volume fraction	103
4.13	The Young's modulus of ballotini filled CT200/HT901 as a function of filler size	104
4.14	The Young's modulus of aluminium filled CT200/HT901 as a function of filler volume fraction	106
4.15	The Young's modulus of aluminium filled CT200/HT901 as a function of filler size	107
4.16	K_{Ic} for ballotini filled CT200/HT901 as a function of filler volume fraction	108
4.17	K_{Ic} for ballotini filled CT200/HT901 as a function of filler size	109
4.18	K_{Ic} for aluminium filled CT200/HT901 as a function of filler volume fraction	110
4.19	K_{Ic} for aluminium filled CT200/HT901 as a function of filler size	111

FIG.		Page
4.20	K_{Ic} for etched aluminium filled CT200/HT901 as a function of filler volume fraction	113
4.21	Fracture energy difference for a ballotini filled CT200/HT901 composite as a function of temperature	116
5.1	Diagrammatic representation of a Charpy impact machine	120
5.2	Diagrammatic representation of the four-point bend apparatus	122
5.3	The "impact energies" of ballotini filled CT200/HT901 as a function of filler volume fraction	125
5.4	The "impact energies" of ballotini filled CT200/HT901 as a function of filler size	127
5.5	The "impact energies" of aluminium filled CT200/HT901 as a function of filler volume fraction	128
5.6	The "impact energies" of aluminium filled CT200/HT901 as a function of filler size	129
6.1	Diagrammatic representation of the long term indenter	140
6.2	Diagrammatic representation of the short term indenter	142
6.3	Circuit diagram of the single shot pulse generator	143
6.4	Oscillographs of 10^{-2}s and 10^{-3}s pulses	145
6.5	Diagrammatic representation of the environment and temperature enclosure	147
6.6	The Vicker's Hardness Number of CT200/HT901 as a function of applied force	151
6.7	The Vicker's Hardness Number of LY558/HT973 as a function of applied force	152
6.8	The Vicker's Hardness Number of EPON828/NMA/BDMA as a function of applied force	153

FIG.		Page
6.9	The Vicker's Hardness Numbers of the three resin systems as a function of load duration	154
6.10	The Vicker's Hardness Number of CT200/HT901 as a function of temperature and environment	155
6.11	The flow stress of the three resin systems as a function of load duration	156
6.12	The flow stress of CT200/HT901 in various environments as a function of temperature	157
6.13	The Young's modulus of CT200/HT901 as a function of temperature	159
6.14	The crack tip and plastic zone in an ideal elastic-perfectly-plastic material	160
6.15	A crack tip in cured CT200/HT901 (magnification x 1500)	161
7.1	The flow stress of PMMA as a function of load duration	173
7.2	The flow stress of "float glass" as a function of load duration	174
7.3	A cracked talc filled CT200/HT901 double cantilever beam specimen showing the "damaged" region around the crack tip	182
7.4	Diagrammatic representation of a simple composite material	184
7.5	The stress components at a crack tip	185
7.6	A single particle in an infinite isotropic matrix	187
7.7	The geometry of the region around a crack tip	190
7.8	The predicted and experimental fracture energies as a function of filler volume fraction	197
7.9	The predicted and experimental fracture energies as a function of filler size	198

CHAPTER 1

Basic Concepts of Strength and Fracture Toughness

1.1. Introduction

The ultimate strength of any solid is determined in principle by the cohesive forces between the constituent atoms or molecules: theoretical estimates of this ultimate strength have been made, in various ways, for a number of different materials. Real strengths approaching this theoretical limit have been attained in several instances; notably in freshly drawn glass fibres, whiskers of high melting point materials and, to a lesser extent, in heavily worked or heat treated alloys. However, if these very strong materials are to find general appliaation then an assurance is needed that they will maintain their strength in service and thus are not prone to sudden or catastrophic failure. Unfortunately, all the above solids are, in practice, prone to failure at much lower fracture stresses than can be obtained in the laboratory where great care may be taken during preparation and in subsequent handling; many will fail, at a relatively low stress, from small surface flaws induced by mechanical damage or chemical attack. The useful structural materials are therefore those that are both strong and have a high resistance to the propagation of cracks which may be nucleated from surface or internal flaws; a material with a high resistance to crack propagation is generally referred to as being tough.

In practice it is extremely difficult to produce a solid that has both great strength and a high degree of toughness since the two characteristics are, to a large extent, in conflict; traditionally the most useful structural materials have been those that exhibit the ability to deform plastically, at least locally around a crack tip. This local plastic deformation will lead to the dissipation of energy, the blunting of the crack tip, and will, as a consequence, increase the resistance to crack propagation. The complexity of the physics of the local, crack tip, plastic deformation is primarily responsible for the problems encountered in assessing the strength and, perhaps of much greater importance, the toughness of a material.

1.2. Basic Energy Concepts of Strength and Toughness

The general conflict between strength and toughness has highlighted the need for separate quantitative assessments of these parameters. Singularly the most important advance in this field was GRIFFITH'S (1920) realization that it was unrealistic to consider flawless materials, for, even where these can be produced in the laboratory it is virtually impossible, during normal usage, to maintain them free from surface damage. Griffith was also the first to appreciate that a finite stress is required to extend a pre-existing crack, even in a hypothetical ideally-brittle material, because work must be done to supply the energy required to produce new area of fracture surface. He introduced the criterion that the rate of decrease of strain energy of a body, during crack extension at constant strain, must be greater than the rate of increase in surface energy as the crack advances,

$$\text{i.e. that:-} \qquad \frac{\partial U}{\partial L} \geq \frac{\partial T}{\partial L} \qquad [1.1]$$

where:

U = Stored strain energy

L = Crack length

T = Surface free energy.

Griffith assumed T to be equivalent numerically to the surface tension and showed that the above criterion provided a necessary and sufficient condition for a pre-existing crack to propagate in an ideal brittle material, i.e. a material in which no plastic deformation occurs during failure.

With the aid of INGLIS' (1913) analysis for the stress distribution around an elliptical cavity in an infinite isotropic solid he was able to calculate the change in the strain energy of the system due to the presence of a crack of known length. This contribution, ΔW, (per unit thickness of sheet) under plane stress conditions is given by:

$$\Delta W = \frac{\pi \sigma^2 c^2}{E} \qquad [1.2]$$

where σ is the stress applied at the boundary, c the half length of the crack and E the Young's modulus. Griffith further associated a characteristic surface energy T with the free surface within the crack and hence the change in energy, ΔU, of the system due to the introduction of a crack into a previously uncracked body is:-

$$\Delta U = 4Tc - \frac{\pi \sigma^2 c^2}{E} \qquad [1.3]$$

If the above criterion is satisfied then the uniaxial tensile stress σ_b required to fracture the body is given by:

$$\sigma_b = \left(\frac{2\,E\,T}{\Pi\,c}\right)^{\frac{1}{2}} \qquad [1.4]$$

Equation [1.4] was apparently successful in predicting the breaking strengths of glass rods containing pre-existing cracks of known size. However, the later work of LINGER and HOLLOWAY (1968), WEIDERHORN (1969) and many others consistently suggest that the energy absorbed during the production of new fracture surfaces even in glass, the archetype brittle material, is much greater than that required simply to overcome the surface tension forces. In addition, values for the energy expended during the fracture of metals and polymers are many orders of magnitude greater than the theoretical surface free energy. Nevertheless it was nearly twenty years before Griffith's ideas were modified to give a more complete explanation of the fracture behaviour of these quasi-brittle materials. IRWIN (1948) and OROWAN (1948-49) independently demonstrated how the work done during plastic deformation at a crack tip could be incorporated into the crack extension criterion. They argued that if plastic deformation occurs at the tip of a crack and if the zone of plastic deformation advances ahead of the tip then additional work will be required to propagate the crack. The basic ideas central to Griffith's hypothesis may however be retained if we replace the surface energy, T, (in for example, equation [1.4] by a fracture energy, γ, which will now be defined as the total energy expended in propagating a crack so as to produce unit area of new fracture surface. The fracture energy, γ, will therefore be the sum of the surface energy, T, and that energy, P, expended during the crack tip plastic deformation. The fracture energy, γ, is a characteristic property of a material and may be determined by direct experiment.

Again with the aid of INGLIS' (1913) analysis of the stress distribution around an elliptically shaped crack in an infinite Hookean solid Irwin and Orowan deduced the

following expression for the uniaxial tensile breaking stress of a quasi-brittle material.

$$\sigma_b = \left(\frac{2\,(T+P)\,E}{\pi\, c}\right)^{\frac{1}{2}} \qquad [1.5]$$

For all materials, including the inorganic glasses, the plastic work contribution to the fracture energy is predominant and hence for most purposes the surface energy may be neglected and we may now write $\gamma \propto P$ and:-

$$\sigma_b = \left(\frac{2\,E\gamma}{\pi\, c}\right)^{\frac{1}{2}}$$

where crack extension occurs under conditions of plane strain or:-

$$\sigma_b = \left(\frac{2\,E\gamma}{\pi c}\right)^{\frac{1}{2}} \quad (1-\upsilon^2)^{-\frac{1}{2}}$$

for plane strain conditions where υ is Poisson's ratio. An important extension to the Griffith - Orowan theory of fracture has been provided by Irwin's "fracture mechanics" concepts. Fracture mechanics is concerned with the mechanical responses of a flawed or cracked body to the application of forces or stresses. For a linear elastic body the stress field produced around the crack tip can be described in terms of the external loads or stresses and the geometry of the body. The crack tip stress field may be characterised by a stress intensity factors K_1, K_2, K_3 which represent the stress singularity surrounding the tip of a crack subjected to the three fundamental modes of crack surface displacement illustrated in Fig. (1.1). For each of the three displacement modes the stress distribution with regard to the angle θ (defined in

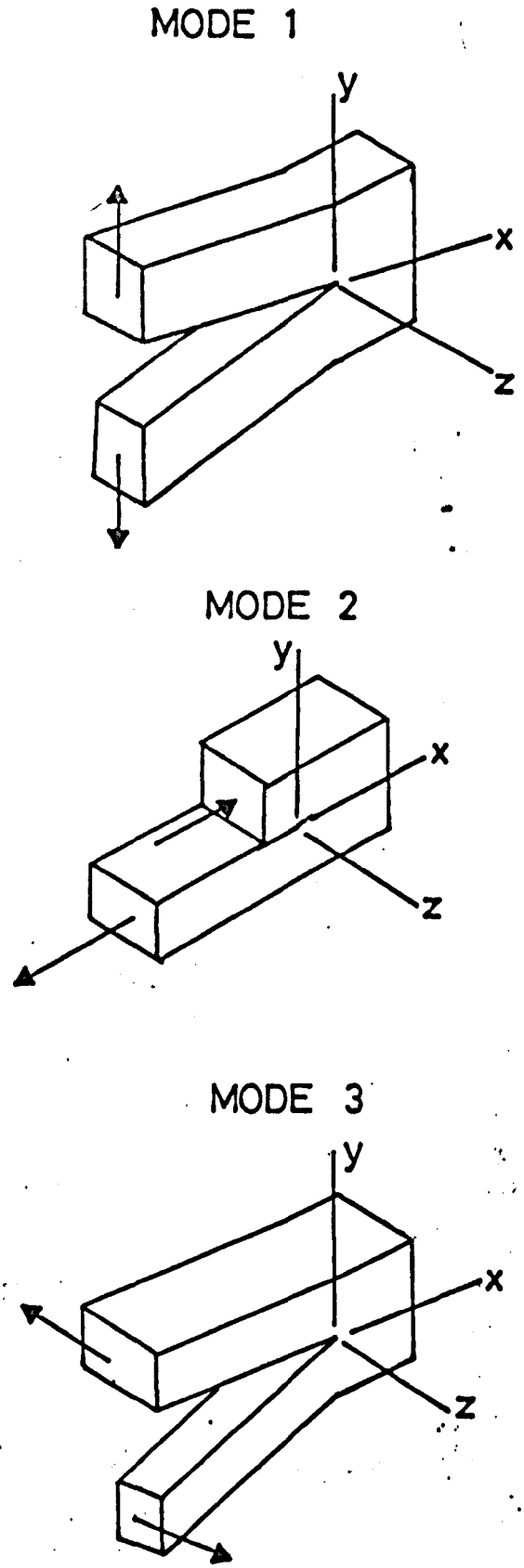

Fig. (1.1) The three fundamental modes of crack surface displacement

Fig. (1.2)) is identical close to the crack-tip regardless of the geometry of the member. Hence the stress intensity factor may be considered as being a single parameter which describes the crack-tip stress field.

Alternately, the magnitude of this stress field may be characterised by an "energy release rate", $\mathcal{G}$, which is associated with the change of elastic - strain energy accompanying an increment of crack extension (IRWIN 1958). When the value of K exceeds a limit characteristic of the material a crack becomes unstable and propagation may occur: this critical stress intensity factor is usually denoted as K_c and serves as a useful empirical toughness parameter which reflects directly, and quantitatively, the complex crack tip plastic deformation.

Irwin also showed by integration across the stress field that:-

$$\gamma = \frac{K_c^2}{2E} (1-\nu^2) \qquad [1.6]$$

when the stress system corresponds to plane strain and hence the fracture is entirely perpendicular to the applied stress direction. Equation [1.6] reduces to

$$\gamma = \frac{K_c^2}{2E}$$

for plane stress conditions where the fracture is entirely shear.

The above expressions may only be justified rigorously for an elastic crack in an ideal, linearly-elastic, brittle material and provide the basis for the so-called "linear elastic fracture mechanics" treatment of brittle fracture. However, they may still be considered as applicable for our purposes even when plastic flow occurs at the crack

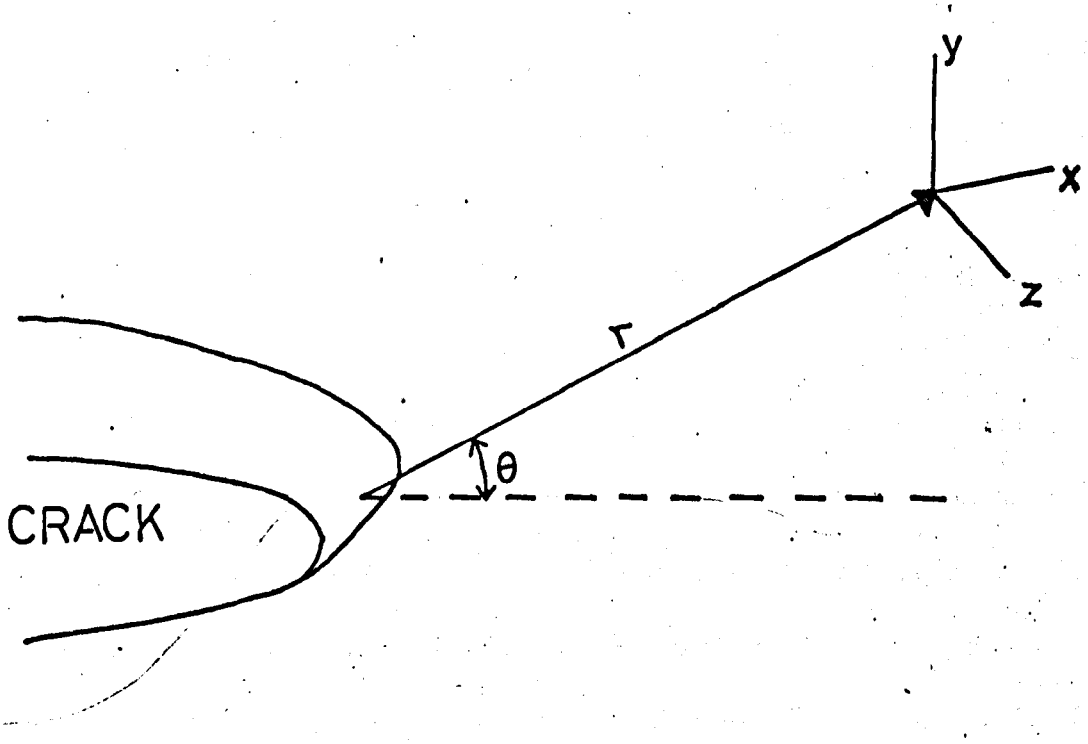

Fig. (1.2) The geometry of the region close to a crack tip

tip provided that the length of the plastic zone and the crack opening displacement are small compared with the specimen dimensions, and the crack length, and also that for the whole specimen, departures from linear elastic behaviour are small.

Both K_c and γ, are referred to in the literature as "fracture toughness" parameters and normally this causes no serious problems. However, if in a systematic study of the dependence of the fracture toughness parameters on the addition of a second phase to a brittle matrix the elastic modulus changes drastically the trend in fracture energy may not be the same as that in the critical stress intensity factor. Generally, in making comparisons between different materials, this critical stress intensity factor is perhaps a more useful parameter for the design engineer since if its value is known, together with the stress applied to a component, then it is possible to calculate the flaw size necessary to cause failure; or alternatively, if the size and orientation of the "worst" flaw is known, then the failure stress may be found. The critical stress intensity factor may therefore be considered as relating directly to the load-bearing capability of a component containing unavoidable cracks. The fracture energy is perhaps a more fundamental parameter since it reflects the extent of inelastic processes occurring at crack tips in non-ideally brittle materials. In this thesis we shall confine ourselves mainly to the determination of fracture energy but in some instances where it is considered necessary critical stress intensity factors will also be quoted.

CLARKE, et.al. (1966) define a "work of fracture" which is essentially an integral form of what we have called fracture energy. This work of fracture may be obtained by determining the total work that has to be done to break a specimen in a manner that is sufficiently slow so that no kinetic energy is imparted to the resulting

fracture pieces. They then divide this work by the projected fracture surface area without taking into account any of the fine scale surface irregularities.

To summarise briefly, we now have two basic parameters, the fracture energy and the critical stress intensity factor, both of which can be determined by experiment, and either of which can be used to represent the toughness of a material, thus enabling comparisons of different materials to be made.

A useful structural material will be one that has a high strength and an adequate toughness. Nature has provided many such materials: bone and bamboo are notable examples and both of these are composites, i.e. they consist of two or more discrete components combined together to produce a final material that has desirable properties not offered by the constituent components on their own. Man has copied nature's composites to produce such materials as glassfibre-reinforced plastics, dispersion strengthened alloys, glass-bonded ceramics, hair-reinforced plaster, straw-reinforced bricks, etc. Such composite materials have received considerable attention over the last decade. Interest has centred primarily on the evaluation of strength, toughness and stiffness and on production techniques with little attention having been paid to the physics of the processes that are involved when a crack propagates through such a material. In addition, much of this work has been concerned with fibre-reinforced matrices and it is now quite well established that increases in toughness, above that of the matrix alone, can be achieved by incorporating fibres into a brittle matrix: for example carbon fibres in glass and glass fibres in polyester resins. On the other hand, the strength of a ductile, and therefore tough, material can be increased by

incorporating strong yet brittle fibres: for example, tungsten in a copper or silver matrix, or silicon carbide whiskers in aluminium.

The main objective of the work to be described in this thesis was to examine in some detail the fracture characteristics of composite materials formed from an epoxy resin matrix and various particulate fillers. It was hoped that a reasonably systematic examination of the effect on toughness of the size, shape, nature, concentration and adhesion of the matrix to the filler particles might lead to some insight into the physical mechanisms involved during crack propagation in this type of composite material. Preliminary work of GRIFFITHS (1968) had already established that the addition of silica flour and aluminium powder to an epoxy resin matrix produced a significant degree of toughening. The choice of composite type, and in particular the matrix material, was governed mainly by practical considerations. Three commercially available epoxy resins were chosen as matrix materials:-

(i) Araldite CT200 cured with HT901 (products of CIBA - Giegy Limited), a casting and laminating system.

(ii) Araldite LY558 cured with HT973 (again products of CIBA - Giegy Limited) a preimpregnation and laminating system.

(iii) EPON 828 cured with NMA and accelerated with BDMA (products of Shell Chemicals Limited), a basic "state of the art" system.

It was hoped that these would provide matrices covering a range of mechanical and thermal properties; the important properties were considered to be, fracture energy, flow stress, elastic modulus, impact energy and thermal expansion coefficient.

The choice of filler was primarily dictated by the availability of particles of suitable sizes. Glass and aluminium were used as fillers in some of the principal series of measurements because they were available in a useful wide range of sizes, but some quite informative results were obtained, in a few tests, using a number of other materials.

1.3. The Determination of Fracture Energy

We have shown that fracture energies or critical stress intensity factors will serve as useful fracture toughness parameters and in the remainder of this chapter we shall review the experimental methods available for the determination of these parameters.

Mica was the first material on which direct measurements of fracture energy were made, OBREIMOFF (1930) used the natural cleavage planes to stabilize the crack propagation direction. The mica was fractured by driving a wedge into the material in a direction parallel to the crystallographic cleavage planes and the fracture energy calculated from the measured crack lengths and opening displacements. The fracture energies of other crystals have been determined in a similar way by, for example, GILLMAN (1960) and WESTWOOD and HITCH (1963). Various other specimen geometries and loading systems have been used or suggested for, fracture toughness testing and a review of many of these is given in the A.S.T.M. SPECIAL TECHNICAL PUBLICATION, Number 381 (1964).

In this thesis the author describes the Double Cantilever Beam or D.C.B. method of fracture toughness determination. The principal advantage of this technique is that it provides a cracked specimen of such geometry that normally the crack has a number of stable positions so that data from a series of propagations, in a single specimen

may be used to estimate the fracture toughness parameters. Other advantages of this method are that, depending on the behaviour exhibited by the material under test, slow crack propagation may be studied or the conditions for both crack initiation and arrest ascertained. The fracture energy presented here is derived from the rate of release of strain energy $\frac{\Delta U}{\Delta L}$ during the fracture of a double cantilever beam type of specimen illustrated in Fig. (1.3). GURNSEY & GILLMAN (1961)have shown that the direction perpendicular to the maximum tensile stress near the crack tip in such a specimen lies at an angle inclined to the longitudinal mid-plane of the specimen which is the required direction of crack propagation and hence, once initiated, a crack will be unstable and tend to run out of the side of the specimen. A number of methods have been employed to stabilize the crack direction in macroscopically isotropic materials; for example, BENBOW and ROESLER (1957) applied longitudinal compression to specimens confined in guides to prevent buckling, and SVENSSON (1961) used an axial loading technique. A simpler method of controlling the propagation direction has been described by BERRY (1963) who cut grooves along the centre line of opposing faces of a long rectangular specimen and was successful in confining the crack to within the grooved central regions; it is this technique that is used throughout this work.

1.4. The Mechanics of the Double Cantilever Beam System

Approximate expressions for the rate of release of strain energy $\frac{\Delta U}{\Delta L}$ and hence the fracture energy may be derived from simple beam theory in terms of specimen dimensions and critical applied load or displacement. Fig. (1.3) again shows schematically a double cantilever system and the following analysis will be concerned

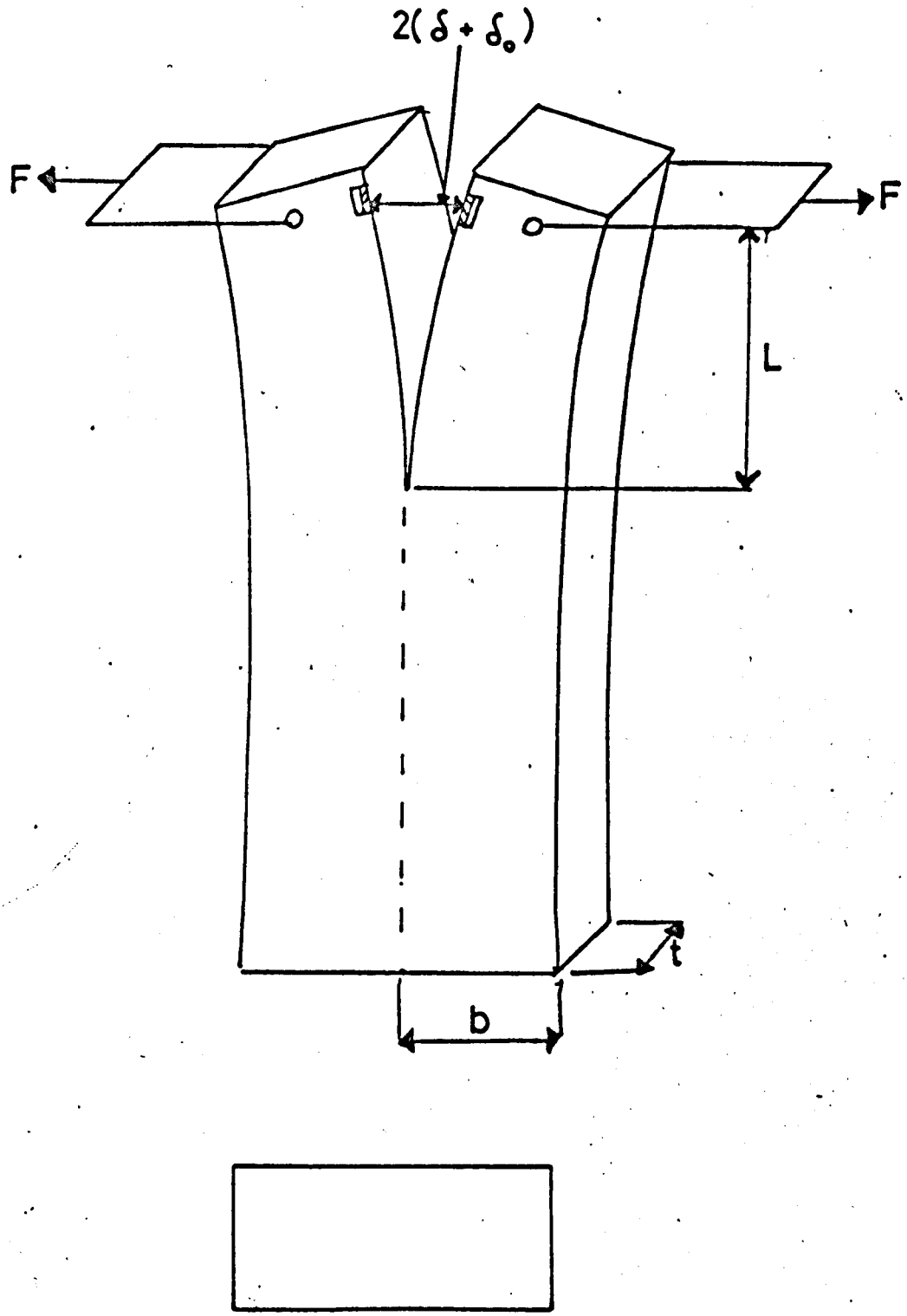

Fig. (1.3) A double cantilever beam specimen.

initially with the simple rectangular form illustrated. For the most elementary case we consider a specimen split along the medium plane such that each half acts as a cantilever whose length is given by the crack length, L. An applied force, F, will produce a bending moment, M (x), along the beams such that M (x) = F (L-x) for $O < x < L$. If we neglect any shear effects then the strain energy, U, in the beam is given by simple beam theory to be:-

$$U = \frac{1}{2EI} \int_{o}^{L} M^2 (x)\, dx = \frac{F^2 L^3}{6EI} \qquad [1.7]$$

where:

E = Youngs modulus

I = Second moment of area of cross section which for a beam of thickness b and width t is given by $I = \frac{tb^3}{12}$

The deflection, δ, at the point of application of the force is given by Castigliano's theorem:-

i.e. $$\delta = \frac{\partial U}{\partial F}\bigg|_{x=L} = \frac{FL^3}{3EI} \qquad [1.8]$$

combining equations [1.7] and [1.8] we have:-

$$U = \frac{3EI\delta^2}{2L^3} \qquad [1.9]$$

Now applying the Principle of Conservation of Energy:

Work done by external force	+	Energy expended in producing new surface	+	Change in stored energy	=	0
$F.d\delta$	+	$\gamma t dL$	+	dU	=	0

where, t, is the width of the fracture surface, i.e. the thickness of the specimen.

From equation [1.8] we have:

$$dU = \left(\frac{\partial U}{\partial L}\right)_{\delta} dL + \left(\frac{\partial U}{\partial L}\right)_{L} d\delta = -\frac{9EI\delta^2}{2L^4} + Fd\delta \qquad [1.10]$$

thus $$\gamma t = \frac{9EI\delta^2}{2L^4} \qquad [1.11]$$

and

$$\gamma = \frac{3Eb^3\delta^2}{8L^4} \qquad [1.12]$$

or alternatively

$$\gamma = \frac{6F^2L^2}{Et^2b^3} \qquad [1.13]$$

A third expression for fracture energy may also be obtained by eliminating E from equation [1.12] and [1.13] to give:-

$$\gamma = \frac{3}{2}\frac{F\delta}{tL} \qquad [1.14]$$

Thus we have three different expressions for fracture energy: if Young's modulus is known, then the fracture energy can be estimated from either measurements of deflection and crack length, or applied force and crack length, alternatively if both force and deflection are measured, then the fracture energy can be estimated directly without the need for a separate measurement of Young's modulus. It will be convenient to denote these different estimates of fracture energy by distinct symbols: viz γ_δ, γ_F and $\gamma_{F\delta}$ respectively. In practice the values of fracture energy obtained from a given set of experimental data using equations [1.12], [1.13] and [1.14] do not always agree to within experimental error; usually $\gamma_\delta \geq \gamma_{F\delta} > \gamma_F$ these differences being a reflection of the approximations involved in using the simple beam theory to evaluate the rate of release of strain energy.

1.5. A More Detailed Analysis

The expressions for fracture energy given in the previous section were developed from a simple beam theory which omits any contribution to the expressions for cantilever arm deflection from shear and from "end rotation". (The finite strain beyond the crack tip, in the unbroken section of the specimen.) These two additional contributions may be considered as corresponding to an extra displacement of the cantilever arms for a given applied stress and hence we may write the total deflection as:-

$$\delta \text{ Total} = \delta \text{ shear} + \delta \text{ end rotation} + \delta \text{ applied stress}.$$

The effect of these additional terms has been considered by GILLIS and GILLMAN (1964), BERRY (1963) and SRAWLEY & GROSS (1967); we will now examine in some detail these three rather different ways of correcting the simple expressions.

1.5.1. Gillis and Gillman

Gillis and Gillman have analysed mathematically the principal deviations from the simple beam case; they considered the main sources of error to arise from the neglect of the effects of the shearing strains in the cantilever arms and the finite strains beyond the crack tip.

Shear

The existence of a finite shear strain within the cantilever arms modifies the simple beam expression [1.7], for stored strain energy to:-

$$U = \frac{F^2L^3}{6EI} + \frac{CF^2L}{2AG} \qquad [1.15]$$

where A and C are constants and G the shear modulus.

If we combine this with equation [1.13] we may write:-

$$\gamma_{F\ (\text{corrected for shear})} = \frac{F^2L^2}{2EIt}\left(1 + \frac{CEI}{AGL^2}\right) \qquad [1.16]$$

Similarly the deflection equation for stored strain energy may be rewritten in its corrected form as:

$$U = \frac{3EI\,\delta^2}{2L^3}\left(1 + \frac{3CEI}{AGL^2}\right)^{-1} \qquad [1.17]$$

and hence the corresponding fracture energy expression becomes:

$$\gamma_{\substack{\text{corrected}\\\text{for shear}}} = \frac{9EI\delta^2}{2L^4}\left(1 + \frac{CEI}{AGL^2}\right)\left(1 + \frac{3CEI}{AGL^2}\right)^{-2} \qquad [1.18]$$

Now following a similar procedure to that used previously and eliminating Young's modulus from equations [1.16] and [1.18] then the force/deflection equation for fracture energy may be written as:-

$$\gamma_{F\delta\ \left(\substack{\text{corrected}\\\text{for shear}}\right)} = \frac{3}{2}\frac{F\delta}{tL}\left(1 + \frac{CEI}{AGL^2}\right)\left(1 + \frac{3CEI}{AGL^2}\right)^{-1} \qquad [1.19]$$

An estimate of the error involved, for an epoxy resin, in neglecting shear effects and using the equations based on the simple theory may be found by substituting typical values into the additional terms in these three corrected expressions.

Such a substitution gives:-

$$\frac{CEI}{AGL^2} \approx \frac{1}{5}\frac{b^2}{L^2}$$

and hence the errors due to neglecting shear are:

$$\left[\begin{array}{l} 5\% \text{ at } L = 2b \\ 1\% \text{ at } L = 4b \end{array}\right]$$

$$\left[\begin{array}{l} 20\% \text{ at } L = 2b \\ 1\% \text{ at } L = 4b \end{array}\right]$$

$$\left[\begin{array}{l} 5\% \text{ at } L = 2b \\ 2\% \text{ at } L = 4b \end{array}\right]$$

for the force, deflection, and force/deflection equations respectively.

End Rotation

Finite stress beyond the crack tip are problematical and if these are present then some movement of what were previously assumed to be the fixed ends of the cantilever arms takes place; this movement is generally referred to as end rotation. If we now confine ourselves to considering specimens with large $\left(\frac{L}{b}\right)$ ratios where, as we have shown previously, shear effects may be neglected, then

$$\delta = \frac{FL^3}{3EI} \left(1 + 3DL^{n-2}\right) \qquad [1.20]$$

where D and n are constants.

Manipulation of equations [1.13] and [1.20] gives the following relationship between the fracture energy and the applied force:

$$\gamma_{\substack{F \\ \text{(corrected for end rotation)}}} = \frac{6F^2L^2}{Et^2b^3} \left[1 + (n+1)\, DL^{n-2}\right] \qquad [1.21]$$

and similarly by combining equations [1.12] and [1.20] the "deflection" equation may be written:-

$$\gamma_{\substack{\delta \\ \text{(corrected for end rotation)}}} = \frac{3Eb^3\delta^2}{8L^4} \cdot \frac{1 + (n+1)\, DL^{n-2}}{(1 + 3DL^{n-2})^2} \qquad [1.22]$$

and as before:-

$$\gamma_{F\delta\ (\text{corrected for end rotation})} = \frac{3}{2}\frac{F\delta}{tL}\left[\frac{1 + (n+1)\,DL^{n-2}}{1 + 3DL^{n-2}}\right] \qquad [1.23]$$

If n = 2 the above equation reduces to simple beam expression: viz $\gamma_{F\delta} = \frac{3}{2}\frac{F\delta}{tL}$. Gillis and Gillman also considered various other departures from simple behaviour including kinetic energy and anisotropy. Kinetic energy contributions which arise from the motion of the cantilever arms are problematical, however, determinations of fracture energy made in this work are dependent upon the rate of release of strain energy at the beginning and end of each increment of crack extension, i.e. where the velocity approaches zero and therefore this effect may be neglected. Specimen anisotropy has also been shown to have little effect on calculated fracture energies provided that a modulus appropriate to the applied stress direction is used (this problem may be avoided if the force/deflection expressions are used since these do not contain a modulus term.)

Further small errors arise from the effects of the suppression of anticlastic curvature near the crack tip. This effect appears to be part of the end rotation already considered since the suppression of this curvature suggests that the strain energy density is higher than that calculated from simple beam theory but only by about 3% at a length to breadth ratio of three. For some materials and specimen sizes it is possible that the deformation of the cantilever arms becomes non-Hookean. This effect is particularly difficult to correct for analytically and the best procedure is to avoid the problem by selecting a specimen size (in particular the width of the cantilever arms) such that the deformation remains linearly elastic.

1.5.2. Berry's Method

The procedure adopted by BERRY (1963) and later by BROUTMAN and Mc GARRY (1965) to obtain accurate estimates of fracture energy from double cantilever beam force and displacement data is best described as being semi-empirical. The essential difference between this method and that of Gillman is that Berry does not specify the form of the errors involved but attempts to determine their influence experimentally whereas Gillman deduces the form of the errors theoretically and evaluates or eliminates them experimentally. Berry assumes that the simple cantilever equation [1.8] is inappropriate, however, he does not specify the sources of error in detail, unlike Gillis and Gillman. Instead he generalises the equation to:-

$$\delta = \frac{FL^m}{3EI} \qquad [1.24]$$

and assumes:

$$F = \frac{H\delta}{L^m} \qquad [1.25]$$

where m and H are constants.

Now since $U = \frac{1}{2} F\delta$ then from [1.25]

$$U = \frac{1}{2} H\delta^2 L^{-m} \qquad [1.26]$$

$$\therefore \quad \frac{\partial U}{\partial L} = -\frac{mH\delta^2}{2L^{m+1}} \qquad [1.27]$$

and hence

$$\frac{\partial U}{\partial L} = -\frac{mF\delta}{2L} = 2\gamma W \qquad [1.28]$$

or rearranging

$$\frac{F\,\delta}{t} = \left(\frac{4\gamma}{m}\right)L \qquad [1.29]$$

The constant, m, may be determined experimentally from a plot of $\log\left(\frac{F}{\delta}\right)$ against log (L) and the fracture energy then calculated using this value of m.

1.5.3. Srawley and Gross

SRAWLEY AND GROSS (1967) have carried out a detailed numerical analysis to evaluate the plane strain, stress intensity factor K_I and the cantilever end deflection in terms of the applied load and beam dimensions. The numerical technique they used is often termed boundary collocation and involves finding, by successive approximation, a stress function χ that satisfies the biharmonic equation

$$\Delta^4 \chi = 0$$

and also the boundary conditions at a finite number of stations along the edge of a specimen. The original results were in numerical form but it is fortuitous, and certainly convenient, that their data can be represented by a relatively simple expression, for K_c and δ which, after manipulation, give the following expressions for fracture energy:

$$\gamma_\delta = \frac{3Eb^3\delta^2}{8L^4}\left[\frac{(1+0.7\frac{b}{L})}{1+2.1\frac{b}{L}+1.5\frac{b^2}{L^2}}\right]^2 \qquad [1.30]$$

$$\gamma_F = \frac{6F^2L^2}{Et^2b^3}\,(1+0.7\frac{b}{L})^2 \qquad [1.31]$$

$$\gamma_{F\delta} = \frac{3}{2}\frac{F\delta}{tL}\left[\frac{(1+0.7\frac{b}{L})^2}{1+2.1\frac{b}{L}+1.5\frac{b^2}{L^2}}\right] \qquad [1.32]$$

1.6. Grooved Specimens

The previous analyses have been concerned only with a simple rectangular form of specimen; but it is necessary to cut grooves along two opposing faces in order to stabilise the direction of crack propagation in the macroscopically isotropic materials to be investigated here. In general the specimens employed throughout this work had the cross section shown in Fig. (1.4) and for calculations of fracture energy the basic equations need slight modification.

For a rectangular, grooved specimen (shown in Fig. (1.4)) having the following dimensions:

t = thickness

w = thickness in the groove

2Y = width of groove

b = distance from the edge of the groove to the side of the specimen

The energy dJ expended in producing new surface during an increment of crack extension dL is therefore:-

$$dJ = 2\gamma w dL$$

For our grooved specimens the second moment of area I is given by:

$$I = \frac{E(b+Y)^3}{12}$$

but provided that $Y \ll b$ then

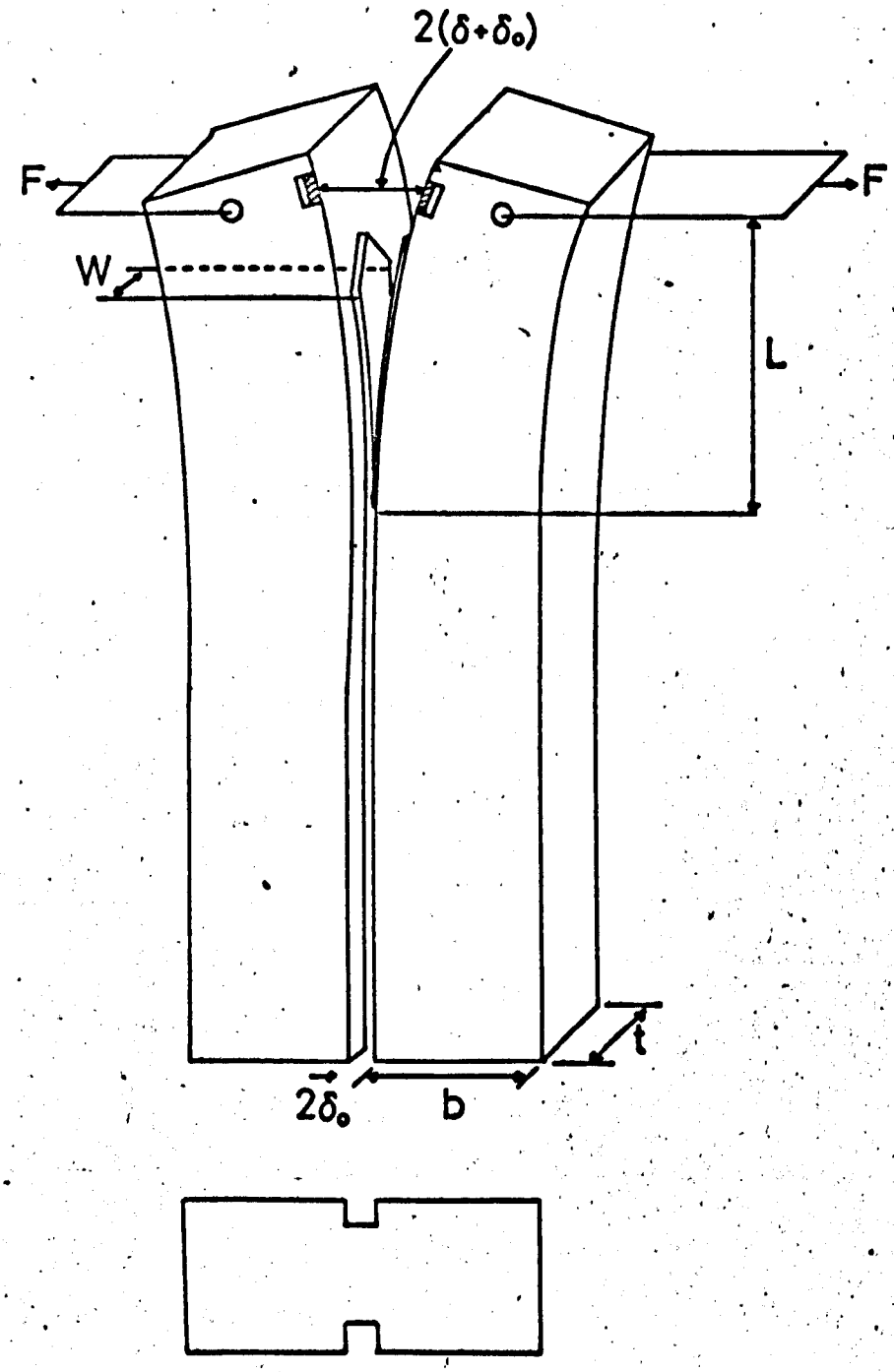

Fig. (1.4) A grooved double cantilever beam specimen.

$$I = \frac{b^3 t}{12}$$

and hence the original Srawley and Gross expressions for fracture energy may be modified to give:-

$$\gamma_\delta = \frac{3Etb^3\delta^2}{8wL^4}\left[\frac{(1+0.7\frac{b}{L})}{1+2.1\frac{b}{L}+1.5\frac{b^2}{L^2}}\right]^2 \qquad [1.33]$$

$$\gamma_F = \frac{6F^2L^2}{Ewtb^3}\left(1+0.7\frac{b}{L}\right)^2 \qquad [1.34]$$

$$\gamma_{F\delta} = \frac{3}{2}\frac{F\delta}{wL}\left[\frac{(1+0.7\frac{b}{L})}{1+2.1\frac{b}{L}+1.5\frac{b^2}{L^2}}\right] \qquad [1.35]$$

1.7. Discussion

The deviations from the simple beam theory have been discussed in detail and it will be shown later that numerical data presented in this thesis fits closely the Srawley and Gross equations provided that the crack length is greater than about twice the specimen width. Gillis and Gillman's analytical arguments were included to illustrate and give some physical basis to the main sources of error for the experiments reported here; these are considered to be shear and end rotation although in general minor contributions are made by the kinetic energy of the cantilever arms, repressed anticlastic curvature, non-linear deformations and anisotropy. Berry's technique was considered primarily for its historical significance and to emphasise that some care must be exercised when comparing published data obtained from different analyses of experimental results. In Berry's case deviations from the simple beam model

are all included in the value of his constant, m, and are therefore reflected directly in the calculated fracture energy. The Srawley and Gross boundary collocation results, which fit very closely the experimentally observed relationships between deflections, applied forces and crack lengths, indicate that the corrections which need be applied to the simple model are not of the first order as Berry assumes: hence deviations are not necessarily reflected directly in the estimated value of fracture energy.

1.8. Summary

This chapter has been concerned primarily with the theoretical background of the double cantilever beam technique for the determination of the fracture energy of a brittle material. Expressions for the fracture energy have been developed from simple beam theory with the aid of Principle of Conservation of Energy and some of the deviations from the simple case have been discussed and the necessary corrections presented. The best available expressions for the calculation of fracture energy are considered to be those published by Srawley and Gross.

CHAPTER II

Basic Experimental Techniques

2.1. Introduction

Some discussion is presented here on the basic epoxy resin cure mechanisms and on the methods of specimen preparation: the experimental procedure adopted for the determination of fracture energy and the apparatus used are also described.

2.2. Basic Cure Mechanisms

The three epoxy resin systems used throughout the experimental programme were Araldite CT200/HT901, Araldite LY558/HT973 (both products of CIBA Geigy Limited), and EPON828/NMA/BDMA (products of Shell Chemicals Limited).

2.2.1. CT200/HT901

CT200 is an "advanced" epoxy resin based on the diglycidyl ether of bisphenol A which is generally used for casting and laminating purposes. The diglycidyl ether is obtained by reacting bisphenol A with epichlorohydrin, in the presence of a sodium hydroxide catalyst. The reaction proceeds via two stages:-

(i) The formation of a chlorohydrin intermediate.

(ii) The dehydrohalogenation of the intermediate to the glycidyl ether.

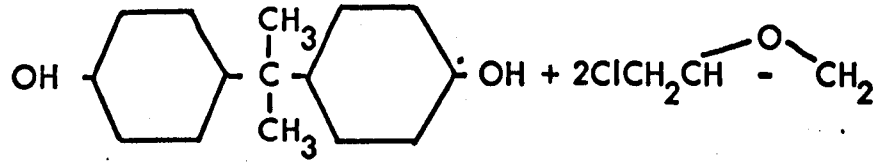

Bispehnol A Epichlorohydrin

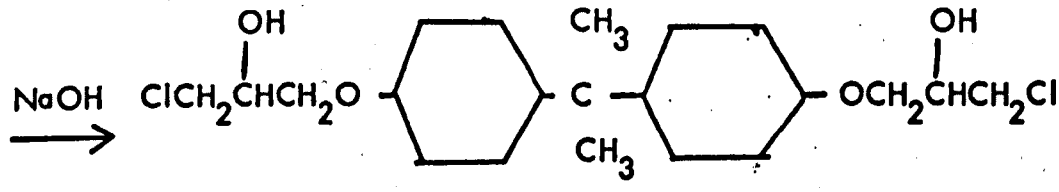

Chlorohydrin intermediate

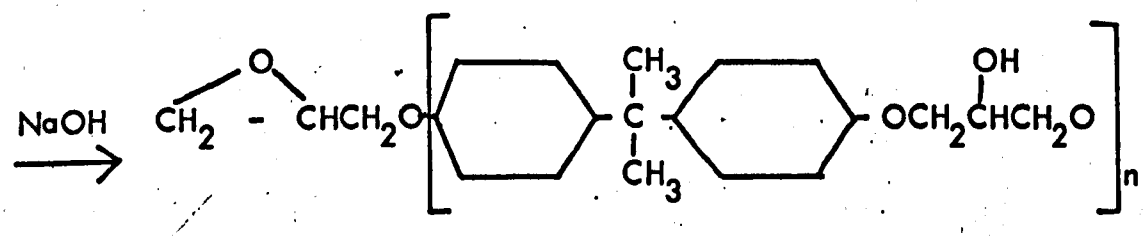

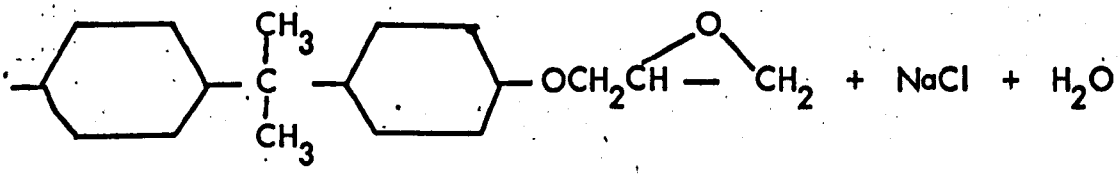

The reactions which occur when the CT200 is "cured" with phthalic anhydride, HT901, to form a thermally more stable material are somewhat complicated and uncertain. Since phthalic anhydride does not react directly with epoxy groups it is first necessary for the anhydride ring to be opened.

The nature and the rate of reaction between the anhydride and the resin will, in general, be governed by the method of ring opening; in this system the ring is opened by the hydroxyl groups of the resin to result in the formation of carboxyl groups.

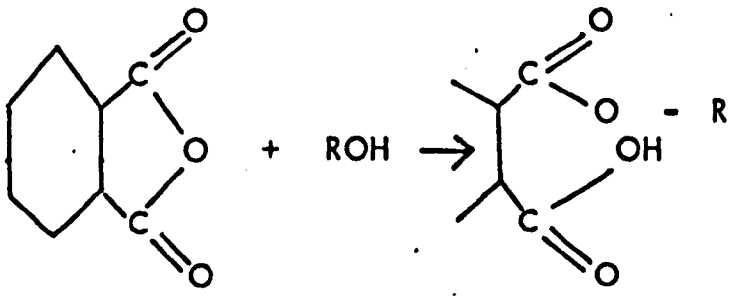

Phthalic
Anhydride

The carboxyl groups produced further react with the eppxy groups by what is initially an addition esterification.

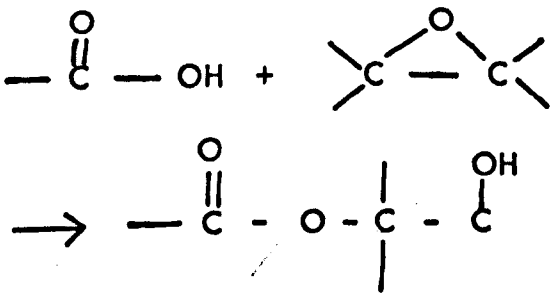

Alcoholic hydroxyl

The alcoholic hydroxyl then undergoes preferential, independent etherification through the reaction of available hydroxyl groups with epoxy groups.

The precise mechanisms have not been too well elucidated in the literature but it is likely that the reaction proceeds in part through the formation of an intermediate oxonium ion.

The final product is however the highly cross-linked polymer:-

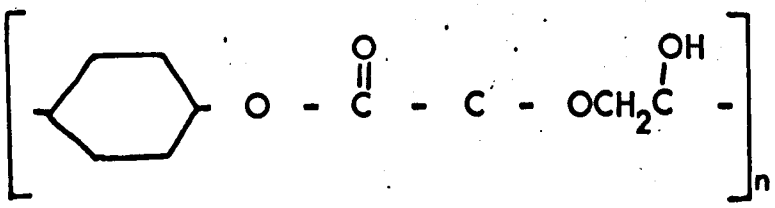

2.2.2. LY558/HT973

LY558 is an epoxy-novolac resin generally used for the production of fibrous composites. The starting novolac may be produced by the reaction of phenol and formaldehyde in acid solution, such novolacs have the following idealised structure:

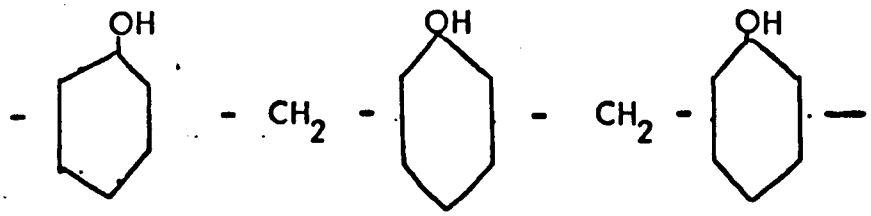

The novolac-based epoxy resins are normally synthesised by a reaction involving epichlorohydrin in a similar manner to that used for bisphenol A resins.

HT973 is a boron triflouride/ethylamine complex, the boron triflouride is used to accelerate the sluggish reaction between amine and resin. Complexing is employed to co-ordinate the unshared electron pair of the nitrogen atoms with the empty boron orbitals and so block any reaction until elevated temperatures are used to dissociate the complex. The above complex dissociates at about 360K and hence this particular system has proved very useful for the preimpregnation of fibrous composites.

$BF_3 \cdot C_2H_5NH_2$ may dissociate to:- $C_2H_5 : BF_3^{(-)} + H^{(+)}$

reaction with available epoxy groups then occurs to give:-

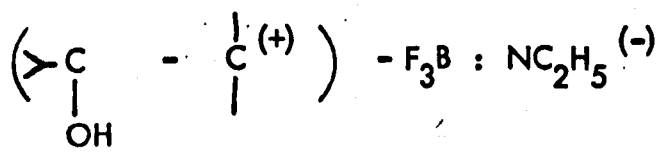

which is capable of chain propagation and cross-linking by ring opening of the epoxy

groups again to produce a highly cross-linked polymer.

2.2.3. Epon 828/NMA/BDMA

Epon 828 is a "state of the art" commercial resin being similar to CT200 and based on the diglycidyl ether of bisphenol A, but has a somewhat lower molecular weight. The mechanism of the cure with nadic methyl anhydride, NMA, and benzyldimethylamine, BDMA is even less well understood, or documented, than the other anhydrides. The tertiary amine, BDMA, is used as an accelerator again to increase the rate of the otherwise very slow reaction of Epon 828 with NMA.

The reaction proceeds in a similar manner to that for CT200 with the BDMA, a Lewis Base, reacting preferentially with the anhydride to accomplish the necessary ring opening and in the process generating a carboxyl ion.

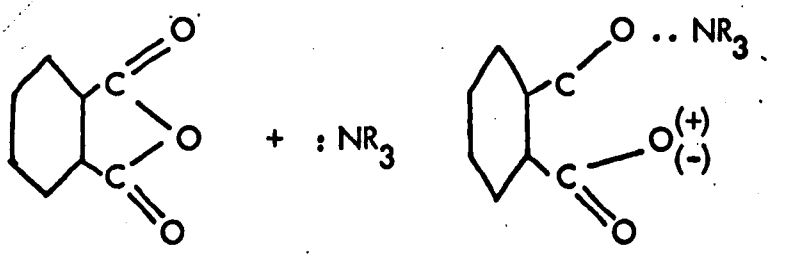

Reaction between an epoxy group and the carboxyl ion produces another ion which is capable of opening a second anhydride ring and so on in a chain process.

2.3. Specimen Preparation

The majority of the specimens produced were cast in preheated steel moulds. These moulds were supported vertically in the curing oven so that transference of mixtures from pre-reaction vessels could be achieved without removing the moulds from the oven. The insides of the moulds were coated with a silicone grease release coating,

(Releasil MS7) which was baked on to the surface at 570K for 24 hours and any excess removed with carbon tetrachloride. This surface treatment allowed about thirty specimens to be cast in any given mould before a re-application of grease was required.

2.3.1. CT200/HT901

Stoichiometric quantities of resin and hardener were used throughout this work, these being 100 : 30 parts by weight of CT200 resin to HT901 hardener. In preliminary experiments it was found expedient to use freshly supplied batches of the components if samples having consistent fracture behaviour were to be produced. Initially some difficulty was experienced in fabricating specimens containing the larger sizes of filler since sedimentation occurred in the vertical moulds in the period after pouring from the pre-reaction vessels and before gellation of the matrix. A somewhat unusual cure schedule was developed in which the CT200 resin was pre-heated in a covered vessel to 433K. In the instances where filled specimens were to be produced, the requisite amount of pre-heated filler was added at this stage and sufficient time allowed for the removal of air bubbles. The appropriate weight of hardener was then stirred into the mix and regular stirring continued for a period of thirty minutes after which time the partially pre-cured mixture was transferred into the heated steel moulds. A mould temperature of 393K was chosen to prevent sedementation by rapidly increasing the viscosity of the mix. Specimens were cured in the moulds for sixteen hours at 393K and cooled slowly at 20K per hour to room temperature where they were broken out, drilled, trimmed and a slot, terminating in a swallow-tail, cut. The samples, supported on a glass plate, were then post-cured at 433K for sixteen hours and again cooled slowly at 20K per hour; thus eliminating

the necessity for a further annealing treatment.

The steel moulds produced specimens having the following dimensions:

Length	=	300 mm
Width of arm b	=	12 mm
Thickness, t	=	7.5 mm
Groove width, 2Y	=	1 mm
Thickness in the groove, w	=	3 mm

which were chosen to satisfy the condition that the ratio of minimum crack length to specimen thickness was greater than three so that errors involved in the use of the Srawley and Gross expressions would be minimal.

2.3.2. LY558/HT973

Specimens were manufactured using LY558 and HT973 in the ratio of 100 : 3 parts by weight respectively, plus the required amount of filler. The cure schedule was of the same form as that employed for CT200 but with the following modifications:

(i) Pre-cure for fifteen minutes at 393K

(ii) Cure at 373K for sixteen hours in steel moulds

(iii) Post-cure and anneal at 393K for sixteen hours.

2.3.3. Epon 828/NMA/BDMA

The preparation procedure differed slightly from the above cases due to the necessity of adding an accelerator. Resin and hardener in the ratio of 100 : 90 parts

by weight were heated separately to 393K and then mixed thoroughly, the required quantity of filler was added at this stage and the mixture allowed to stand in a covered vessel until all the air bubbles had been removed. 0.5 parts by weight of accelerator was then thoroughly stirred into the mixture. The complete cure schedule was as follows:-

(i) Pre-cure at 393K and pour ten minutes after the addition of the accelerator.

(ii) Cure at 388K for sixteen hours.

(iii) Post-cure and anneal for sixteen hours at 433K.

The above procedures when allied with a little experience enabled composites to be produced having bubble volume fractions of less than 0.01 and with no appreciable sedementation. A generally good surface finish could also be obtained such that unfilled specimens were transparent; light not being scattered appreciably from surface imperfections. Examination under crossed polaroids revealed only slight residual strains.

2.4. Description of Apparatus and Experimental Procedure Used for Determination of Fracture Energy-

We have previously indicated that the double cantilever beam technique, for the determination of fracture energy, has a number of advantages over other possible methods. In particular it is generally possible to control the propagation of the crack such that data may be obtained from a number of increments of crack extension. This technique also makes it possible to study slow crack growth in materials in which this occurs and to determine conditions for crack initiation, propagation and arrest.

The determination of fracture energy involves the measurement of cantilever opening displacement, applied force and crack length for separate discrete values of opening displacement.

The test apparatus shown in Figs. (2.1) and (2.2) was constructed using a commercial Hounsfield tensometer as a basis and enabled the fracture energy of specimens, having the dimensions given previously, to be determined. The cantilever opening displacement, 2δ, was derived from observations of the relative positions of fiducial marks attached to the specimens; these were followed with the aid of a low power X10 microscope, mounted on a vernier scale, which could be read to within $\pm$ 0.05 mm. The crack length was obtained with the aid of a second low power microscope attached to a vertical scale. Some problems were encountered in deciding upon the precise location of the crack front because of its finite curvature; this difficulty applied particularly to the filled material where it was impossible to see into the body of the specimen. Quoted values of crack length may therefore be considered to be accurate to within $\pm$ 0.5 mm although the error in relative values are much less. There are also more profound implications of the curved crack front since all the theoretical models including that of Srawley and Gross assume a straight crack front. The situation is further complicated by the fact that the curvature depends on the crack velocity. A typical crack front in cured CT200 is shown in Fig. (2.3), for the sake of consistency all the crack lengths were measured from the line of application of load to the point where the front intersects the specimen surface. Provided that the curvature is not too large, this approximation should not produce an appreciable error in the calculated fracture energies.

The applied force, F, was recorded with an Ether U.F.2. dynamometer and a TOA chart recorder. Specimens were precracked in a simple hand-operated machine to

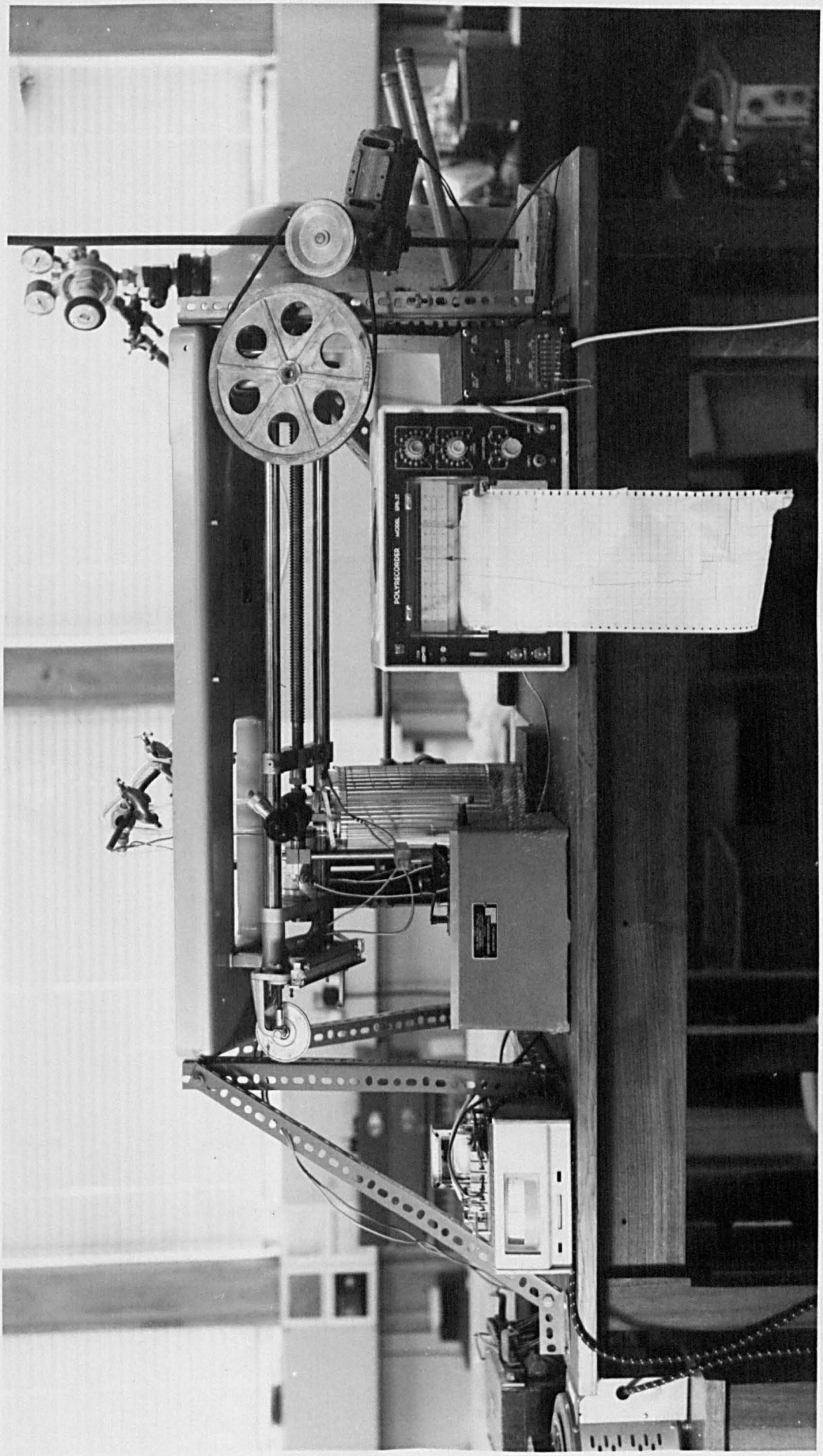

Fig. (2.1) Basic apparatus used for the determination of fracture energy

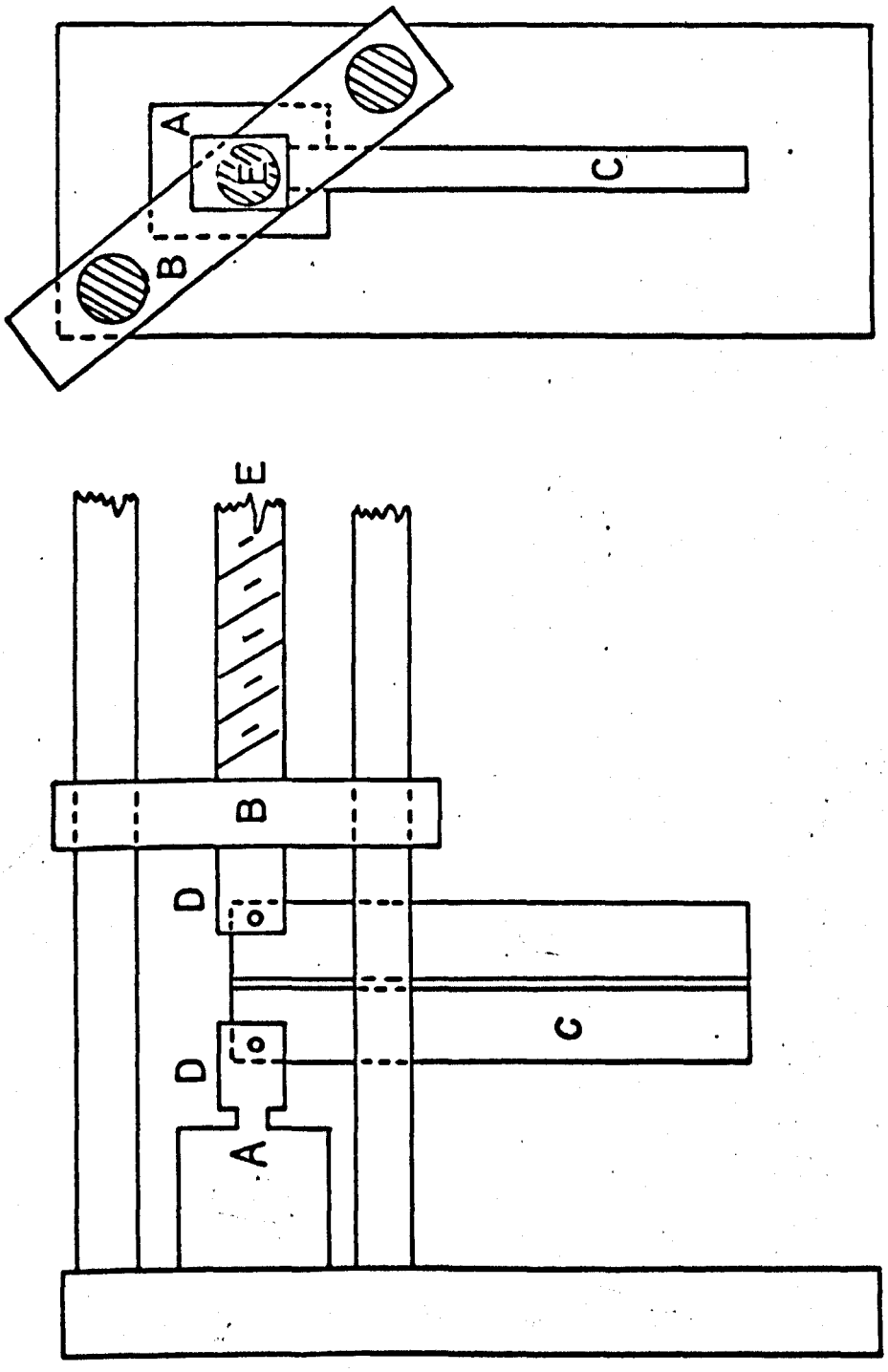

Fig. (2.2) Diagrammatic representation of basic test apparatus

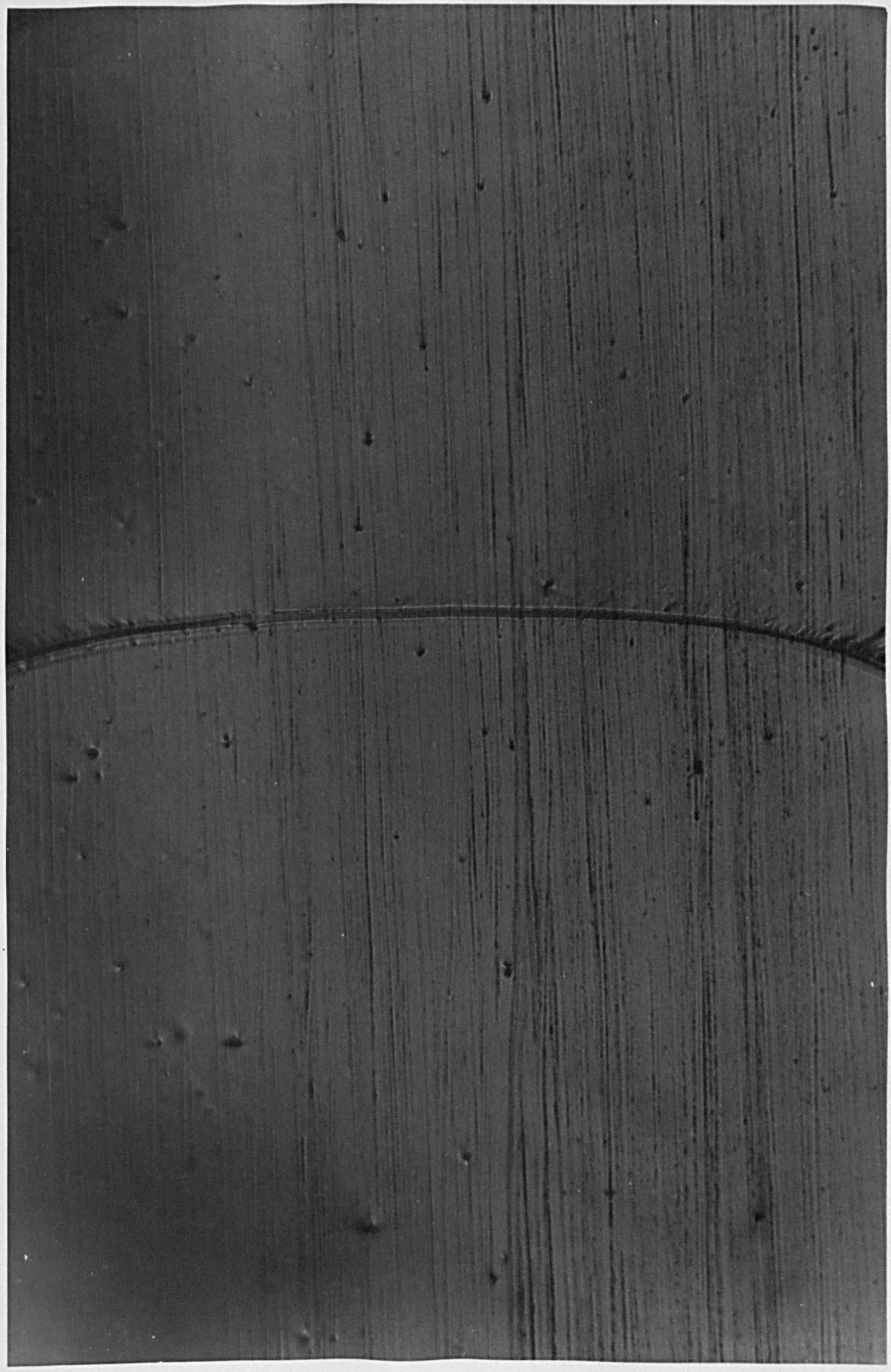

Fig. (2.3) Typical crack front in cured CT200/HT901

(magnification x 75)

produce a crack length of about 100 mm. A sensitive load cell could then be used, in the more sophisticated testing machine, without possible damage by the high loads required to initiate a crack from a swallow-tail cut. The above combination of dynamometer and chart recorder then allowed the applied force to be determined to within $\pm$ 2% irrespective of the range of dynamometer.

Samples under test were placed in the machine jaws and the distance between the fiducial marks, $2\delta_o$, recorded in the unstressed state. The cross-head drive motor was then started and the fiducial marks followed with a travelling microscope until the crack was observed to propagate, at which instant readings of $2(\delta + \delta_o)$, crack length and applied force, F, were recorded.

The width, w, of the fracture surface was estimated after fracture with the aid of a travelling microscope, about ten readings being taken at different points along the length of the specimens. The width, b, and thickness, t, of the cantilever arms were taken as the mean of four micrometer readings from each limb of the double cantilever specimens.

In practice, for many of the materials tested here, a complication arises since the crack does not propagate in a continuous manner as the displacement of the cantilever arms is increased, but in a series of discrete, well-defined jumps. It is therefore possible, as we shall see later, to calculate fracture energies corresponding to conditions of crack initiation and arrest.

2.5. Processing of Observational Data

Fracture energies were determined from the observational data, by a graphical method using co-ordinates based on the Srawley and Gross equations: In general the force-deflection equation [1.35]was used since a knowledge of Young's modulus was

not necessary when only the fracture energy was to be calculated. A typical graphical representation of corrected data from two unfilled, cured CT200 specimens is shown in Fig. (2.4), the correction factor

$$\left[\frac{(1+0.7\frac{b}{L})^2}{1+2.1\frac{b}{L}+1.5\frac{b^2}{L^2}}\right]$$

having been found, for each group of data, with the aid of a desk top computer.

An interesting feature of the graphical representation of the experimental data is the small negative intercept, on the ordinate, which is found reproducibly on plots for unfilled specimens fractured at a constant cross-head speed. These intercepts were not found on graphs plotted from data obtained when hand cranking the Hounsfield testing machine. This apparent anomaly will be considered in some detail in Chapter III.

The Young's modulus of the specimens, where needed, was determined using a Srawley and Gross corrected formula since it may readily be shown by manipulation of equations [1.32] and [1.33] that:-

$$E = \frac{4FL^3}{tb^3\delta}\left(1+2.1\frac{b}{L}+1.5\frac{b^2}{L^2}\right)$$

The data was again analysed graphically and a typical example is given in Fig. (2.5).

2.6. Summary

The somewhat incomplete information at present available on the chemistry of the cure mechanisms of the three basic resins is presented; this is not intended to

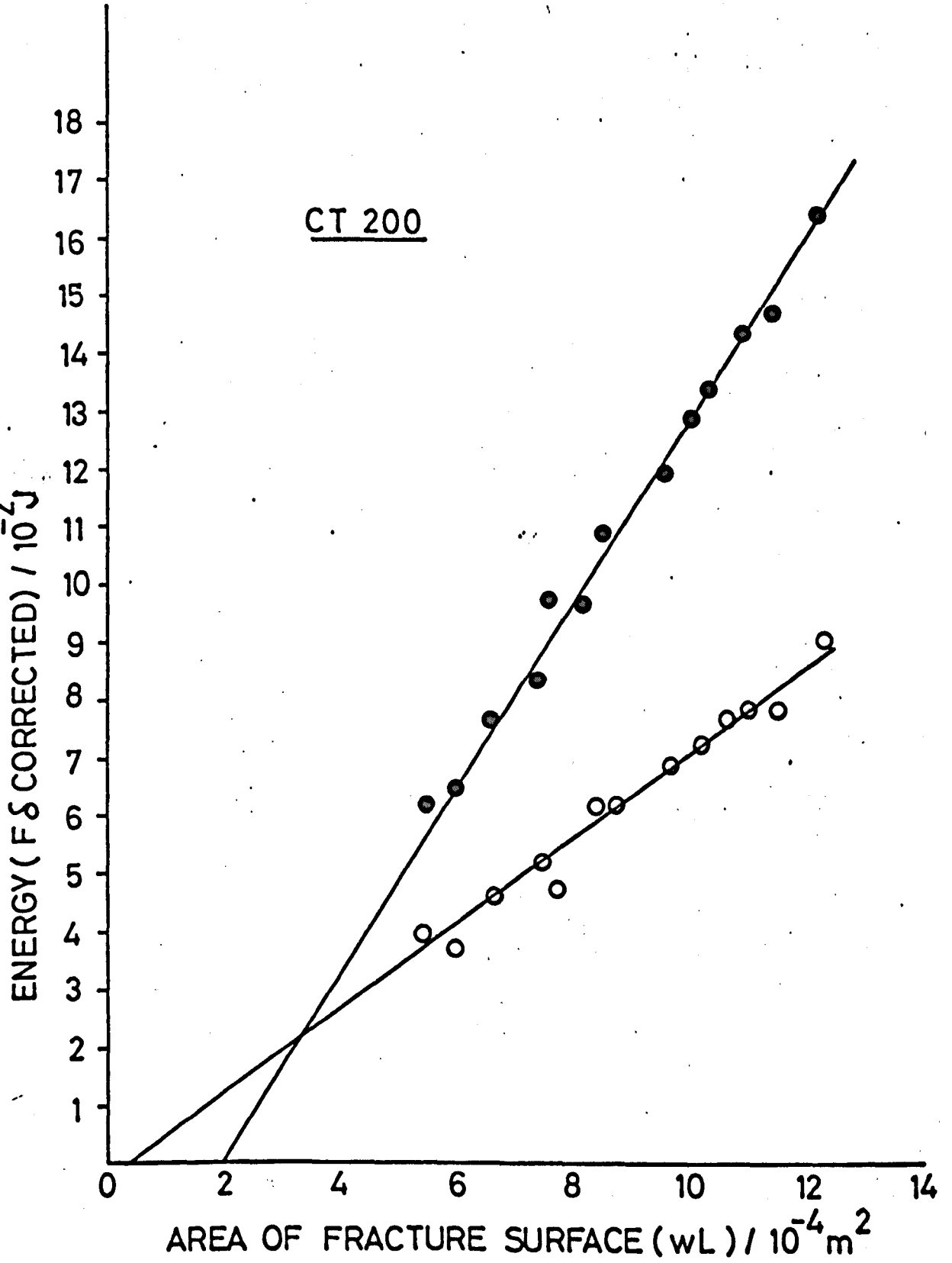

Fig. (2.4) Typical corrected data used for the determination of the fracture energies ($lγ_{F\delta}$ and $Aγ_{F\delta}$) of unfilled CT200/HT901.

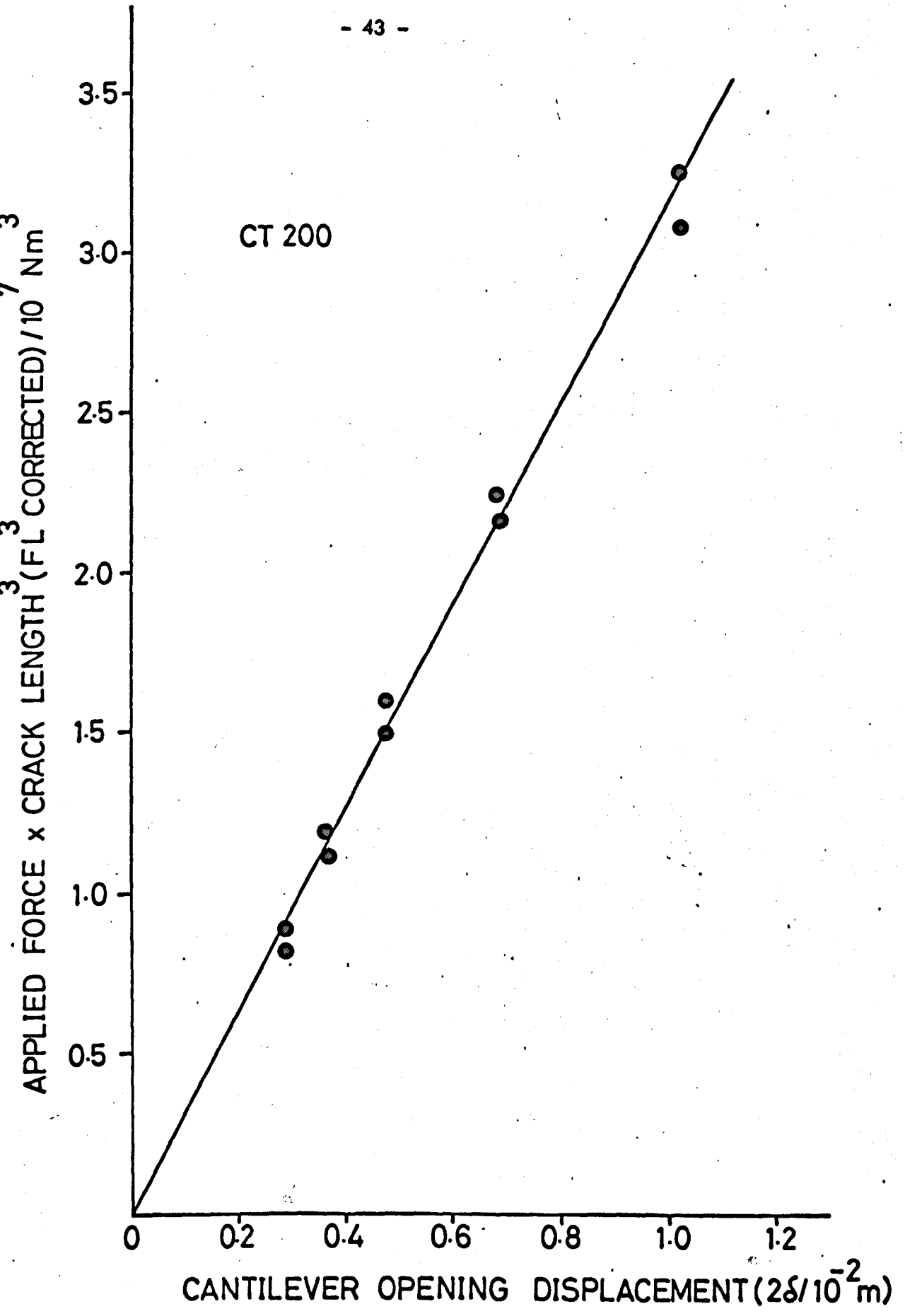

Fig. (2.5) Typical corrected data used for the determination of the Young's modulus of CT200/HT901

be a comprehensive review of the epoxy resin literature but to illustrate the complexity of the cure processes involved. The salient feature, however, of these materials is that what is initially a liquid or low melting point solid may be cross-linked to produce a polymer having excellent mechanical properties. Techniques employed for the production of composite materials with an epoxy resin as a matrix are also described as are the measurement of the various parameters needed for the determination of fracture energy.

CHAPTER III

Preliminary Experiments with Unfilled Resins

3.1. Introduction

Early experiments with fillers highlighted the need for some basic information on the fracture behaviour of the matrix resins. A series of experiments was therefore performed to examine the behavioural features of the three selected resins and to investigate the effects of temperature and environment. These experiments, which reveal a number of interesting features, will be described in this chapter. Some new effects have been observed, in particular that the fracture energy is strain-rate dependent and also at 350K, where a pronounced increase in toughness occurs, the crack-tip plastic deformation is augmented by the formation of a considerable number of small "craze-like" defects.

3.2. General Behaviour

Two effects were observed during very early experiments when using a simple hand-cranked machine to fracture double cantilever beam specimens. Firstly, the crack does not propagate continuously as the testing machine cross-head is displaced at a constant rate, but advances in a series of well-defined jumps. Secondly, the fracture energies of these materials are sensitive to the effective extension rate at the crack tip, which as we shall see later is a function not only of the applied extension rate but also the crack length.

Specimens of all three resin systems prepared as described previously, exhibit a type of crack propagation behaviour that will be described throughout this thesis as "crack jumping". It is observed, for these materials when low strain rates are used, that during double cantilever beam experiments the crack does not advance in a continuous fashion as the cross-head displacement is increased but in a series of discrete increments. There are therefore a range of values of cantilever opening displacements and/or applied force over which the crack will not propagate, and hence a number of stable crack positions may be obtained along the length of a specimen. It may be useful at this stage to compare some of the phenomenological characteristics that obtain during the propagation of a crack in these materials with that expected for an ideal brittle material which has a unique, single-valued, time and temperature independent, fracture energy. If a double cantilever beam fracture test were performed on this hypothetical material with the testing machine cross-head driven at a constant rate then the crack would be observed to propagate continuously down the length of the specimen. The rate of crack propagation being controlled by the rate at which the system is supplied with strain energy, that is by the speed at which the cross-head is displaced. A similar experiment performed on the three cured epoxy resins would yield very different results: if the cross-head was extended slowly then the crack would be observed to advance in a series of well-defined jumps. For materials exhibiting this mode of crack propagation it is possible to determine fracture energies for conditions of crack initiation and arrest. If we assume that L_1, δ_1, and F_1 are the observed values of crack length, end deflection and applied force respectively, at a stable crack arrest position, then it is found that in order to propagate the crack the applied force and hence the end-deflection must be increased to higher values of say F_2 and δ_2. In what we shall assume, for the moment, to be a perfectly rigid

machine, the crack advances then at constant end-deflection to a new, stable position at a length L_2 as the applied force falls to F_3. Values of L_1, δ_2 and F_2 at the instant of initiation can be used to evaluate an "initiation" value of fracture energy, I^{γ}; an arrest value, A^{γ}, may also be calculated from $\delta_2 L_2$ and F_3 with the aid of equations [1.33], [1.34], and [1.35].

The number of stable positions obtainable from a specimen of given length is not only dependent upon the relative magnitude of the initiation and arrest fracture energies but also as may be deduced from equations [1.33], and [1.34], on the width, b, of the cantilever arms. Although we have shown by direct experiment that the fracture energies are themselves independent of specimen size. Unfortunately there is no simple, single parameter which characterises the overall crack jumping behaviour of these materials but there are practical situations where quantitative comparisons may be made, for example, by comparing the ratio of initiation and arrest fracture energies of one material with the next, when subjected to a typical cross-head speed. This ratio of fracture energies, however, does not have a unique value for a given material for as we will see later the fracture energies of individual resins are rate sensitive and are therefore functions of the effective extension rate that is experienced by the crack tip. The initiation and arrest values of fracture energy are, in general, affected in different ways by changing the extension rate.

Table 3.1. summarizes the fracture energies of the three cured resins which have been determined at a fixed, arbitary cross-head speed of 6.3×10^{-3} mm s^{-1}.

Cured CT200 has the largest fracture energy ratio. In this material the crack advances from one stable position to the next in a violent manner; during propagation it is impossible to follow the crack front visually. The other two systems, cured LY558 and cured EPON 828, behave in a less violent manner, as reflected by the lower fracture energy ratios; in these materials the crack front advances at about 10 mm s^{-1}.

TABLE 3.1.

The Fracture Energies of the Three Resin Systems

Material	${}_I\gamma/10^2 Jm^{-2}$	${}_A\gamma/10^2 Jm^{-2}$	$\frac{{}_I\gamma}{{}_A\gamma}$
CT200/HT901	1.2	0.75	1.60
LY558/HT973	0.33	0.28	1.18
EPON828/NMA/DBMA	0.58	0.53	1.09

3.3. The Role of Effective Crack Tip Extension Rate

It was observed during early experiments with a simple, hand-cranked testing machine that the crack in our double cantilever specimens could be made to propagate without jumping provided that the cross-head was displaced at a sufficiently high rate. In addition, it was found that it became increasingly more difficult to propagate the crack in this non-jumping manner as the crack length increased. The above observations led us to suspect that the fracture energies of these materials were rate sensitive since if a specimen is fractured at a constant cross-head speed then the actual extension rate experienced by the crack tip decreases as the crack length increases.

We will now define an effective crack-tip extension rate $E^{\bullet}_{\epsilon}$ as:-

$$E^{\bullet}_{\epsilon} = \frac{\text{applied cross-head speed}}{(\text{crack length})^2}$$

If a specimen having rate sensitive fracture energies is fractured at a constant applied cross-head speed, then the observed fracture energies will be functions of crack length since both ${}_I\gamma$ and ${}_A\gamma$ are functions of $E^{\bullet}_{\epsilon}$. It may be recalled that it was proposed to use a graphical method, with axes based on the Srawley and Gross factors, for the

estimation of fracture energy from our experimental data. Unfortunately this technique is inappropriate for the base matrices for linear plots are obtained with large negative intercepts on the ordinate: an example for cured CT200 fractured at a cross-head speed of 6.3×10^{-3} mm s^{-1} has already been shown in Fig. (2.4). In such instances point fracture energies were calculated, with the aid of equations [1.33], [1.34], and [1.35] at the beginning and end of each crack jump. We will see later, however, that the graphical technique may be used for the more heavily filled materials, where the fracture energies are essentially independent of effective crack-tip extension rate and therefore of crack length.

Some additional experiments were undertaken to test the hypothesis that the effects described above were due to variations in fracture energy with effective extension rate and not to a geometrical effect or to a systematic error that may have been overlooked. Three cross-head speeds were chosen which would give some overlap of effective extension rates in specimens tested at different applied rates. The speeds chosen were:-

$$1.5 \times 10^{-2} \text{ mm s}^{-1}$$
$$6.3 \times 10^{-3} \text{ mm s}^{-1}$$
$$1.5 \times 10^{-3} \text{ mm s}^{-1}$$

and, for example, a specimen fractured at a cross-head speed of 6.3×10^{-3} mm s^{-1} and having a crack length of 200 mm will have the same effective rate as another fractured at 1.5×10^{-3} mm s^{-1} and having a crack length of 96 mm.

By using these three applied cross-head speeds the point values of fracture energy calculated from equation [1.35] and presented in Figs. (3.1), (3,2) and (3.3) were obtained for the three resin systems. The excellent overlap of fracture energies

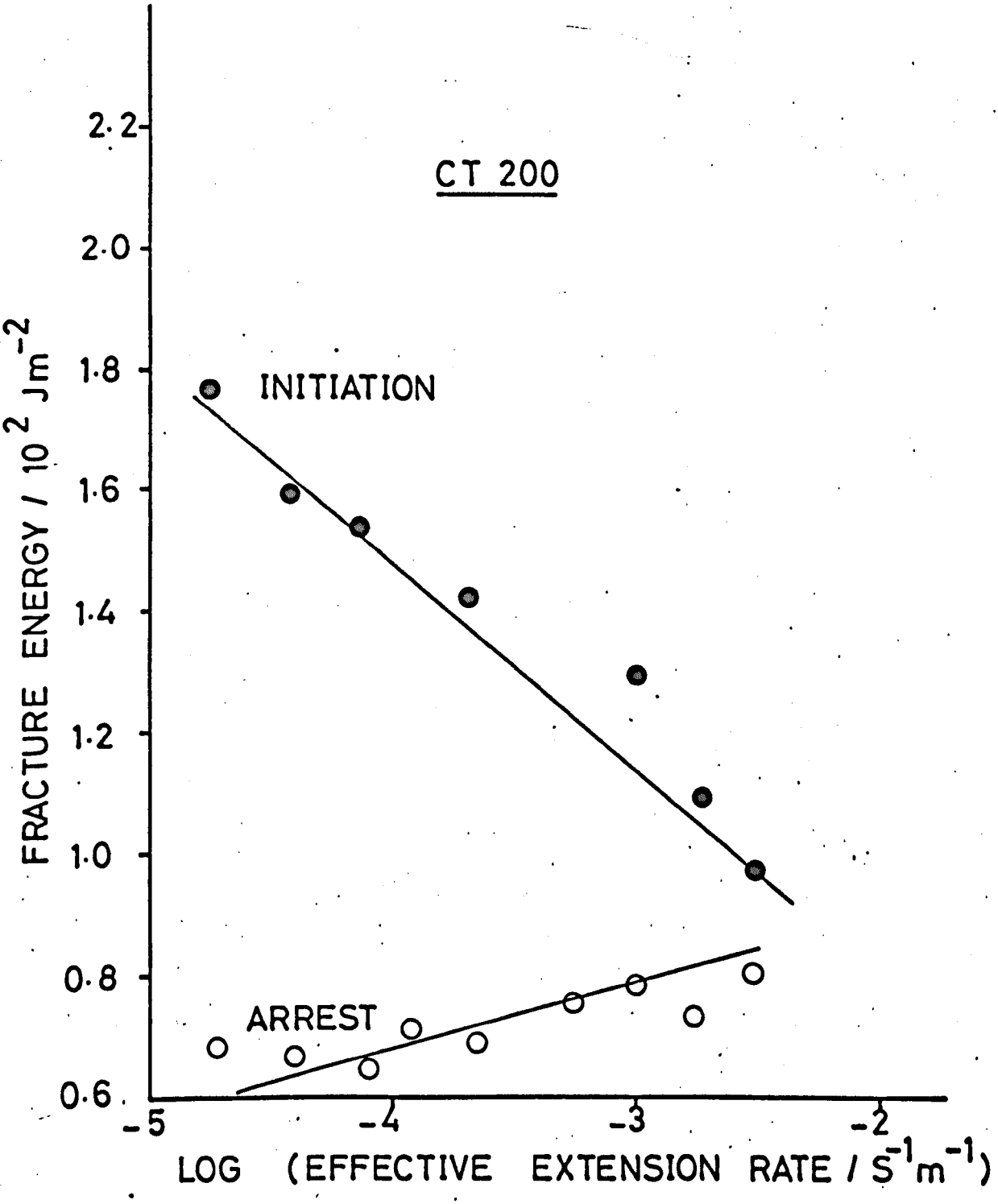

Fig. (3.1) The fracture energies of CT200/HT901 as a function of effective extension rate.

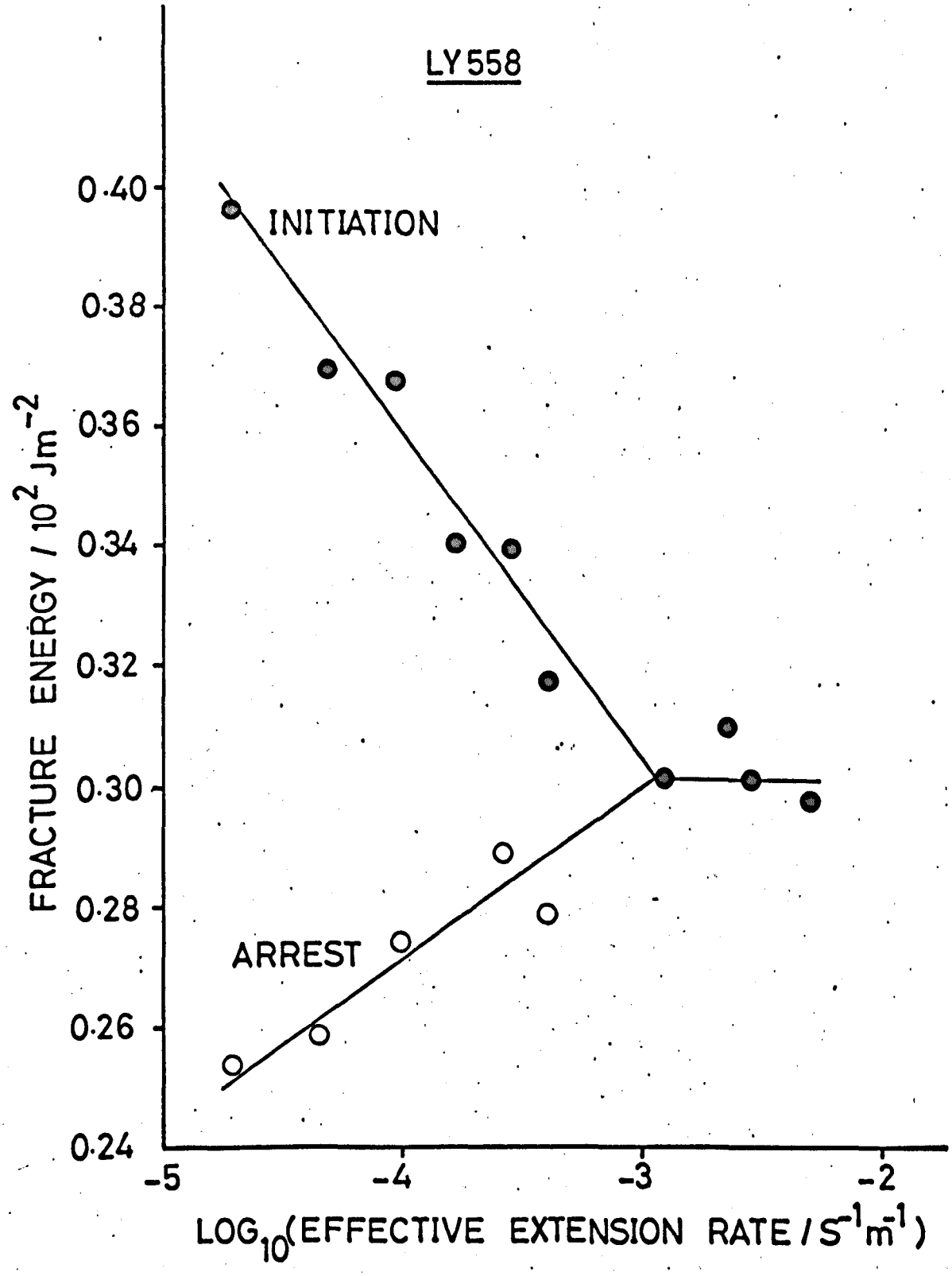

Fig. (3.2) The fracture energies of LY558/HT973 as a function of effective extension rate

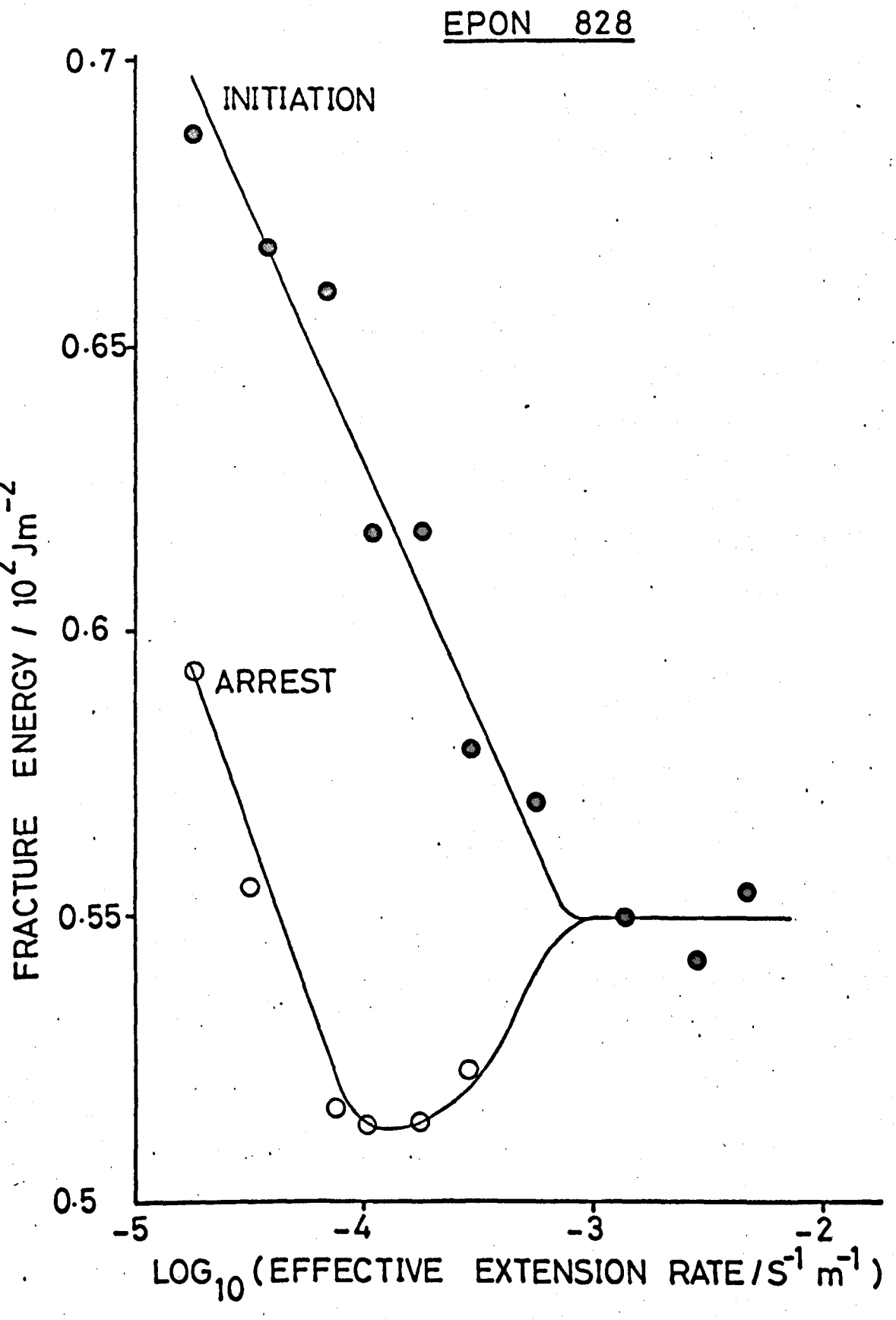

Fig. (3.3) The fracture energies of EPON828/NMA/BDMA as a function of effective extension rate

estimated at effective rates derived from different applied rates suggests that the variation in fracture energy is a real phenomenon.

3.4. The Effect of Temperature and Environment on Fracture Energy

A series of experiments were carried out to explore the influence of temperature and environment on the fracture energies of the three epoxy resin systems. The effect of temperature and environment has obvious practical significance but as we shall see later the data presented in this chapter will also enable us to make some inferences about the physical processes involved during crack propagation in these materials.

The environments chosen for preliminary investigation were:-

(i) Moist laboratory air, approximately 10g of $H_2O\,Kg^{-1}$ of air

(ii) Silicone oil (MS 550) dried over freshly prepared sodium wire

(iii) Water

A detailed study was conducted in the temperature range 263K to 393K.

3.4.1. Experimental Procedure

To allow temperature and environmental studies to be performed, an environment and temperature enclosure and some temperature control and stirring apparatus was added to the basic testing machine. The enclosure was constructed from a tall, 1½ litre, glass bottle with the top sawn off. In an attempt to reduce the temperature gradient over the height of the necessarily rather tall jar, heating elements were wound on glass formers, with the wire spacing such as to provide the greatest heat input at the bottom of the vessel. Temperature sensing was achieved with a copper/

constantin thermocouple and the heating element driven via a Eurotherm controller. Even with the graduated spacing of the heater windings some difficulty was encountered in obtaining a uniform temperature distribution over the height of the enclosure. Various stirring methods were investigated and it was found that the best results were obtained by vigorously bubbling dry nitrogen through the liquid environments, or blowing preheated laboratory air through the container during experimental runs requiring the use of moist air.

Specimens were precracked as before in the simple, hand-operated machine and allowed to soak, in an unloaded state, in the chosen environment, and at the required temperature, for one hour prior to use. Tests were performed as before and the data obtained is presented in Figs. (3.4), (3.5) and (3.6). Some cured CT200 specimens were stressed to 90% of the calculated load required to initiate propagation from a crack of known length and were soaked, under load, in specific environments, for a known time and temperature. The specimens were then returned to room temperature but maintained in the original environment and the critical load required to initiate propagation from the aged crack determined. The results are presented in Table 3.2. along with some comparative data from specimens fractured at the test temperature.

3.5. Survey of Results

Figs. (3.1), (3.2) and (3.3) indicate that the fracture energies of all three epoxy resin systems as estimated using double cantilever beam specimens are sensitive to the actual cross-head extension rate experienced at the crack tip. Cured CT200 and LY558 exhibit broadly similar dependencies of fracture energy on effective rate over the range investigated. Although larger fractional changes are observed in both

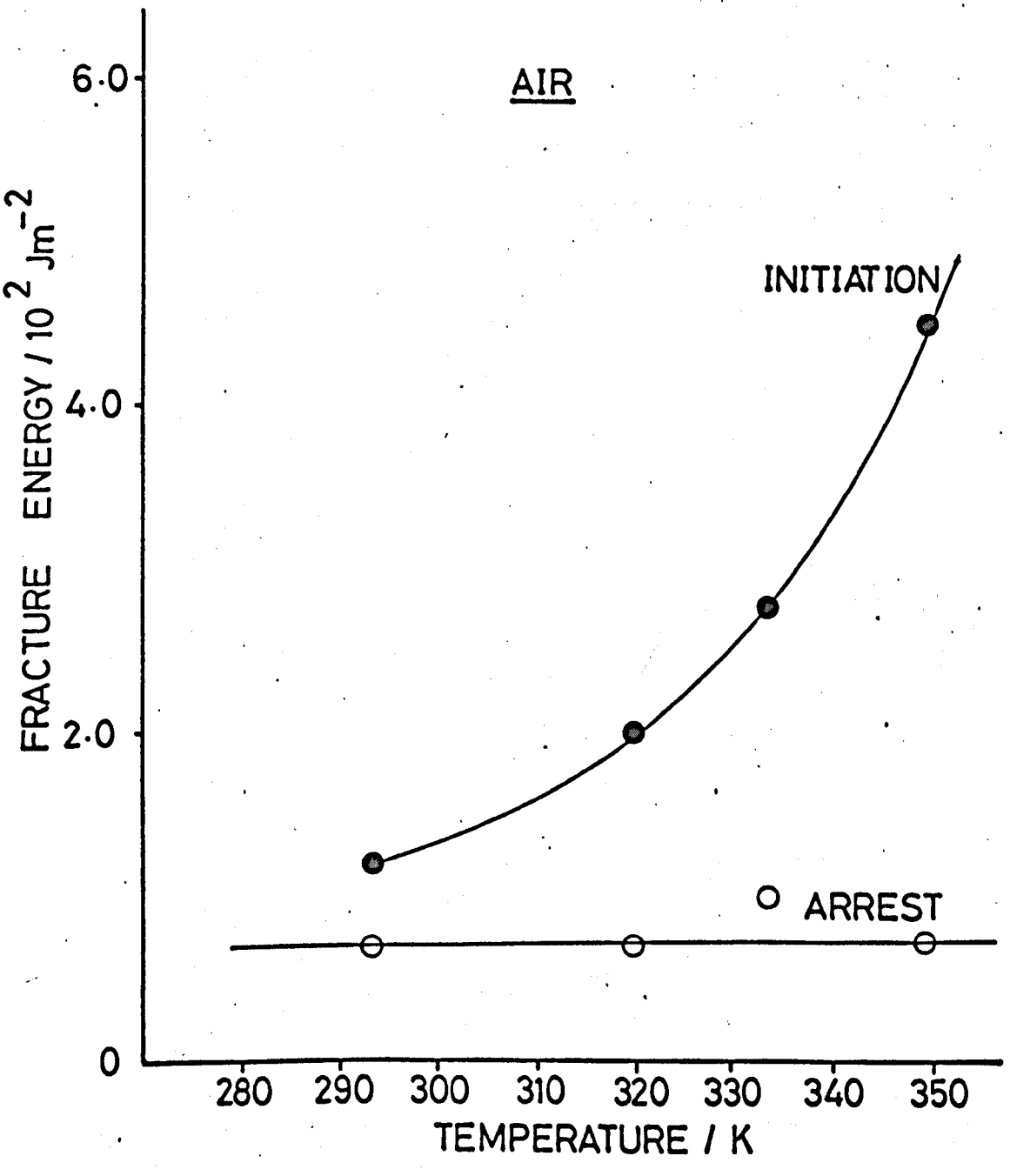

Fig. (3.4) The fracture energies of CT200/HT901 in air as a function of temperature

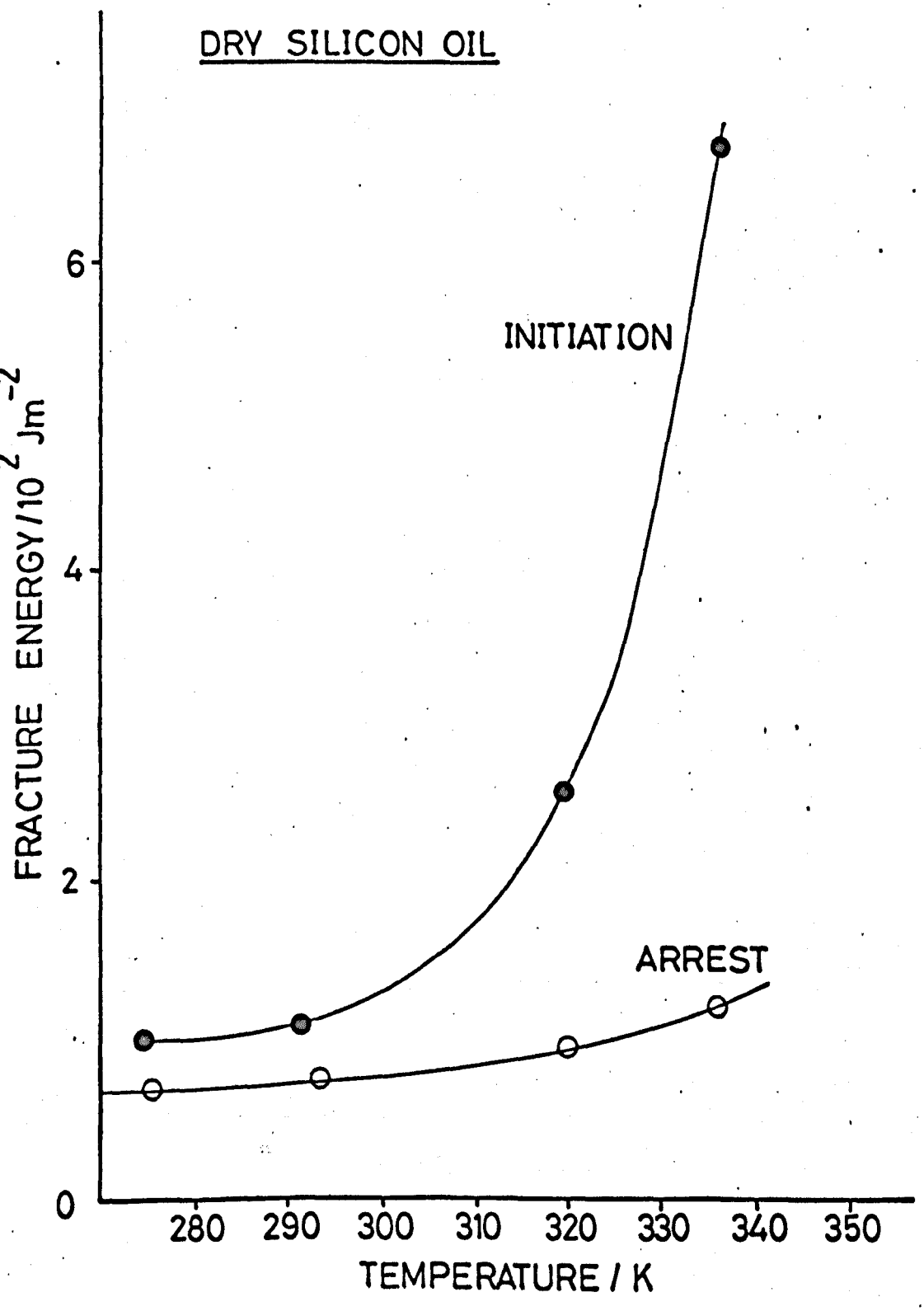

Fig. (3.5) The fracture energies of CT200/HT901 in dry silicone oil as a function of temperature

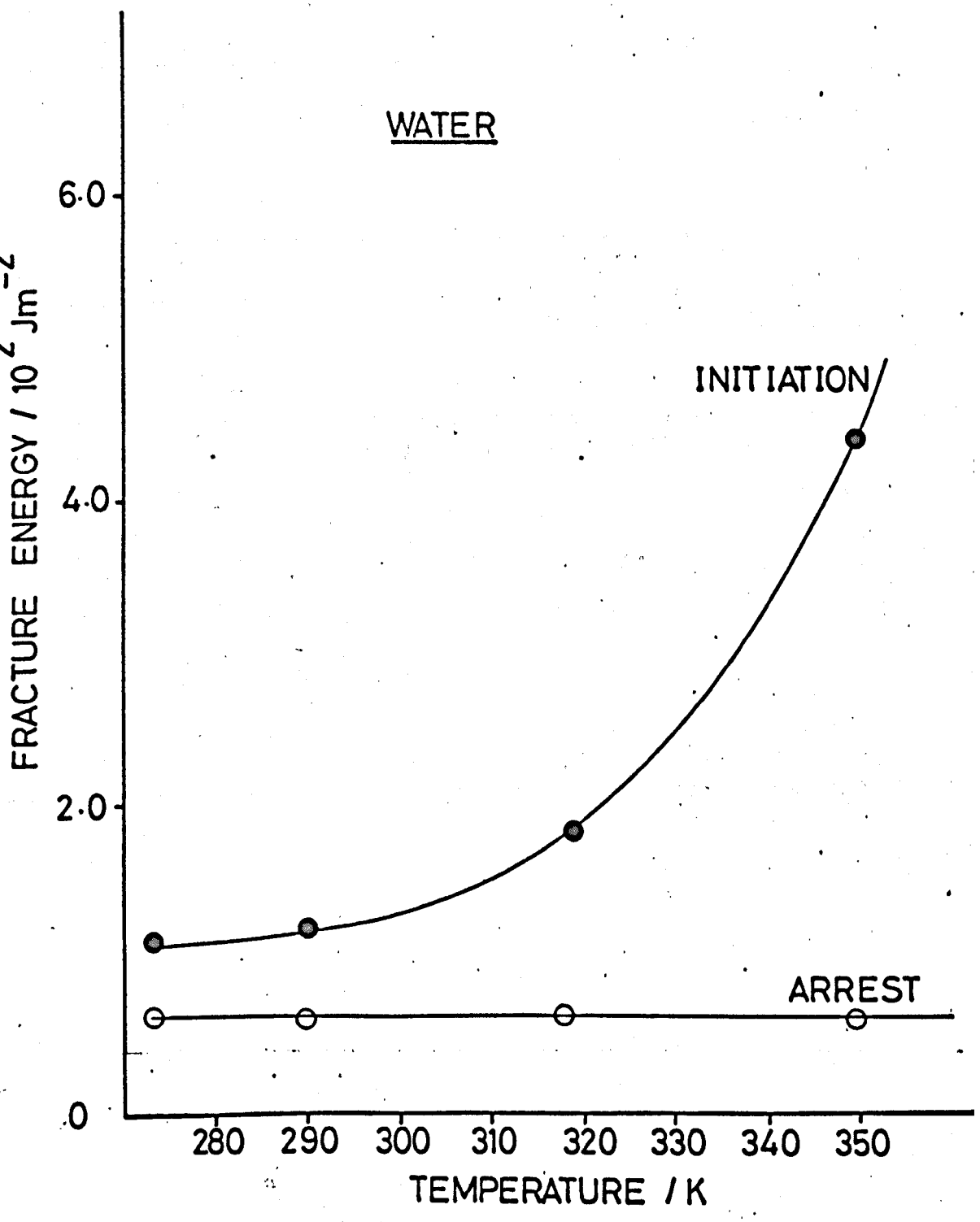

Fig. (3.6) The fracture energies of CT200/HT901 in water as a function of temperature

TABLE 3.2.

Comparative Fracture Energy Data for Specimens Tested at the Soaking Temperature and Room Temperature

Tested at Soaking Temperature		Tested at Room Temperature	
Fracture Energy/10^2 Jm^{-2}		Fracture Energy/10^2 Jm^{-2}	
I^{γ}	A^{γ}	I^{γ}	A^{γ}
Water 350K		Water 350K	
4.40	0.70	4.38	0.70
Silicone Oil 335K		Silicone Oil 335K	
6.68	1.20	6.57	1.20
Air 350K		Air 350K	
4.42	0.70	4.45	0.68

I^{γ} and A^{γ} for cured CT200, the initiation fracture energy decreases whilst the arrest fracture energy increases with increasing effective extension rate until a common fracture energy is reached, where the crack is observed to propagate without jumping. Cured Epon 828 behaves in a somewhat different manner: both the initiation and the arrest fracture energies initially decrease with increasing effective extension rate but this is followed by a rapid increase in the arrest value to produce again a common fracture energy.

Figs. (3.4), (3.5) and (3.6) reveal that a large increase in the fracture energy for crack initiation of cured CT200 occurs at about 340K; this is some 30K to 40K below the glass transition temperature of the material, Careful microscopic examination of the region close to the crack tip, in a specimen that had been loaded for one hour at 350K, revealed what appeared to be extensive "crazing".

Crazing is a common feature in glassy thermoplastics such as polystyrene, PMMA, polycarbonate, polystyrene, etc. and the phenomenon has been extensively studied by KAMBOUR (1965), HULL (1970), HAYWOOD (1972) and many others. It has been established that crazes are local regions of very high strain and at low optical magnifications they appear to be flat, almost crack-like defects which are formed in time perpendicular to the local principal stress when this exceeds a critical value. They are however load-bearing and, in the above thermoplastic materials, consist of thin strips of oriented polymer material containing a high proportion of very small voids (KAMBOUR and HOLIK (1969)) and as a consequence have a significantly different refractive index from the normal material. It is this difference in refractive index within the craze which gives it the appearance of a crack. In linear polymers crazes form, provided the stress is sufficiently high, perpendicular to the local principal tensile stress and this results in the production of a characteristic pattern of crazes

around a crack tip, especially when this has been, for some time, under a load less than that required to cause rapid crack extension.

The micrograph in Fig. (3.7) shows the crazes near the crack tip in a small rectangular specimen of polystyrene containing an edge-crack which was loaded by driving a small wedge into the end of the crack. The details of the craze pattern vary with load history and with the geometry of the crack tip profile. Fig. (3.8) shows the features observed near the crack tip in a similar specimen of a fully cured CT200 in which the edge crack was loaded by wedging after the specimen had been immersed in water at ~ 350K for about 10 minutes.

It is the striking similarity in the appearance of Fig. (3.7) for polystyrene, and Figs. (3.8.) and (3.9) for cured CT200 that makes it tempting to interpret the "lines" appearing round the loaded crack tip in the epoxy at 350K as crazes, Patterns of features similar to that shown in Figs. (3.8) and (3.9) appeared around loaded crack tips within a few minutes at 340 ÷ 350K for all three resins when immersed in air, water or in silicone oil (MS 550). Similar features have been detected near the crack tips in specimens of CT200/HT901 and EPON828/NMA/BDMA loaded for much longer times, (100 hours), at room temperature in air. The distribution of individual features formed at the lower temperature is much less intense so that, in isolation, the similarity between the features formed at room temperature and crazing in thermoplastics is much less striking.

If some form of crazing can occur in the cured polymer, then it should be possible to produce it other than around a crack tip. We have in fact established that craze-like flaws are produced on the tensile surface of a rectangular beam of CT200/HT901 which was loaded in bending at 350K in an air oven. Fig. (3.10) shows some of the crazes which have grown perpendicular to the tensile stress and it was

Fig. (3.7) Crazes around a crack tip in polystyrene

(magnification x 100)

Fig. (3.8) "Crazes" around a crack tip in cured CT200/HT901

(magnification x 800)

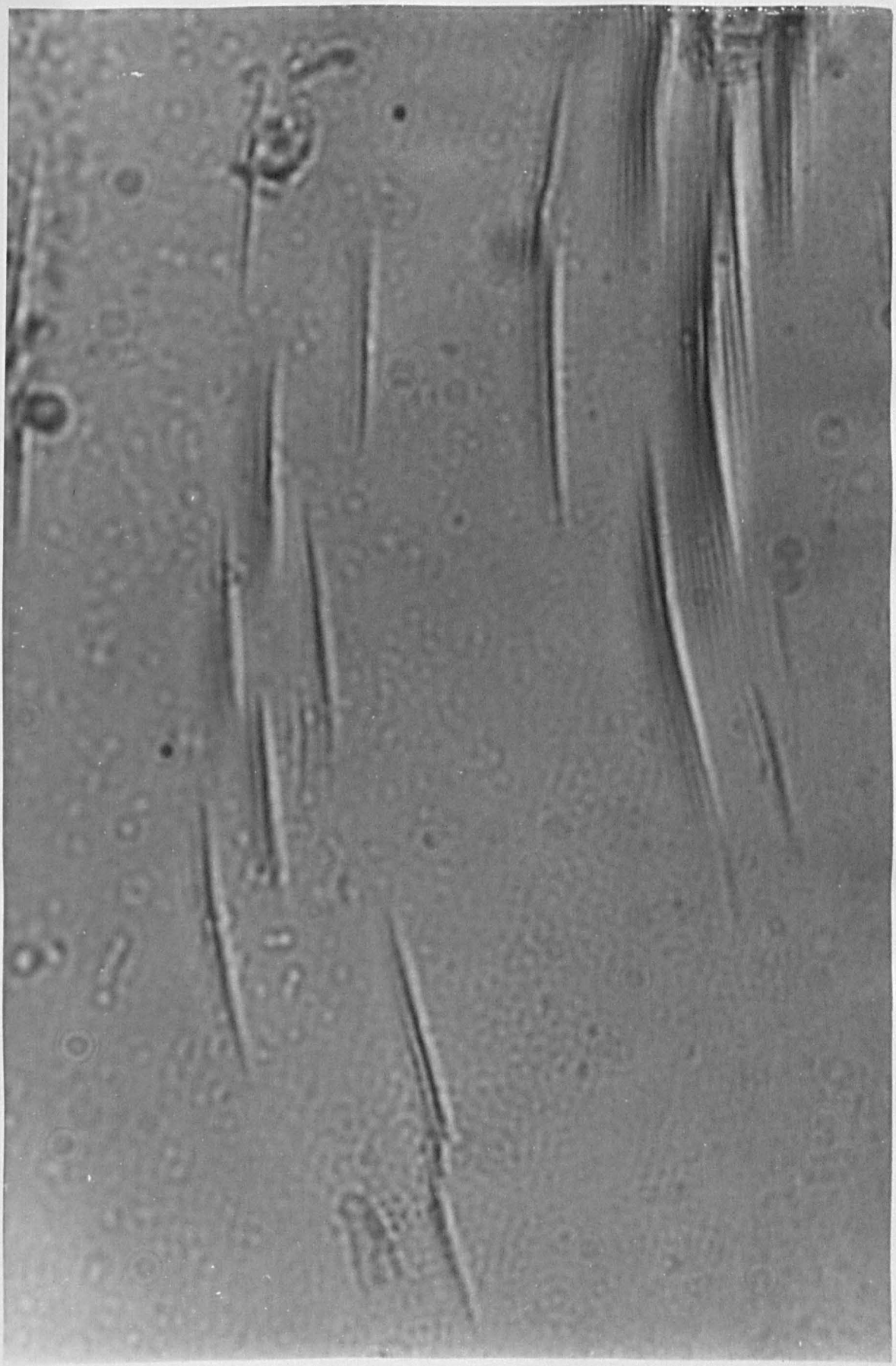

Fig. (3.9) "Crazes" ahead of a crack tip in cured CT200/HT901 (magnification x 2000)

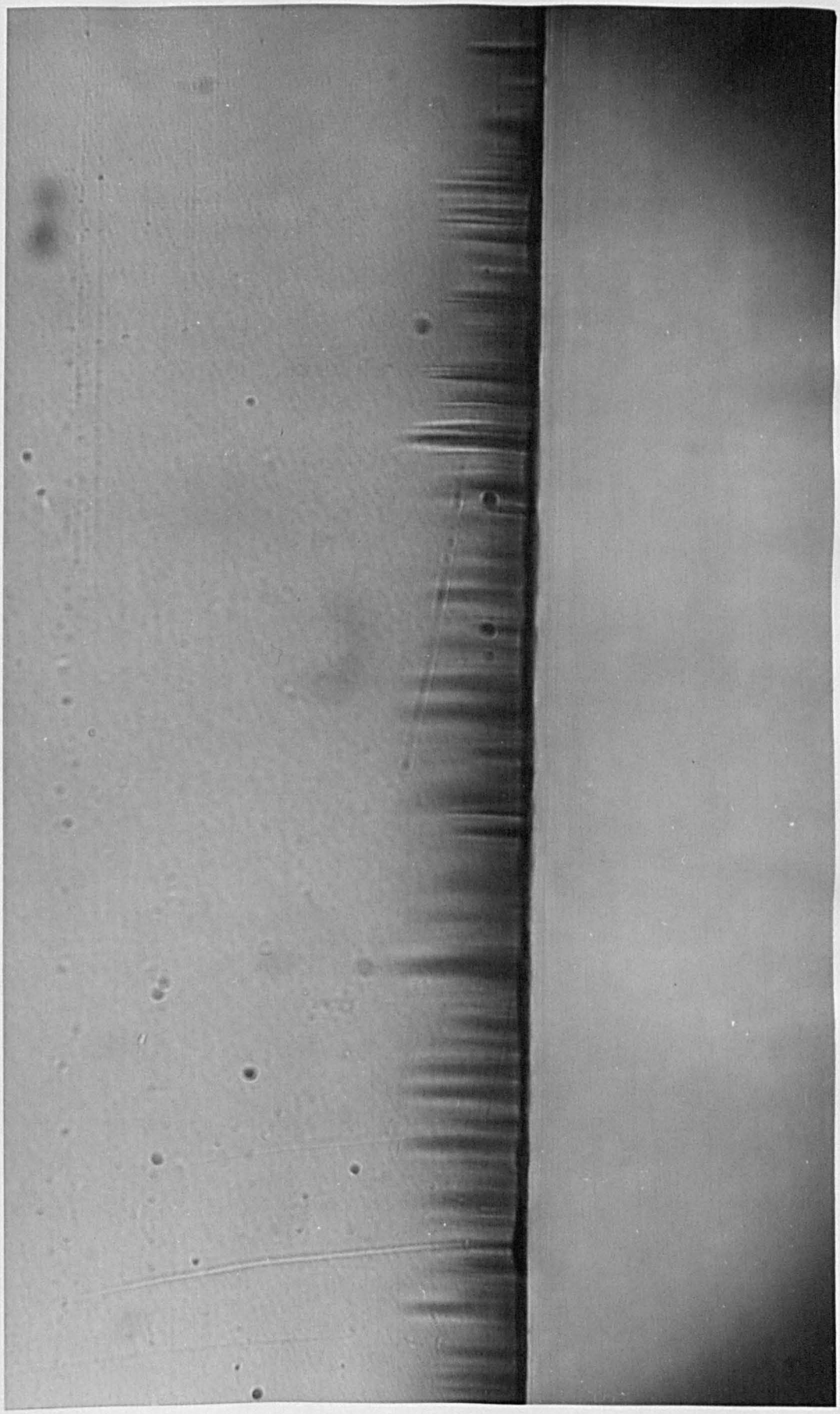

Fig. (3.10) "Crazes" normal to the tensile surface of a simple cantilever beam of cured CT200/HT901

(magnification x 400)

particularly interesting to note the existence of pairs of these flaws, which, although separated by a very small distance, appeared to have grown without interacting with one another.

All the craze-like features observed, whether near crack tips or on cantilever specimens, grew perpendicular to the local principal stress. Detailed examination of Fig. (3.10) suggests that there is little interaction between adjacent but closely spaced features and hence they appear to be load bearing. Thus these features appear to satisfy the qualitative phenomenological criteria for crazes.

Most of the crazing described so far was observed in, or very close to, the outer surface layers of the resin specimens which were in contact with the mould surface and/or were exposed to the atmosphere during post-curing. Thus it is a priori possible that the material in these layers is depleted of hardener and therefore not fully cross-linked. Although it has been observed that much longer, more pronounced crazes occur in cured CT200/HT901 resins which contain only one half the stoichiometric proportion of anhydride hardener (15 instead of 30 parts of HT901 to 100 parts of CT200), it is believed that crazing does occur in the normal, fully cured resins. Crazes have been detected in the central part of the upper, tensile surface of beams loaded as simple cantilevers at 340K, even though that surface had been formed by fracturing after the original specimen had been given the normal post-curing heat treatment. Moreover, microscope examination of the fracture surfaces of double cantilever beam specimens of both CT200/HT901 and EPON828/NMA/BDMA, used to determine fracture toughness of these materials at room temperature, reveals similar craze-like features over the whole width of the specimen; these are particularly dense near crack arrest positions, (see Fig. (3.11)). Corresponding features were found in equivalent positions on the matching fracture surfaces and they are believed to be small crazes

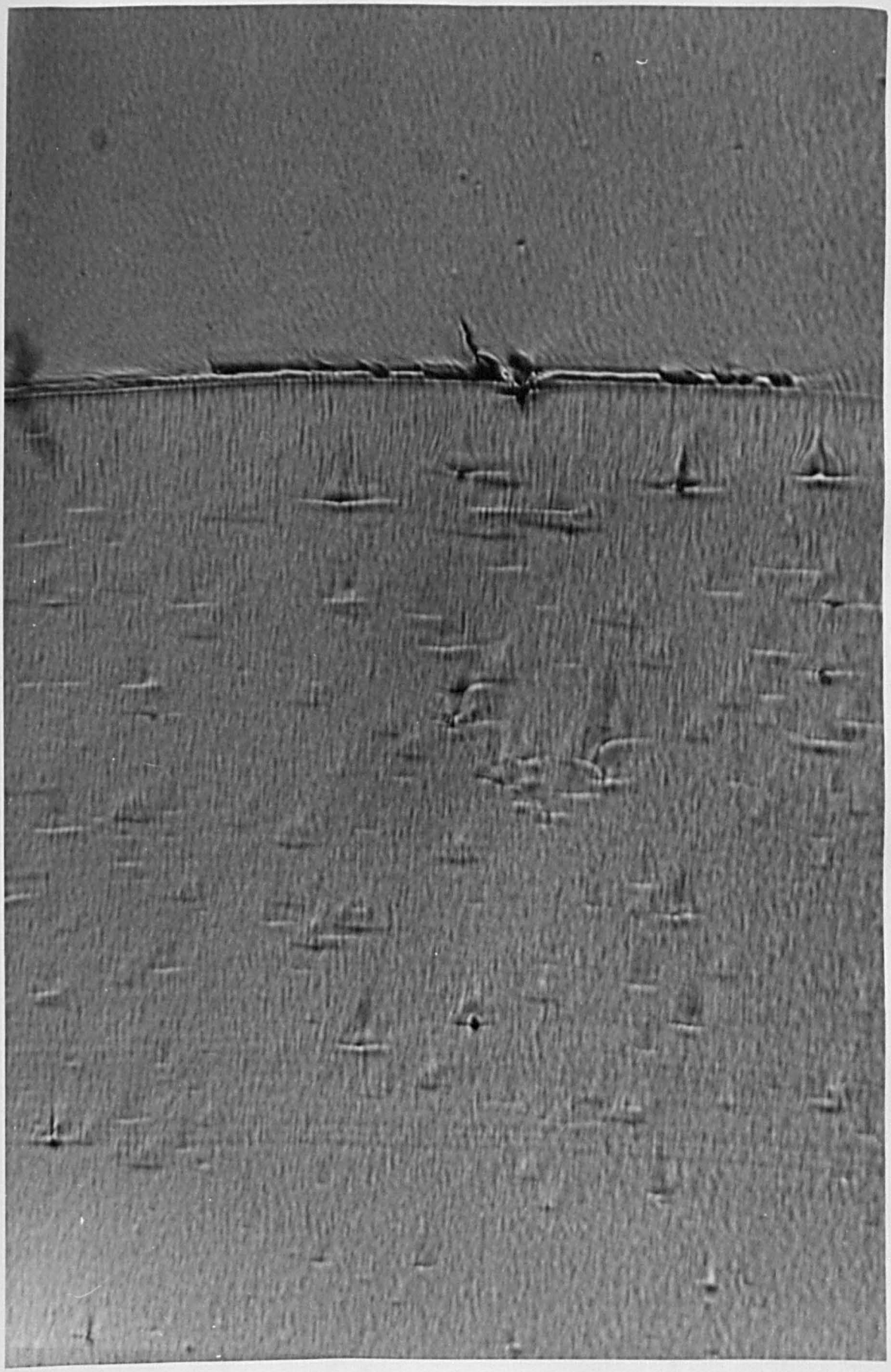

Fig. (3.11) Region close to a crack arrest position in cured CT200/HT901 (magnification x 400)

formed oblique to the fracture plane. HULL (1970) has reported the formation of crazes at an angle to the fracture surfaces of polystyrene, and these produced features on the fracture surface which are remarkably similar to those illustrated in Fig. (3.11). We could not detect any features of this kind on fracture surfaces of LY558/HT973. However, Fig. (3.12) shows that the cleavage fracture surfaces of this material have quite pronounced striations roughly parallel to the direction of crack propagation and these would make it more difficult to detect the lateral marks corresponding to oblique crazes. On the other hand, our few simple tests failed to reveal, unambiguously, any crazes around crack tips at room temperature in this resin, and it might be that crazing occurs in LY558 only at elevated temperatures.

The evidence outlined here strongly suggests that crazes, i.e. localised, planar regions of intense plastic strain, can occur in these highly cross-linked network polymers. If this is the case, although the structure of the craze material is still problematic , it seems likely that an intimate connection exists between the growth of crazes and fracture similar to that now well established for glassy thermoplastics. (See e.g. KAMBOUR (1965), HULL (1970), HAWARD (1972).)

It is believed that the above observations provide the most direct evidence, presently available, that crazes can form in thermosetting epoxy resins. However, it must be admitted that this evidence is still somewhat circumstantial.

A further important aspect of the behaviour of cured CT200 at elevated temperatures is also shown in Figs. (3.4), (3.5) and (3.6). It is that the initiation fracture energy increases while the arrest fracture energy either remains essentially constant, or increases only slightly, as the temperature is raised above room temperature. This observation is in direct contradiction to the preliminary results of Griffiths that led him to postulate that the crack jumping behaviour in these epoxy resins could be

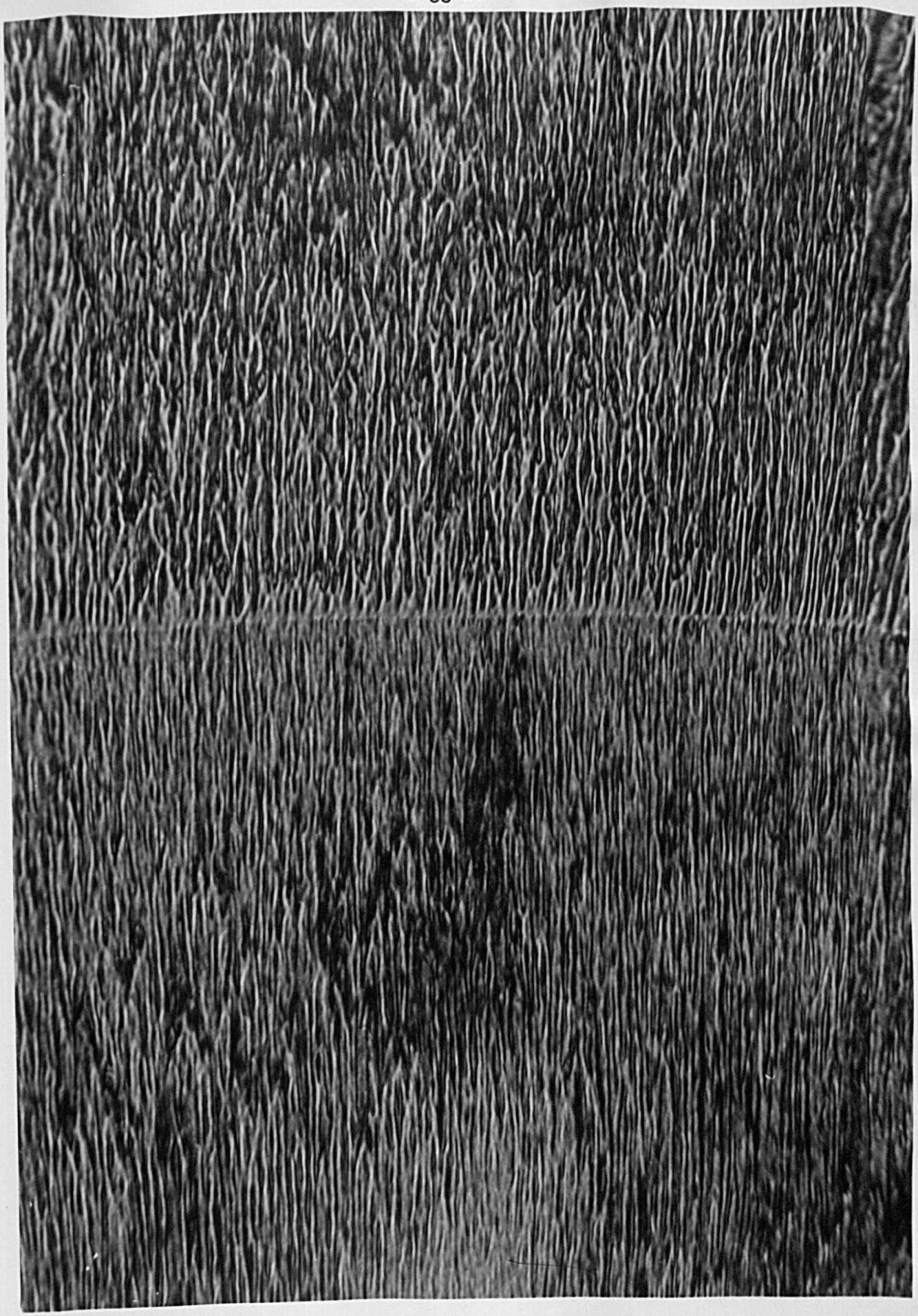

Fig. (3.12) Region close to a crack arrest position in cured LY558/HT973

(magnification x 400)

attributed to adiabatic heating effects at the crack tip, Griffiths' hypothesis, in the light of the results presented here, will be discussed elsewhere in this chapter and in some detail in the final chapter. Comparison of Figs. (3.4), (3.5) and (3.6) shows that both the initiation and arrest fracture energies are higher in a water-free environment. Table (2.2.) will reveal also that both the initiation and arrest fracture energies of specimens soaked at an elevated temperature, in a chosen environment, in a cracked and stressed state, and then tested at room temperature are essentially the same as the values that would have been obtained if the specimens had been fractured at the soaking temperature. This, therefore, implies that the processes which occurred at the crack tip, at the elevated temperature, were not reversed by unloading and cooling to room temperature.

3.6. Preliminary Discussions

Ultimately, the crack propagation behaviour of materials is related to their internal structure, and probably to their microstructure, however, for epoxy resins as for the majority of amorphous materials, knowledge of the structural arrangements at an appropriate level is not available. In the case of the epoxy resins even the chemistry of the cure mechanisms is still rather uncertain. One may, however, sympathise with the organic chemist since he is faced with following an extremely complex reaction and analysing a final product that has a high degree of chemical, and physical stability: it is these very properties that have led, in part, to the epoxy resins finding such wide-ranging use. In view of the complexity of the reaction involved during curing, it is perhaps plausible to expect that epoxy resins will have a microstructure consisting of adjacent regions of high and low cross-link density. This is certainly not inconsistent with the results of simple etching experiments performed in

these laboratories by the author and B.R. McQuillin; both chromic acid and argon ion bombardment in a radio frequency glow discharge consistently reveal the type of structure shown in Figs. (3.13) and (3.14). However, it is considered that the "scale" of this structure is too small to allow any simple correlations to be made with, for example, the size of the crack tip plastic zone.

In the absence of any detailed information on either structure or the processes of inelastic deformation which lead to the blunting of the crack tip, we can attempt only a rather naive phenomenological explanation of the processes occurring during crack propagation in these materials. Although we shall return to this problem in more detail in the final chapter, it may be useful, briefly, to discuss the possibility of such interpretations of the fracture behaviour of unfilled resins, before we meet the additional complications apparent when fillers are added.

One of the most striking features of the cured epoxy resins being considered here, is the jumping mode of crack propagation which obtains during the fracture of a double cantilever beam specimen, as distinct from the more familiar continuous propagation that occurs in many of the other, macroscopically brittle, materials such as the inorganic glasses, PMMA and PVC. Notwithstanding these striking differences in the mode of crack propagation all these materials have fracture energies that are much greater than their respective surface free energies. Irwin first showed that for an ideal elastic-plastic material:-

$$\gamma = \tfrac{1}{2} \sigma_y \alpha \qquad [3.1]$$

where: γ = fracture energy

σ_y = uniaxial flow stress

α = plastic zone extension

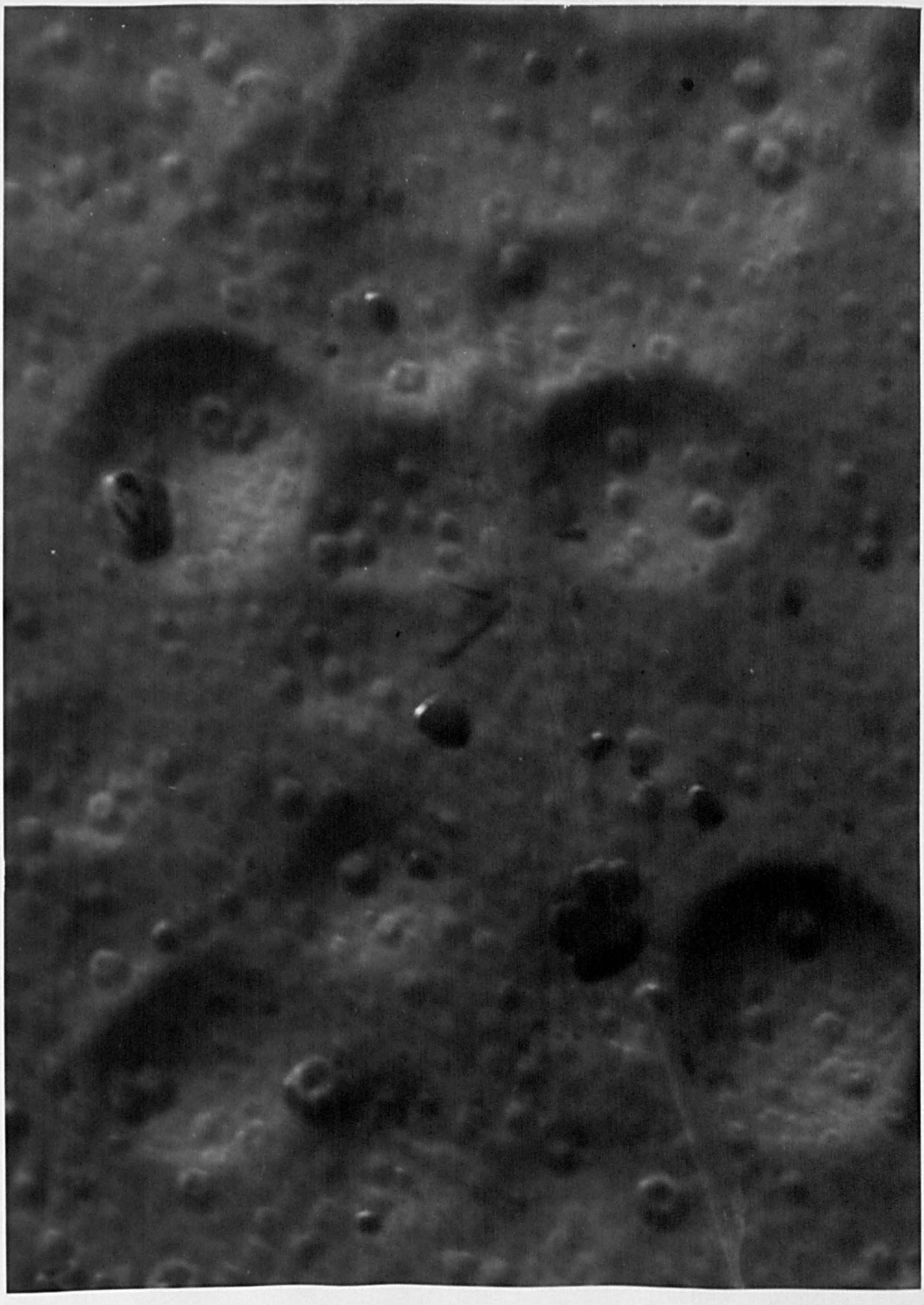

Fig. (3.13) The fracture surface of CT200/HT901 having been etched in chromic acid (magnification x 40,000)

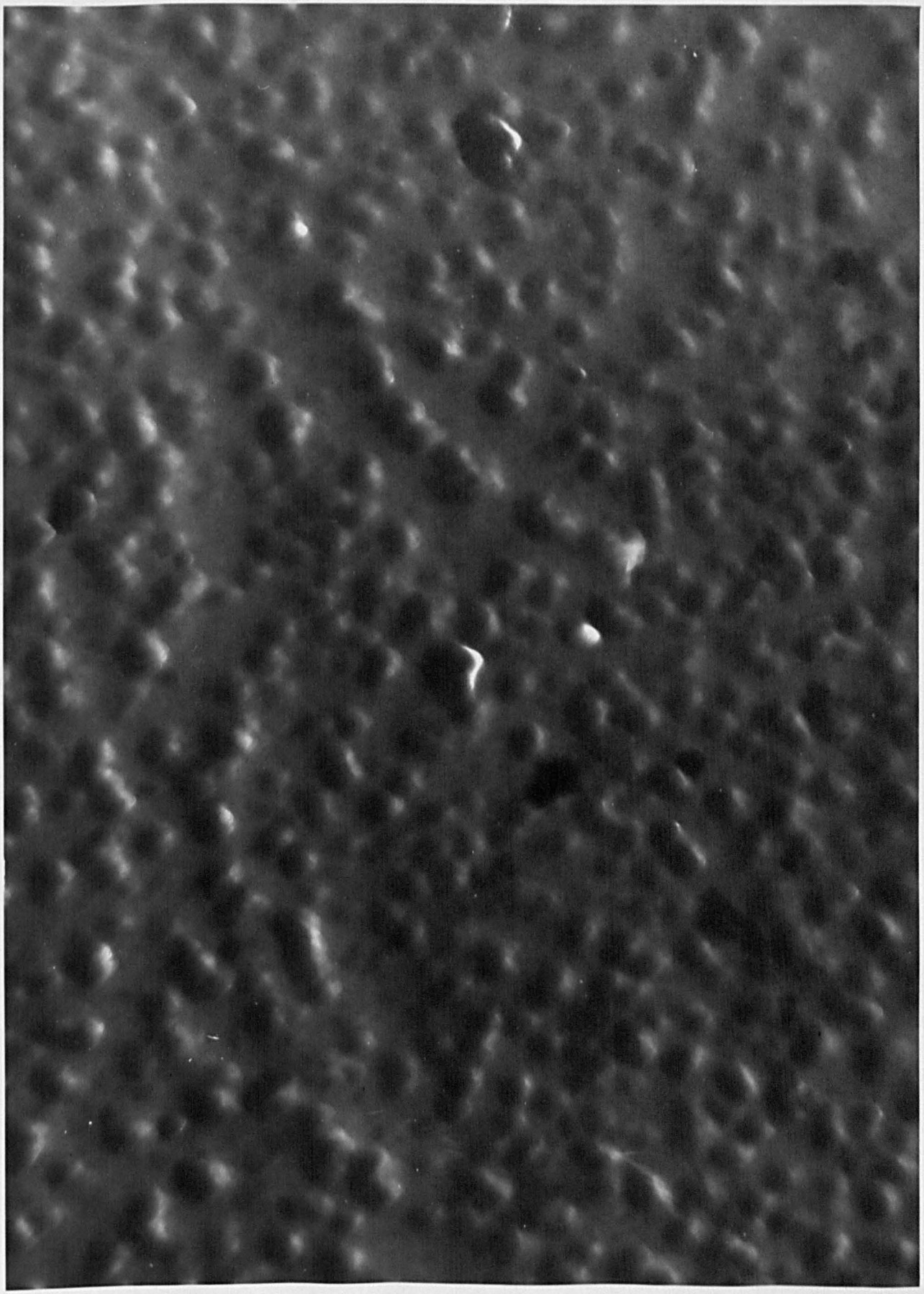

Fig. (3.14) The surface of CT200/HT901 having been etched by argon ion bombardment in a radio-frequency glow discharge (magnification x 40,000)

Microscopic examination of crack tips in our matrix materials showed a measurable difference between the extension of the plastic zone just prior to crack initiation and immediately after arrest, i.e. before the applied load or opening displacement were again increased. This observation suggested that some information on the flow stress and the plastic zone extension might be helpful in constructing a phenomenological model. Experiments to determine both these parameters will be discussed at a later stage but in the meantime it may be appropriate to review Griffiths' adiabative heating hypothesis which was offered as an explanation for the jumping mode of crack propagation.

Griffiths postulated that crack jumping was the result of the behaviour of the material near the crack tip under the influence of adiabatic heating, which is a consequence of the heat liberated during plastic deformation being unable to diffuse away completely as the crack propagates. Preliminary work had indicated that the fracture energies fell as the temperature was raised above ambient. He therefore argued that when the applied extension rate was low any extension of a plastic zone at the tip of a stationary crack would occur under essentially isothermal conditions. In addition WILLIAMS (1965) has shown that adiabatic heating during crack propagation may lead to quite high crack tip temperatures and therefore if the fracture energy falls as the temperature increases, excess energy will be available for further propagation. Thus propagation will occur until the crack tip temperature falls again and raises the fracture energy; the crack may therefore be expected to advance in a series of jumps. The more extensive data presented here does not confirm the few results obtained by Griffiths and fails to support his hypothesis: the fracture energy does not decrease with increasing temperature and hence Griffiths' hypothesis appears to be inapplicable.

Finally, the preliminary results presented here highlight the problem of which

values of fracture energy should be used for the comparison of different epoxy resin-based materials, since the fracture energies are functions of the effective extension rate experienced by a crack tip. It is clear from the complex behaviour that there is no single parameter which can be used to compare all aspects of the crack propagation behaviour of these materials. However, from a practical or design point of view the minimum arrest value of fracture energy has important practical significance. There are also three sets of fracture energies which may be used when seeking to compare the effects of various fillers.

(i) The fracture energy at a very low effective extension rate where variations over the length of a specimen are negligible.

(ii) The fracture energy at an effective extension rate where the initiation and arrest values are equal and hence the crack propagates continuously.

(iii) The fracture energy at an arbitrary effective extension rate.

Methods (i) and (ii) although perhaps of more fundamental importance than (iii) are difficult values to obtain in practice since in the first case the applied extension rates are so low as to render the collection of data an extremely lengthy and tedious process. A value for (ii) is readily obtainable for the three unfilled epoxy resin systems but this proved to be impossible for the more heavily filled materials since, with the apparatus available, a continuously propagating crack could not be produced. The compromise method (iii) is employed throughout this work. The fracture energies for the various materials are all determined in effect for a similar, but arbitrary effective extension rate, i.e. for a given cross-head speed of 6.3×10^{-3} mm s^{-1} and a crack length of 150 mm. It will be shown later that the fracture energies of the heavily filled

composites are essentially independent of effective extension rate over the range investigated and in these cases the fracture energy values quoted, in subsequent chapters, are mean figures over the length of a specimen fractured at an applied extension rate of: 6.3×10^{-3} mm s^{-1}.

3.7. Summary

We have discussed some of the more important behavioural features of the three base matrix materials: firstly, under our test conditions a crack does not propagate continuously but in a series of discrete jumps; secondly the estimated fracture energies are functions of the actual extension rate experienced at the crack tip. In addition it is apparent that the inelastic processes occurring at a crack tip may be augmented by the formation of craze-like defects. The fracture energies of these materials increase or at least remain constant as the temperature is raised above room temperature which suggests that Griffiths' adiabatic heating hypothesis may not give an appropriate account of the jumping mode of crack propagation.

CHAPTER IV

The Effect of Fillers on the Fracture Toughness of Epoxy Resins

4.1. Introduction

We shall examine here the effect of a variety of particulate fillers on the fracture toughness of an epoxy resin: originally this was the main aim of the experimental programme. The choice of fillers was dictated by the availability of materials in suitable small sizes and as a result the main body of the data presented here will be concerned with glass and aluminium particles. These were readily available in a range of shapes and sizes and permitted various surface treatments to be used which it was hoped would enable us to modify the adhesion between the matrix and the filler. Glass was chosen to represent a filler type more "brittle" than the matrix and aluminium to represent one more "ductile".

Some additional experiments were performed using mineral fillers; the most interesting of these was talc which produced a large increase in fracture energy. This chapter will be confined to describing the experiments performed and the results obtained; the main discussion will be held over until the final chapter.

4.2. Experimental

The experiments were centred on the matrix, CT200/HT901 as it was found to be relatively simple to control the preparation and cure conditions such that composites

having consistent fracture properties were produced. It was considered that spherical glass beads (ballotini), roughly equi-axed glass frit, and short chopped glass fibres would provide a useful range of filler shapes. The ballotini was purchased from R.W. Jennings Limited, the frit prepared by wet milling crushed Float Glass (Pilkington Brothers Limited) and the chopped glass fibres, of length 5 mm and 10 μm diameter were purchased from CIBA-Geigy Limited. The frit and ballotini were mechanically sieved to render the following particle size fractions:-

25	to	50 μm
50	to	75 μm
75	to	105 μm
105	to	150 μm
150	to	300 μm

A typical particle size distribution for the 75 to 105 μ m fraction is given in Fig (4.1) and was obtained by measuring the size of one hundred balls from a representative batch with a Cambridge Instruments "Quantimet" microscope.

All the glass fillers were dried prior to use by heating to 570K and composites prepared and tested as described previously. The short glass fibres proved to be a most difficult filler to handle from both the testing and fabrication aspects. It was impossible with the standard preparation technique to produce specimens containing more than about a 0.05 volume fraction of fibres since the addition of quite small quantities produced a very viscous mix which was difficult to pour. A modified casting technique was therefore employed in which the hot mix was poured into the usual moulds but instead of being supported vertically they were arranged horizontally and filled by removing one of the

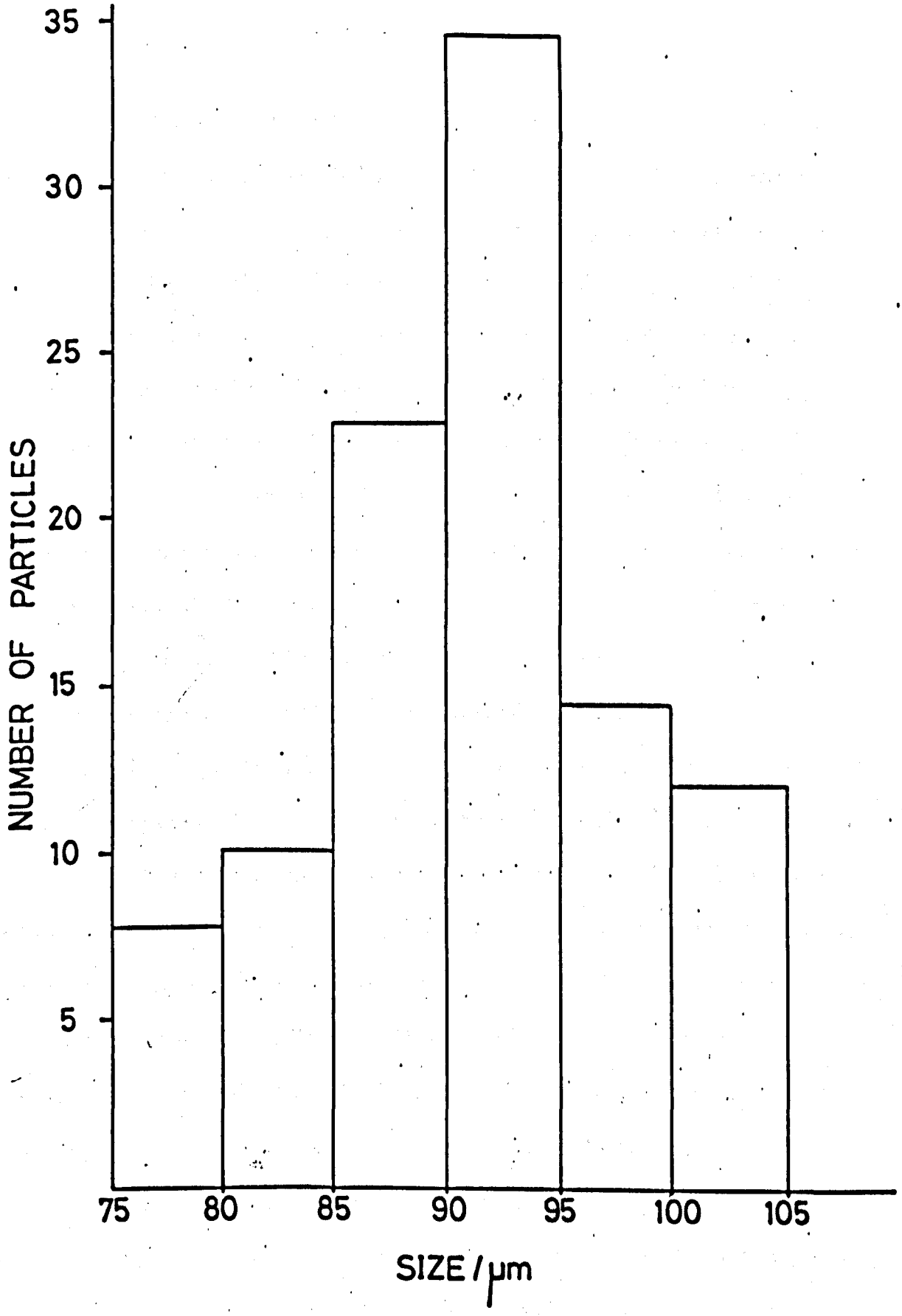

Fig. (4.1) Typical particle size distribution for 75 to 105 μm ballotini

side plates.

Composites produced in this manner were however considered to be unsatisfactory since they had a considerable bubble content of about a 0.1 volume fraction but in addition, and of more importance, considerable anisotropy was introduced by the modified casting technique. This anisotropy was particularly pronounced near the central groove as the fibres were longer than the thickness of the specimen at this point and were therefore limited in their possible orientations. The problem was alleviated to some extent by casting ungrooved specimens and milling to the final shape, but unfortunately it was impossible to propagate a crack for more than about 40 mm from the starting notch before the crack deviated into one of the cantilever arms and resulted in the fracture of that arm. An approximate fracture energy was calculated however from the little data that had been obtained.

Aluminium was chosen as a representative ductile material since it was readily available as flake and roughly equi-axed powder. No attempt was made to investigate chopped aluminium wire because of the problems already encountered with the short glass fibres. The aluminium powders were supplied by B.D.H. Limited. It was found that the finer powder was coated with a mineral-oil, apparently to prevent rapid and explosive oxidations of the aluminium when exposed to the atmosphere. The oil film vapourised when the filler was added to the hot resin and a considerable time was required to remove all the bubbles from the mixture. It was also suspected that the oil might in some way effect the physical properties of the base matrix. This was demonstrated to be the case by adding some of the oily residue that had been removed from the aluminium to a hot mixture of resin and hardener before gellation had occurred; a 0.01 volume fraction increased the fracture energy by about 10%.

For normal aluminium-filled specimens the oil film was removed from the

aluminium powder by repeated washing in trichloroethylene which enabled bubble-free composites to be manufactured. Composites containing more than a 0.05 volume fraction of this filler were again difficult to fabricate invertical moulds because of the high viscosity of the hot mixture. Some specimens were prepared, however, using a similar technique to that employed for glass fibres. The aluminium particles were sieved to produce the same series of size fractions as for glass. Microscopical examination of sieved fractions of the material supplied by B.D.H. Limited revealed that the shape of the particles was dependent upon their size, the smaller particles being lamellar, the larger ones roughly equi-axed. Powders supplied by other manufacturers were also found to exhibit a similar shape/size dependence.

One of the original aims of this work was to examine the role of the degree of matrix-particle adhesion on the fracture energy of a composite material. The usual technique for modifying the bonding between an epoxy resin and an inorganic glass filler is to use a silane pre-treatment of the glass surface. Silanes are commercially available which are claimed to be capable, when applied correctly, of either increasing or decreasing the adhesion between an epoxy resin and a glass surface. Such silanes have found wide application in the glass-reinforced plastics industry where pre-treatment of glass fibres with silane "adhesion promoters" has been shown to improve various mechanical properties of the final composite.

Two different silanes were used to pre-treat samples of ballotini in an attempt to explore the effect of adhesion on the toughness of glass/epoxy resin composites. They were A1100, on adhesion promoter, and A186, on adhesion inhibitor, both products of Union Carbide Limited.

Details of the application of the above silane coupling agents to glass surfaces are given by WAMBATCH (1971): the procedure described was followed closely. The

initial series of results from a matrix containing ballotini treated with the two types of silane suggested that the treatment did not affect the toughness or the crack propagation behaviour of the composite. Microscopic examination of the fracture surfaces also failed to reveal any distinction between the fracture surfaces of composites prepared from either untreated ballotini or that treated with the A1100 or A186 silanes.

It was considered advisable to attempt to check directly that the silane pre-treatment of the glass was in fact changing the adhesion between the resin and the glass before concluding from the above experiment that the adhesion between the particles and the matrix was not a major factor influencing the toughness. A method was therefore developed for estimating directly the degree of bonding between large strips of glass plate and cured CT200. The technique employed was similar to the double cantilever beam method and enabled the "debonding energy" of the interface to be found.

Fig. (4.2) shows a typical specimen in which two laths of glass are bonded together with cured CT200. PTFE tape was used to limit the width of the bonded region to a 5 mm strip down the centre of the 20 mm wide and 5 mm thick glass plates so that failure occurred either in the resin or at the resin/glass interface and not by fracture of one of the cantilever arms. These experiments, the results of which are described in detail in a later section, showed that the materials and the techniques employed here did not affect the degree of adhesion between the glass and the resin.

The effect of pre-etching the aluminium on the toughness and crack propagation behaviour of epoxy resin-aluminium composites was also examined. COATES (1971) has shown that a chromic acid etch will promote the adhesion between an epoxy resin and aluminium and hence his technique was employed. The etching time in the

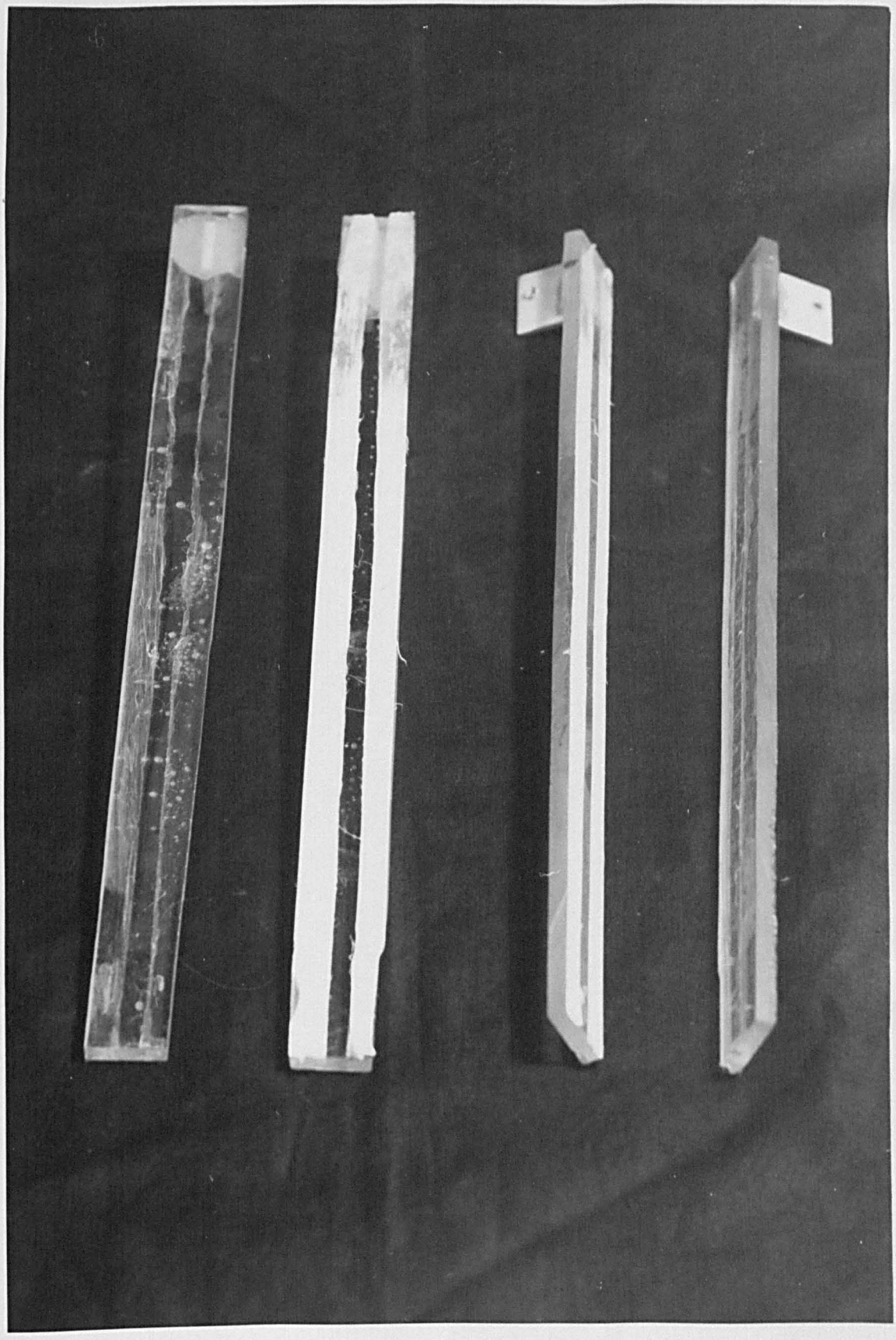

Fig. (4.2) Typical specimens used to determine the adhesion between silane treated glass and cured CT200/HT901

recommended 0.1N chromic acid was limited to 300 s after which a microscopic examination revealed that 100 μm particles had undergone a reduction in size of about 10%, mainly by the removal of sharp edges.

Some additional experiments were performed with other fillers, including: alumina, slate, mica, graphite, antimony trioxide, lead, silica flour, copper, talc and rutile. Slate, mica, graphite and talc were chosen because they were known to be lamellar and it was thought that they would offer a means of comparing filler types of the same shape since the aluminium used previously was predominantly lamellar. Antimony trioxide and rutile were thought to be acicular and it was hoped that they would provide a useful comparison with the short glass fibres. Lead was considered because it had a very low flow stress as had the talc; silica flour was used for comparison with the glass frit and copper and aluminium are similar.

The alumina was selected largely because of its availability in fairly precisely graded and very fine sizes (1 μm and 0.05 μm) but unfortunately it proved difficult to form composites in which these fine particles were well dispersed. Microscopic examination of the cast composites revealed that the standard stirring procedure would not fully disperse the particles in the matrix; a commercial hand mixer (F.W. Woolworth) was tried but this offered little improvement in the particle dispersion and greatly increased the fine bubble content of the final composite. A second technique was examined which involved dissolving the CT200 in acetone . The powder and HT901 hardener were then added to this solution and the final mixture agitated in an ultrasonic bath for two hours; this was followed by the evaporation of the acetone in a well-ventilated oven and curing in the normal manner. This rather laborious process offered little improvement in the particle dispersion over that achieved by the standard mixing technique.

To gain some further information on the effect of the adhesion between the matrix and the filler a coating of a silicone release agent (Releasil MS7) was applied to the mica powder in an attempt to reduce the matrix adhesion. The release coating was applied by soaking the particles in a dilute solution of the silicone in carbon tetrachloride. The adhesion "promotor" A1100 was also applied to the talc in the recommended manner.

4.3. Results

All the results presented in this chapter, unless otherwise stated, have been obtained using an applied cross-head speed of 6.3×10^{-3} mm s^{-1}. The humidity and temperature of the laboratory air were not controlled but were generally within the ranges 294 K to 298 K and 5 to 12 g of H_2O K_g^{-1} of air respectively.

4.3.1. The Fracture Energies of Glass Filled CT200/HT901

For any given range of particle sizes, the fracture energies of ballotini/CT200 composites increase linearly with the volume fraction of filler. Fig. (4.3) illustrates this for the 75 to 105 μm particles. The energy for crack initiation however increases slightly more rapidly than the energy at arrest. This is well illustrated by the fracture energy ratios

$$\frac{I^{\gamma}}{A^{\gamma}} = 1.65 \text{ at a volume fraction of } 0.025$$

and

$$\frac{I^{\gamma}}{A^{\gamma}} = 1.60 \text{ at a volume fraction of } 0.3$$

a difference of only about 4%.

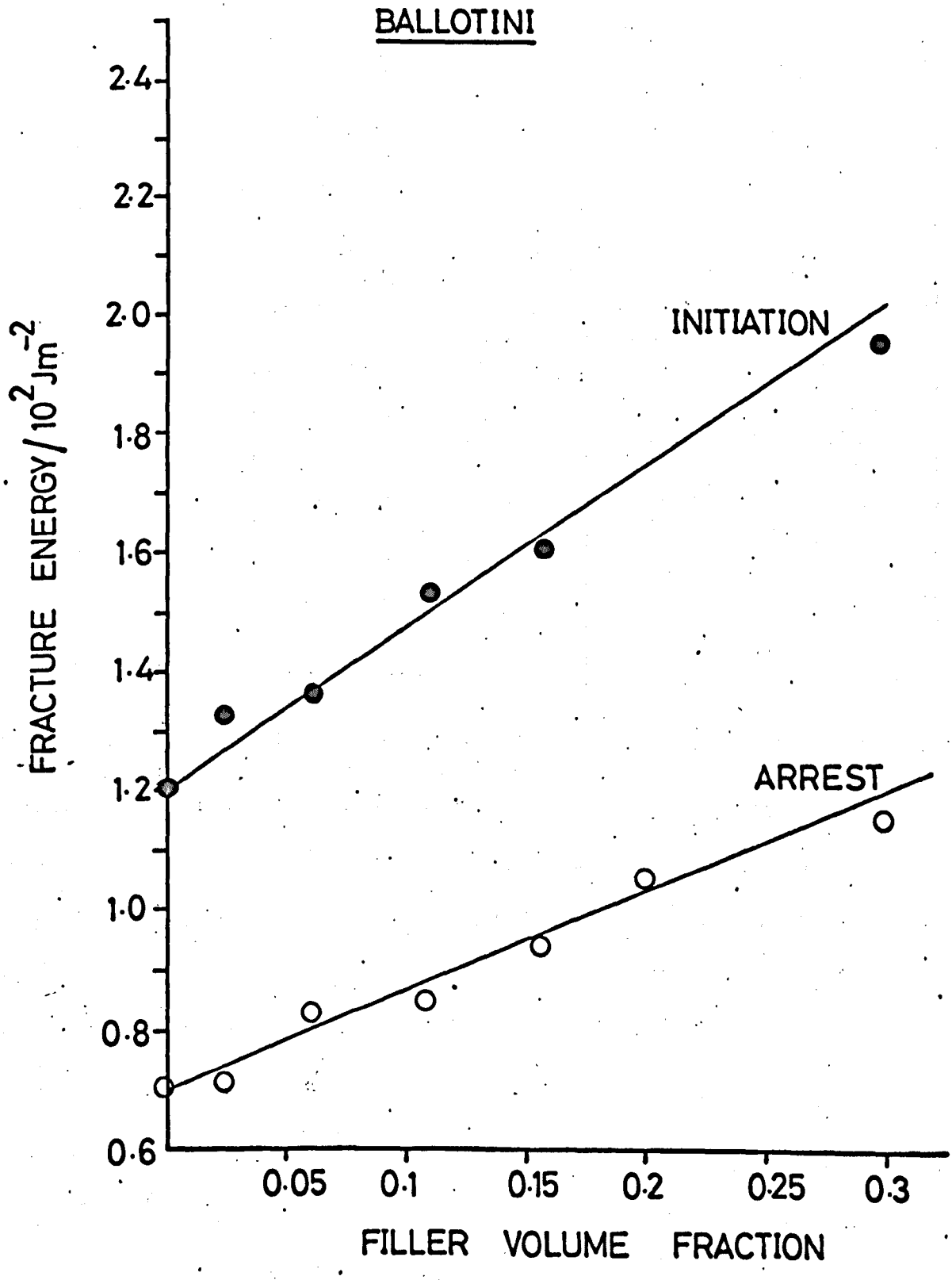

Fig. (4.3) The fracture energies of ballotini filled CT200/HT901 as a function of filler volume fraction

Table (4.1) indicates that both frit and ballotini produce essentially similar results; the fracture energies of frit-filled material being only slightly higher than those of a ballotini composite with the same volume fraction of filler.

TABLE 4.1

The Fracture Energies of Frit and Ballotini Filled Composites

Volume fraction of filler	75 to 105 μm Ballotini		75 to 105 μm Frit	
	Fracture energy/10^2Jm^{-2}		Fracture energy/10^2Jm^{-2}	
	I^{γ}	A^{γ}	I^{γ}	A^{γ}
0.025	1.32	0.75	1.33	0.74
0.06	1.36	0.83	1.40	0.82
0.11	1.53	0.84	1.57	0.88
0.155	1.61	0.94	1.64	0.97
0.3	1.95	1.15	2.00	1.23

Fig. (4.4) which summarises the data obtained from composites containing a 0.1 volume fraction of ballotini in various size fractions, indicates that both fracture energies are independent of particle size within the range 75 to 300 μm. A particularly interesting feature is the possible large increase in the initiation fracture energy when particles smaller than 50 μm are incorporated into the matrix.

It was indicated in the previous section that it was extremely difficult to fabricate and test the chopped glass strand filled composites and as a result little quantitative information was obtained. An approximate initiation fracture energy of $2 \times 10^3 Jm^{-2}$ was however calculated from the limited amount of data that had been collected.

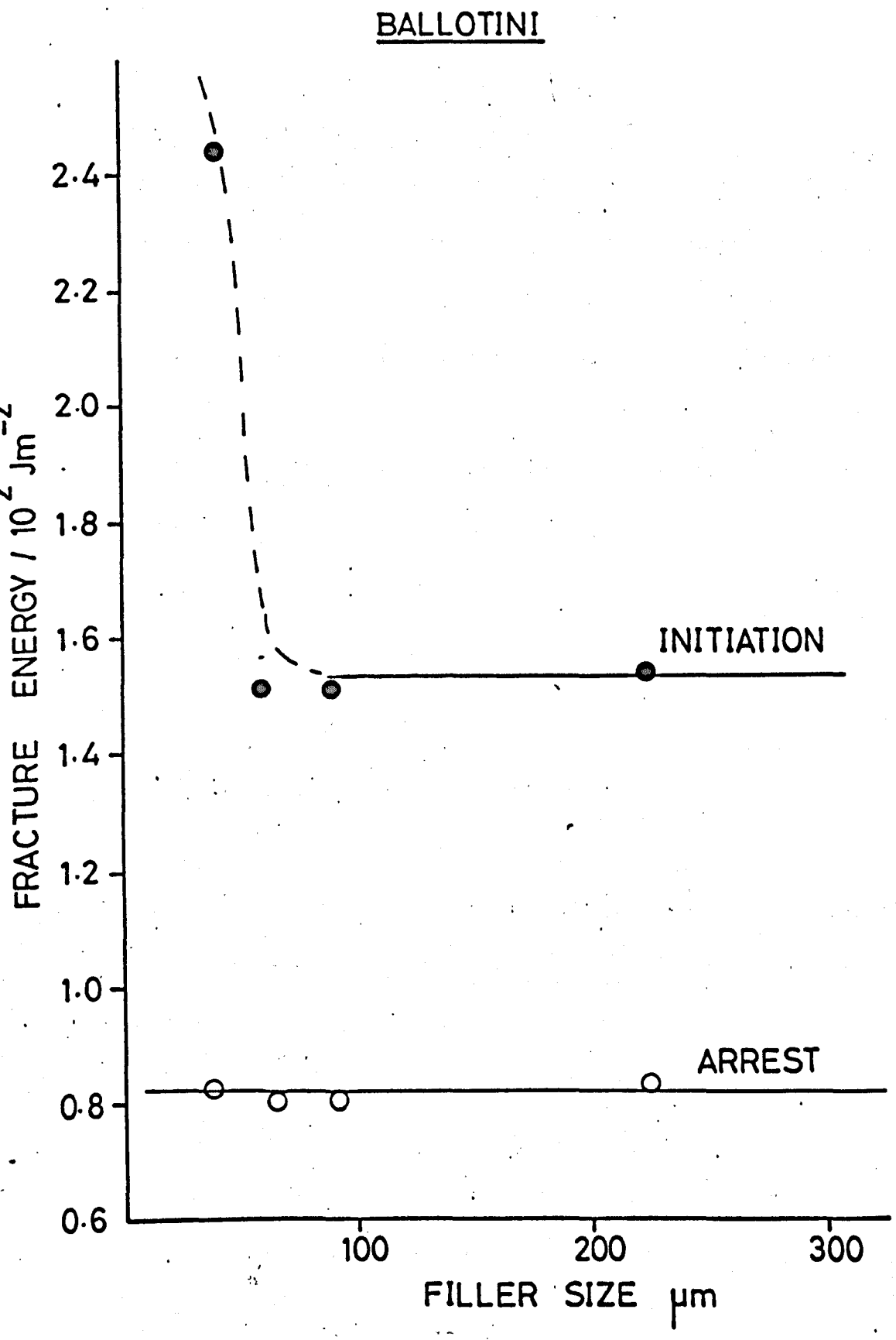

Fig. (4.4) The fracture energies of ballotini filled CT200/HT901 as a function of filler size

4.3.2. The Fracture Energies of Aluminium Filled CT200/HT901

Again for any given range of particle sizes the fracture energies of aluminium/CT200 composites increase approximately linearly with the volume fraction of filler. Fig. (4.5) shows this to be the case although there is an ill-defined reduction in both values of fracture energy below a volume fraction of 0.01. The above figure also illustrates that the initiation fracture energy increases more rapidly with the volume fraction of 75 to 105 μm powder than does the arrest value; this is reflected in the fracture energy ratios:

$$\frac{I^{\gamma}}{A^{\gamma}} = 2.0 \text{ at a volume fraction of } 0.012$$

and

$$\frac{I^{\gamma}}{A^{\gamma}} = 2.65 \text{ at a volume fraction of } 0.04$$

a difference in this case of about 30%. Comparison of Fig. (4.5) with the corresponding Fig. (4.3) for ballotini shows that, at a given volume fraction of filler, aluminium produces more marked increases in both fracture energies.

Fig. (4.6), which summarises the data obtained from composites containing a 0.025 volume fraction of aluminium powder, in various size fractions, illustrates that in the range 75 to 300 μm, both fracture energies are independent of particle size. An ill-defined increase in the initiation fracture energy is again evident when particles smaller than 50 μm are used.

4.3.3. The Fracture Energies of Alumina Filled CT200/HT901

Both glass and aluminium appeared to give increases in fracture energies when

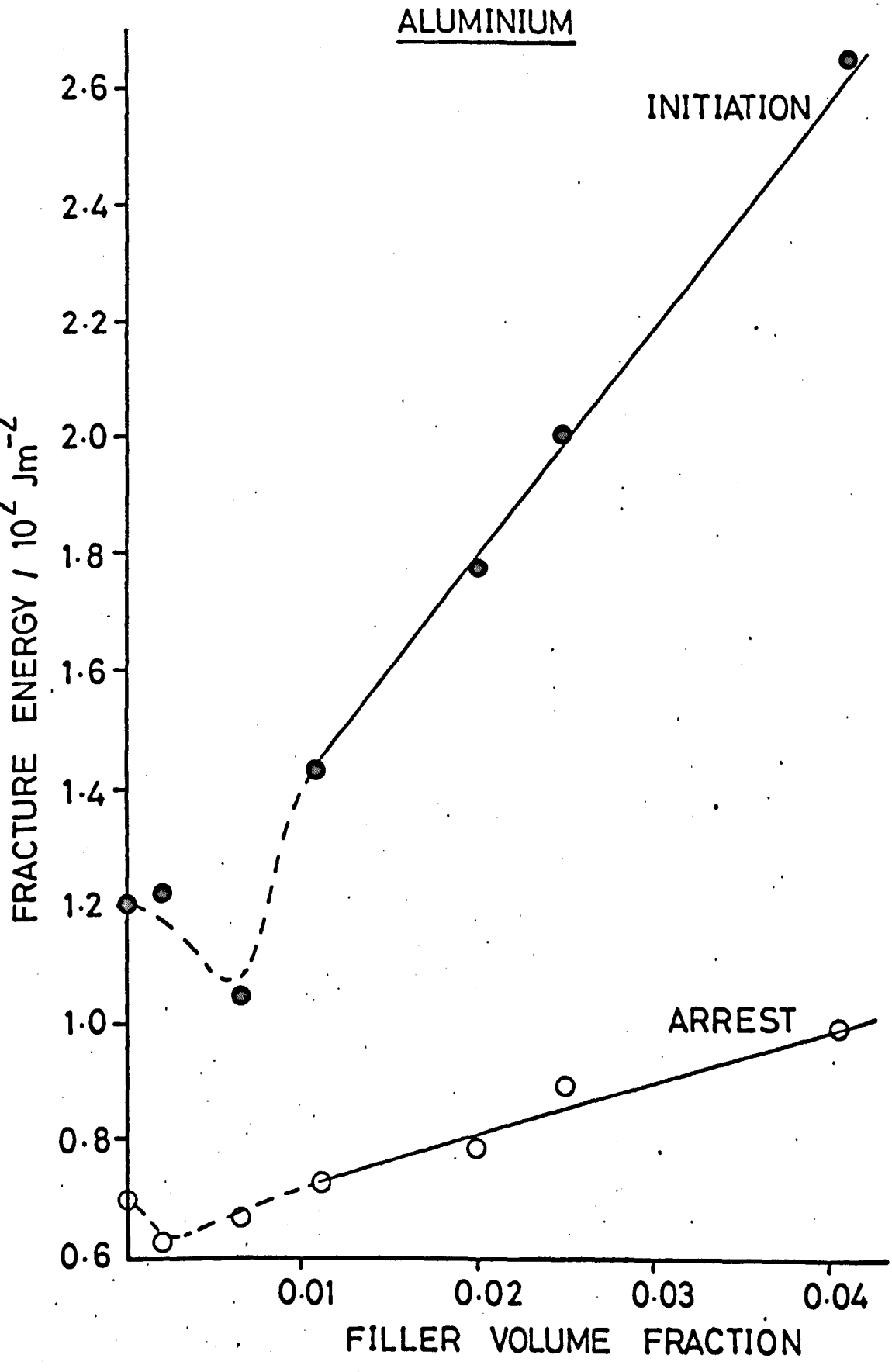

Fig. (4.5) The fracture energies of aluminium filled CT200/HT901 as a function of filler volume fraction

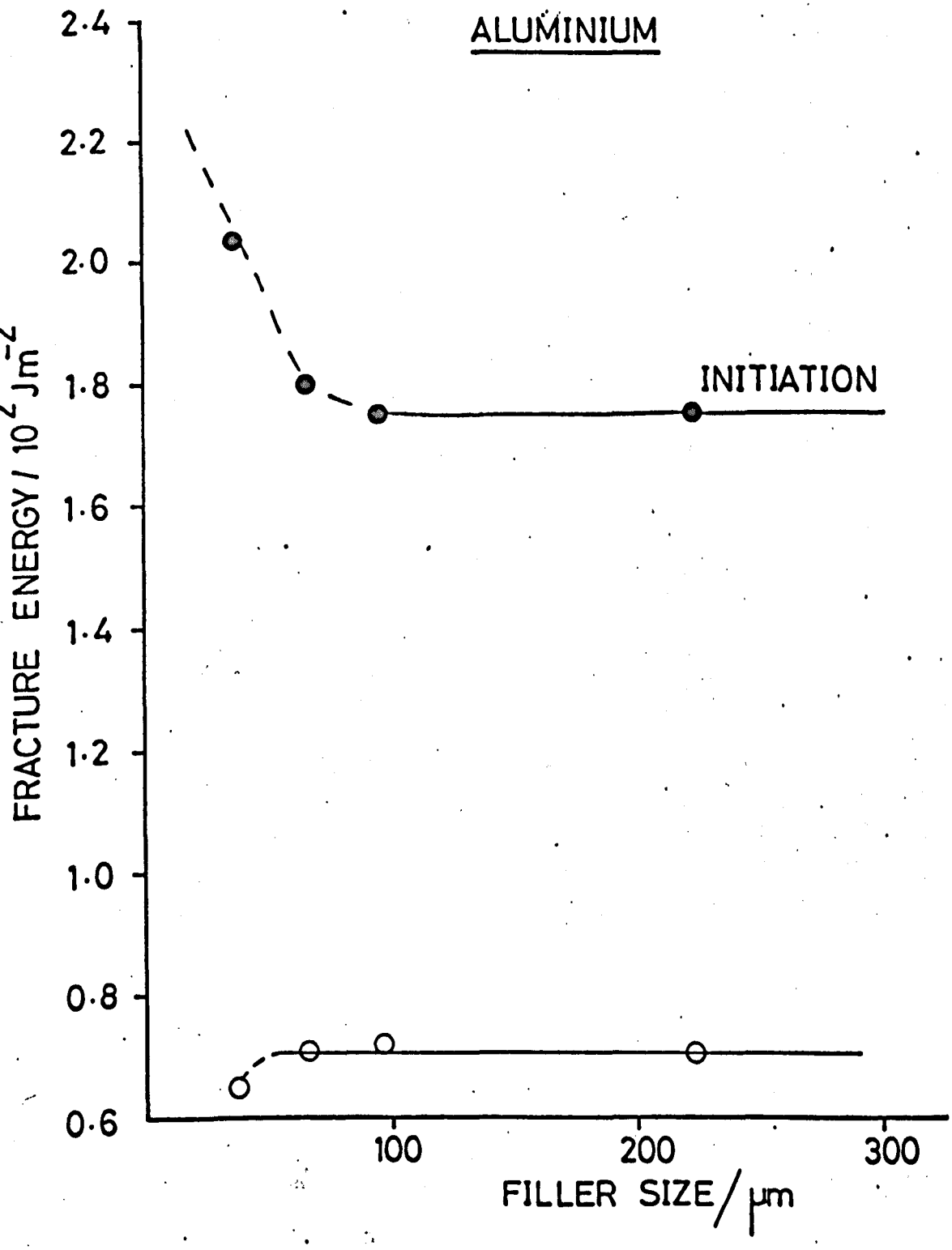

Fig. (4.6) The fracture energies of aluminium filled CT200/HT901 as a function of filler size

particles smaller than about 50 μm were incorporated into the CT200/HT901 matrix. The above two materials were not readily available as very fine powders and hence alumina was used in an attempt to explore this size range in more detail since this was obtainable in fairly precisely graded and very fine sizes.

Particle sizes of 1 μm and 0.05 μm were used but some difficulty was experienced in dispersing these very fine powders in the CT200 matrix; microscopic examination revealed that only a small proportion of the 0.1 volume fraction that was added to the matrix had in fact been dispersed. The data obtained using the three mixing techniques is presented in Table (4.2), along with some comparative results for 50 μm aluminium and ballotini.

TABLE 4.2

The Fracture Energy of Some Alumina, Aluminium and Ballotini Filled Composites

Material CT200/HT901 plus a:-	Fracture Energy/10^2Jm^{-2}	
	$I\gamma$	$A\gamma$
0.025 Vol.fraction of 50 μm Al	2.04	0.65
0.1 Vol.fraction of 50 μm Ballotini	2.45	0.82
0.1 Vol.fraction of 0.1 μm Al_2O_3	2.38	0.74
0.1 Vol.fraction of 0.05 μm Al_2O_3 (hand mixed)	2.44	0.78
0.1 Vol.fraction of 0.1 μm Al_2O_3 (machine mixed)	2.29	0.78
0.1 Vol.fraction of 0.1 μm Al_2O_3 (ultrasonically vibrated)	2.40	0.72

Table (4.2) indicates that large increases in the initiation fracture energy were not realised by using fine alumina powder and either of the three mixing techniques.

4.3.4. The Fracture Energies of Two Composites as a Function of Effective Extension Rate

Some insight into the role of effective extension rate can be gained if one recalls that it was impossible to obtain a continuously propagating crack in the filled materials when "normal" cross-head speeds were used to fracture our double cantilever beam specimens. The role of effective extension rate was examined directly, and in some detail, by means of a series of experiments at selected cross-head speeds similar to those used for the unfilled resins. Results are presented in Figs. (4.7) and (4.8) for the following two composite materials:

(i) CT200/HT901 plus a 0.025 volume fraction of 75 to 105 μm aluminium.

(ii) CT200/HT901 plus a 0.1 volume fraction of 75 to 105 μm ballotini.

Evidently the addition of a 0.025 volume fraction of aluminium and a 0.1 volume fraction of ballotini to the CT200 resin matrix removes the dependence of fracture energy on effective extension rate.

4.3.5. Other Fillers

Table (4.3) presents the fracture energy values for composites generally containing an 0.1 volume fraction of a variety of other fillers. (Note the 0.025 volume fraction in the case of copper particles.)

The most effective of these fillers at increasing both the initiation and arrest fracture energies is talc; a volume fraction of 0.1 produced an order of magnitude increase in these parameters. It is also observed that at a 0.1 volume fraction of talc the initiation and arrest fracture energies are co-incident and hence at normal cross-head speeds the crack propagates continuously. In these specimens a "whitening" of

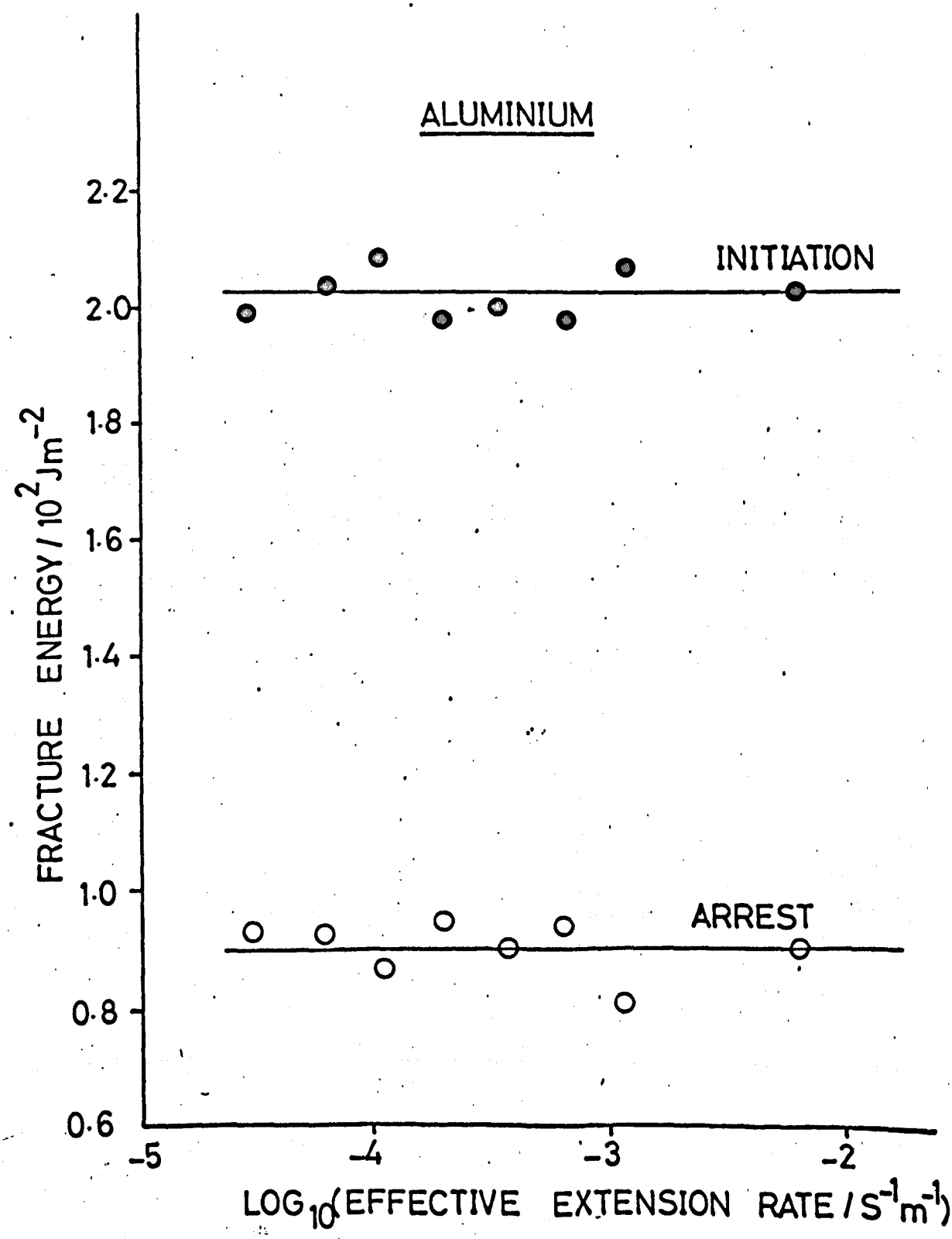

Fig. (4.7) The fracture energies of ( ) aluminium filled CT200/HT901 as a function of effective extension rate

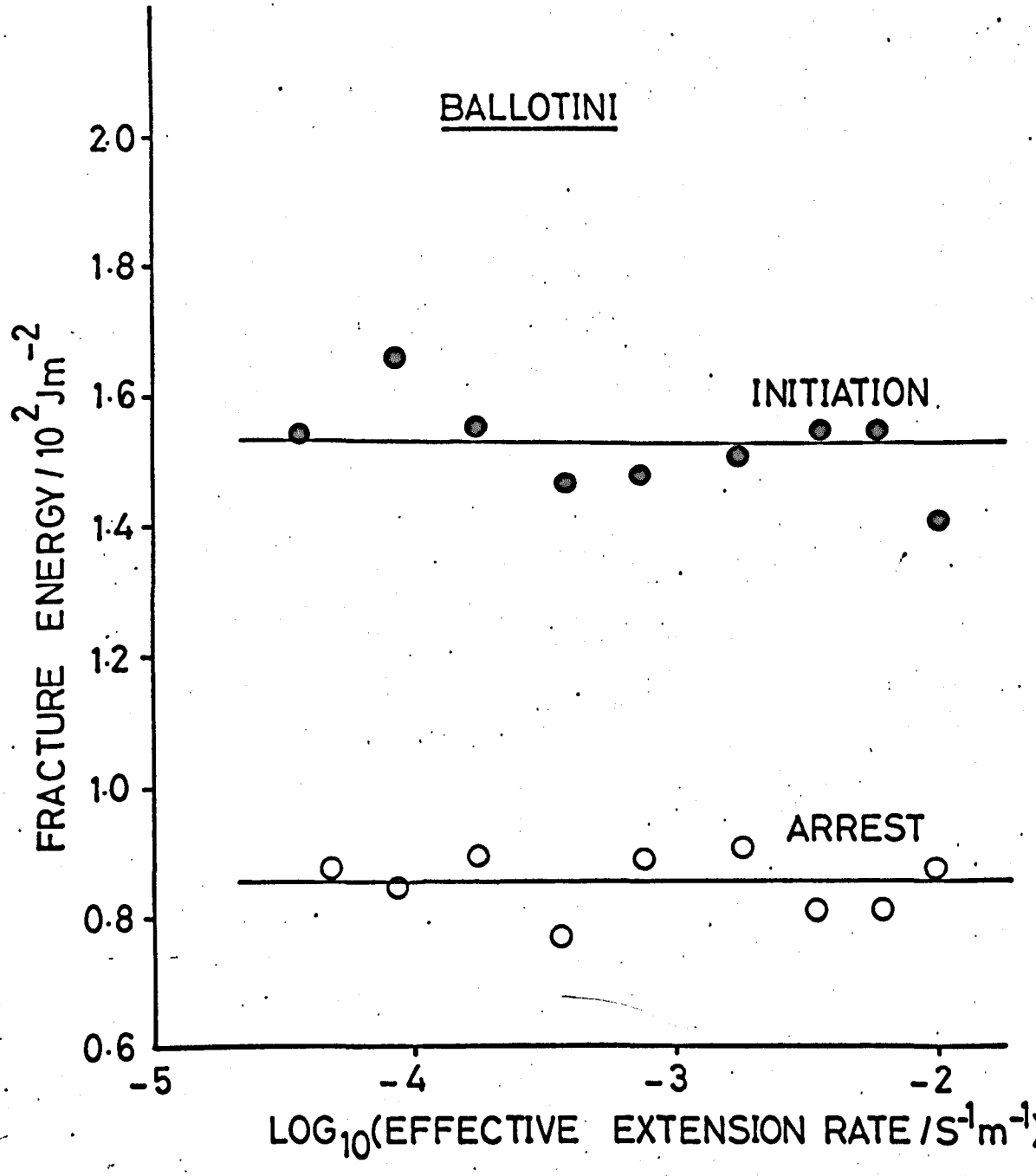

Fig. (4.8) The fracture energies of ballotini filled CT200/HT901 as a function of effective extension rate

TABLE 4.3

The Fracture Energies of CT200/HT901 Composites Containing Various Particulate Fillers

Filler	Volume Fraction	Shape and approx. size	Fracture Energy/$10^2 Jm^{-2}$	
			I^γ	A^γ
Alumina	0.1	equi-axed 0.1 μm	2.4	0.7
Slate	0.1	lamellar 150 μm	2.0	1.0
Mica	0.1	lamellar 150 μm	1.8	1.4
Graphite	0.1	lamellar 150 μm	6.1	1.7
Antimony trioxide	0.1	acicular 100 μm	4.2	1.6
Lead	0.1	equi-axed 100 μm	3.7	2.0
Silica flour	0.1	equi-axed 100 μm	1.5	1.0
Copper	0.025	lamellar 100 μm	2.0	0.8
Talc	0.1	lamellar 100 μm	9.1	9.1
Rutile	0.1	acicular 100 μm	1.3	1.1

the material around to the crack tip was evident and this often extended into the arms of the double cantilever specimens. The variation in the fracture energies with volume fraction of talc in a CT200/HT901 matrix is illustrated in Fig. (4.9) and the fracture energies of composites containing 0.1 volume fraction of talc in all three epoxy matrices is summarised in Table (4.4). The results illustrate that a small proportion of talc increases substantially the fracture energies of both CT200/HT901 and EPON828/NMA/BDMA but not LY558/HT973.

4.3.6. The Effect on Fracture Energy of Filler Surface Pre-treatment

The results quoted in Table (4.5) show that pre-treatment of the ballotini with silanes have a negligible effect on the fracture energies of composites based on CT200/HT901 and containing a 0.1 volume fraction of 75 - 105μm particles.

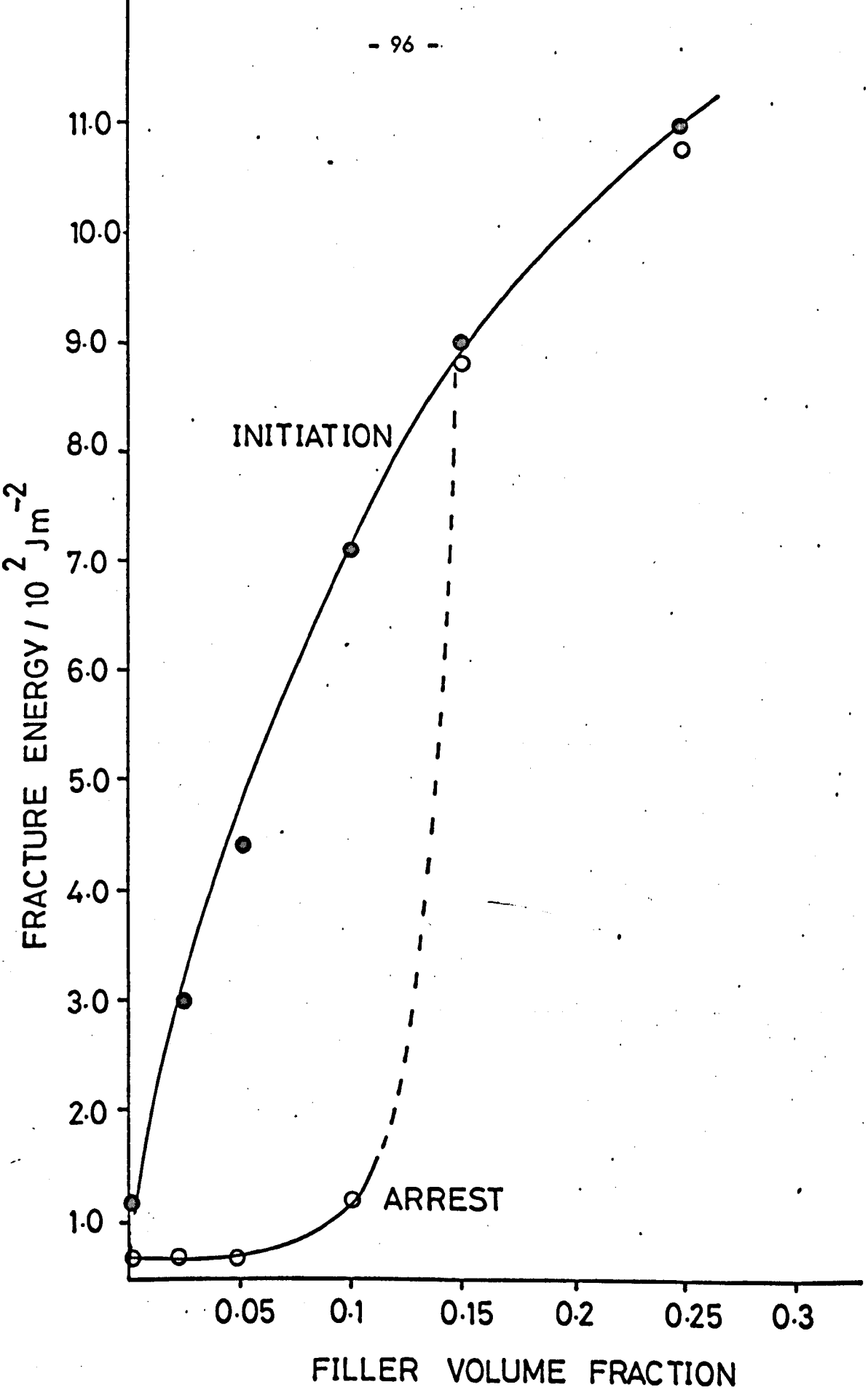

Fig. (4.9) The fracture energies of talc filled CT200/HT901 as a function of filler volume fraction.

TABLE 4.4

The Fracture Energies of Talc Filled Resins

Matrix	Fracture Energy/$10^2 Jm^{-2}$			
	Unfilled		Plus a 0.1 volume fraction of talc	
	I^γ	A^γ	I^γ	A^γ
CT200/HT901	1.2	0.75	9.1	9.1
EPON828/NMA/BDMA	0.59	0.53	3.4	1.9
LY558/HT973	0.33	0.28	0.52	0.45

TABLE 4.5

The Fracture Energies of Some Composites Containing Silane Treated Ballotini

CT200/HT901 plus a 0.1 volume fraction of 75 to 105 μ m ballotini	Fracture Energy/$10^2 Jm^{-2}$	
	I^γ	A^γ
Untreated	1.52	0.82
A1100 treated (adhesion promotor)	1.50	0.77
A186 treated (adhesion inhibitor)	1.56	0.78

As mentioned earlier, these results suggest that the silane pre-treatments were unsuccessful in modifying the fracture behaviour of CT200/HT901 based composites. That the silane treatment had little effect on the adhesion between the glass and the matrix is confirmed by the results given in Table (4.6) for the energy required to debond the glass plate specimens. Debonding occurred in a "creep like" mode; i.e. the debonded length increased at constant end deflection for a period of more than one hour after an increment of deflection. The debonding energy therefore decreases with time and hence the energies quoted were calculated from values of

TABLE 4.6

The Energy Required to Debond the Glass Plate Specimens

Surface Treatment	Debonding Energy at 120 s/10^2 Jm^{-2}
None	4.1
A1100	4.5
A186	4.0

cantilever end deflection, applied force, and length of debonded region at an arbitrary period of 120 s after each increase in end deflection.

Microscopic examination of the surfaces, after separation, revealed that in general the resin had debonded from only one interface to leave a "clean" glass surface and thus indicates that failure had occurred at the resin-glass interface and not by crack propagation within the resin. The data contained in Table (4.6) illustrates that for our resin system and methods of application that no significant modification of adhesion was produced by the use of the silane coupling agents. The reason for this was not fully resolved but may be due to an incorrect method of application or the use of an inappropriate resin system. Our CT200 resin was anhydride cured whereas the manufacturer of silanes recommend an amine curing agent.

Chromic acid etching of aluminium was successful in increasing the initiation value of fracture energy but reduced the arrest value. The data from a number of composites employing a particle size range of 75 to 105 μm (prior to etching) is summarised in Fig. (4.10) which warrants comparison with Fig. (4.5) for the unetched filler. The two additional experiments, using talc treated with the so-called adhesion promotor, A1100, and mica coated with a silicone release agent produced no significant changes in fracture energy. The results are summarised along with some from untreated materials, in Table (4.7).

4.3.7. The Effect of Temperature on the Fracture Energies of a CT200/Ballotini Composite

The effect of temperature on the fracture energies of the composite, CT200/HT901 plus a 0.1 volume fraction of 75 to 105 μm ballotini is illustrated in Fig. (4.11).

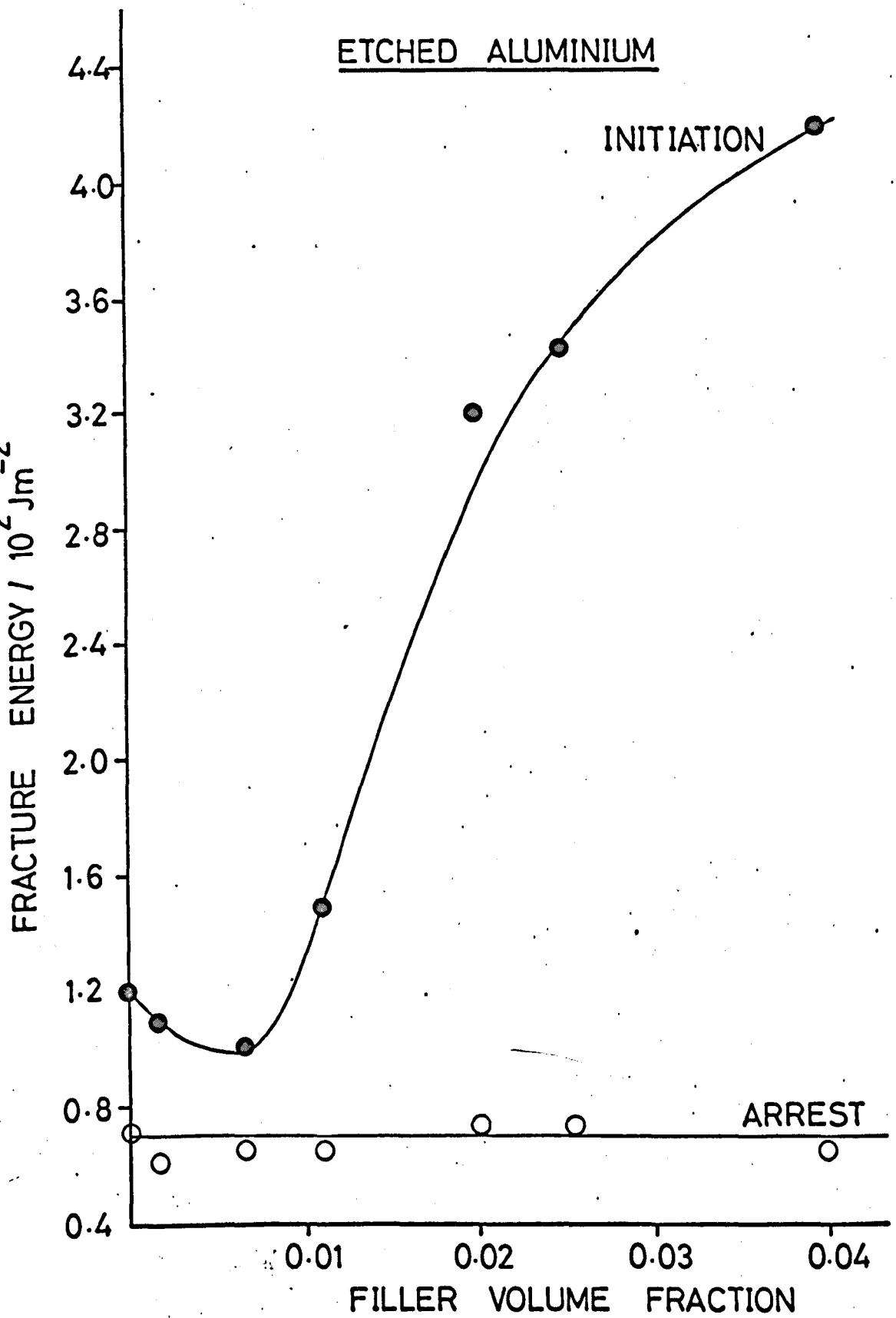

Fig. (4.10) The fracture energies of etched aluminium filled CT200/HT901 as a function of filler volume fraction

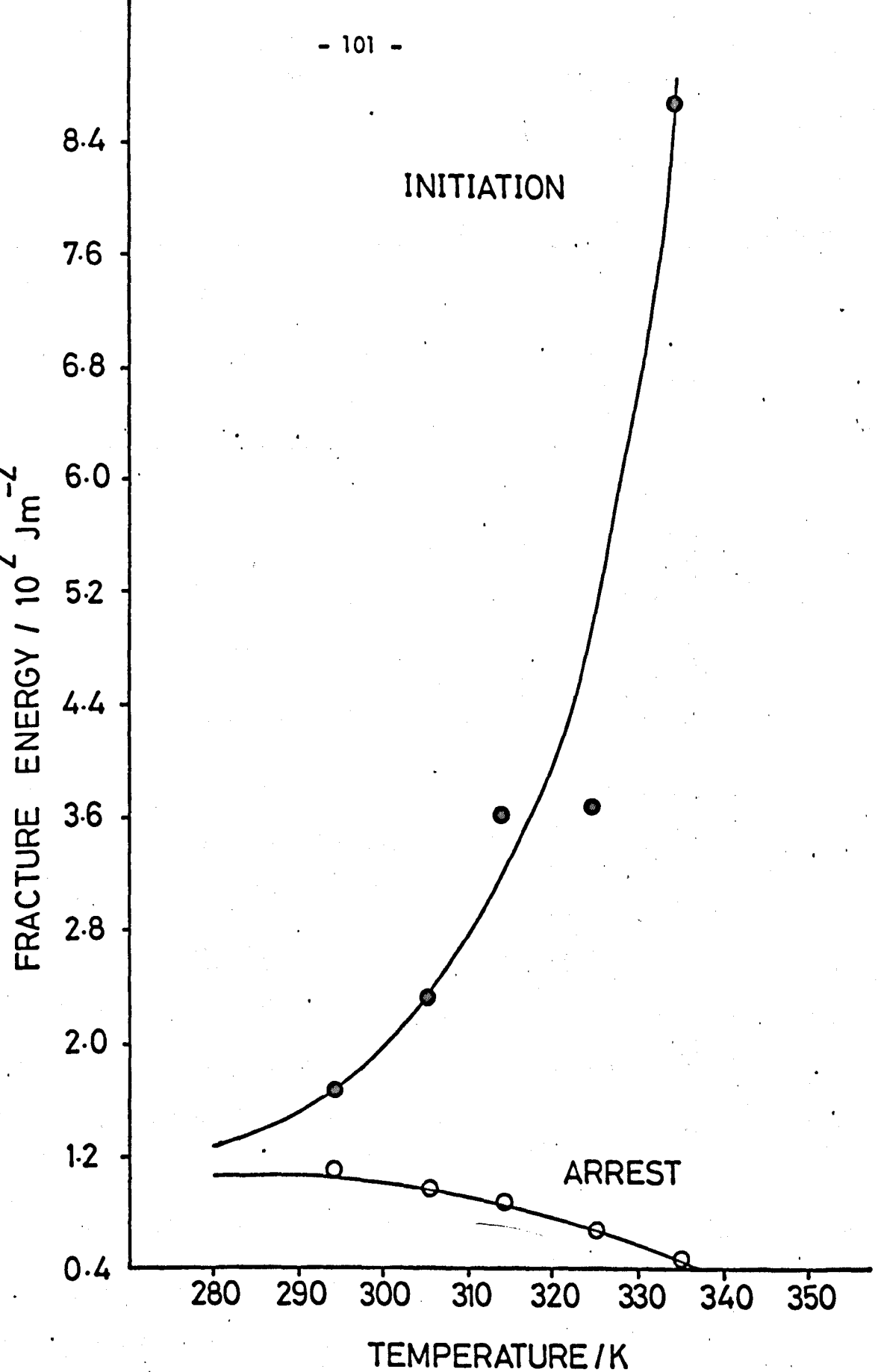

Fig. (4.11) The fracture energies of ballotini filled CT200/HT901 as a function of temperature

TABLE 4.7.

The Fracture Energies of Composites Containing Mica and Talc Fillers having undergone a Surface Treatment

CT200/HT901 plus a 0.1 volume fraction of:	Fracture Energy/$10^2 Jm^{-2}$	
	I^{γ}	A^{γ}
Talc	9.1	9.1
Talc treated with A1100	9.8	9.8
Mica	1.8	1.4
Mica treated with a silicone release agent	2.1	1.4

Tests were carried out in dry silicone oil over the temperature range 273K to 353K. Very similar results were also obtained in water and moist air environments.

4.3.8. The Young's Modulus of Ballotini Filled CT200/HT901

For any given particle size the Young's modulus of ballotini/CT200 composites increases linearly with volume fraction of filler; Fig. (4.12) illustrates this for the case of 75 to 105 μm particles in the compositional range from zero to a 0.3 volume fraction of filler.

Fig. (4.13) which presents the data from composites containing a 0.1 volume fraction of ballotini in various size ranges, indicates that the Young's modulus decreases in a non-linear fashion as the filler size is increased.

4.3.9. The Young's Modulus of Aluminium Filled CT200/HT901

Again for a given range of particle sizes the Young's modulus of aluminium

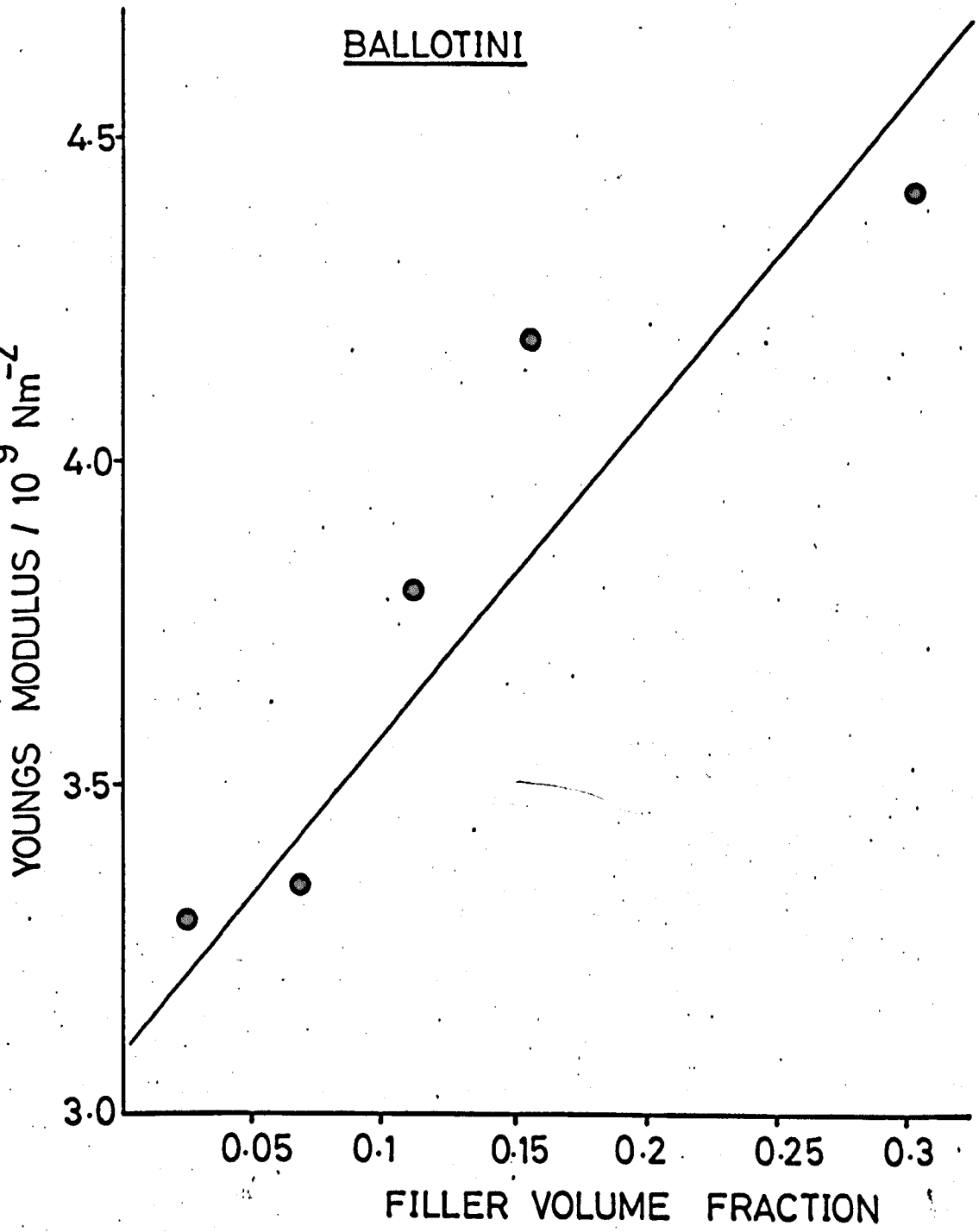

Fig. (4.12) The Young's modulus of ballotini filled CT200/HT901 as a function of filler volume fraction

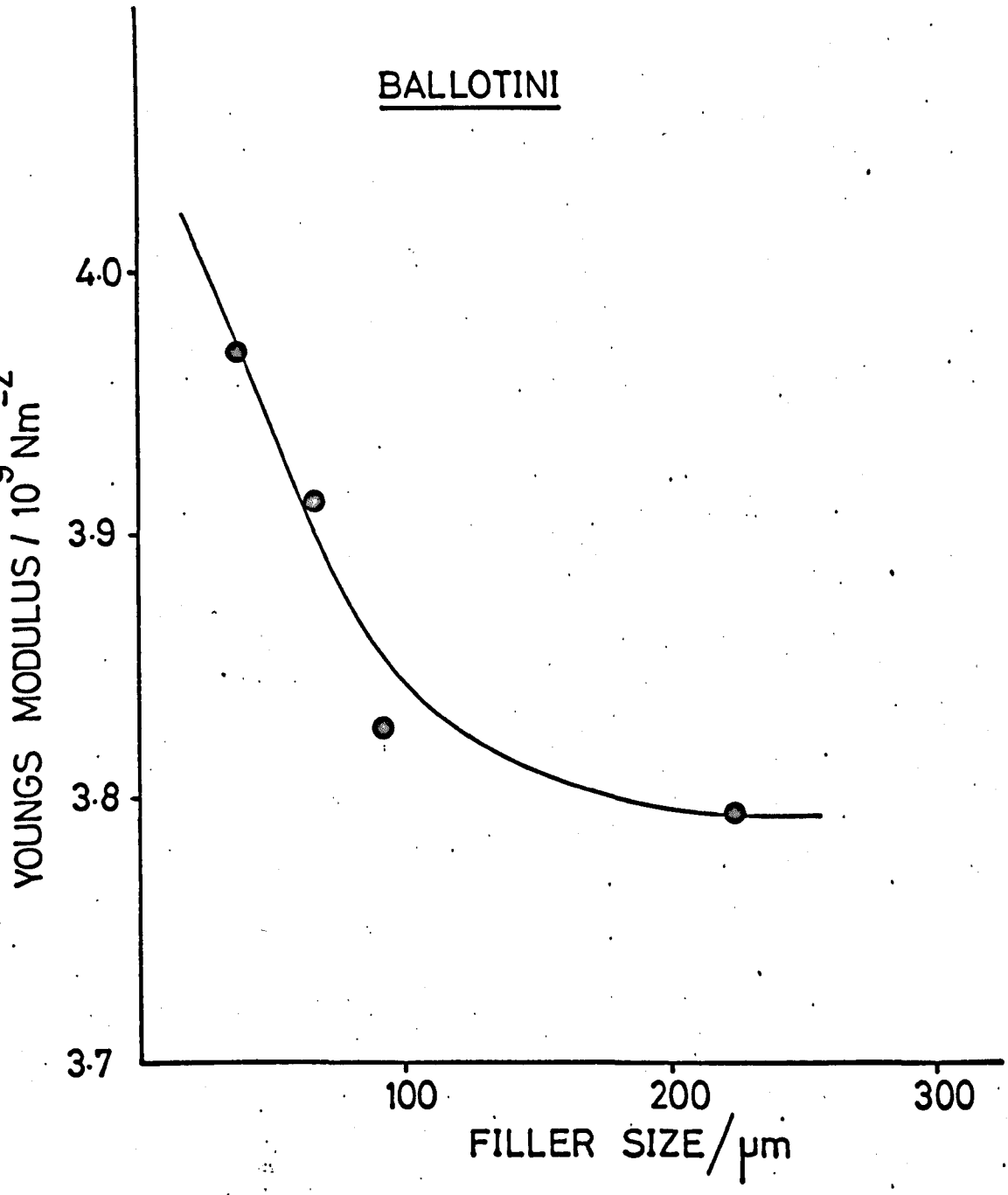

Fig. (4.13) The Young's modulus of ballotini filled CT200/HT901 as a function of filler size

/CT200 composites increases linearly with the volume fraction of filler. Fig. (4.14) shows this to be the case although there is an initial ill-defined reduction in the modulus of composites containing unetched filler. In addition, the modulus of composites containing etched filler particles are generally higher than those for the unetched filler.

The Young's modulus of aluminium-filled, CT200/HT901 also decreases in a non-linear fashion as the particle size of a 0.025 volume fraction of filler is increased, see Fig. (4.15).

4.3.10 K_{Ic} for Ballotini Filled CT200/HT901

Figs. (4.16) and (4.17) indicate that the general trends in the critical plane strain stress intensity factors are similar to those for fracture energy. The critical stress intensity factors for both crack initiation and arrest increase approximately linearly with filler volume fraction and are essentially independent of filler size above about 75 μm although a marked increase is observed in the critical stress intensity factor for crack initiation below this size.

4.3.11 K_{Ic} for Aluminium Filled CT200/HT901

Figs. (4.18) and (4.19) show for aluminium/CT200 composites that similar trends are exhibited in the critical stress intensity factors and in fracture energies. The critical plane strain stress intensity factors for both crack initiation and arrest are observed to increase in a non-linear fashion with the volume fraction of unetched 75 to 105 μm aluminium powder, although to qualify this a little, there is an ill-defined reduction at about a 0.005 volume fraction. Composites containing etched, as opposed to normal aluminium, particles but in similar volume fractions and in the same size

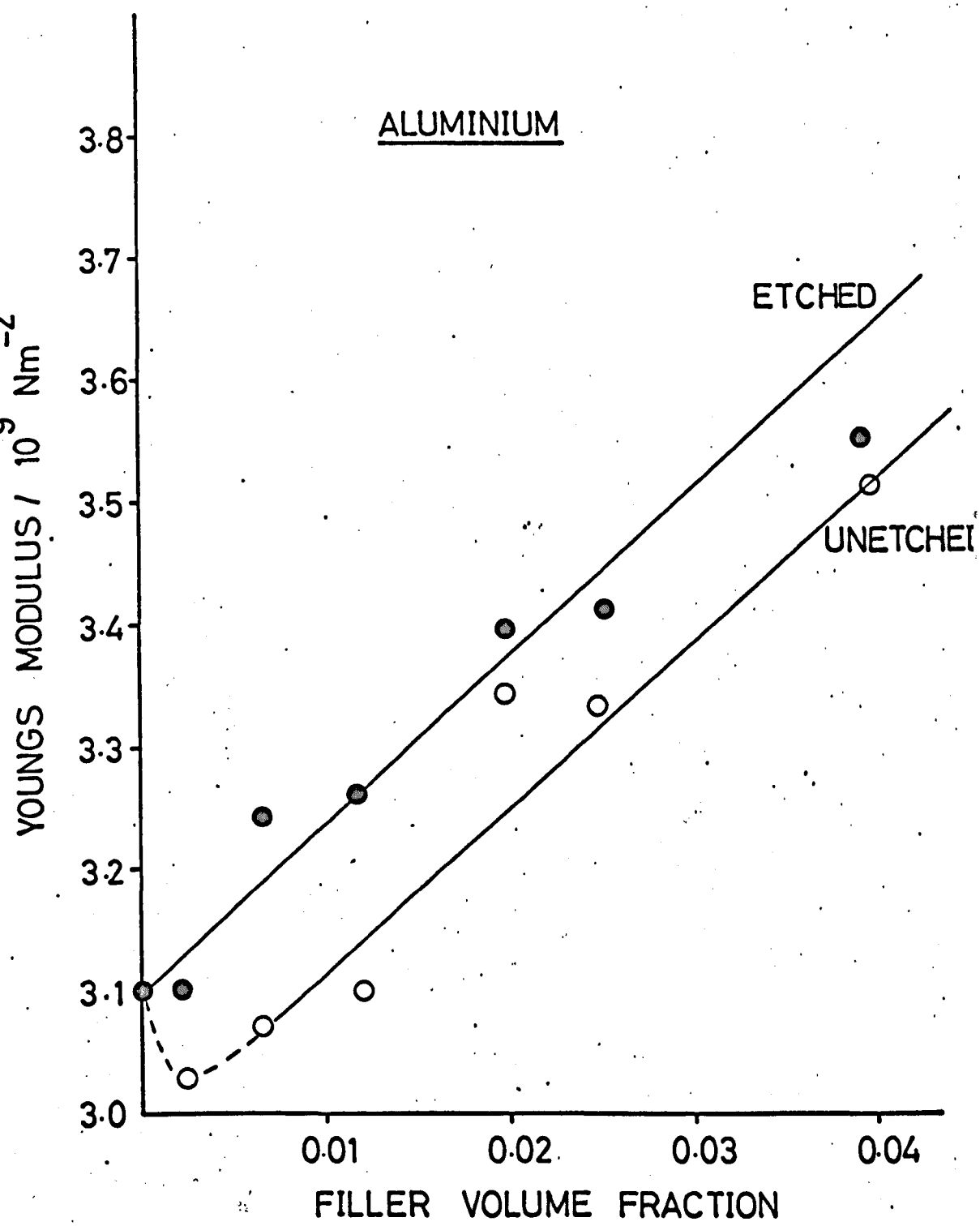

Fig. (4.14) The Young's modulus of aluminium filled CT200/HT901 as a function of filler volume fraction

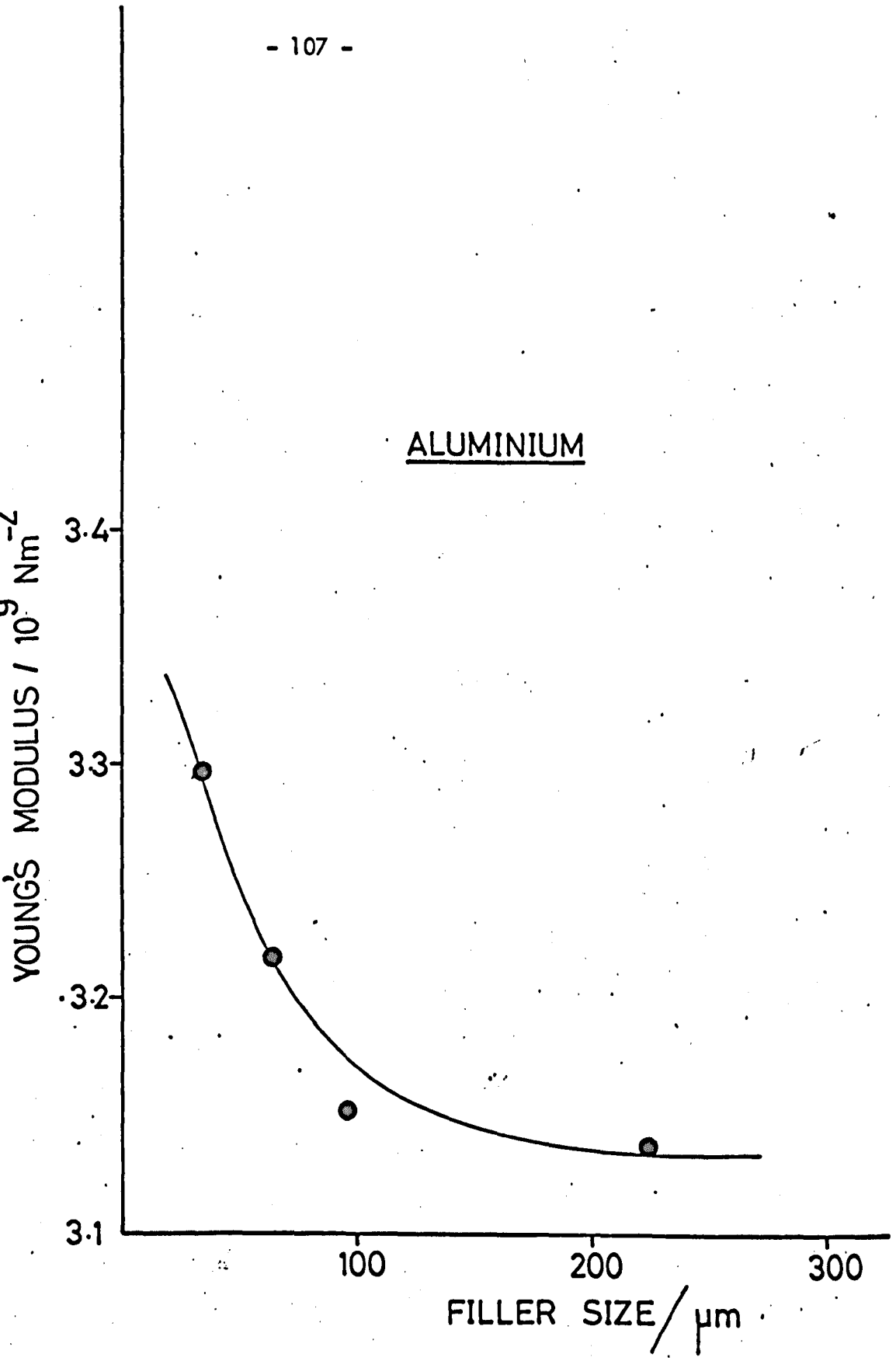

Fig. (4.15) The Young's modulus of aluminium filled CT200/HT901 as a function of filler size

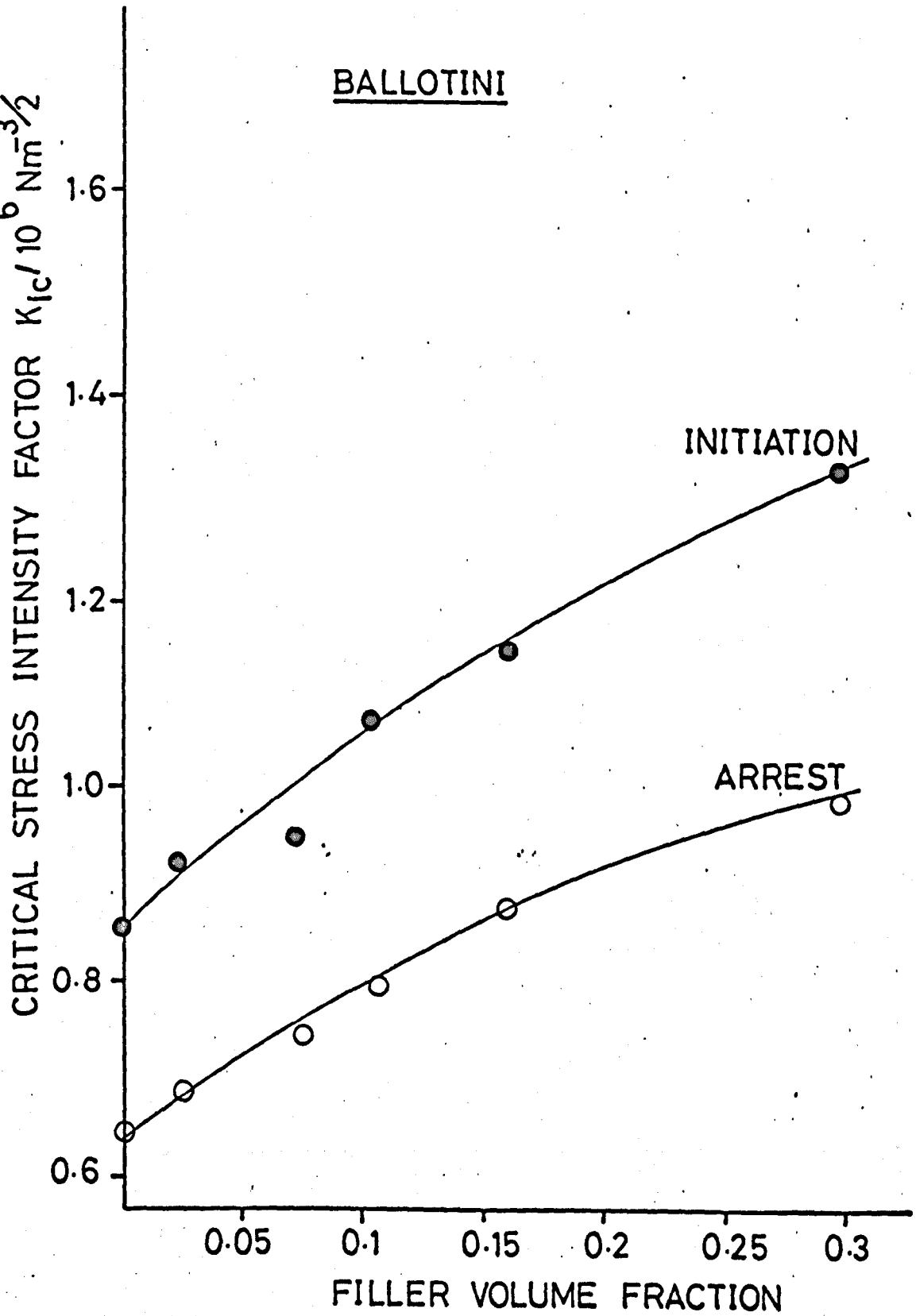

Fig. (4.16) K_{Ic} for ballotini filled CT200/HT901 composites as a function of filler volume fraction

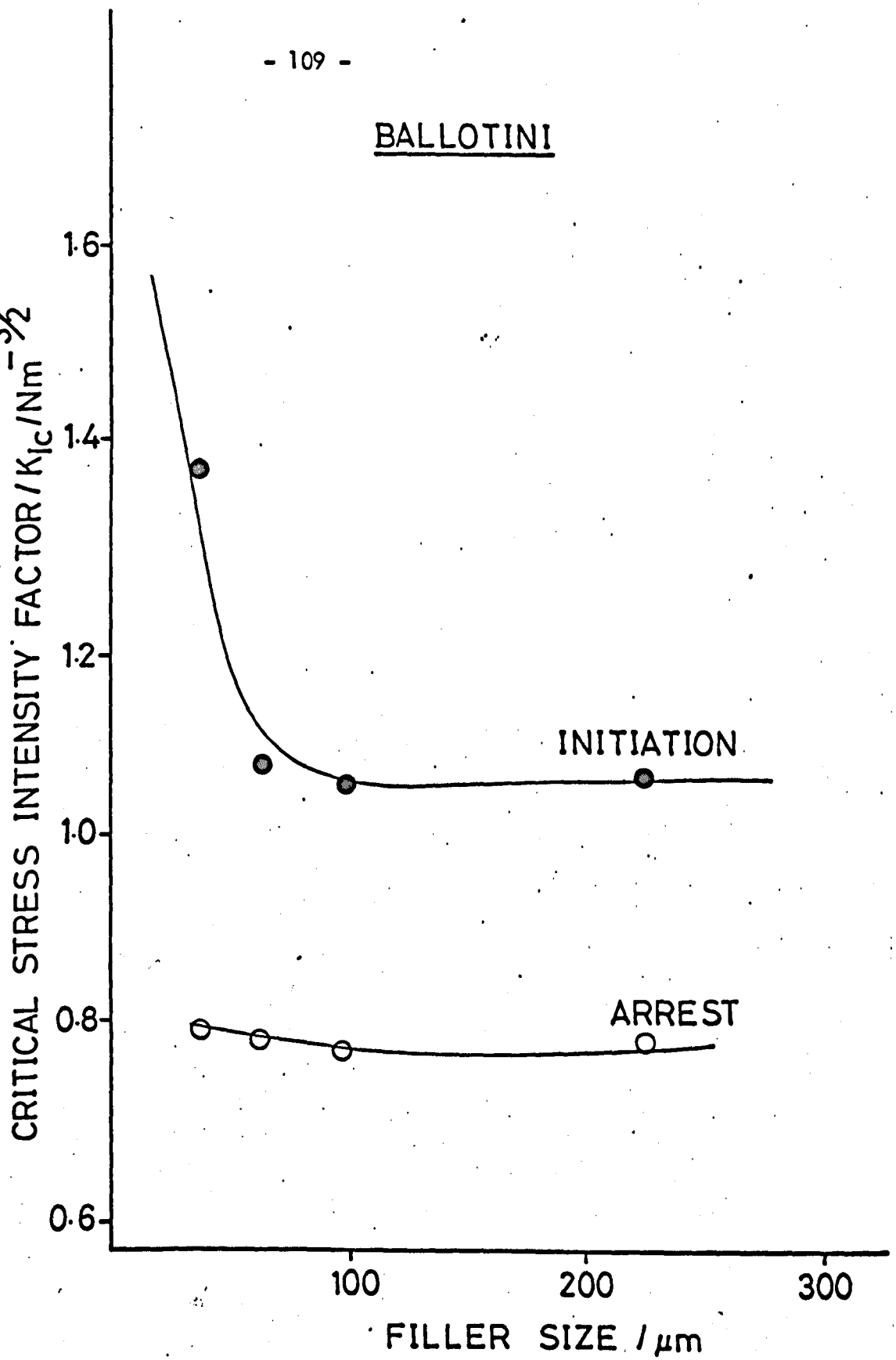

Fig. (4.17) K_{Ic} for ballotini filled CT200/HT901 as a function of filler size.

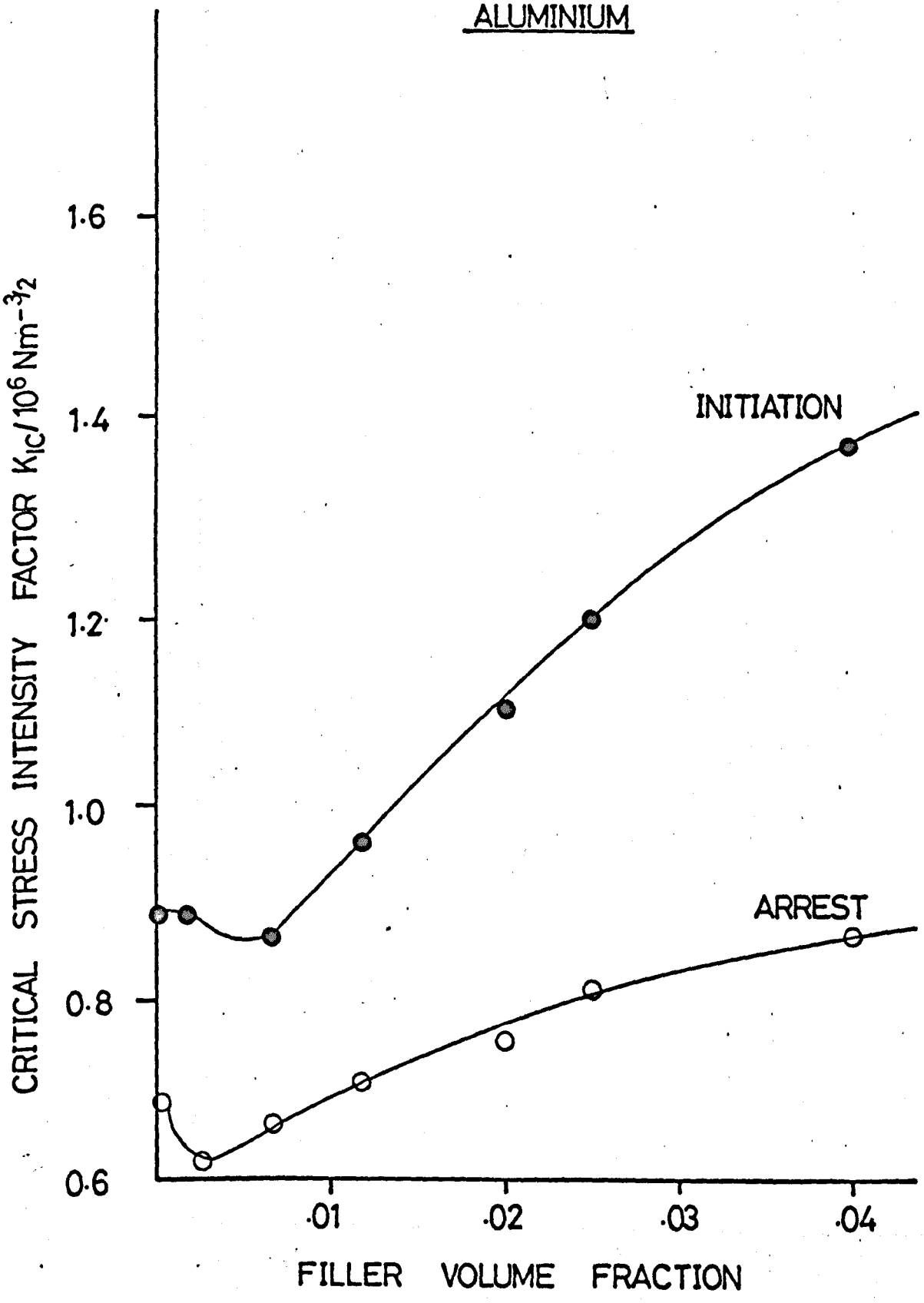

Fig (4.18) K_{Ic} for aluminium filled CT200/HT901 as a function of filler volume fraction

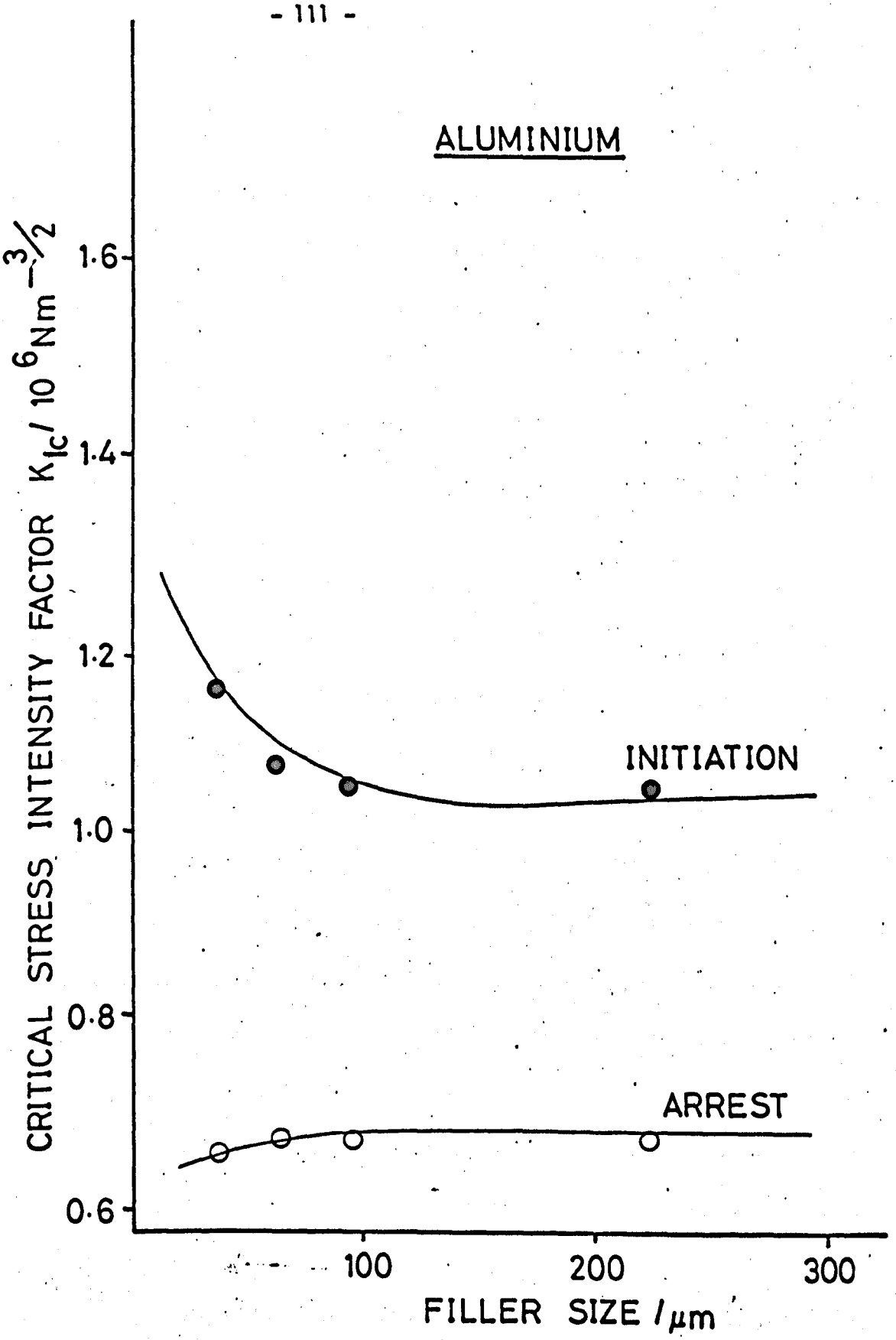

Fig. (4.19) K_{Ic} for aluminium filled CT200/HT901 as a function of filler size.

range, have a higher initiation value of critical stress intensity factor but a lower arrest value. The general trends in K_{Ic} with volume fraction are however similar, see Fig. (4.20). The critical stress intensity factors are yet again essentially independent of particle size above about 75 μm, a possible increase in the initiation value being observed below this figure: Fig. (4.19) demonstrates this for composites containing a 0.025 volume fraction of unetched aluminium.

4.4. Preliminary Discussion

The main unambiguous feature of the addition of our particulate fillers to an epoxy resin matrix is to produce a general increase in fracture energies, critical plane strain stress intensity factors and Young's moduli over and above that of the base matrix. Glass and aluminium, although brittle and ductile respectively, produce qualitatively similar changes both in fracture roughness and in Young's modulus; the fracture toughness of the ballotini filled composites increases linearly with filler volume fraction. A non-linear increase is observed in the fracture toughness of the aluminium filled composites. Within the size ranges examined, size has little effect on the fracture toughness parameters although a possible ill-defined increase in the initiation fracture energies and critical stress intensity factors is observed for glass and aluminium powders which have a particle size of less than about 50 μm. Glass and aluminium filled composites show similar non-linear reductions in Young's modulus as the particle size is increased.

Alumina was used in the hope of exploring the apparent increases in fracture toughness when particles smaller than about 50 μm were used; unfortunately it was impossible to disperse the 1.0 μm and the 0.05 μm alumina in the epoxy resin matrix.

A double cantilever beam technique was successful in demonstrating

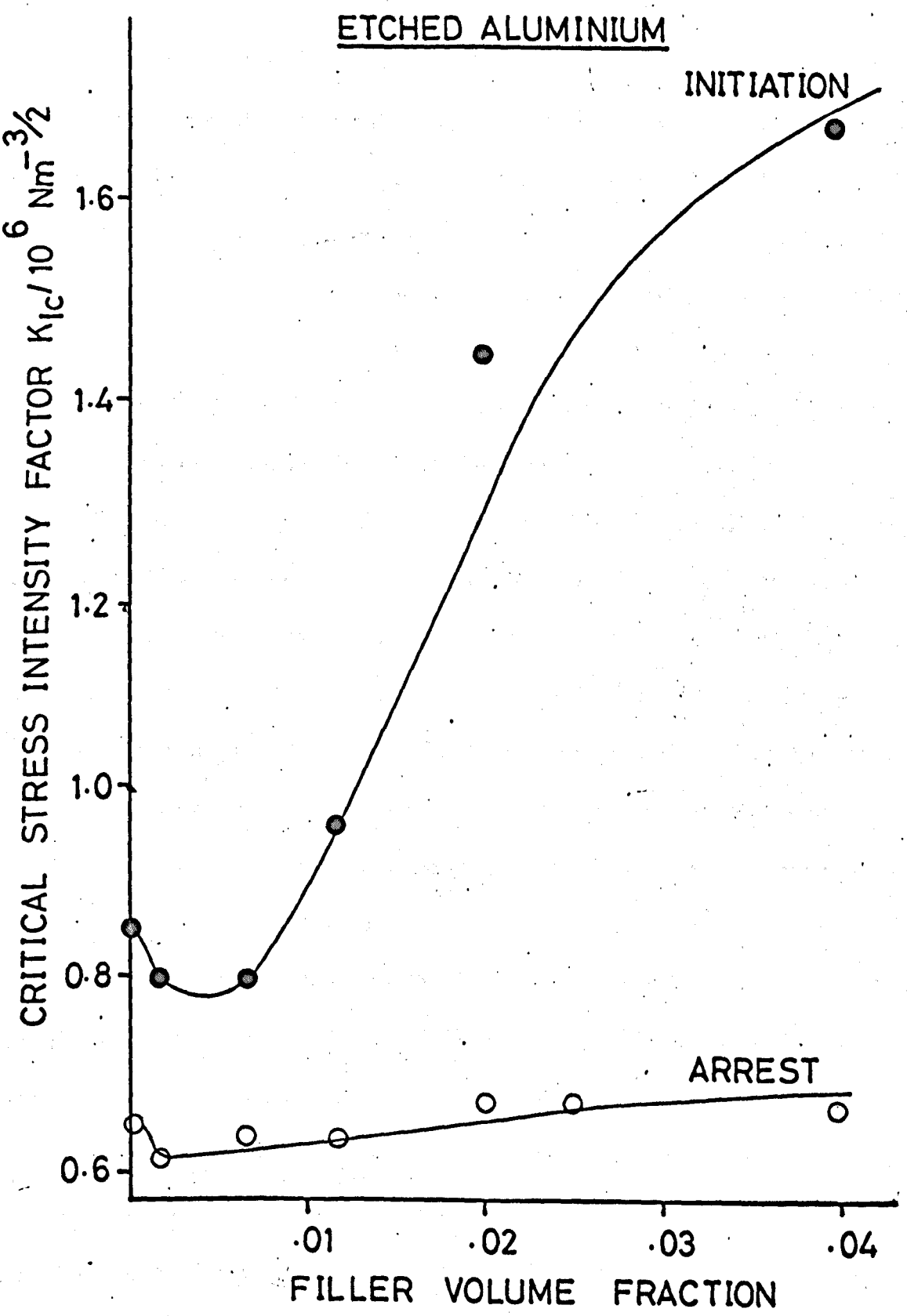

Fig. (4.20) K_{Ic} for etched aluminium filled CT200/HT901 as a function of filler volume fraction

that silane etching treatments do not modify the adhesion between an anhydride cured epoxy resin and a clean glass surface. In addition, the treatment of talc with an adhesion promotor and mica with a silicone release coating did not affect the fracture behaviour. However, etching of the aluminium with chromic acid was shown to affect the fracture toughness of composites produced using such a powder as a filler. The crack initiation fracture toughness parameters were increased and the crack arrest parameters decreased, when etched rather than normal aluminium particles were used.

The fracture energies of the two composites investigated, CT200/HT901 plus a 0.1 and 0.025 volume fraction of ballotini, and aluminium respectively are insensitive to effective extension rate over the range investigated. Similar results may also be expected for composites containing up to a 0.3 volume fraction of ballotini and a 0.04 volume fraction of aluminium. This conclusion may be drawn since intercepts were not observed on the graphical representation of data used for determining $\gamma_{F\delta}$ from the Srawley and Gross corrected formula. One may recall that intercepts on these graphs were shown to arise from the variation in the fracture energies, of the material under test, with effective extension rate. The physics of the time-dependent processes occurring at the tip of a crack in these filled materials is likely to be quite complex because, when a second phase is added to the matrix, a range of local effective extension rates are found in different regions around the crack tip. The effective rate will be dependent not only upon the crack length and applied cross-head speed but also upon the stress raising properties of the filler particles, their distribution and concentration.

The effect of temperature on our composite materials is interesting not only for practical reasons but may provide very useful insight into the mechanism of particle toughening. One of the more important features of a composite material that has been

fabricated from components with different thermal expansion coefficients are the "frozen-in" stresses produced when the composite is cooled from the glass transition temperature, or melting point of the matrix, to the test temperature. These stresses cannot be relieved by an annealing treatment and, during fracture, a crack has to propagate through an extremely complex stress field which will be the resultant of these frozen-in stresses and those produced by the applied load and stress raising properties of the filler particles. The magnitude of these frozen-in stresses may be reduced by fracturing composites at an elevated temperature. The interpretation of data from such experiments is complicated by the additional fact that the fracture energy of the matrix is itself temperature sensitive. Fig. (4.21) was derived from Figs. (3.5) and (4.11), which summarise the variation with temperature of the fracture energies of the CT200/HT901 matrix and the given composite and shows the difference between the fracture energies of the matrix and the composite at each selected temperature. The initiation fracture energy difference shown in Fig. (4.21) increases as the temperature is raised towards the glass transition temperature of the matrix, i.e. the fracture energy difference increases as the frozen-in thermal stresses decrease This suggests strongly that the existence of frozen-in microstresses due to the miss-match in thermal expansion of the matrix and the filler are not responsible at least for the major part of the increase in toughness of the filled materials. We shall, however, return to the discussion of this problem in the final chapter.

There are no obvious trends in the effectiveness of filler types; the data summarised here perhaps presents a rather gloomy picture from an engineering stand-point since, excluding the specific case of chopped glass fibres, only talc, and to a lesser extent graphite, offer any means of producing a useful increase in crack arrest fracture toughnesses by the addition of finely dispersed particles. It is this parameter,

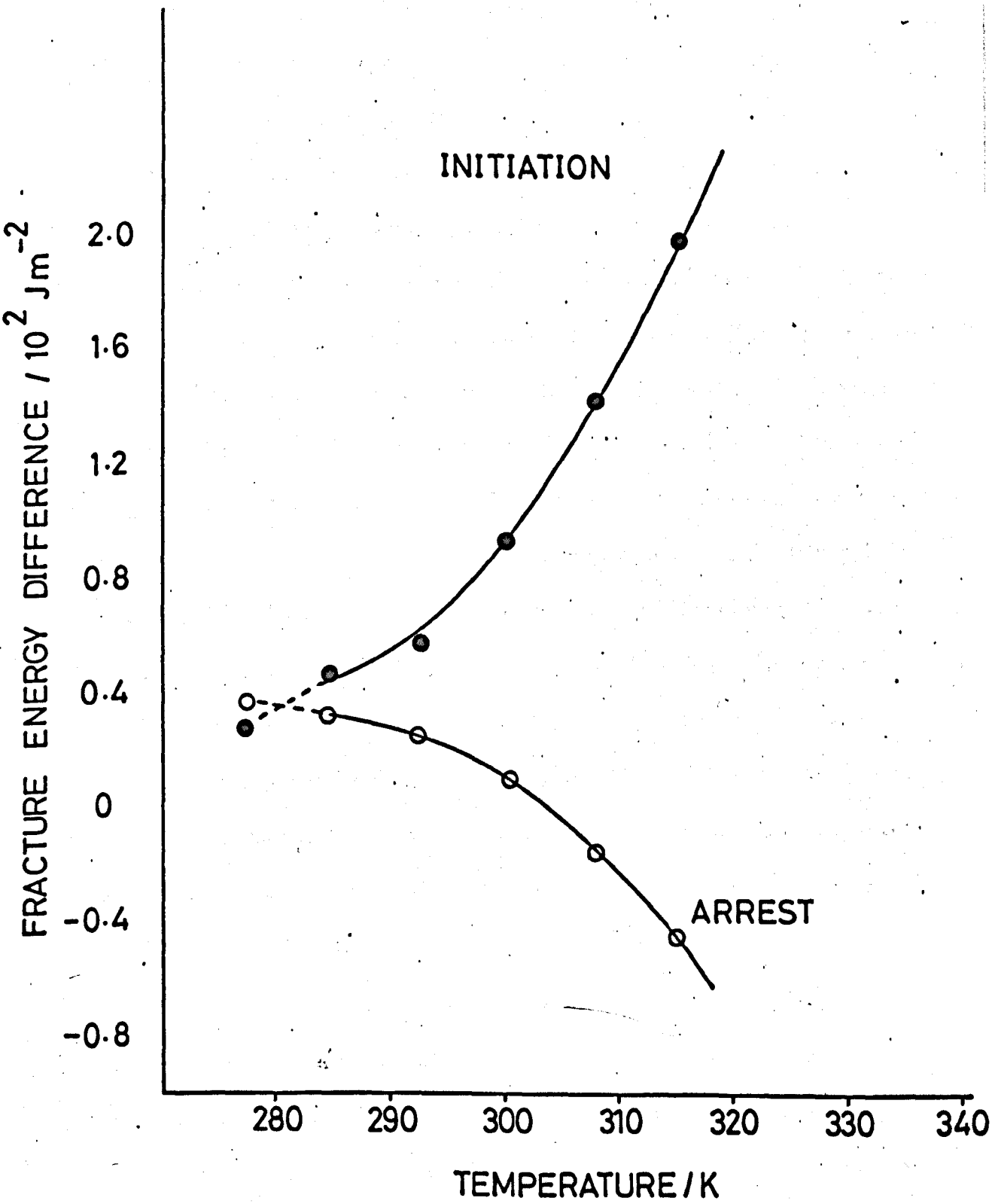

Fig. (4.21) Fracture energy difference for a ballotini filled CT200/HT901 composite as a function of temperature

as opposed to the crack initiation toughness, that is of principal interest to a design engineer since he must calculate the maximum applied stress that can be tolerated at any time in a structure having a crack of a known length. Unfortunately, further complications arise in our tests of the talc and glass-strand filled composites since double cantilever beam specimens are only appropriate for a plane strain test if the crack tip plastic zone is small compared with the thickness of the specimen. In practice this implies that our standard size of specimens are only appropriate for plane strain tests if the fracture energy is less than about $5 \times 10^2 Jm^{-2}$. If both plane strain conditions and homogeneity are to be maintained, then chopped-fibre filled specimens about ten times larger than those used here would be required. The effort involved in producing and testing such large specimens is the principal reason why only a few results were obtained with this filler. Similar arguments are applicable to the talc-filled materials; the difficulty is underlined by the observation of large inhomogeneous, inelastic deformation zones around the crack tip. The whitening which is a consequence of this deformation was seen to extend for some distance into the cantilever arms. Although the results quoted for the talc and chopped glass strand filled materials were not obtained under true plane strain conditions they do indicate, however, that these two types of filler offer a means of dramatically increasing the fracture toughness of an epoxy resin.

We shall leave the main discussion and interpretation of the results and observations presented here until a later chapter since it will be useful to describe next the experiments performed and the results obtained with some materials when their relative engineering merits were assessed by the more conventional, though arbitrary Charpy impact test.

CHAPTER V

The Charpy Impact Energy "Notch Toughness Parameters" and Modulus of Rupture of Various Composites

5.1. Introduction

The Charpy impact test has been used for many years by engineers to rank the traditional, structural metals and alloys which exhibit untoward brittle fracture under impact loading or are "notch sensitive". The results of these tests are extremely difficult to interpret from a fundamental viewpoint but have, nevertheless, proved useful in practice since the information obtained does correlate with the in service behaviour of many of these materials.

The results presented here are from Charpy impact tests performed on samples cut from the cantilever arms of specimens that had already been fractured during the determination of fracture energies and critical stress intensity factors. Care was therefore taken to remove any material from the region close to the fracture surface which may have been "damaged" during the earlier experiments. The impact results showed a pronounced inverse correlation with the fracture toughness parameters, i.e. those materials with the highest fracture energies or critical stress intensity factors in general had the lowest Charpy impact energies, and vice versa. Tentatively, this was thought to be due to the fact that the impact energies of these materials reflected the difficulty in initiating a crack from a relatively blunt notch.

To explore further this tentative hypothesis some additional measurements

were made of the modulus of rupture and the value of $\left(\frac{\Delta U}{\Delta L}\right)_N$ when fracture is initiated from an arbitrarily blunted crack. $\left(\frac{\Delta U}{\Delta L}\right)_N$ is a measure of the rate of release of strain energy when a "sharp" propagating crack is nucleated at the tip of the notch. These experiments will be described in the course of this chapter, but first we shall review the Charpy impact test and summarise the results obtained with our materials.

5.2. The Charpy Impact Test

The Charpy impact test determines the energy expended by a standard pendulum in breaking, in a single blow, a standard beam specimen. A diagrammatic representation of a Charpy impact machine is shown in Fig. (5.1). A standard specimen which is supported as a simple beam is broken by a blow delivered midway between the specimen supports, and if the specimen is notched, opposite a standard notch. The so-called impact strength is given by the difference in energy of the pendulum before and after impact, suitable corrections having been made for friction and air resistance. (For the sake of consistency we shall call this parameter the impact energy.) Machines used for determining the impact energy of metals are generally designed so that the velocity of the pendulum is 3.5 m s^{-1} which implies an initial elevation of the pendulum of 650 mm. A commercial machine for the testing of "plastics" and manufactured by Tensometer Limited was used throughout this work and employs a pendulum elevation of 300 mm: corrections for friction and air resistance were included in the calibration of the instrument which was supplied by the manufacturers.

The specimens used for the impact tests were produced from the separated arms of the double cantilever beam specimens which had already been used for fracture

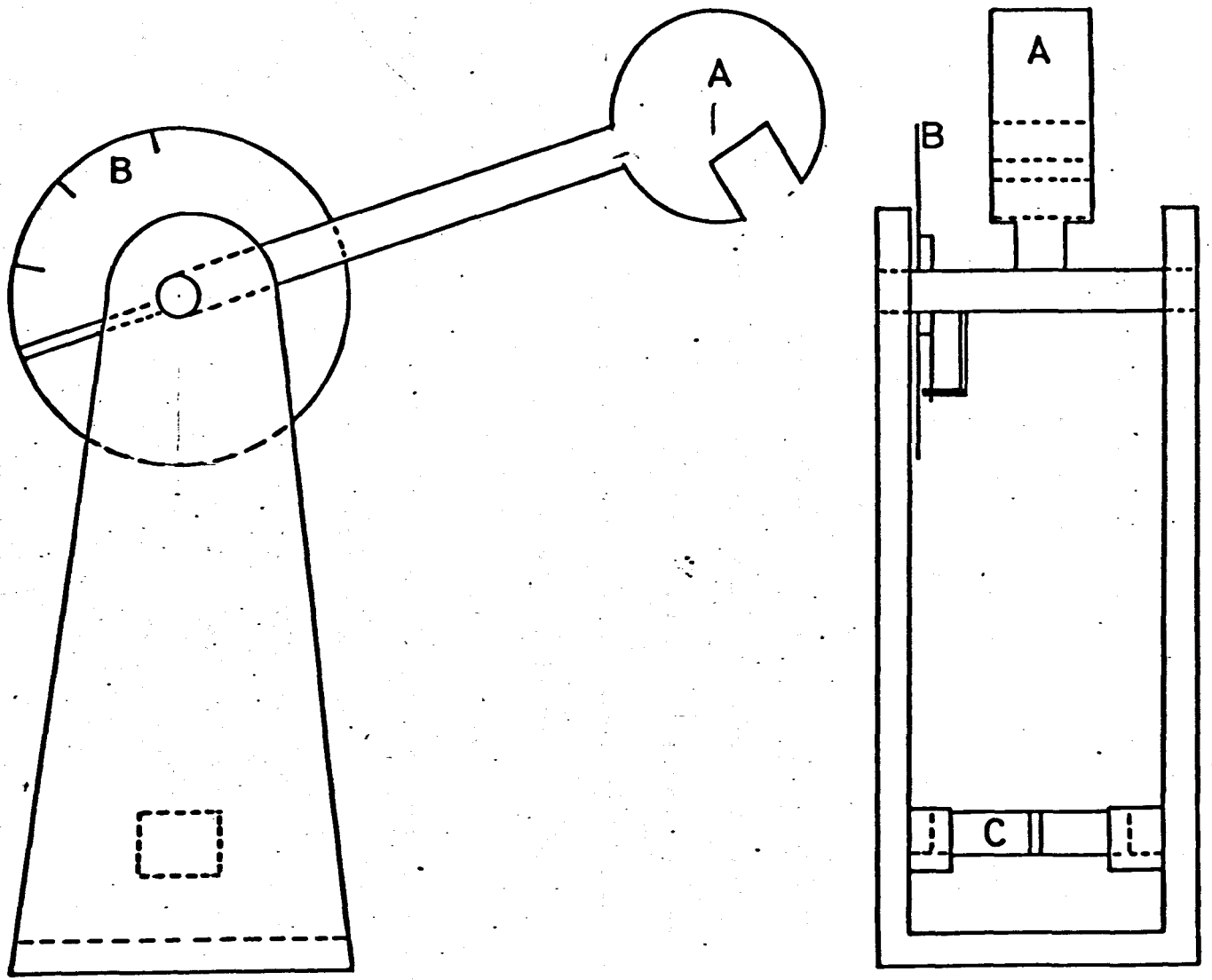

Fig. (5.1) Diagrammatic representation of a Charpy impact machine

energy determinations. The only preparation required was cutting to length, and the milling away of the original fracture surface, to produce a section of 10 x 6 mm. Care was however taken, particularly with the talc filled composities, to remove all the whitening associated with the earlier crack propagation. Most of the tests were conducted on notched specimens but some data was taken using unnotched samples. Where notching was required, a machine, also supplied by Tensometer Limited, was used to produce a notch, 1 mm deep and with a root radius of 0.25 mm always in what was a side face of the original double cantilever specimen. Samples were broken, after centering the notch between the anvils, with a pendulum chosen to give an instrument scale reading between 2 and 8. Unnotched specimens were fractured in a similar manner and the energy lost by the pendulum was obtained from the instrument scale reading using the conversion tables supplied with the instrument. The energy lost was then divided by the area of the fracture surface.

As is common with impact tests performed on many materials, a considerable scatter in the results existed and hence all the data quoted later in this chapter are mean values obtained from at least twenty specimens: 90% confidence limits, which were calculated in the normal manner with the aid of the Student's t distribution, are included on the graphs to give an indication of the magnitude of this scatter.

5.3. The Modulus of Rupture of Various Materials

The modulus of rupture of various samples was obtained using the four-point bend configuration illustrated diagrammatically, with relevant dimensions, in Fig. (5.2). A four-point bend rupture test was used to assess the "strength" of our materials rather than the tensile test that is commonly used for ductile materials. The four-point bend arrangement was preferred since it avoids the specimen gripping problems normally

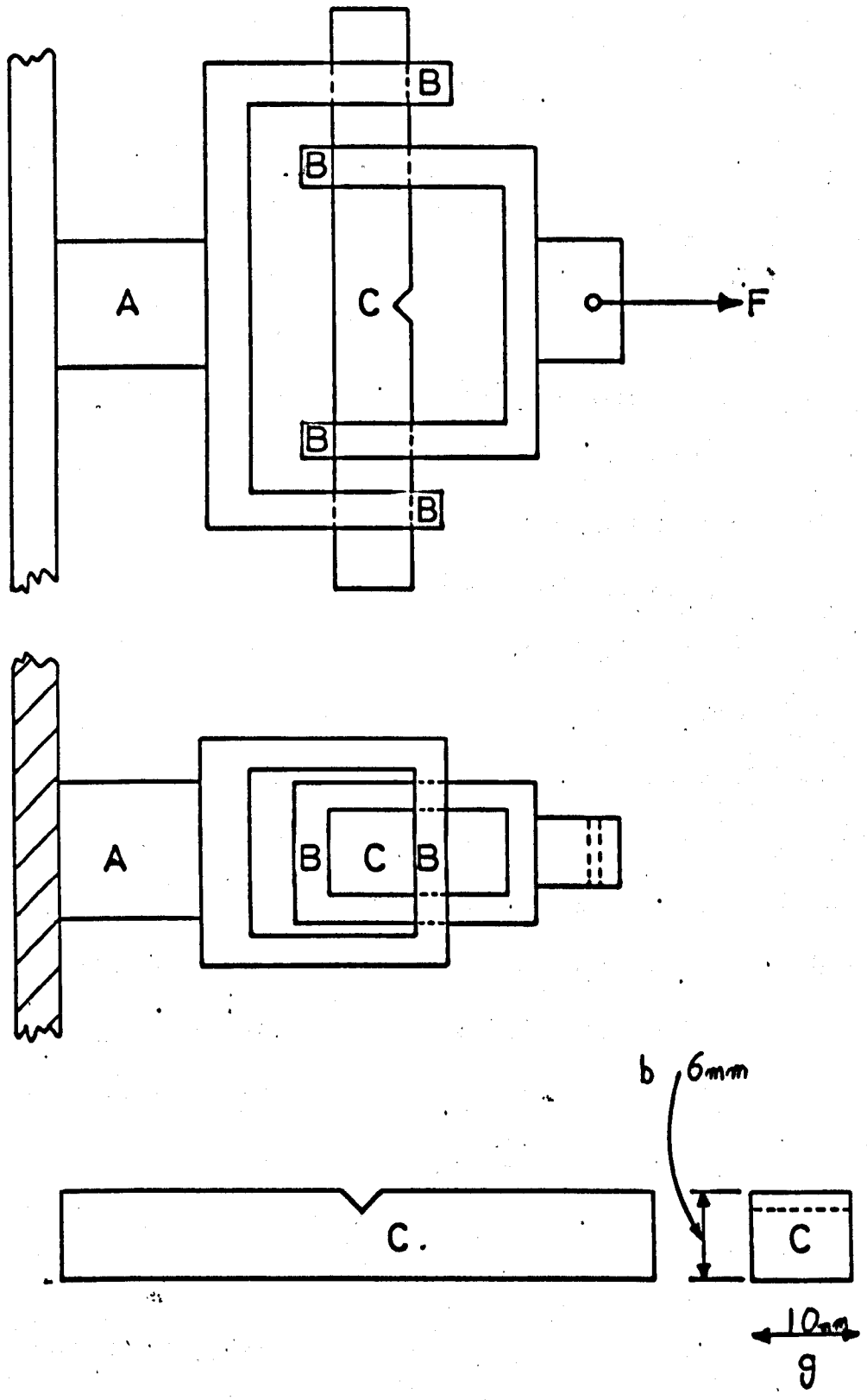

Fig. (5.2) Diagrammatic representation of the four-point bend apparatus

associated with tensile tests of brittle materials and is thus easier to perform. Experiments were again carried out using both notched and unnotched specimens. Notches 1 mm deep were cut with the same tool as used for the impact tests but a horizontal shaping machine was employed to accommodate the longer specimens required in this case. The separate arms of double cantilever beam specimens each provided two samples for modulus of rupture tests, the fracture surfaces again being removed with a milling machine to give specimens of the same cross-section as for the impact test. Notched specimens were positioned in the four-point bend rig such that the notch was on the tensile face and mid-way between the inner pair of knife edges; centralization of the notch was achieved with the aid of a pair of callipers although this is not absolutely necessary because in the four-point bend configuration the bending moment between the inner knife edges is constant. The unnotched specimens were orientated such that one of the cast faces of an original double cantilever beam formed the tensile surface. The load at fracture was recorded using an Ether type U F 2 dynamometer and a TOA chart recorder, the system having first been calibrated by dead-weight loading. Specimen dimensions were determined with a micrometer. The modulus of rupture was obtained from the load at fracture and the above dimensions using the expression:

$$Z = \frac{Mq}{2I} \qquad [5.1]$$

where: Z = modulus of rupture

M = bending moment between inner two knife edges

I = second moment of area of cross section which for a rectangular specimen of the form is shown in Fig. (5.2) is $\frac{bg^3}{12}$

5.4. The "Notch Toughness Parameters" of Some Arbitrarily Blunted Cracks

A value of $\left(\frac{\Delta U}{\Delta L}\right)_N$, the rate of release of strain energy, when fracture is initiated from an arbitrarily blunted crack was determined using the standard double cantilever beam technique. A hole of 0.25 mm radius, i.e. the same as the root radius of the notches used for the impact and modulus of rupture tests, was drilled through the thickness at a point 150 mm down the length of a double cantilever specimen and a crack propagated with the aid of the simple hand-cranked machine until it terminated in this hole. The "notch energy", and the related "notch critical stress intensity factor", K_{NC} were determined in the standard manner, i.e. by using the "crack length", cantilever opening displacement and the peak load required to initiate fracture in equation [1.35]. These parameters will clearly not be fundamental material characteristics but rather a function of both the material and the hole size. The expressions used to calculate these plane strain values were derived using assumptions based on linear elastic fracture mechanics which may only be justified rigorously for elastic cracks. These expressions may however be used without significant error in cases where the plastic zone size is small compared with the crack length and specimen dimensions. In the present case, although the hole size is small compared with crack length, it is not small when compared with the thickness of the specimen in the central groove. However, we are concerned here with specimens and holes all of the same size and hence we may compare the values of $\left(\frac{\Delta U}{\Delta L}\right)_N$ and K_{NC} for different materials even though these do not correspond unambiguously either to loading conditions of plane strain or plane stress.

5.5. Results

The results of the notched Charpy impact tests are summarized in Figs. (5.3),

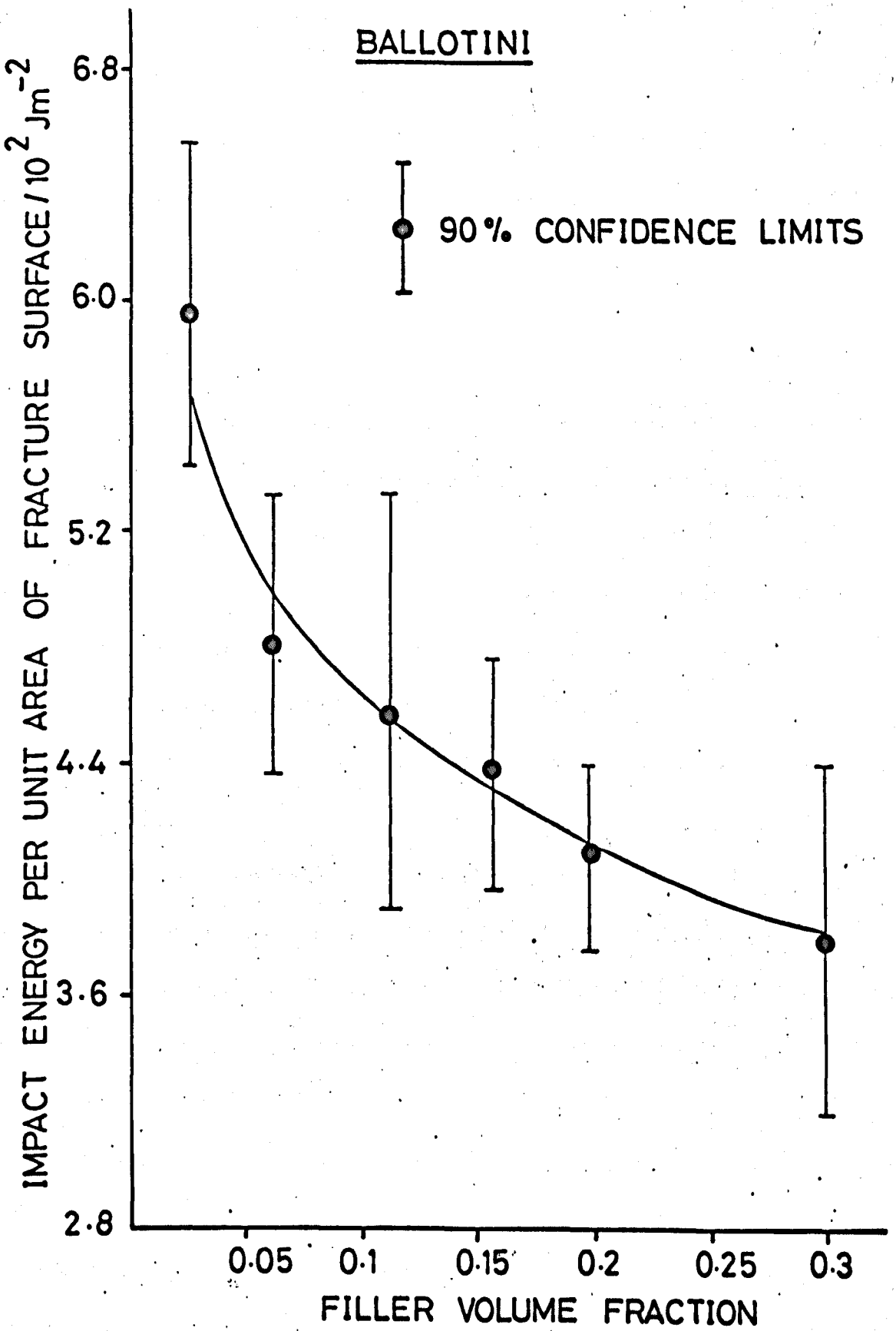

Fig. (5.3) The "impact energies" of ballotini filled CT200/HT901 as a function of filler volume fraction

(5.4), (5.5) and (5.6). The additional results from the modulus of rupture tests, the unnotched Charpy impact tests and the "notch toughness parameters" are presented in table (5.1).

5.6. Discussion

The most striking feature of the notched Charpy impact values is the inverse correlation with the normal material fracture energy: i.e. the materials within this group which have higher fracture energies have lower Charpy impact energies. A general non-linear decrease in the impact energy occurred when the volume fraction of filler and the filler sizes were increased although there appears to be an anomalous value at a 0.04 volume fraction of aluminium. Reasonable correlations do however exist between the notched impact energies, the "notch toughness parameters" and the notched modulus of rupture.

Any comparison of unnotched impact and modulus of rupture results is unfortunately rather difficult without some further work because of the large inherent scatter in the data, (the 90% confidence limits are included in table (5.1) to give some indication of this scatter.) It does however appear that the impact energies of the unnotched specimens correlate with the modulus of rupture.

At first sight the inverse correlation of fracture energy with notched impact energy may appear rather alarming as both these methods of "ranking" materials are often referred to in the literature as fracture toughness tests. However, the energy extracted from the falling pendulum and used as a measure of the resistance of a standard specimen to fracture under a specific rate of loading may be considered to be resolvable into the following components:

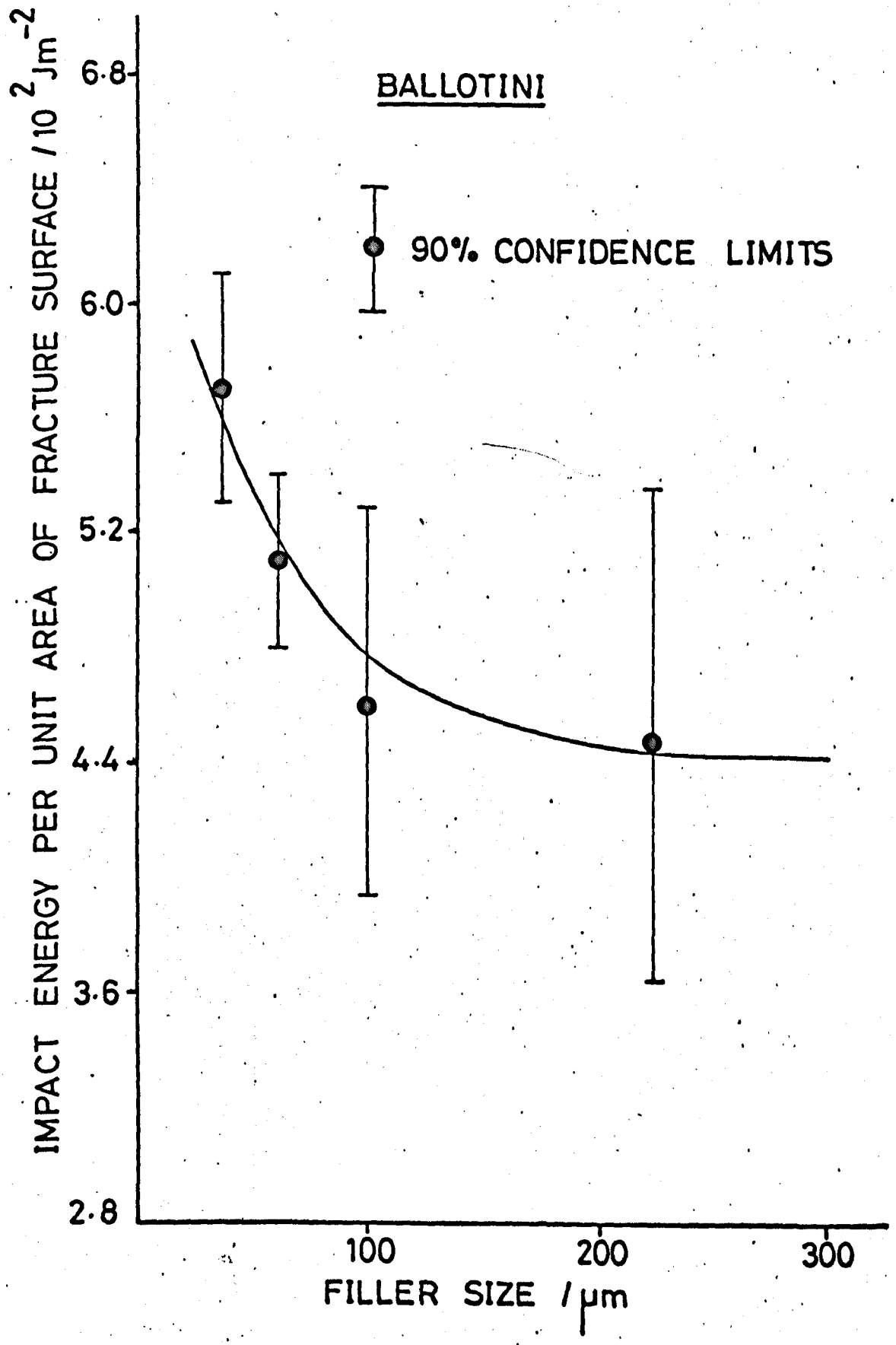

Fig. (5.4) The "impact energies" of ballotini filled CT200/HT901 as a function of filler size

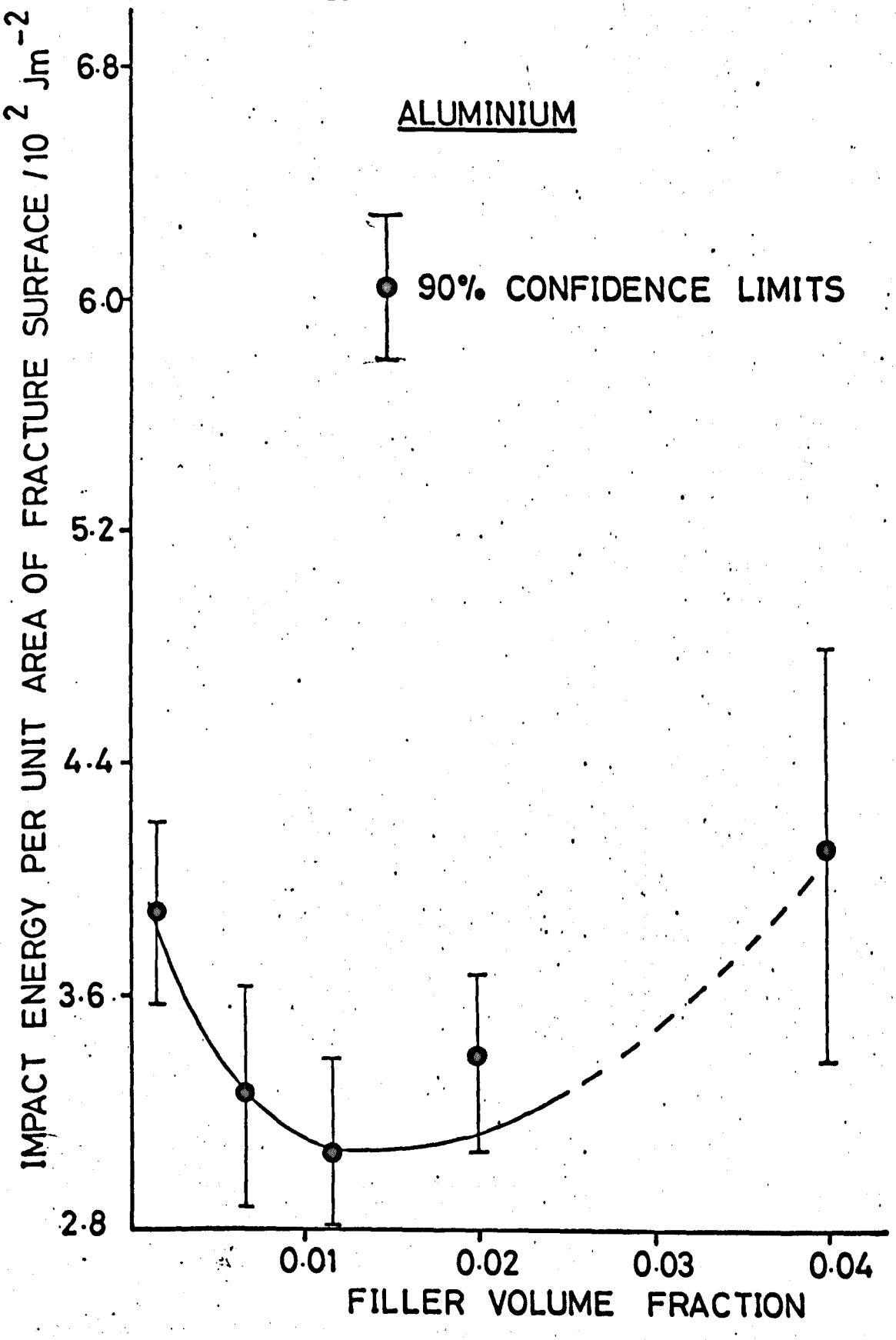

Fig. (5.5) The "impact energies" of aluminium filled CT200/HT901 as a function of filler volume fraction

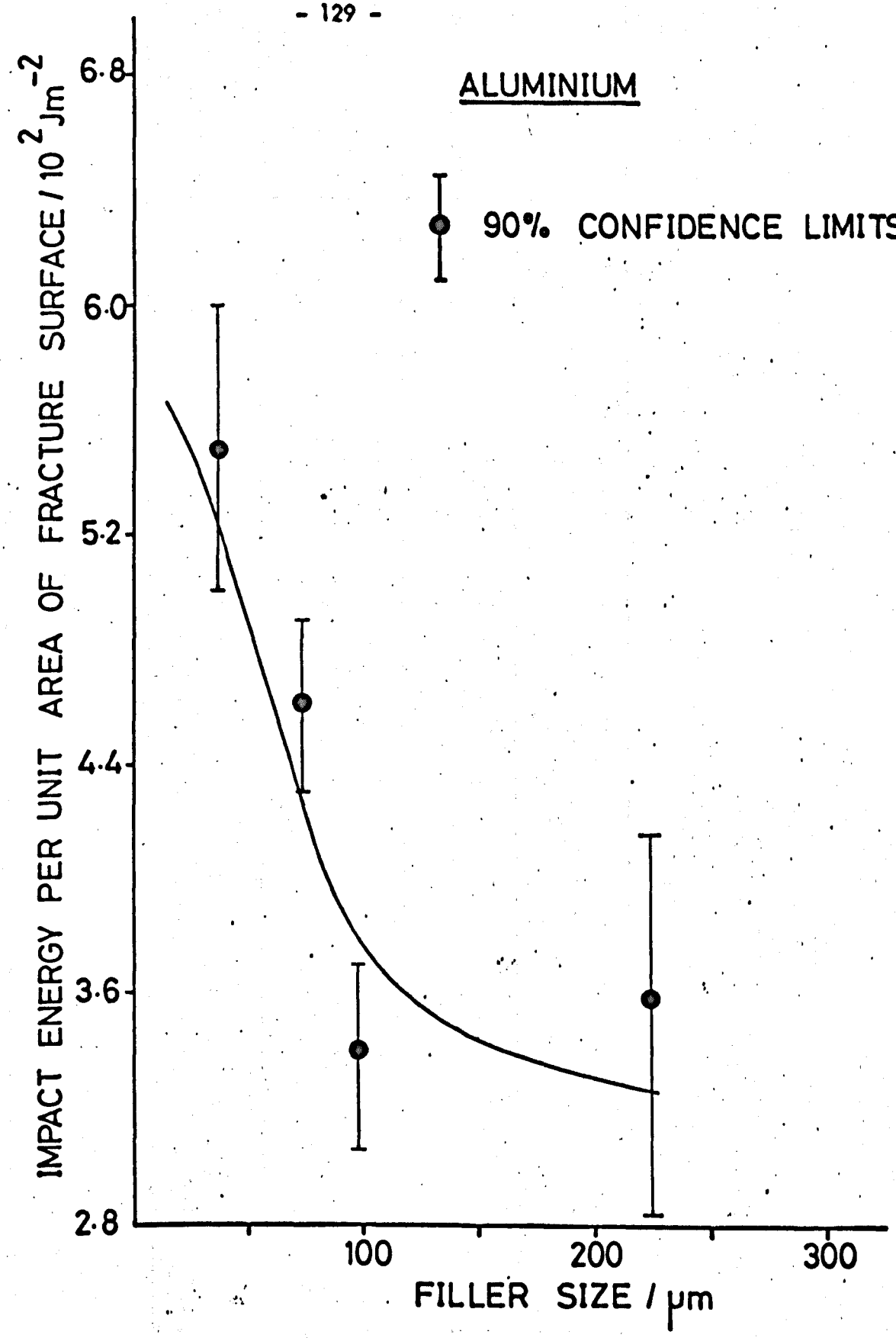

Fig. (5.6) "The "impact energies" of aluminium filled CT200/HT901 as a function of filler size

TABLE (5.1)

The Fracture Energies, γ, Moduli of Rupture, Z, Impact Energies, IE, and "Notch Toughness Parameters" of Various Materials

Material	I^{γ} / $10^2 Jm^{-2}$	A^{γ} / $10^2 Jm^{-2}$	Z unnotched / $10^8 Nm^{-2}$	Z notched / $10^8 Nm^{-2}$	IE unnotched / $10^2 Jm^{-2}$	IE notched / $10^2 Jm^{-2}$	$\left(\frac{\Delta U}{\Delta L}\right)_N$ / $10^2 Jm^{-2}$	K_{NC} / $10^6 Nm^{-\frac{3}{2}}$	2IE notched / $\left(\frac{\Delta U}{\Delta L}\right)_N$	Z notched / IE notched / $10^4 m^{-1}$
CT200/HT901	1.2	0.75	1.1 (90% limits at 1.5 & 0.7)	0.35	36.0 (90% limits at 45.0 & 27.0)	6.0	142	6.3	0.085	5.8
CT200/HT901 + a 0.1 volume fraction of 100μ m ballotine	1.45	0.85	0.85 (90% limits at 1.1 & 0.6)	0.26	32.2 (90% limits at 38.2 & 26.2)	4.6	25.6	3.0	0.36	5.6
CT200/HT901 + a 0.025 volume fraction of 100μ m aluminium	2.0	0.80	0.65 (90% limits at 0.95 & 0.35)	0.16	22.4 (90% limits at 32.4 & 12.4)	3.2	15.36	2.25	0.42	5.0

(i) The elastic energy to deform the specimen.

(ii) The energy to initiate fracture.

(iii) The energy to propagate the fracture through the specimen.

(iv) The energy to impart kinetic energy to the broken specimens.

(v) Energy lost through friction, vibration of the base, air resistance, etc.

The components in (v) need not concern us greatly as these are usually eliminated by careful design, or corrected for by a calibration procedure.

Let us now consider each of the other components in turn. The energy of the pendulum at the point of impact will be dependent only upon the mass of the pendulum since its length and drop distance were held constant. Some of the pendulum kinetic energy will be expended in deforming the specimen up until the point of initiation of a crack from the machined notch, i.e. in imparting elastic strain energy to the specimen. A necessary condition for crack initiation is that the stress at the tip of the notch must exceed a critical value and therefore the kinetic energy of the pendulum will be extracted as strain energy up until the point at which the stress at the notch is sufficient for the crack to be initiated. The amount of elastic energy present in the specimen at initiation will therefore be a function of the critical stress required for initiation, the elastic modulus of the material, the depth and shape of the notch, and the dimensions of the specimen.

Some additional energy will be consumed, before the criterion for crack initiation is satisfied, to produce a plastic zone at the tip of the notch. The excess energy over and above the amount normally associated with the plastic work at a crack tip may be considered as being the energy consumed during crack initiation.

Component (iii), i.e. the energy to propagate the fracture across the specimen

is related to the fracture energy as determined by the double cantilever beam technique, although it is not immediately obvious which of either the initiation or arrest fracture energies should be considered, The initiation fracture energy is the energy required to propagate a pre-existing crack, whilst the arrest value gives essentially the minimum energy to propagate a crack that is already extending. The fracture energies presented here are quasi-static parameters since estimates were made at the beginning and end of a crack jump whereas the fracture energy we now require is for a rapidly propagating crack. However, we can set some limits on its value since it must clearly lie between the initiation and arrest fracture energies.

Component (iv), the kinetic energy given to the fracture pieces may be estimated using simple Newtonian mechanics; experimenters often apply such corrections to obtain what they consider to be more appropriate impact energies. The average kinetic energy of the resulting fracture pieces was estimated as being about 2×10^{-2} J; this is a considerable fraction, typically about half, of the total energy required to fracture the impact specimens. By contrast the energy required to propagate the fracture across the specimen is on average about 40% of the total impact energy, although this figure varies from one of our materials to another because of the inverse correlation between fracture and impact energies.

It may be tentatively concluded from the results presented, and the preliminary discourse, that the impact energy of our epoxy resin and associated composite materials is determined by the amount of plastic and elastic strain energy that must be supplied to the impact specimen, in order to achieve a stress at the root of the notch sufficient to initiate the fracture. All the other components of energy are then extracted from the strain energy and not from the remaining energy in the pendulum. If this is the case, then we would expect the impact energy values to correlate not with the fracture

energy but with the "notched toughness parameters", this is in fact is observed. Table (5.1) also indicates that there is not only a correlation between impact energies and "notch toughness parameters" but that these also correlate with the modulus of rupture of notched four point bend specimens. This is again to be expected since this modulus of rupture is a measure of the stress at which failure occurs from the blunt notch.

Any attempts at correlating the unnotched impact and modulus of rupture results is unfortunately somewhat difficult because of the large scatter in the estimated values. It is expected, however, that similar principles apply but in this case we will be concerned with the critical stress required to initiate fracture from a pre-existing surface flaw, or an internal defect, which may well be a filler particle.

The above discussion has been concerned primarily with attempts to explain why the fracture energies of our materials, do not correlate with Charpy impact energies. We have not yet considered why it is more difficult to propagate a pre-existing crack in our composite materials than it is in the base matrix, but, on the other hand, it is easier to initiate a crack from a blunt notch in a composite than in the base matrix. Discussion, from a phenomenological viewpoint, of these central and fundamental features of the results will be taken up in the final chapter. It will be convenient first of all to describe a series of measurements of the flow stress which were made as part of the experimental programme, since these provide useful additional information for the discussion.

Before concluding this present chapter it may be appropriate to consider briefly the practical problem facing the design engineer who may be presented with two sets of data both of which it may be claimed give an estimate of the "toughness"

of a range of composites but one set ranks the materials in inverse order. Clearly both tests may not be used to rank possible materials for a given application and hence he must decide which test gives information that is appropriate for the application he has in mind. We have shown by the correlations presented in this chapter that the Charpy impact energies reflect the strength of our materials and this leads us back to the initial discussion of strength and toughness parameters. The latter are appropriate for design purposes only when one can specify inspection procedures to limit, or define, the maximum size of any crack produced during fabrication or by damage whilst in service and may also determine the maximum load and the loading geometry.

CHAPTER VI

The Plastic Zone Extension, Vicker's Hardness Numbers and Flow Stresses of the Epoxy Matrix Materials

6.1. Introduction

In an earlier chapter it was pointed out that the work involved in creating unit area of new surface area, during the propagation of a crack, is much greater than the normal surface free energy T and that the difference between the fracture energy, γ, and the surface free energy, T, may be attributed to the formation of a plastically deformed region ahead of the crack tip. For an elastic perfectly-plastic material where $\gamma >> T$, Irwin first showed that:-

$$\gamma = \frac{1}{2} \sigma_y \alpha$$

where:

γ = fracture energy

σ_y = flow stress

α = crack opening displacement.

The possibility of interpreting the crack propagation behaviour in terms of variations in crack opening displacements and flow stresses seemed attractive and therefore these parameters were determined.

The primary object of this digression from the main theme of the experimental

programme was to provide data that could be used in conjunction with the fracture energy results presented in Chapter III in the hope that some inferences could be made concerning the propagation of a crack in the base matrix materials and perhaps also in the composites.

Determination of the plastic zone extension, α, is in principle relatively straight forward and simply involves the measurement of the displacement at the crack tip. However, some practical complications do arise and these will be discussed later. A common, and certainly very convenient, method of finding the flow stress of a material involves the measurement of the indentation hardness; this technique is employed here and results are presented concerning the hardness and flow stress of the matrix materials as a function of the duration of loading, temperature, and environment.

6.2. The Microhardness Test

Indentations made under standard conditions may be used to define a hardness of a given material, the size of the indentation and the applied load being used to determine the required parameter. An indenter that is frequently used for this purpose is a diamond pyramid generally known as a Vicker's Diamond; the hardness figures obtained using such a pyramid are termed Vicker's Hardness Numbers or V.H.N.s. The Vicker's Hardness Number is defined as the applied force divided by the contact area under the indenter, and for a pyramid having an inclined angle of 136° the area of contact is given by:

$$\text{Contact area} = \frac{d^2}{2 \sin 68^{\circ}} \qquad [6.1]$$

where d is the length of a diagonal of the indent. If P is the applied load in Newtons

which produced an indentation of d metres then:-

$$\text{hardness number} = \frac{1.82\ P}{d^2} \qquad [6.2]$$

An indentation test is usually performed by bringing a loaded diamond into contact with a specimen at a well defined rate, known as the contact speed, until the full load rests on the specimen. This load is maintained for a specific length of time, referred to as the load duration, after which the diamond is removed.

Vicker's hardness tests are generally performed on metals but TAYLOR (1949, 1950) has demonstrated that it is possible to determine the hardness of amorphous, non-metalic materials by the same technique. An extensive study of the hardness of glass was performed by Taylor who was able to show that consistent hardness numbers, of a soda glass, could be obtained with a contact speed of 1 $\mu m\ s^{-1}$ and a load duration of 15s. Subsequent work by BREARLEY (1971), in these laboratories, has indicated that contact speeds of up to 100 $\mu m\ s^{-1}$ may be used with a given load on the diamond without producing significantly larger indents and correspondingly lower hardness numbers, MARSH (1964), in his detailed and now classic work, demonstrated that a continuous increase in the hardness of soda glass occurred when the load duration was reduced from 10^5s to 10^{-3}s; a similar effect was observed during exploratory experiments on our epoxy matrix materials and in addition it is very well documented than an analogous effect occurs in metals.

TABOR (1951) has shown that for the "softer" materials, i.e. aluminium, copper, silver, low carbon steels, etc. that the Vicker's Hardness Number is related to the uniaxial tensile stress at which plastic deformation occurs

viz: V.H.N. $\simeq$ $3\,\sigma_y$

where σ_y = flow stress after an 8% strain.

This simple relationship does not hold for the "harder" materials, such as epoxy resins, tool steels, glass, etc., or for indenters having a large included angle, where substantial elastic strains occur before the onset of plasticity. In these circumstances deformation under a Vicker's diamond may be considered analogous to that of an hemispherical cavity, in an elastic-plastic material, which is being expanded by an internal pressure numerically equal to the hardness. The hardness, P, is then related approximately to the flow stress σ_y and the Young's modulus, E, by the following expression:-

$$\frac{P}{\sigma_y} = A + B \ln \frac{E}{\sigma_y} \qquad \text{HILL (1950)} \qquad [6.3]$$

where A and B are constants. Marsh has since demonstrated that for a range of highly elastic materials, which included epoxy resins of the type used here, the ratio of hardness to flow stress varies linearly with $\ln\left(\frac{E}{\sigma_y}\right)$ and that:

$$A \simeq 0.07 \qquad B \simeq 0.6$$

We may therefore write:

$$\frac{P}{\sigma_y} = 0.07 + 0.6 \ln\left(\frac{E}{\sigma_y}\right) \qquad [6.4]$$

Marsh obtained the constants A and B by comparing the flow stresses of, "an epoxy resin", five carbon and carbon-chromium steels, P M M A , polystyrene, and a number of other materials obtained by both the indentation method and under uni-axial compression.

6.3. Basic Apparatus

It was proposed to measure the Vicker's Hardness Number as a function of load duration at several different temperatures and in a range of environments in order to provide information which could be compared with the fracture energies reported previously. GUNASEKERA (1970) had already developed, in these laboratories, the basic equipment suitable for this purpose although some modifications, recalibrations and the addition of a temperature controlled bath were required before his apparatus could be used to fulfill our requirements. Gunasekera had designed and demonstrated two separate hardness testing machines which enabled the V.N.H. of a given material to be determined for load durations from approximately 10^{-3} s to 10^{5} s with reasonable speed and accuracy. Both machines were intended to be used in conjunction with a Vicker's Projection Microscope and will now be described briefly.

The primary requirement of a hardness tester is to bring a loaded indenter into contact with a specimen at a controllable rate, maintain a constant load and then remove the indenter after a known time. The long term indenter which was used for periods of greater than 10s is illustrated diagrammatically in Fig. (6.1). The machine consists essentially of a simple cantilever (A) which carries the Vicker's Diamond (E), the height of the diamond above the microscope table may be adjusted to suit various specimen thicknesses to ensure that the diamond is vertical at the point of contact with the specimen (S). The diamond is brought into loaded contact, and

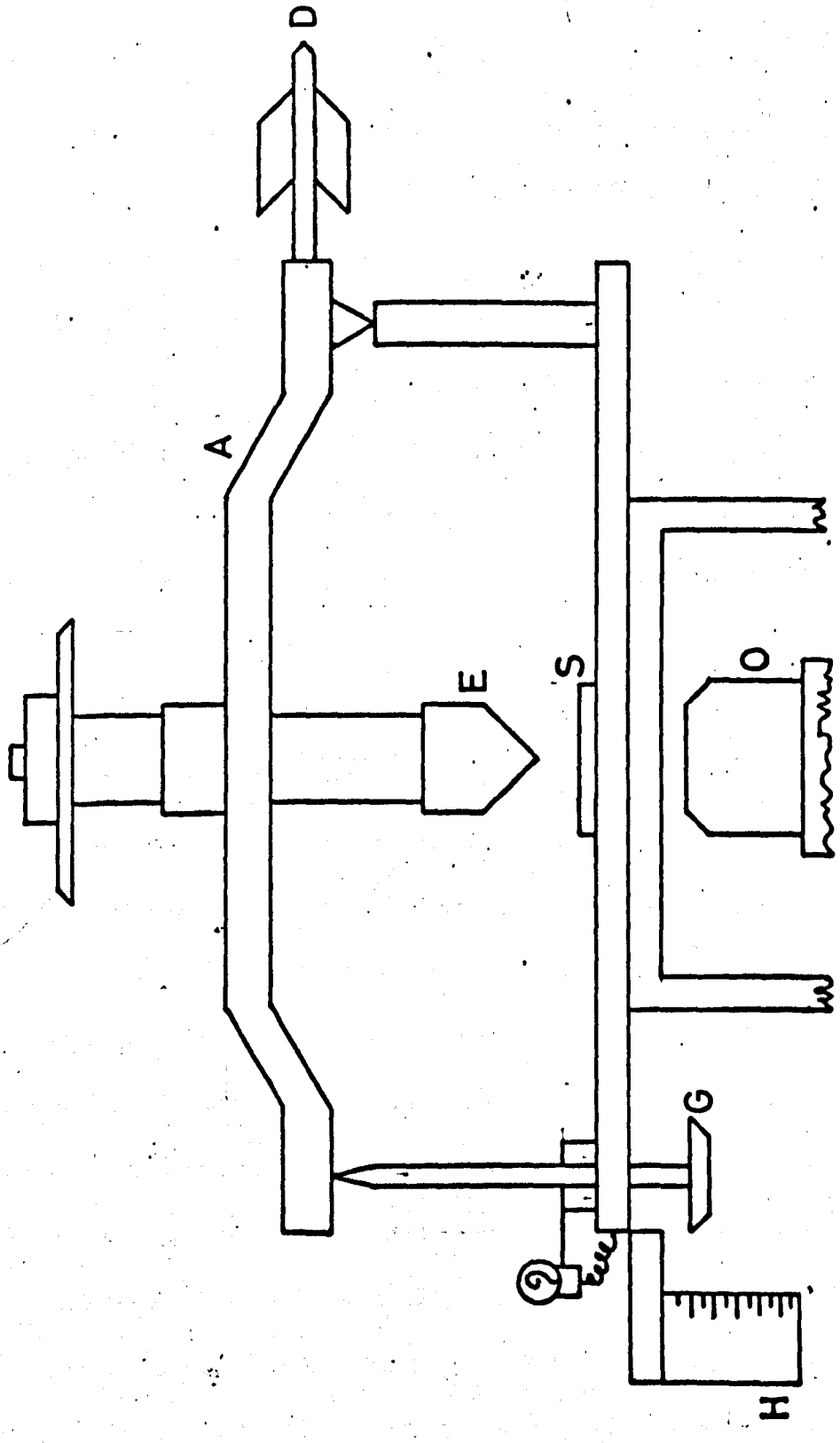

Fig. (6.1) Diagrammatic representation of the long term indenter

subsequently removed after the required time, by manual rotation of the supporting screw (G). Before any indentations were made screw (G) was adjusted to level the cantilever arm and the position of (G) marked on scale (H) so that this horizontal position could be reproduced. The lever was then balanced by adjustment of the brass counter balance weight (D); the addition of a 0.5 g weight was sufficient to deflect the arm and hence, since the lowest force used in this study was 0.5 N any error in force should not be more than 1%. Measurements of the lengths of the diagonals of the indentations were made with a bifilar eyepiece(O) used in conjunction with the projection microscope, readings being taken at each of the four corners of an indent.

The above simple cantilever machine clearly cannot be used for the short load durations and in this work was restricted to periods greater than 10s. An electromagnetic system was used for periods down to 10^{-3}s; no data was obtained for periods shorter than this because of the inherent limitations of the instrument. Gunasekera's apparatus consists essentially of an electromagnetic transducer driven by a "single shot" pulse generator. The transducer arrangement illustrated in Fig. (6.2) consists essentially of a loudspeaker magnet (A), between which was positioned in a freely moving coil (B), wound on a plastic former. The indenter (D) was supported by four leaf springs (C) and the complete system mounted on the specimen table of a Vicker's Projection Microscope. The specimen itself (H) was supported on a jig (G) in the objective mount, so that the fine focusing arrangement of the microscope could be used to lower the indenter slowly into contact with the surface of the specimen and by so doing avoid any impulsive loading effects that may have otherwise occurred.

A circuit diagram of the single shot pulse generator is shown in Fig. (6.3); the pulse length was determined by the values of capacitor selected by (SW_2) and a

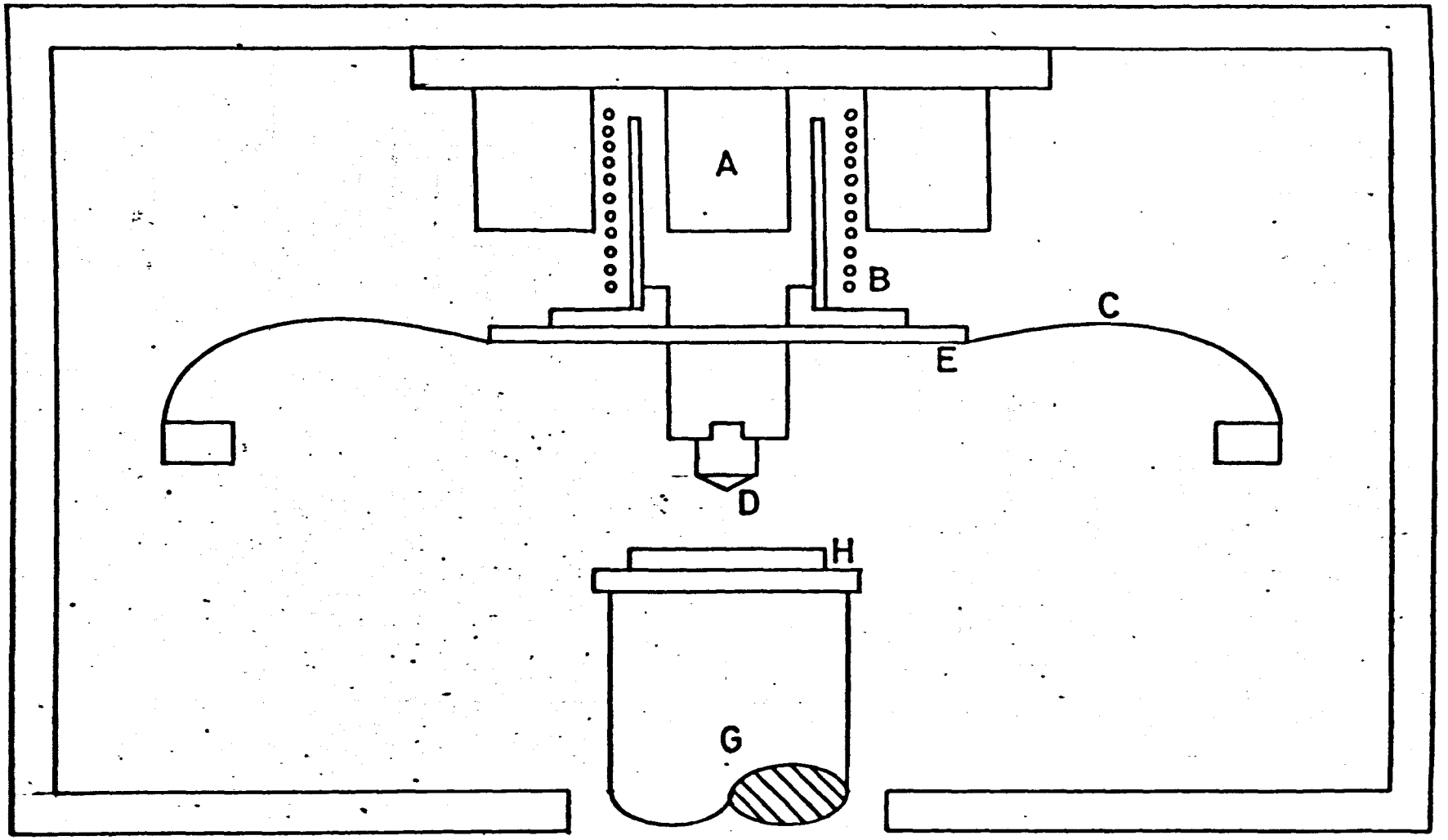

Fig. (6.2) Diagrammatic representation of the short term indenter

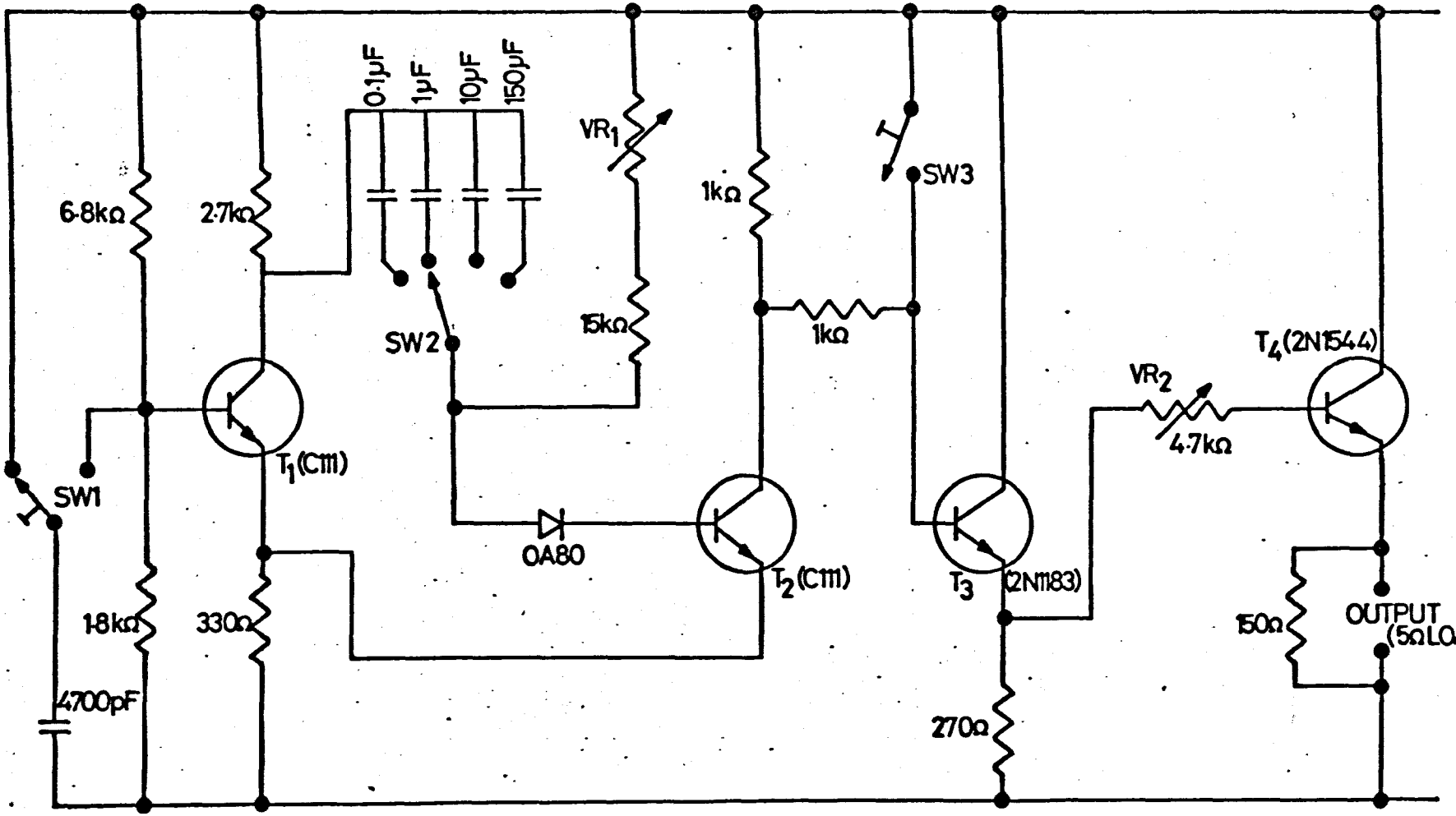

Fig. (6.3) Circuit diagram of the single shot pulse generator

variable resistor (VR_1) which allows fine adjustments of the pulse length to be made. Switch (SW_3) enables pulse lengths of greater than one second to be obtained by manual operation of the monostable multivibrator. Capacitors were chosen to give pulse lengths of 10^{-3}s, 10^{-2}s, 10^{-1}s and 1s. Oscillographic examination of the current output waveform showed that the pulse generator was supplying excellent square wave pulses to the loudspeaker coil. The load output from the whole system was investigated by placing a piezo-electric ceramic slab under an epoxy resin specimen. It was found necessary to damp the system electromagnetically, by winding an additional coil around the original coil, in order to reduce the vibration of the diamond that was observed during the indentation period.

The oscillograph, Fig. (6.4), for a 10^{-3}s pulse indicates that the complete system takes about 0.3×10^{-3}s to attain the peak load; this is 3% of the 10^{-2} pulse and hence these and the longer period pulses may be considered essentially square, provided that we ignore the small transient oscillations. However, the 10^{-3}s loading cycle is far from ideal and all hardness numbers obtained using this pulse length were assigned an arbitary load duration of 0.5×10^{-4}s. So far we have only been concerned with the shape of the load/pulse envelope but in order to calculate a V.H.N. the applied load must be determined. A direct method, as opposed to the indirect procedure adopted by Gunasekera, was used in this work. A 45N capacity Ether Load Cell was positioned under the indenter while the load from the transducer was maintained by closing (SW_3). The load cell was calibrated up to a force of 1.5N by a dead weight technique and the output potential from the strain gauge bridge system measured with a precision potentiometer since the force produced by the transducer of 1.16N was only about 2.5% of the maximum range of the dynamometer.

The environment and temperature enclosure was designed by the author

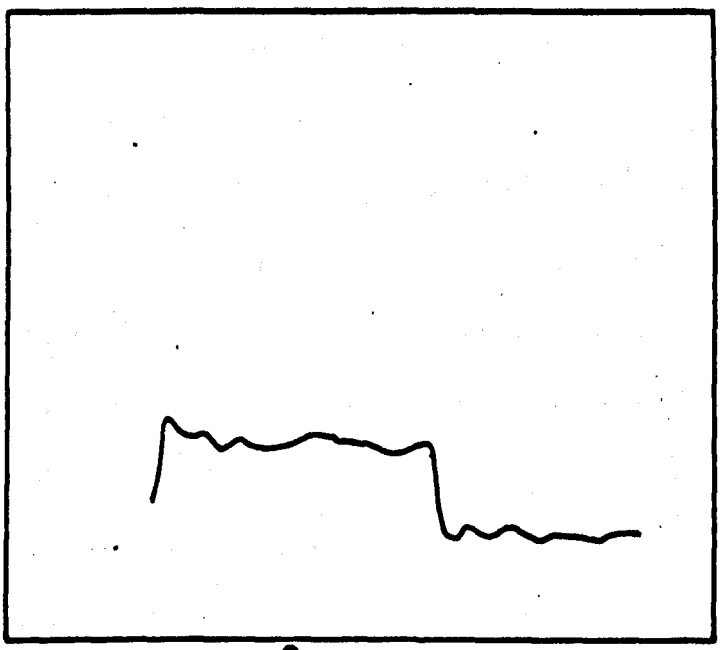

10^{-2}s PULSE

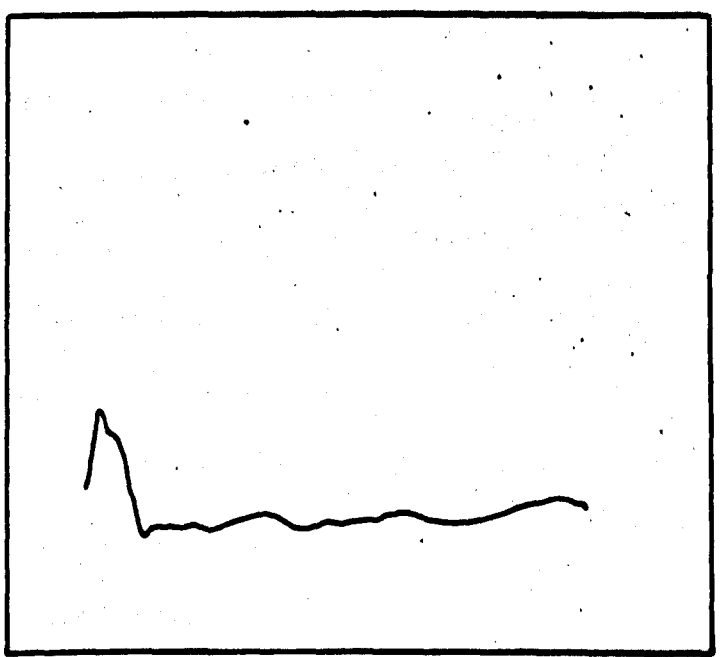

10^{-3}s PULSE

Fig. (6.4) Oscillographs of 10^{-2} s and 10^{-3} s pulses

and is shown in Fig. (6.5). It consisted of an aluminium block (A) onto which was wound a heating coil (B); temperature sensing was achieved by means of a copper/constantin thermocouple (E) attached to a spring clip (D) which enabled the thermocouple to be held firmly in contact with the specimen (C) and close to the indenter.

A Eurotherm controller was used to maintain the required temperature. The specimen itself was contained in a cavity milled in the centre of the block and viewed through a glass window (F).

For the short indentation periods it is impossible to avoid very high contact speeds and still achieve square load pulses; it was calculated that the electromagnetic transducer produced a contact speed of about 10^4 $\mu m\ s^{-1}$. Marsh has demonstrated that these high loading rates produce significantly larger indentations in glass and postulated that this was due to the occurrence of local adiabatic heating. He was able to minimise this effect by a double indentation technique in which the majority of the adiabatic heating occurred during the first indentation; the second indentation, which was performed using a slightly higher load than the first, then enlarged the indentation to equilibrium size under essentially isothermal conditions. However, crack propagation in our materials may not occur under isothermal conditions and hence isothermal hardnesses determined by Marsh's technique were not considered to be any more appropriate than the adiabatic hardnesses, which is simpler to measure. All results quoted here are therefore from single indentations performed at these high loading rates.

6.4. Specimen Preparation

Resin samples were cast in the normal manner but in a chromium plated and polished mould from which as much of the silicone release coating had been removed

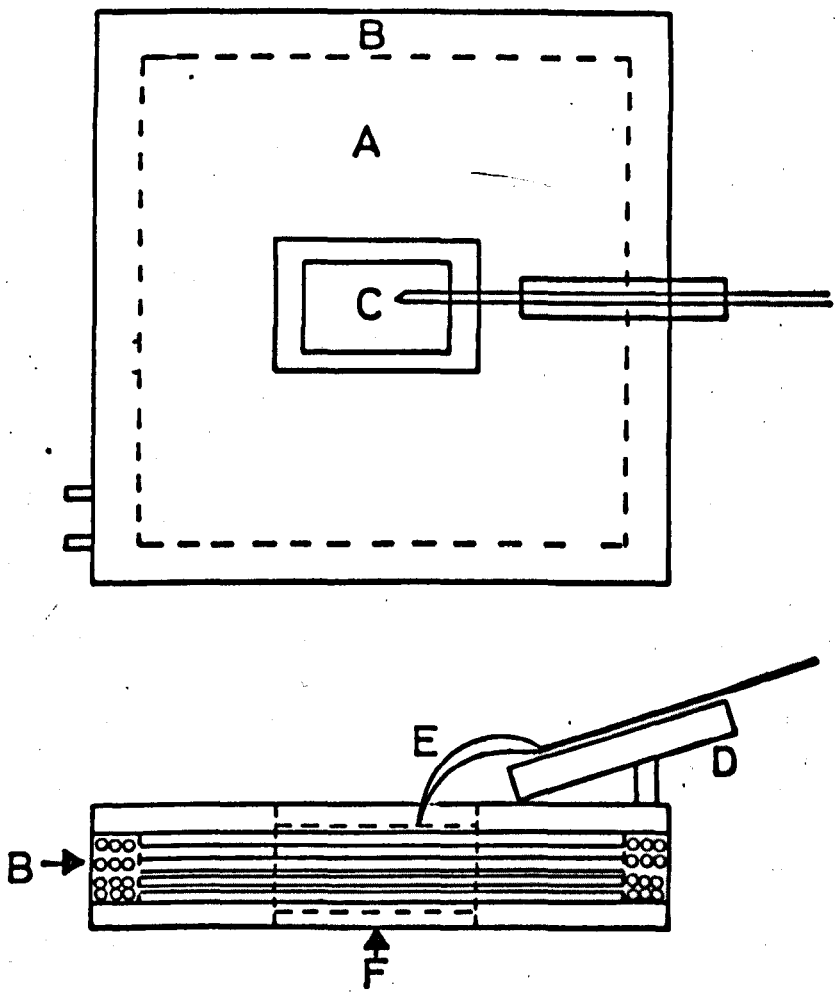

Fig. (6.5) Diagrammatic representation of the environment and temperature enclosure

as would allow a "non-stick" surface to be maintained. Some additional experiments were also performed on specimens from which approximately 0.5 mm had been removed from the "as cast" surfaces. The majority of the material was removed using silicon carbide paper lubricated with water; this rather severe treatment of the samples was followed by a final polishing with diamond paste on an unlubricated selvyt cloth.

6.5. Experimental Procedures

The experimental techniques applied to long and short term hardness tests are necessarily quite different and will therefore be considered separately.

6.5.1. Long Term Loading

The loaded cantilever was lowered slowly at about 5 $\mu m\ s^{-1}$ by manual rotation of screw (G) until the full load was applied to the specimen, timing was started immediately this had been achieved. The required diagonal lengths of an indentation were determined using a double cross-hair bifilar eyepiece. A period of about 30s was required to complete a set of bifilar diagonal readings at the four corners of the indent and therefore at load durations of 10^3s or more the error in time would not be more than 3%. At shorter periods only one diagonal was measured and in this case the time required was only about 3s, alternate readings were taken with the bifilar eyepiece rotated through 90^o. Indentation sizes at periods of 10^3s, 10^4s and 10^5s were obtained from the same indent without removing the diamond. Unfortunately, the removal of the diamond from the specimen surface is accompanied by an elastic contraction of the material surrounding the indent which changes the shape of the impression from a square to that resembling a pin cushion. The diagonal lengths are not however reduced significantly and any reductions were within the general

experimental scatter.

The temperature and environmental studies were conducted in a similar manner to that described above; the specimen was allowed to soak in the required environment, at a chosen temperature, for twenty minutes prior to the indentation. During this period the diamond was left in contact with the specimen surface to enable it to attain the same temperature as the specimen.

6.5.2. Short Term Indentations

Clearly in this case it is not possible to observe the indentations with the load applied and hence pin-cushion shaped, elastically contracted, indentations were measured in all cases; however, as mentioned above, the diagonal contraction was within the experimental scatter and a significant error does not result.

Specimens were again allowed to soak in the required environment at a specific temperature for twenty minutes prior to the recording of any data. During this period the indenter was held in contact with the specimen by closing switch (SW_3) to allow the diamond pyramid and the specimen to reach thermal equilibrium. The pulse length was chosen by rotation of switch (SW_3) and twenty indentations performed in rapid succession.

To ensure that "virgin" material was being examined the specimen was moved after each indentation in such a way that the distance between any two indentations was at least ten times the mean diagonal length. It is a priori possible that, at the higher temperatures some annealing and subsequent reduction in diagonal lengths, may have occurred in the period after producing an indentation and before measurements were taken. However, no reduction in diagonal lengths was observed at 353K in the period between 5s and 600s after performing an indentation.

6.6. Results

The hardness numbers of "as cast" surfaces of cured CT200, LY558 and EPON 828, for a load duration of 600s are plotted as a function of applied force in Figs. (6.6), (6.7) and (6.8). Hardness numbers obtained under similar conditions for specimens that had been polished to remove 0.5 mm from the cast surfaces are also summarized in these figures.

In Fig. (6.9) the hardness of the resins is shown as a function of time; results were obtained from polished surfaces using an applied force of 2.0N for the long term indenter and 1.16N for the short term machine. An increase in hardness of all the resins is observed as the indentation period is reduced from 10^{4}s to 5×10^{-4}s, the rate of increase of hardness as the period is reduced is however more pronounced for CT200 than it is for the other two resin systems. Over the temperature range of 280K to 390K the hardness of cured CT200 decreases rapidly in a non-linear fashion as the temperature is raised, this effect is illustrated in Fig. (6.10) for an applied force of 2.0N and a loading time of 600s. Fig. (6.10) also indicates that the hardness is environment sensitive, the highest hardness at a given temperature being exhibited in dry silicone oil.

Similar variations in flow stress with the duration of the indentation and temperature are observed for all three resins. The flow stresses presented in Fig.(6.11) and Fig. (6.12) were calculated with the aid of equation [6.4] from the appropriate hardness numbers using the values of Young's moduli, at 295K, given in Table 6.1.

The conversion of the hardness numbers of cured CT200 (which were obtained in three different environments and as a function of temperature) into the required stress is a little more complex since the Young's modulus of the material is a function of temperature; the calculations may however be performed using the values of Young's

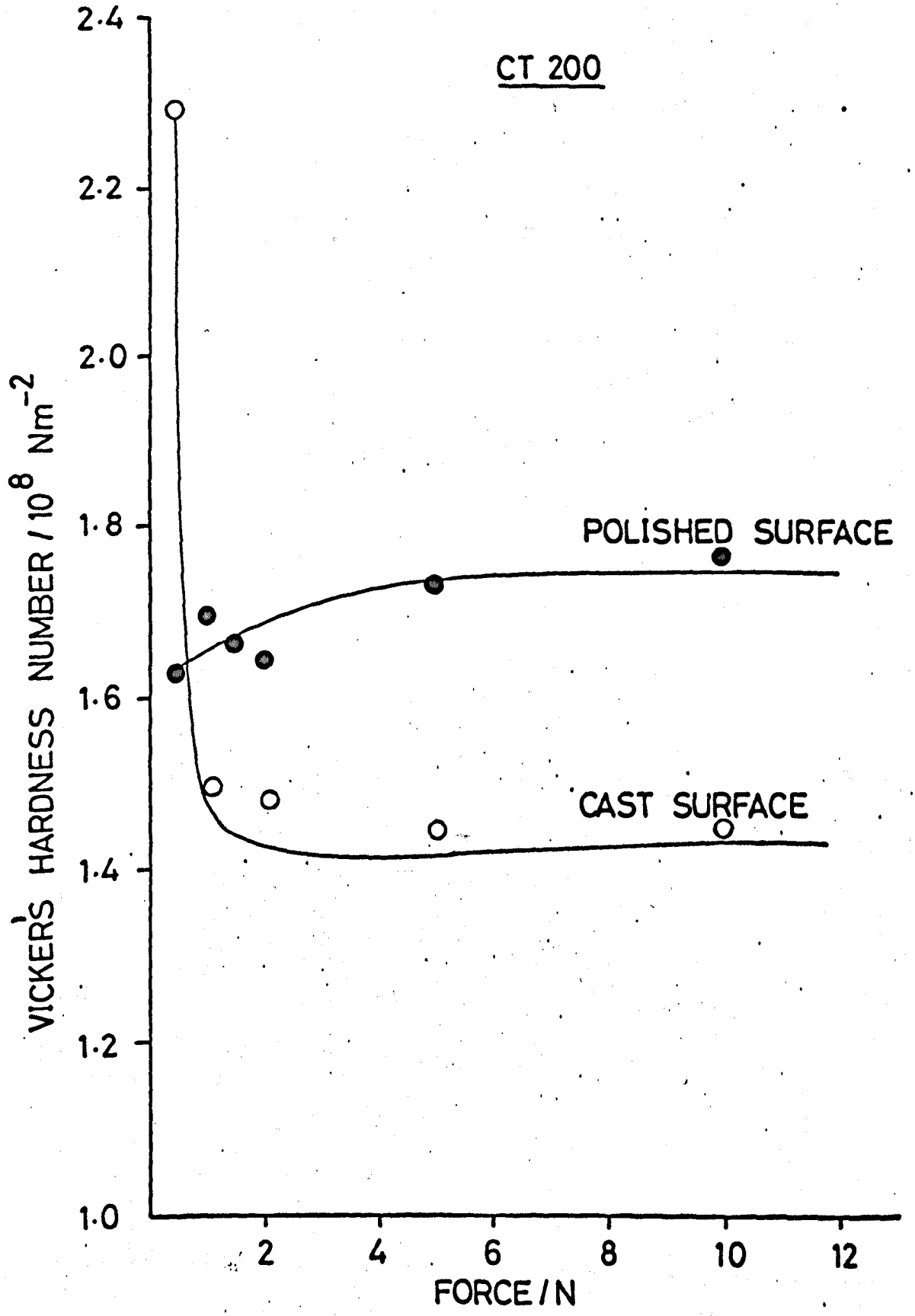

Fig. (6.6) The Vicker's Hardness Number of CT200/HT901 as a function of applied force

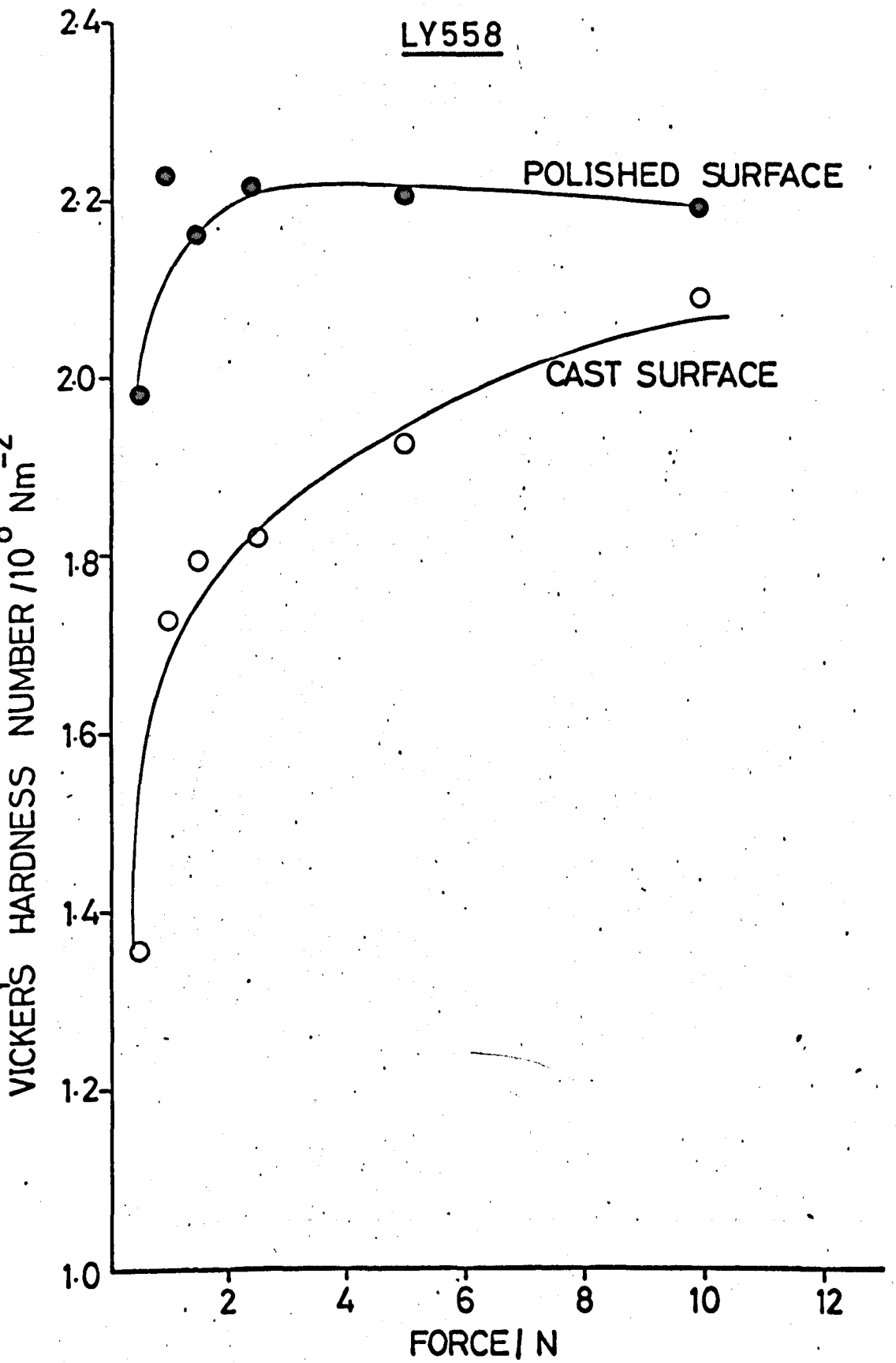

Fig. (6.7) The Vicker's Hardness Number of LY558/HT973 as a function of applied force

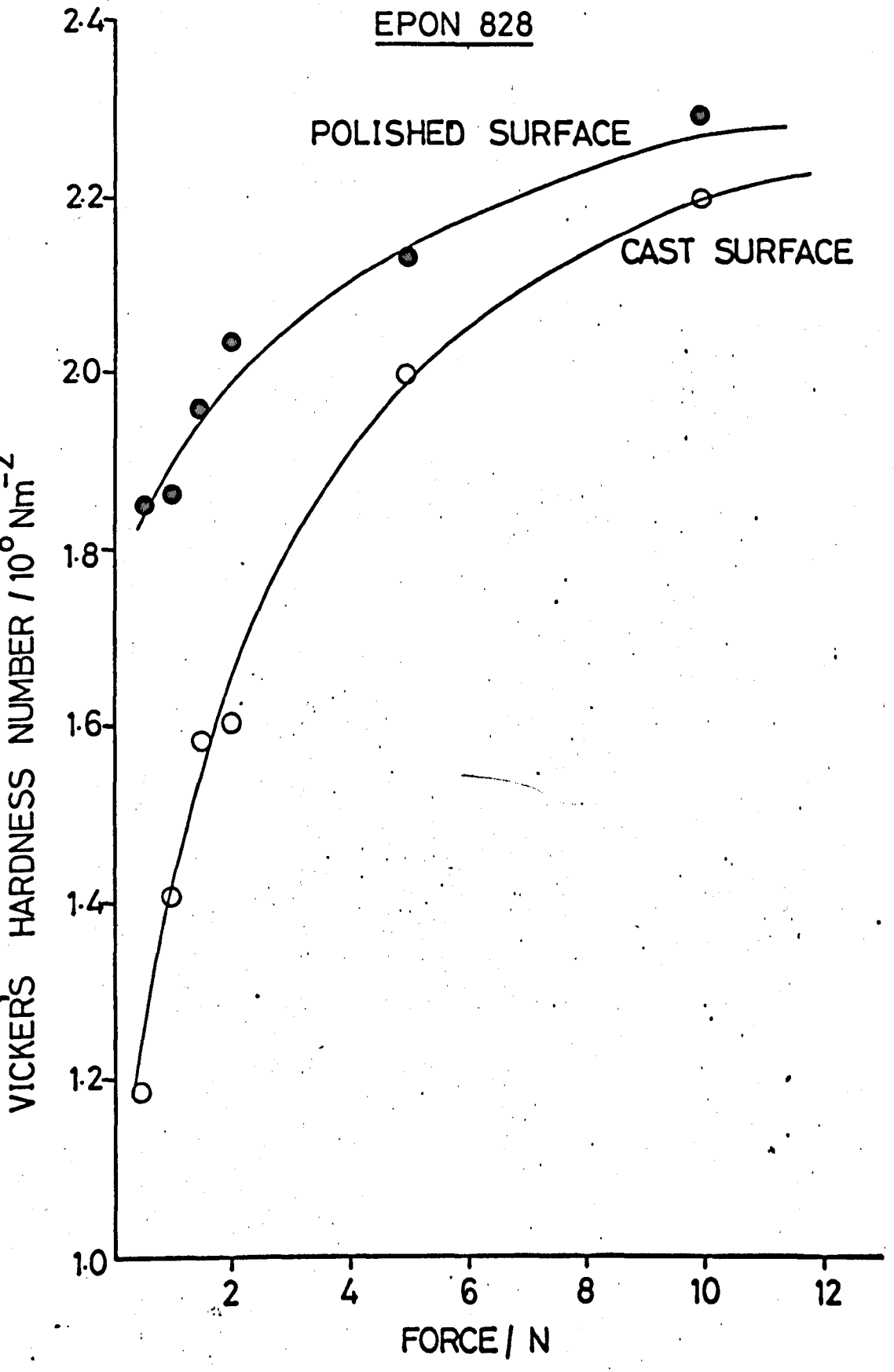

Fig. (6.8) The Vicker's Hardness Number of EPON828/NMA/BDMA as a function of applied force.

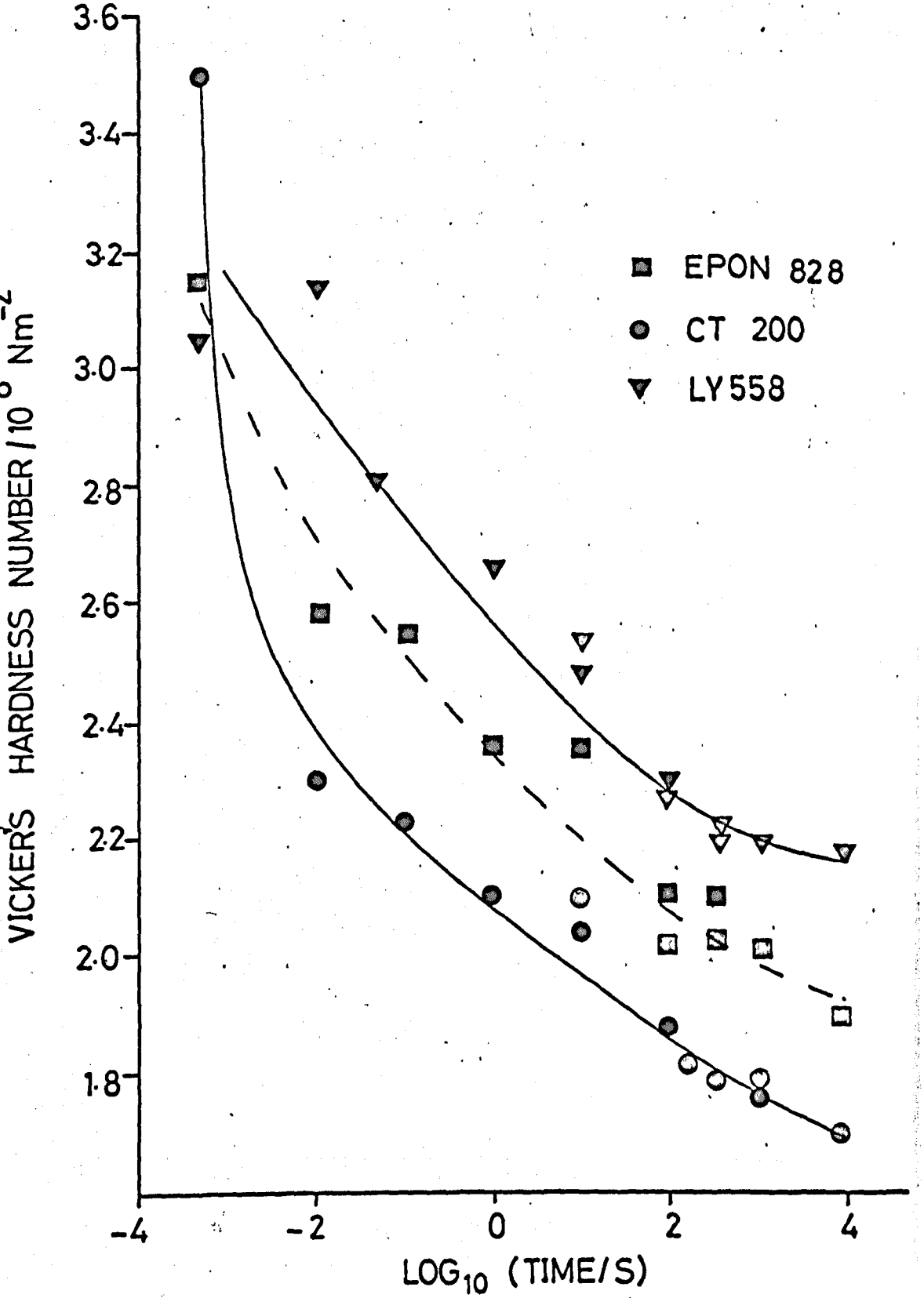

Fig. (6.9) The Vicker's Hardness Numbers of the three resin systems as a function of load duration

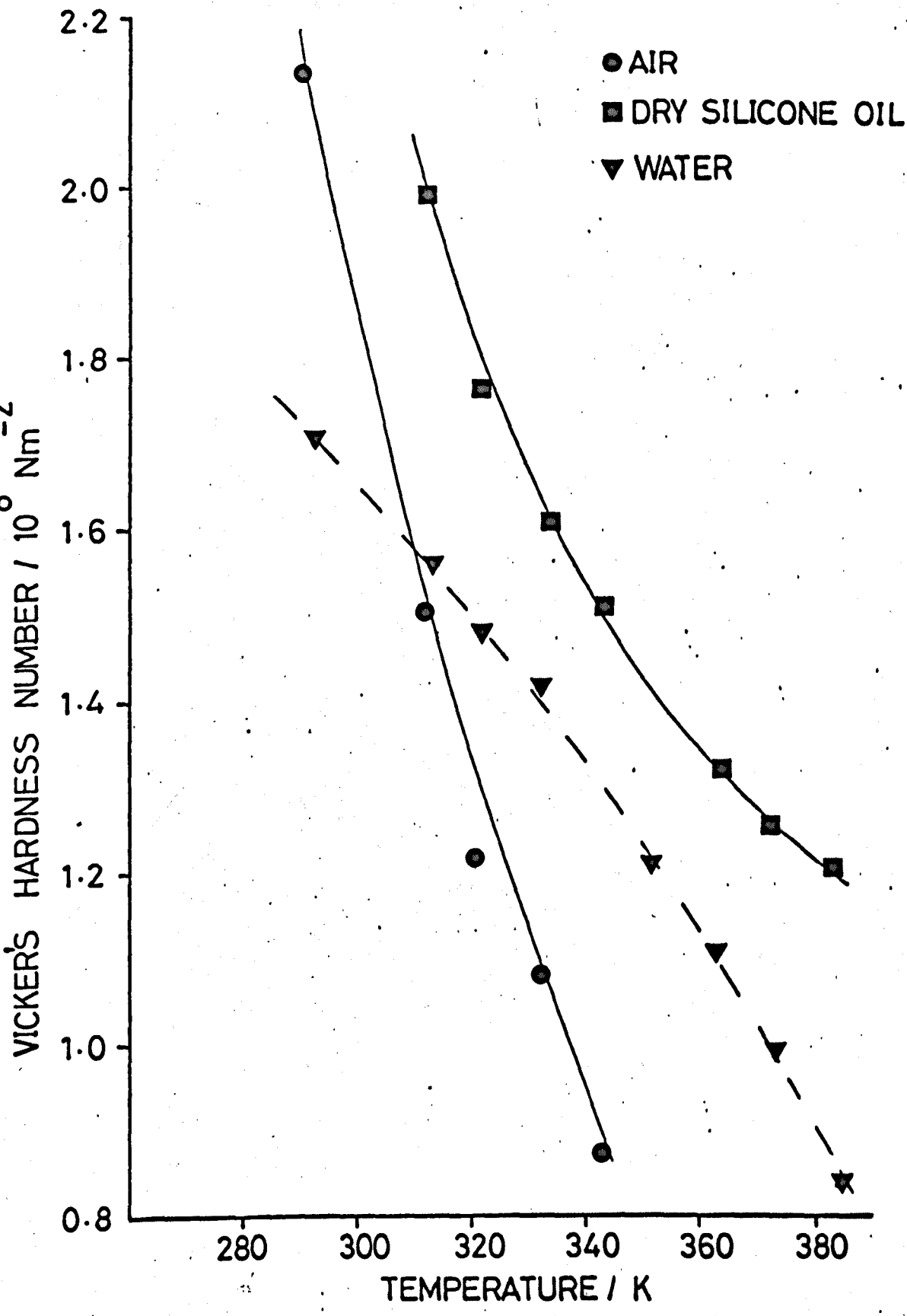

Fig. (6.10) The Vicker's Hardness Number of CT200/HT901 as a function of temperature and environment

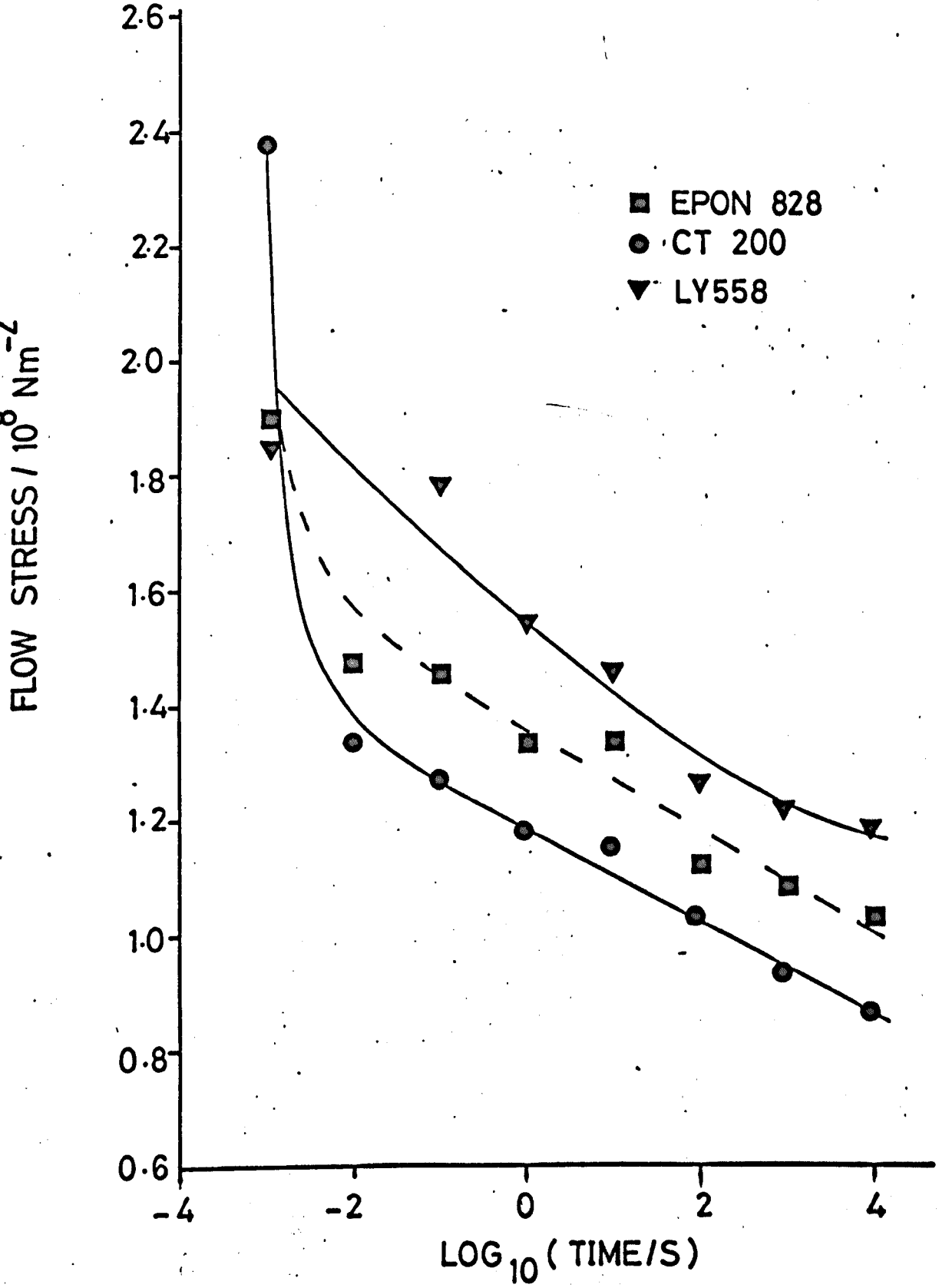

Fig. (6.11) The flow stress of the three resin systems as a function of load duration

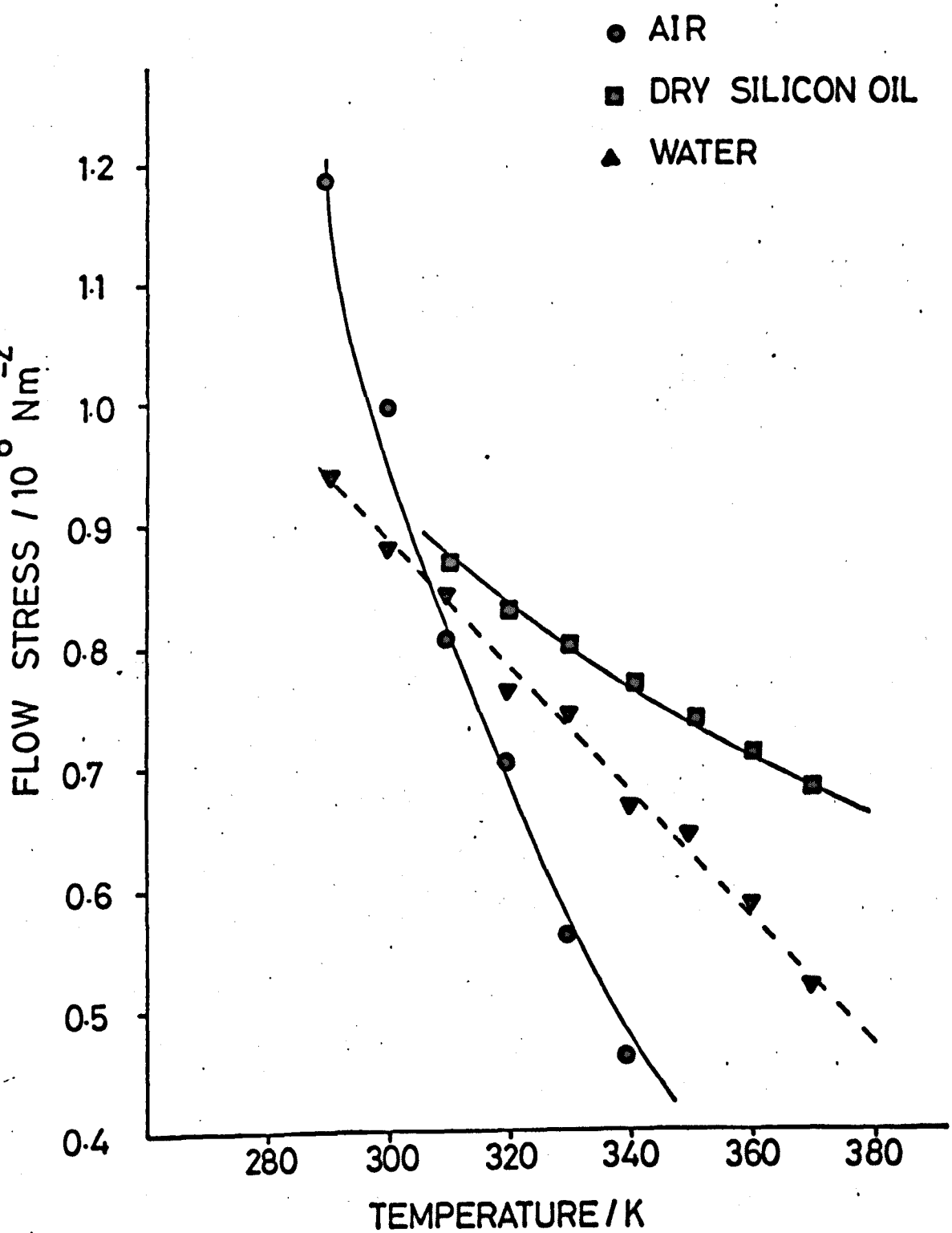

Fig. (6.12) The flow stress of CT200/HT901 in various environments as a function of temperature

Table 6.1.

The Young's Moduli of the Base Matrices at 295K

Material	Young's Modulus/$10^9 Nm^{-2}$
CT200/HT901	3.1
LY558/HT973	3.5
EPON828/NMA/BDMA	3.5

modulus as a function of temperature summarized in Fig. (6.13). The results presented in this figure were recorded during one of the earlier double cantilever experiments.

6.7. The Plastic Zone Extension, α

A plastic zone in an ideal elastic-perfectly-plastic material is shown diagrammatically in Fig,(6.14). It would therefore be a relatively simple matter to determine the required extension, α, provided that it is large enough to be measured by "standard" physical techniques. A photomicrograph of a real crack tip in CT200/HT901 is shown in Fig. (6.15) where it is apparent that the shape of the tip is far from the ideal and hence since the crack faces are not parallel some ambiguity exists as to which crack tip dimension should be measured. A further complication arises for it is only possible to measure the plastic zone extension at the surface of the specimen, i.e. where conditions of plane stress exist, and not as we would prefer, for comparison with our values of fracture energy, under plane strain conditions. However, since the values of plastic zone extension quoted here are only to be used in simple order of magnitude calculations, the above difficulties need not concern us greatly, although it is expected that the values to be presented are within $\pm$ 30% of the appropriate plane strain extension.

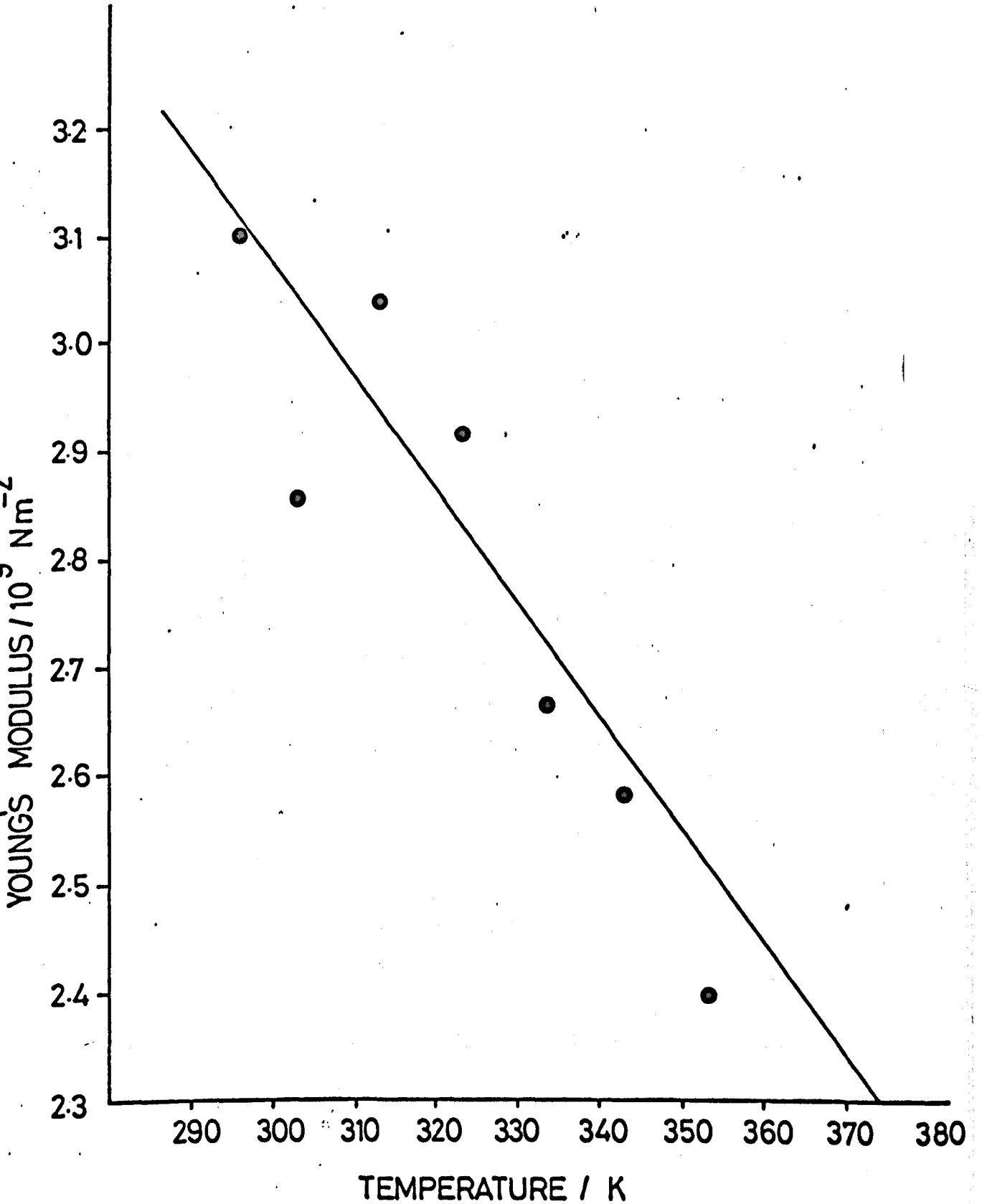

Fig. (6.13) The Young's modulus of CT200/HT901 as a function of temperature

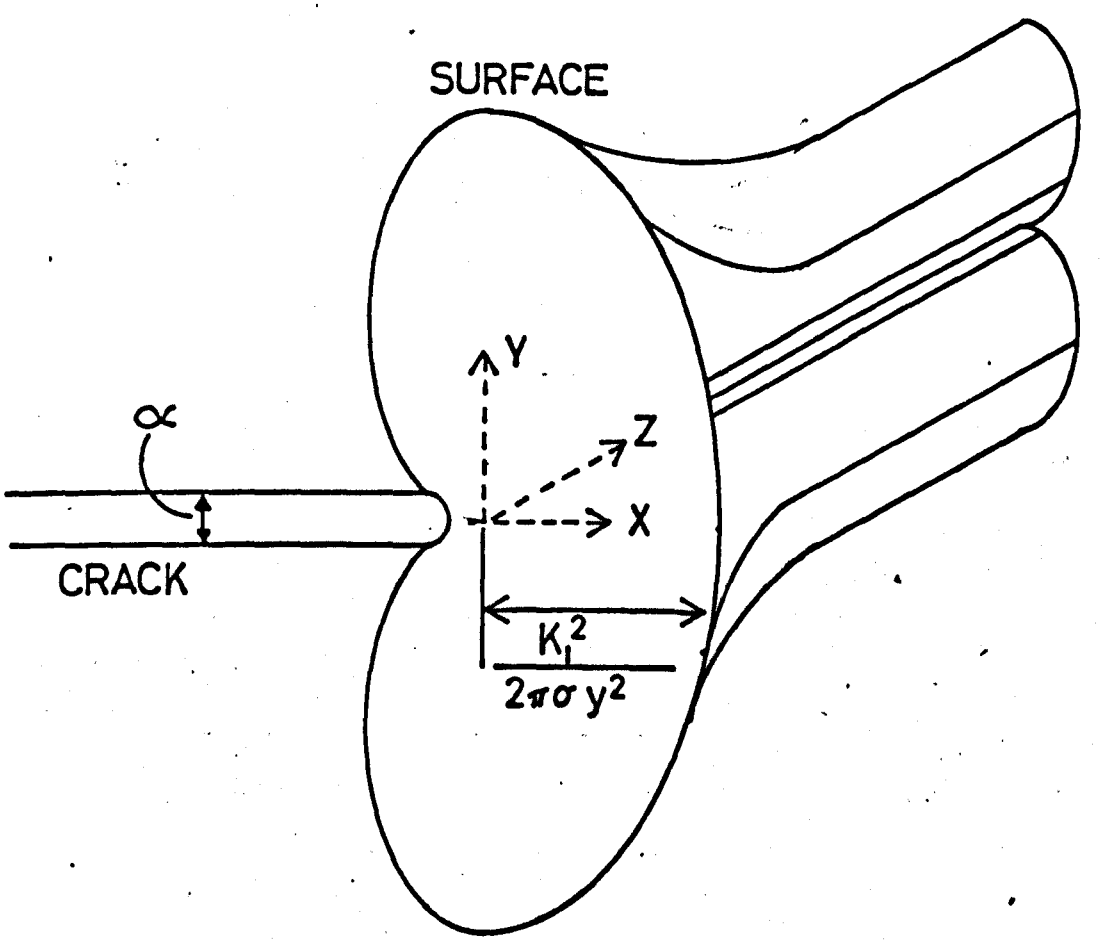

Fig. (6.14) The crack tip and plastic zone in an ideal elastic-perfectly-plastic material

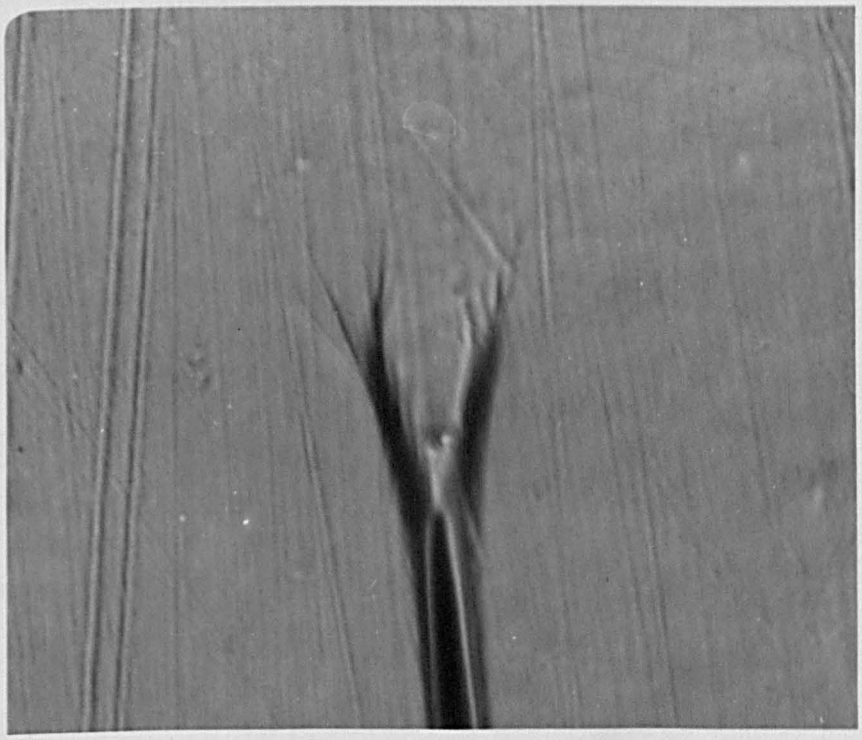

Fig. (6.15) A crack tip in cured CT200/HT901

(magnification x 1500)

The plastic zone extension is required both at the instant of crack initiation and for arrest. The latter is readily obtainable using a simple screw driven fracture machine to propagate a crack. If the screw is stopped as soon as the crack jumps, the tip can be examined with an optical microscope and the necessary dimension measured with a bifilar eyepiece. The extension at crack initiation is more difficult to determine because one cannot easily measure the extension at the instant of initiation. An approximate value was obtained, however, by increasing the cantilever opening displacement whilst continuously monitoring the crack opening displacement; the last recording prior to crack initiation was taken as the required parameter.

6.8. Results

The measured plastic zone extensions for cured CT200, LY558 and EPON828 are presented in Table 6.2.

Table 6.2.

The Plastic Zone Extension of Various Materials

Material	Plastic Zone Extension α / μm	
	Initiation	Arrest
CT200/HT901	25	6
LY558/HT973	5	2.5
EPON828/NMA/BDMA	10	5

6.9. Preliminary Discussion.

The experiments performed to determine the hardness of "as-cast" and polished surfaces of our matrix materials as a function of applied force were undertaken.

to investigate whether the as-cast surface of the materials differed significantly in hardness from the bulk of the sample. Such differences are a priori possible and, for example, may result from the loss of curing agent from the surface, from absorption of the release agent or from other surface effects. The hardness numbers have been plotted against the applied force rather than the indentation depth since these experiments were performed merely to investigate whether a "modified" surface layer exists on these materials. Cured CT200 is shown to have a hard surface layer whilst the surfaces of cured LY558 and EPON828 are softer than the bulk material. This variation in hardness with depth could not be tolerated in our experiments to explore the effect of loading time on flow stress since the flow stresses will not only be a function of the load duration but also of indentation depth. In an attempt to avoid ambiguity in the results 0.5 mm was polished off the "as cast" surfaces, to expose the inner layers of the cast samples. Figs. (6.6) to (6.8) indicate that the hardness is sensibly independent of depth for forces above about 1N, although a thin surface layer, perhaps produced by the final polishing, still appears to be significantly different from the bulk material.

Hardnesses as well as flow stresses are quoted in many instances throughout this chapter; this may appear to be superfluous but it was considered advisable to present, in the first instance, the parameter that was actually measured rather than simply a flow stress which is derived indirectly from the hardness. Some difficulty existed in deciding which flow stresses should be used in the Irwin expression:-

$$\gamma = \tfrac{1}{2}\, \sigma_y\, \alpha$$

The problem arises because time scale differences may exist between the formation of a plastically deformed zone at the crack tip and under the pyramid indenter. Such

time scale differences are a priori possible and may arise because of the different conditions under which the deformation is produced. At this stage it is not obvious what load duration, and hence flow stress, should be assigned to the material at the tip of a crack that has been in a loaded state for a known time. The flow stresses presented with the crack initiation information in Table (6.2) correspond to indentation periods equal to the mean time between successive propagations of a crack in a double cantilever specimen fractured at the standard applied cross head speed of 6.3×10^{-3} mm s^{-1}. Clearly this is a somewhat arbitrary choice of period and cannot be justified rigorously but again we are concerned with changes in these parameters as opposed to the precise period that should be assigned to them.

The average periods between crack jumps are:-

120s for CT200/HT901

35s for LY558/HT973

45s for EPON828/NMA/BDMA

Arbitrary periods of 10^{-3}s were assigned to the crack arrest data although the relevant period is probably much shorter than this especially in CT200 where the crack propagates extremely rapidly between successive arrest positions.

The principal features suggested by the data presented in this chapter are:

(i) The Irwin expression is applicable to these materials (See Table 6.3).

(ii) The flow stresses of the three cured resins are very similar and the differences in the fracture energies may be expressed in terms of

TABLE (6.2)

The Fracture Energies, γ, Crack Opening Displacement, α, and Flow Stresses, σ_y, of the Matrix Materials

Material	$I^{\gamma}/10^2 Jm^{-2}$	$A^{\gamma}/10^2 Jm^{-2}$	$I\alpha/\mu m$	$A\alpha/\mu m$	$I\sigma_y/10^8 Nm^{-2}$	$A\sigma_y/10^8 Nm^{-2}$	$\frac{I\sigma_y I\alpha}{2I^{\gamma}}$	$\frac{A\sigma_y A\alpha}{2A^{\gamma}}$
CT200/HT901	1.2	0.75	25	6	1.05	2.4	1.1	0.96
LY558/HT973	0.33	0.28	5	2.5	1.4	1.85	1.02	0.82
EPON828/NMA/BDMA	0.58	0.53	10	5	1.3	1.9	1.12	0.90

differences in the plastic zone extension.

(iii) The plastic zone extension of a propagating crack is less than that at the instant of initiation: this difference in extension is reflected in the fracture energies:-

viz: initiation fracture energy > arrest fracture energy

initiation plastic zone extension > arrest plastic zone extension

(iv) An inverse correlation exists between the flow stresses and the fracture energies at different temperatures. Hence changes in the plastic zone extensions with temperature must be larger than those changes in flow stress.

In addition, the initiation fracture energy of the CT200/HT901 used in this work was 1.2×10^{2} Jm^{-2} whereas Griffiths used a different cure schedule and obtained a value of 0.8×10^{2} Jm^{-2}. He estimated the flow stress for a load duration of 15s to be 1.0×10^{8} Nm^{-2}, which agrees very well with the value obtained here. He also found the plastic zone extension just prior to initiation to be 15 μm which compares with a value of 25 μm for our material. The ratio of these plastic zone extensions correlates well with the ratio of the initiation fracture energies of the two differently cured materials, i.e.

$$\frac{l_{\alpha}\,(\text{Griffiths})}{l_{\alpha}\,(\text{this work})} = 0.6$$

$$\frac{l_{\gamma}\,(\text{Griffiths})}{l_{\gamma}\,(\text{this work})} = 0.65$$

It is also worthy of note that at room temperature the flow stress of solid uncured CT200 at a load duration of 15s is again about 1.0×10^{8} Nm^{-2} although the fracture energy is extremely low (approximately 2.0 Jm^{-2}). The crack tip plastic zone extension in this material is so small that the crack tip cannot be resolved on an optical microscope having a resolving power of about 1 μm. This is to be expected since the Irwin expression predicts a plastic zone extension of 4×10^{-2} μm.

The information presented in this chapter strongly suggests that the fracture energies of our epoxy resins are dictated primarily by the plastic zone extension and again leads us to speculate that the fracture energy of these apparently amorphous materials may be determined largely by their microstructure. Some further discussion on this topic will follow in the next chapter where it will be set in context with the rest of the information that has been obtained.

CHAPTER VII

The Fracture of Epoxy Resin Based Composite Materials

7.1. Introduction

The principal object of this work was to examine the behaviour of a range of composite materials in the hope that this might provide information on some of the physical processes involved during crack propagation in these materials. However, it soon became apparent that before any detailed attempt could be made to interpret the behaviour of the composites, more fundamental information than was at present available was required on the behaviour of the matrix materials. We shall, therefore, begin this chapter by considering some of these features and then extend the discussion to cover the composite materials.

A considerable amount of information has been presented in this thesis concerning both the matrices and the related composites. Clearly, because of space and time limitations not all of this can be discussed in depth although many of the individual effects which were observed in the course of this empirical survey have already been considered briefly in the earlier chapters following the description of the various results. It will be useful here to collect together some of the major points; to examine the possibility that the results do suggest the physical mechanism responsible for toughening in these "dilute" composites and to introduce a simple model which may explain some features of their behaviour.

We shall, therefore, confine ourselves primarily to:

a) discussing the jumping mode of crack propagation in relation to the results presented concerning the flow stresses and crack opening displacements of the matrices, and

b) considering the variation in fracture energy with the effective extension rate at the crack tip. A model will also be presented which attempts to explain, in a very general sense, why the addition of a particulate phase to an epoxy resin matrix increases the toughness of that material.

7.2. Base Matrices

One of the more striking behavioural features of the epoxy resin family of materials is the "jumping"mode of crack propagation. This type of crack propagation is exhibited not only by the epoxy resins but occurs more generally and has been observed in these laboratories in other polymers, notably polystyrene and polycarbonate, and elsewhere in some aluminium alloys. Any general interpretation that is offered for this behaviour must therefore be capable of application to a variety of materials of quite different structure. It is clearly not appropriate to postulate one unique mechanism which depends on the nature or structure of our particular type of material. Although, ultimately, the physical mechanism responsible for this behaviour may well be quite different, for example in crystalline aluminium alloys, in a linear polymer and in a network polymer, it is probable that these are manifested in a common, phenomenological, microscopic mechanism, such as a change in the critical plastic zone size with crack speed, or with the adiabatic heating brought about in the material ahead of a rapidly advancing crack. Indeed, as we have seen, GRIFFITHS (1968) postulated that crack jumping was a consequence of the behaviour of the material around the crack tip under the influence of the adiabatic heating normally associated with crack

propagation. WILLIAMS (1965) had shown previously that quite high local crack tip temperatures could be attained during propagation and the preliminary work of Griffiths had indicated that the fracture energy of cured CT200 fell as the temperature was raised above room temperature. This was in contrast to the increase in fracture energy with increasing temperature that he had observed in glass and PMMA, both of which exhibit the continuous type of crack propagation behaviour. The more detailed results presented in Chapter III show unambiguously that the fracture energy of cured CT200 does not fall with increasing temperature between 273K and 390K but in fact both the initiation and arrest values increase, albeit rather slowly in the latter case. Griffiths adiabatic heating hypothesis would therefore appear to be inappropriate and hence we now examine, at a phenomenological level, other possible explanations of "crack jumping" behaviour.

It may, however, be useful first to summarise some of the results obtained during the course of this work. A material that exhibits the jumping type of crack propagation may be characterised by two fracture energies which correspond to conditions of crack initiation and arrest. The extent of the jumping behaviour, that is the ratio of the two fracture energies, varies from one material to the next. Table (3.1) shows that at an arbitrarily chosen cross head speed of 6.3×10^{-3} mm s^{-1}, cured CT200 exhibits the largest crack jumps. The extent of crack jumping is also a function of the effective crack tip extension rate, $\dot{\varepsilon}_e$, temperature, and to a lesser extent, environment. In addition there is a characteristic extension rate at the crack tip at which the crack will propagate without jumping. Crack jumping was also observed in all the composites, apart from the materials containing a relatively large volume fraction of talc. The situation is somewhat complex in the latter materials because the plastic zone size is approaching the specimen thickness and hence crack extension does not

occur under plane strain conditions.

Data reported in Chapter VI demonstrates that the flow stresses of all three epoxy resin systems are functions of load duration although the actual flow stresses are all about the same magnitude and show similar differences between very short and very long loading times. CT200 does, however, exhibit a pronounced increase in hardness as the indentation period is reduced below 5×10^{-3} s. It is probable that the appropriate flow stress of the material at the crack tip is lower at crack initiation than during propagation, or at the instant of crack arrest: the material close to a stationary tip has been subjected to an applied stress for a greater period of time. Some difficulty exists in assigning an appropriate load duration and related flow stress, to the material near the crack tip, at the beginning and end of each increment of crack extension because of problematic time scale effects. In addition, there is no reason, a priori, why the compressive flow stress measured by the indentation technique employed here should give the required flow stress, even if an unambiguous period could be found. We have shown earlier, however, that the Irwin expression: viz

$$\gamma = \tfrac{1}{2} \sigma_y \alpha$$

works for our materials if we use the measured values of crack opening displacement at the beginning and at the end of each increment of crack extension and flow stresses for a load duration of 10^{-3} s. and for a period equal to the mean time between successive crack jumps when a standard cantilever beam specimen is fractured at an arbitrary cross head speed.

Observations of the crack opening displacement immediately prior to crack initiation, α_1, and immediately after crack arrest, α_2, reveal that $\alpha_1 > \alpha_2$, i.e.

the plastic zone extension at initiation is greater, and in the case of CT200 much greater, than at the instant of crack arrest. This is to be expected if, as we have already shown, the Irwin expression is appropriate for these materials. It is, however, apparent that the lower flow stress at crack initiation must be more than compensated by an increase in plastic zone extension if the initiation fracture energy is to be greater than the arrest value. This point is well illustrated in CT200 which has the highest ratio of short to long time flow stresses but an even greater ratio of initiation to arrest plastic zone extensions. Fig. (7.1) and Fig. (7.2) which are reproduced by courtesy of B.R. McQuillin and S.P. Gunesekera give the change in flow stress, with time, of PMMA and float glass. It may be observed by comparing these figures with Fig. (6.11), that over the range of periods investigated, the scale of the increase in flow stress as the period is reduced is much greater in glass and PMMA than for the epoxy resins.

A crack may therefore be expected to exhibit the jumping mode of propagation, as opposed to the continuous propagation that occurs in glass and PMMA if the variation in flow stress with time can be more than compensated for by a change in the critical plastic zone extension. It is suggested that the phenomenological basis of the crack jumping behaviour lies in the dependence of the critical crack tip plastic zone size on crack speed. If the change in the critical plastic zone size is large enough it will more than compensate for any rise in flow stress with reducing load duration. This condition is more easily satisfied in materials where the flow stress does not increase rapidly as the load duration is reduced from, for example, 10^{2}s to 10^{-3}s.

A more detailed interpretation other than this rather naive model appears to be inappropriate at this juncture since little information is at present available on the plastic flow mechanism in these materials.

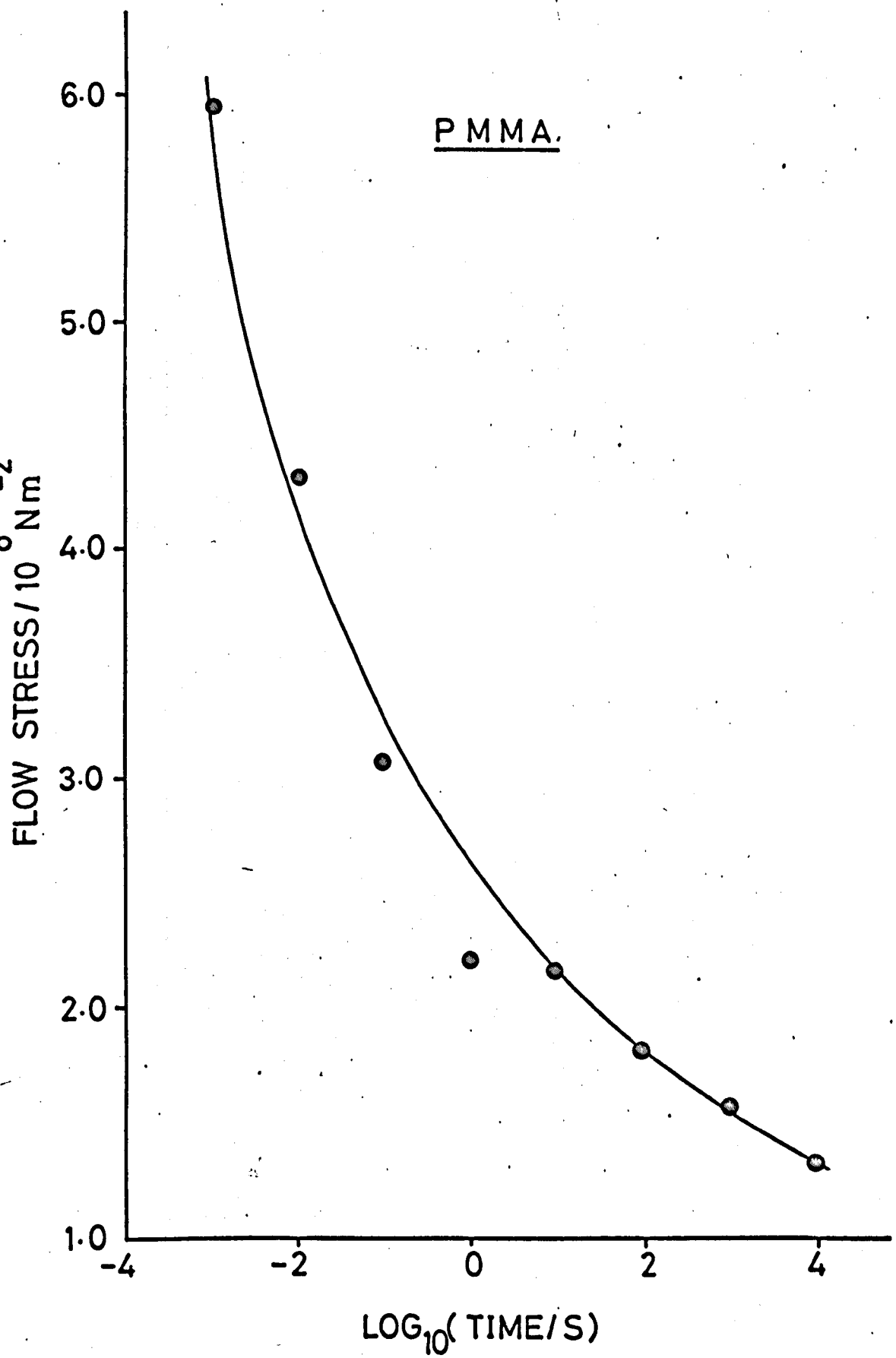

Fig. (7.1) The flow stress of PMMA as a function of load duration

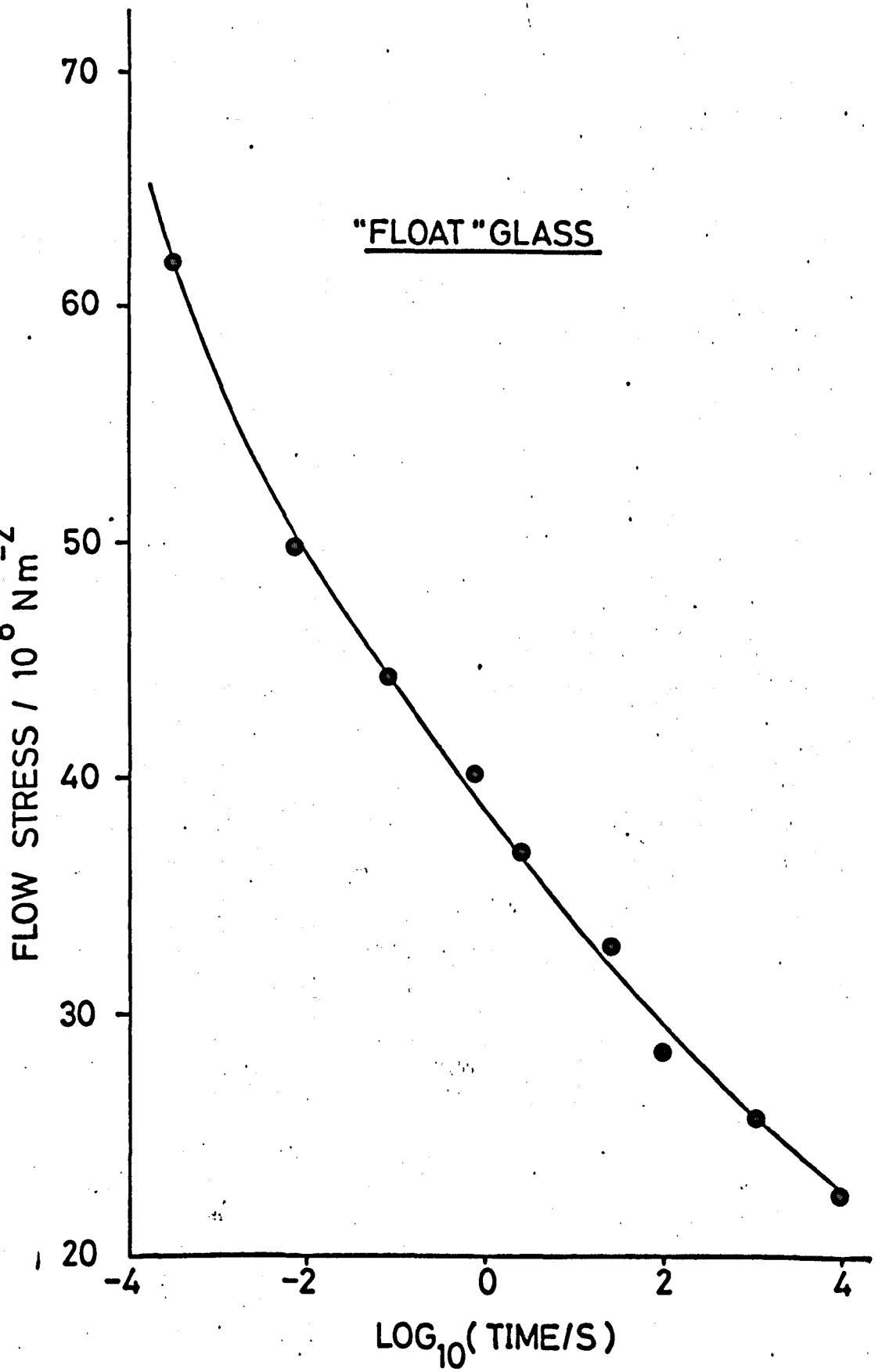

Fig. (7.2) The flow stress of "float glass" as a function of load duration

An important contribution to the understanding of the plastic flow mechanism in the epoxy resin matrices has been made during the process of this work by the identification of the craze-like defects, that occurred within 10 minutes at 350K around loaded crack tips in all three resin systems. Similar features have also been detected near the crack tips in specimens of CT200/HT901 and EPON828/NMA/BDMA loaded for much longer times (100 hours) at room temperature. Crazes could not, however, be detected at room temperature in LY558/HT973 and it may be that crazing occurs in this system only at elevated temperatures.

In view of the paucity of information on the plastic flow mechanism in our materials, what inferences can be drawn about the physics of the crack propagation processes? We know, for example, that the fracture energy of these materials is much greater than the surface energy and there is direct evidence of plastic deformation at a crack tip. Indeed, the magnitudes of the work done during crack propagation estimated using Irwin's expression and selected values of flow stress and observed crack opening displacements, appear to agree with the measured fracture energies. Hence the major parameter determining the different fracture energies of the matrices must be the critical plastic zone extension, α_c, since the flow stresses are similar. A fundamental question is therefore what determines the critical plastic zone extension, or alternatively what limits the size of the plastic zone to a magnitude above which it becomes more favourable to propagate the crack than it is to further extend the plastic zone?

In some metals and alloys it has been demonstrated that the plastic zone extension at which instability occurs is related to the grain or subgrain size. Again no unambiguous information is at present available on the internal structure of our epoxy resins. It is common, tacitly, to assume that they are structureless. However, etching experiments, performed by the author in collaboration with B.R. McQuillin provide

some direct evidence of a microstructure in cured CT200. Etching either with hot chromic acid or by an argon ion bombardment in a radio frequency glow discharge, reveals a structure of the type shown in Fig. (3.13) and Fig. (3.14). Much further work is required, but at first sight the scale of this structural detail appears to be too small to enable any simple correlation to be made with the size of the plastic zone. The identification of a microstructure now presents us with the possibility of being able to modify the structure, to monitor the changes, and examine the behaviour of these materials in relation to their structure; this may be a first step which could lead to an understanding, in fundamental mechanistic terms, of their physical properties.

Figs. (3.1), (3.2) and (3.3) indicate that the fracture energies of our epoxy resins are rate sensitive; this is new information as far as the epoxy resins are concerned although the effect is well known for other types of material, for example, many metals, glasses and polymers have rate sensitive failure conditions. CT200 and LY558 exhibit broadly similar variations in fracture energy with effective extension rate. The same is true of EPON 828 if we ignore, for the moment, the initial decrease in arrest fracture energy, although for EPON 828 the range of the variation of fracture energy is much smaller than in the other two systems. The arrest fracture energy of CT200 is insensitive to effective rate: in this material the crack propagates between arrest positions at such a rate that the actual advance of the crack tip cannot be followed visually and hence the crack may be considered to propagate at constant cantilever opening displacement. This is not the case for EPON 828 and LY558: the crack propagates relatively slowly in these materials and hence we may expect the applied cross-head speed to influence the fracture energy of these non-ideally elastic-plastic materials. Any further discussion of this particular aspect of the behaviour of the base

matrices appears to be inappropriate at the moment without more detailed information on the plastic flow mechanism. The experiments performed here have however highlighted the fact that it is impossible to quote a single fracture energy for any of these materials and hence effective extension rate, temperature and the environment which correspond to any particular value of fracture energy must be specified.

7.3. The Composite Materials

We now discuss some of the behavioural features of our composite materials and attempt to explain the origin of the increase in toughness that occurs when particulate fillers are added to an epoxy resin matrix. Before doing this it may however be useful to review briefly some of the suggestions which have been offered by previous workers to explain this kind of effect. We shall argue that the surface roughness, "frozen in" stresses, and crack front pinning are each inadequate to explain the magnitudes of the observed effects.

The expressions that have been used throughout this work for the estimation of fracture energies were developed with the tacit assumption that the fracture surfaces of our specimens were planar. One may readily conclude however that the extent of the toughening is not simply due to the increase in true surface area of the principal fracture surface, which is brought about by the deviation of the crack front around the second phase inclusions, since it is simple to show that the increase in area is small compared with the observed increase in fracture energy. Results presented and discussed in Chapter IV demonstrate, quite clearly, that the "frozen-in" microstresses which are generated around the particles due to the mismatch of thermal expansion between the filler and the matrix, are not responsible for the major proportion of the toughening. WEYL (1959) and SELSING (1961) have shown that a single spherical particle in an

infinite isotropic matrix will experience a pressure P, due to this mismatch in thermal expansion, given by:

$$P = \frac{(\varepsilon_m - \varepsilon_p)\,\Delta T}{\left(\frac{1+\upsilon_m}{2E_m}\right) + \left(\frac{1-2\upsilon_p}{E_p}\right)} \qquad [7.1]$$

where ε_m and ε_p are the thermal expansion coefficients of the matrix and particle respectively, υ_m and υ_p are the Poissons ratios of the matrix and particle and E_m and E_p are the Young's moduli. ΔT is the temperature range over which the stresses are considered to have developed and where the thermal expansion is a simple linear function of temperature.

Associated with this pressure are radial and tangential stresses in the matrix of

$$\frac{-Pa^3}{r^3} \qquad \text{and} \qquad \frac{Pa^3}{2r^3}$$

respectively. Where a is the particle radius and r is the distance from a point in the matrix to the centre of the particle. Ideally these equations hold only for the case of a single particle in an infinite isotropic matrix but they may be considered to be reasonably accurate at low particle volume fractions. If we substitute typical values into equation [7.1] then we may determine the maximum matrix stress, which occurs at the matrix/particle interface, as being approximately 10^7 N. This is, typically, an order of magnitude lower than the flow stress of our epoxy resins. It is also of note that the stresses which are developed in the matrix are highly localised around the particles since the stress falls as the inverse cube of the distance from the centre of the particle. In addition these thermal stresses are small compared with those that

may be produced under an applied stress because of differences between the elastic moduli of the filler particles and the matrices. It is therefore to be expected, as indeed was observed, that any contribution that the "frozen-in" stresses might make to the fracture energy of the composite material must be masked by other processes.

LANGE (1970) has investigated the effects, on fracture toughness, of adding hydrated alumina (alumina trihydrate) to an epoxy resin matrix. He postulates that the increase in toughness observed, after adding the filler, results from the pinning of the crack front by the second phase particles and the subsequent bowing of the crack front between the pinning positions. Lange argues that the crack front may be considered to have line energy (an assumption which appears to be difficult to justify) and then uses this concept in attempting to show that a significant amount of energy must be supplied to the system to bow the crack front between the particles and this in turn leads to a toughening of the material.

If we consider for the moment that the concept of a line energy is physically admissible then Lange's expression for the fracture energy of a composite material may be written:

$$\gamma_c = \gamma_m + \frac{F}{\eta} \qquad [7.2]$$

where γ_c and γ_m are the fracture energies of the composite and matrix respectively, F the line energy of the crack front and η the mean interparticle spacing. Equation [7.2] predicts that the fracture energy of the composite material is directly proportional to the inverse of the interparticle spacing: we shall see later that this is not borne out in practice.

Any model that we develop to explain the observed effects of adding a filler to an epoxy resin matrix must take into account the fact that the magnitude of the

increase in fracture energy cannot be wholly attributed to a roughening of the fracture surface, thermal stresses, or as Lange suggests, to the pinning of the crack front. In addition we have shown that glass and aluminium although representing filler types that are more brittle and tougher, respectively, than the matrix produce essentially similar increases in the fracture energies of the composite materials above that of the matrix. Within the ranges of particle sizes and volume fractions considered the fracture energy increases approximately linearly with particle volume fraction and at a constant volume fraction the fracture energy is insensitive to particle size above a size of about 50 μm.

We postulate here that the predominant effect leading to increases in toughness is the production of secondary plastic deformation around, or adjacent to, some of the filler particles at a distance from the intrinsic plastic zone at the crack tip. This extra plastic deformation will augment the crack tip plastic zone and will produce a larger, although highly inhomogenous region of plastic deformation. The fillers may produce this additional deformation because of the ability of the particles to magnify the applied stress to produce locally a stress exceeding the matrix flow stress; plastic deformation near a filler particle may in turn lead to local rupture, i.e. to the formation of subsurface cracks. The stress raising properties of a filler particle will be a function of its shape, Young's modulus, orientation with respect to the macroscopic applied stress and to some extent upon the adhesion between the matrix and the filler materials. Glass and aluminium particles of a given shape would therefore be expected to behave in an essentially similar fashion because of their similarity in modulus. Lamellar-shaped aluminium particles should however produce a much greater increase in toughness, at a given volume fraction (or particle spacing), than ballotini because the lamena suitably orientated is a more potent stress raiser than the sphere.

Evidence of additional "damage" produced at some distance from the crack tip is presented in the photomicrograph of a talc-filled specimen shown in Fig. (7.3). This provides direct evidence to support our hypothesis that toughening is due to an increase in the "effective" plastic zone size. The whitened region around the crack tip is believed to be the result of the formation of microcracks that are nucleated at the talc particles. The talc filler is a particularly potent stress raiser because of the lamellar shape of the particles. In addition, talc has a very low flow stress and can readily be deformed and hence the role of talc particles may be like that to be expected from pre-existing penny-shaped cracks.

A very simple physical model will now be presented which predicts the magnitude of the increase in toughness that is observed when particulate fillers are added to an epoxy resin matrix. We have already postulated that the role of the particles is to produce additional plastic deformation remote from the intrinsic plastic zone at the crack tip. To estimate the extent of this secondary deformation and hence the fracture energy of the composite we will assume that the criterion for fracture of the composite is the same as that of the matrix, i.e. the crack will become unstable when the local crack tip plastic zone exceeds a critical length, R_c. However, the total work done in advancing the crack in the filled material is greater than in the unfilled matrix, because additional deformation occurs around the particles.

We shall now follow through a rather crude calculation to estimate the magnitude of the effects to be expected. This should be regarded simply as a preliminary examination of the implications of our model; a much more sophisticated and rigorous calculation is possible in principle but was beyond our scope in the time available.

From Linear Elastic Fracture Mechanics we know that at a constant matrix flow stress that:-

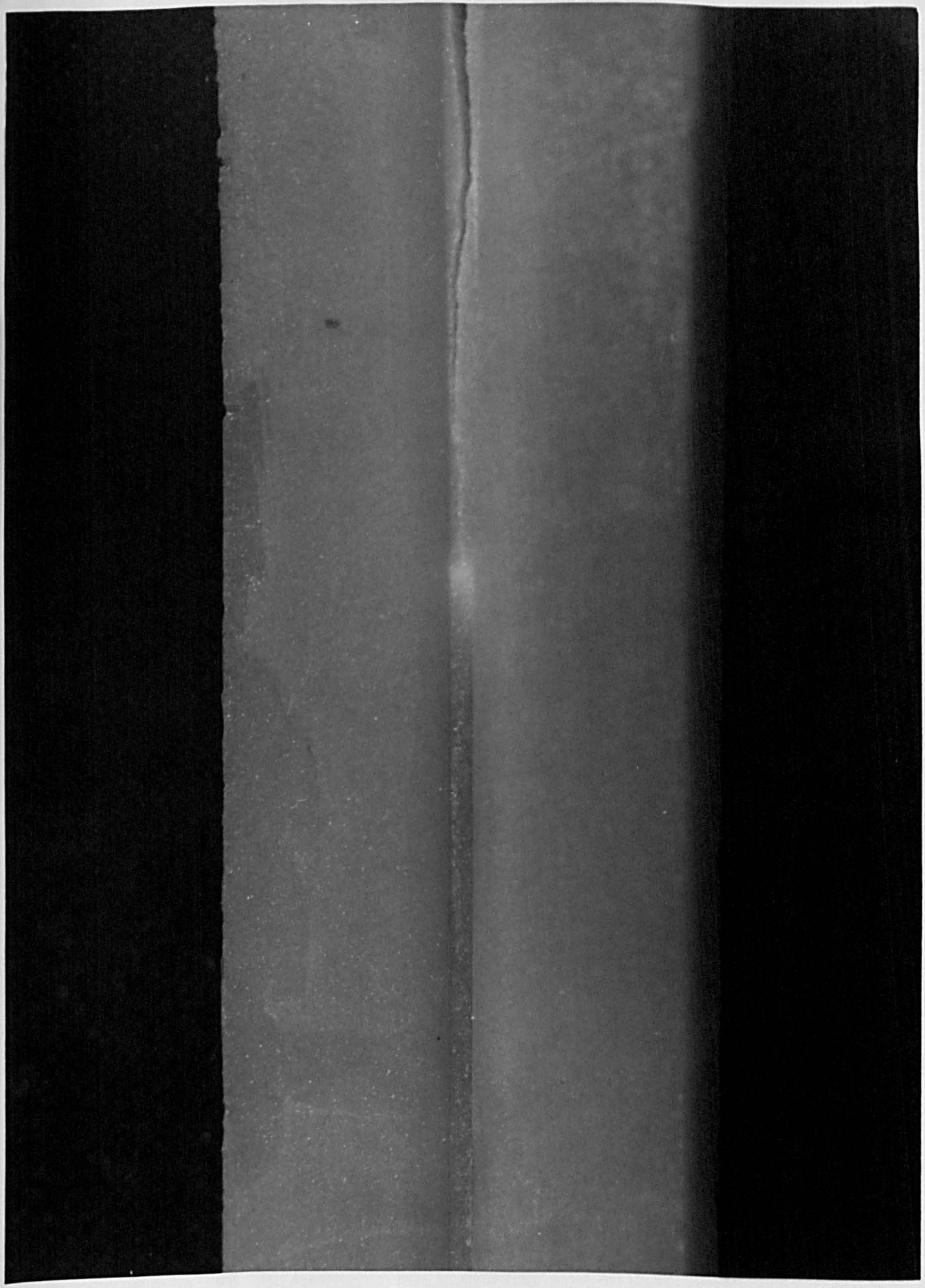

Fig. (7.3) A cracked talc filled CT200/HT901 double cantilever beam specimen showing the "damaged" region around the crack tip

$$\gamma \propto K_{Ic}^2 \propto R_c$$

and hence we will assume that contributions from the extra plastic deformation to the fracture energy are additive This assumption seems reasonable since the total work done in extending the crack to produce unit area of new fracture surface is given by: $\sigma_y \alpha/2$ from the crack tip zone plus $\sigma_y \sum \alpha_p$ from the filler particles which contribute to the work done during the formation of this new fracture surface where

σ_y = Matrix flow stress

α = Plastic zone extension at the crack tip

α_p = Plastic zone extension at a filler particle

A simple composite material is represented in Fig. (7.4). The probability of any given particle producing secondary deformation zones will depend not only on the factors already discussed (Young's modulus, shape and orientation) but also upon its position in the stress-field produced by the crack itself.

The stress components, defined in Fig. (7.5) at a point (r, θ) away from a crack tip in a linearly elastic material are given for loading conditions appropriate to plane strain by:

$$\sigma_{xx} = \frac{K_I}{(2\pi r)^{\frac{1}{2}}} \frac{1}{4} \left(3\cos\frac{\theta}{2} + \cos 5\frac{\theta}{2}\right) \qquad [7.3]$$

$$\sigma_{yy} = \frac{K_I}{(2\pi r)^{\frac{1}{2}}} \frac{1}{4} \left(3\cos\frac{\theta}{2} - \cos 5\frac{\theta}{2}\right) \qquad [7.4]$$

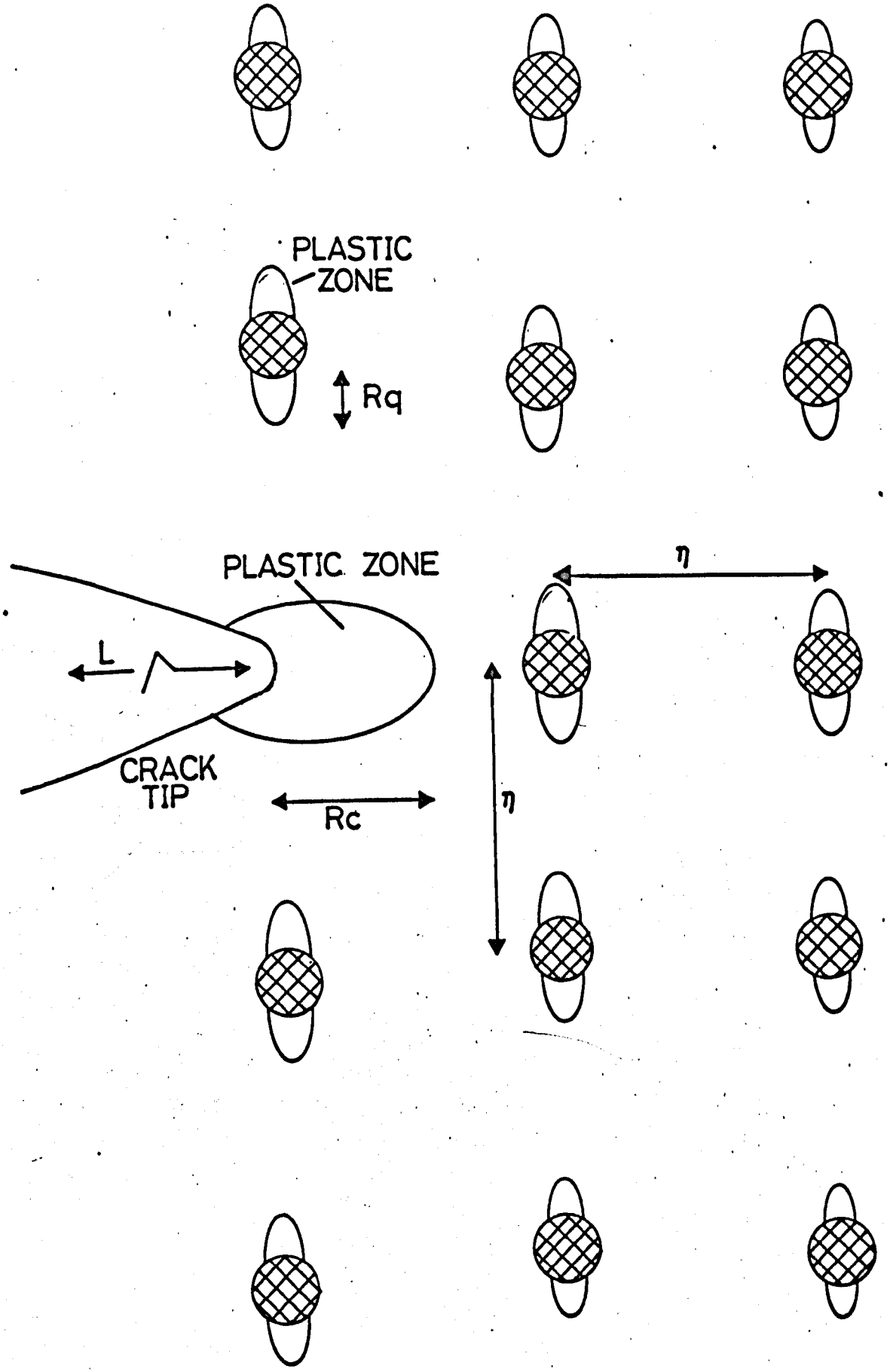

Fig. (7.4) Diqgrammatic representation of a simple composite material

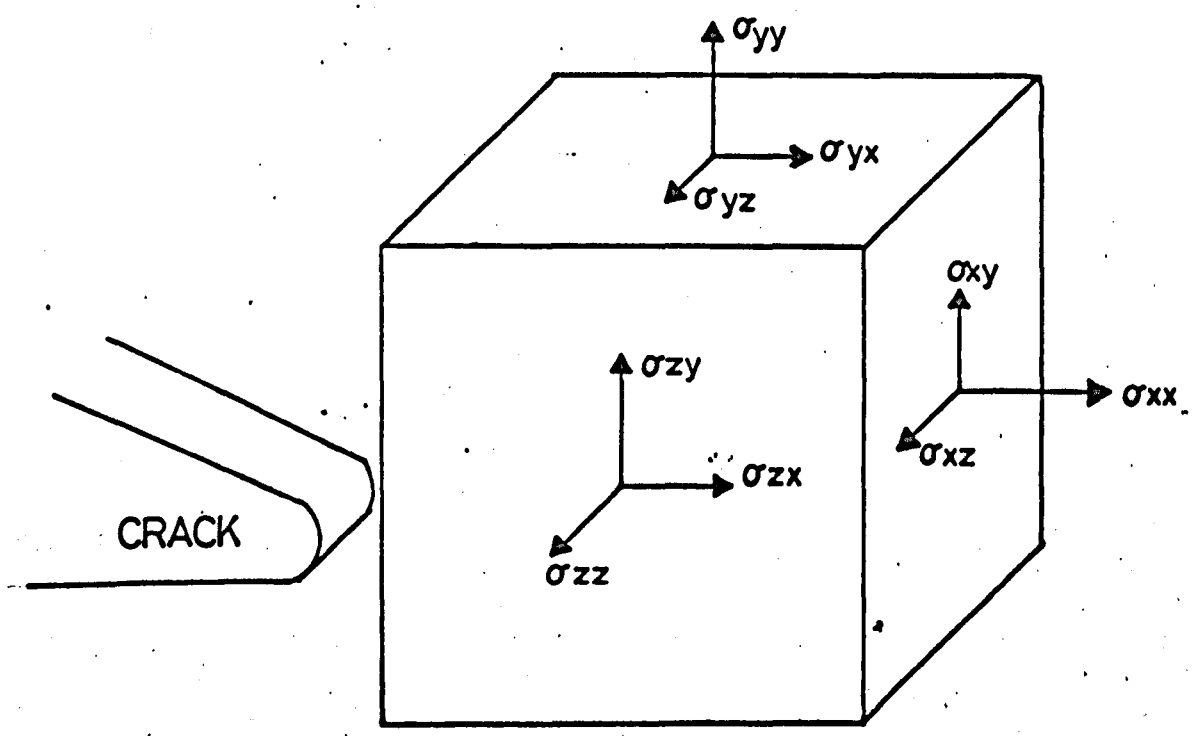

Fig. (7.5) The stress components at a crack tip

$$\sigma_{xy} = \frac{K_I}{(2\pi r)^{\frac{1}{2}}} \cdot \frac{1}{4} \left(-\sin\frac{\theta}{2} + \sin\frac{5\theta}{2} \right) \qquad [7.5]$$

These components may be resolved to give the maximum and minimum principal stresses, σ_p, at a point (r, θ)

$$\sigma_p = \frac{K_I}{(2\pi r)^{\frac{1}{2}}} \left[1 \pm \sin\frac{\theta}{2} \right] \qquad [7.6]$$

We can use the above expression to calculate the total energy expended in producing plastic deformation around the filler particles and hence estimate from first principles the fracture energy of an idealised composite material.

From equation [7.6] we can see that the maximum principal stress σ_p is not a sensitive function of the angle, θ, for $\frac{\pi}{2} \geq \theta \geq 0$ and hence we may write that the principal stress at a distance, r, from the tip of an unstable crack (i.e. when $K_I = K_{Ic}$) is:-

$$\sigma_p = \frac{K_{Ic}}{(2\pi r)^{\frac{1}{2}}} \qquad [7.7]$$

where K_{Ic} is the critical plane strain stress intensity factor for the unfilled matrix since we have already assumed that the critical plastic zone extension in the local zone at the crack tip is the same in the composite materials as it is in the base matrix.

If we continue to confine ourselves, for the moment, to a two dimensional situation represented in Fig. (7.6) then the local maximum stress, σ, in the matrix, at the matrix/particle interface is given by $\sigma = 3\beta\,\sigma_a$ [7.8]

where: β is a function of the elastic coefficients of the particle and the matrix and,

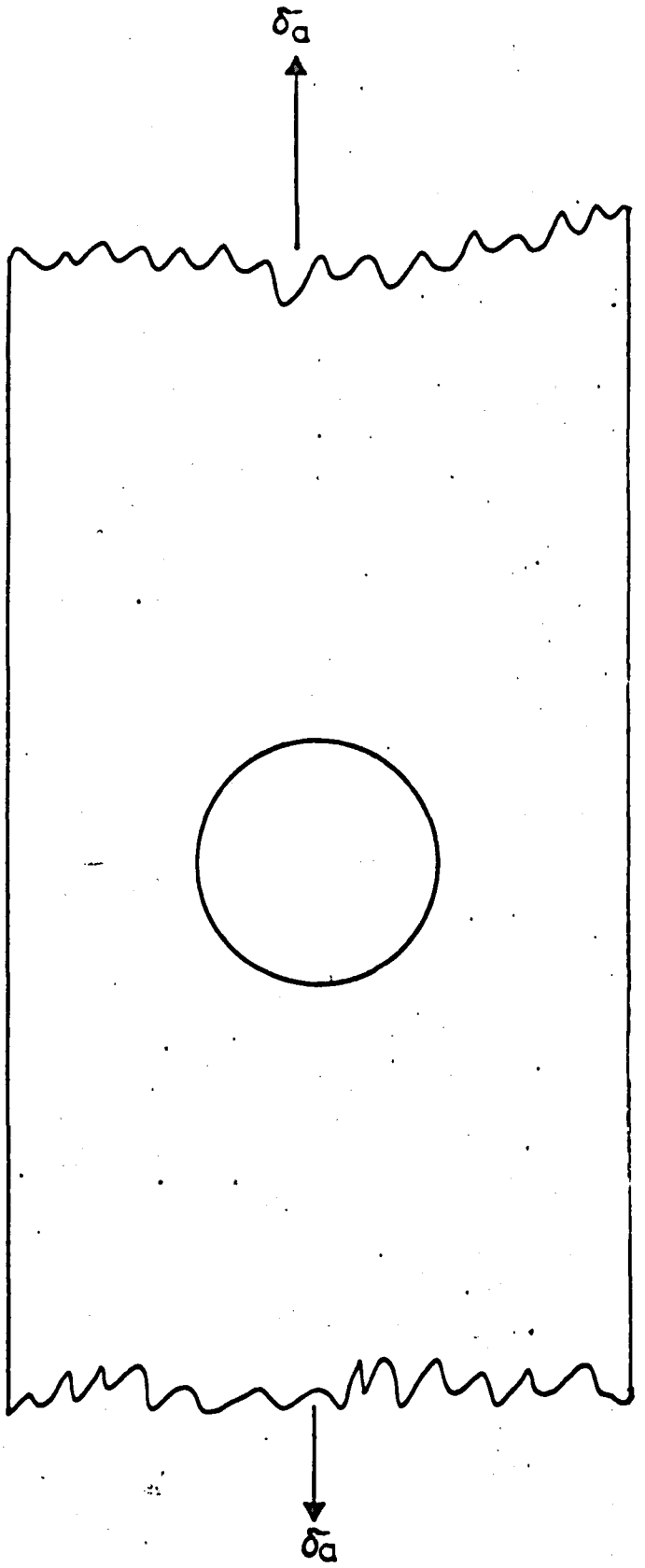

Fig. (7.6) A single particle in an infinite isotropic matrix

σ_a, is the uniaxial stress applied to the matrix. If we consider that the situation illustrated in Fig. (7.6) represents a single filler particle in the composite material then the stresses will produce a pair of plastic zones each of length R_q, one on each side of the particle. Now the normal stress σ_q, across a plane perpendicular to the local applied stress, σ_a, at a distance q, from the particle will be given by an expression of the form:

$$\sigma_q = \frac{K_p}{(2\pi q)^{\frac{1}{2}}} \qquad [7.9]$$

where K_p is the "stress intensity factor" of the particle and is given by:

$$K_p = \sigma_a (2\pi a)^{\frac{1}{2}} \qquad [7.10]$$

where, a, is the radius of the particle, Hence:

$$\sigma_q = \frac{3 \beta \sigma_p (2\pi a)^{\frac{1}{2}}}{(2\pi q)^{\frac{1}{2}}} \qquad [7.11]$$

since the stress at the matrix particle interface will be $3\beta\sigma_p$. By analogy with the situation at a simple crack tip in a homogenous material these stresses, if they are of sufficient magnitude will produce a pair of plastic zones each of length, R_q, where:

$$R_q = \frac{18\beta^2 \sigma_p^2 \pi a}{2\pi \sigma_y^2} \qquad [7.12]$$

and hence the total length of the two zones that are associated with each particle will

be:

$$R_q = \frac{18\beta^2\sigma_p^2 a}{\sigma_y^2} \qquad [7.13]$$

Now from equation [7.7]

$$\sigma_p^2 = \frac{K_m^2}{2\pi r}$$

and therefore:

$$R_q = \frac{9\beta^2 a K_m^2}{\pi r \sigma_y^2} \qquad [7.14]$$

where K_m is the plane strain stress intensity factor for the matrix.

We now represent our composite material by a simple cubic array of particles having an interparticle spacing as defined in Fig. (7.4) of η. Suppose that the crack advances by a distance dL, this will be accompanied by an increase in the total length of the zones around adjacent filler particle of ΔR_q.

Therefore from equation [7.14] and with reference to Fig. (7.7):

$$\Delta R_q = \frac{9\beta^2 a K_m^2}{\pi \sigma_y^2}\left(\frac{1}{r_{ij}} - \frac{1}{r_{ij}'}\right)$$

$$= \frac{9\beta^2 a K_m^2}{\pi \sigma_y^2}\left(\frac{\delta_{ij}}{r_{ij}^2}\right)$$

$$= \frac{9\beta^2 K_m^2 a}{\pi\sigma_y^2}\left(\frac{dL\cos\phi}{r_{ij}^2}\right) \qquad [7.15]$$

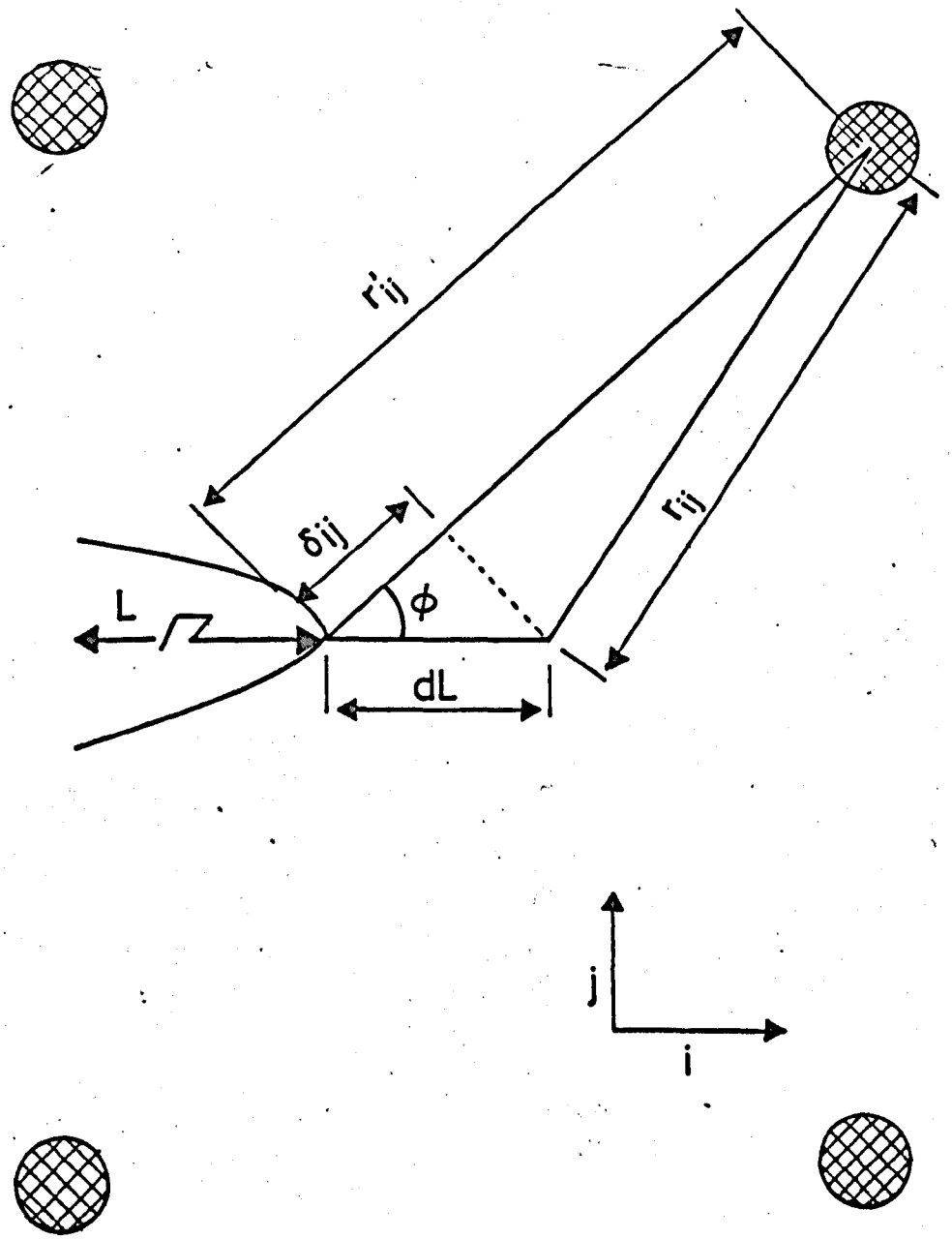

Fig. (7.7) The geometry of the region around a crack tip

We now require the total work done during the increment of crack extension from L to L + dL. If all the secondary plastic zones that are formed involve an extension α and these are produced in a matrix having a constant flow stress σ_y (i.e. no work hardening occurs) then the work done in producing these zones will be approximately:

$$dw = \sigma_y \left[2a \sum \Delta R_q \right] \alpha \qquad [7.16]$$

$$= \text{stress [area] displacement}$$

where, a, is again the radius of the particle. The above expression cannot be justified rigorously but it is considered that the mean depth of the plastic zone will be of the same order as the radius of the particle. Equation [7.16] strictly applies (if we may ignore end effects) to cylindrical rods of radius, a, and length α which are oriented with their longitudinal axis parallel to the crack front.

So far we have only considered a single "plane" containing these particles, if the interparticle spacing is, η, then there will be $\frac{t}{\eta}$ of these "planes" in a specimen of thickness, t. Hence the total work Δw, done during the extension dL will be the sum of the plastic work done at the crack tip and that around the particles, therefore:-

$$\Delta w = \sigma_y \alpha \, dL t + \sigma_y \alpha a \frac{t}{\eta} \left[\sum Rq \right] A_p \qquad [7.17]$$

where A_p is a coefficient that depends upon the orientation of the particles.

Hence:

$$\Delta W = \sigma_y \alpha dL.t + \sigma_y \alpha \frac{at}{\eta} A_p \frac{9\beta^2 K_m^2 a.dL}{\Pi \sigma_y^2} \sum \frac{\cos\phi}{r_{ij}^2} \qquad [7.18]$$

but $$\gamma = \frac{\Delta W}{2dL.t}$$

$$\therefore \quad \gamma = \frac{\sigma_y \alpha}{2} \left(1 + \frac{9a^2\beta^2 K_m^2 A_p}{\Pi \sigma_y^2 \eta} \sum \frac{\cos\phi}{r_{ij}^2}\right) \qquad [7.19]$$

or rewriting:

$$\gamma = \frac{\sigma_y \alpha}{2} \left(1 + \frac{9a^2\beta^2 K_m^2 A_p}{\Pi\sigma_y^2 \eta} \cdot \frac{1}{\eta^2} \sum \frac{i}{(i^2+j^2)^{3/2}}\right) \qquad [7.20]$$

and since the fracture energy γ_m of the matrix is given by:

$$\gamma_m = \frac{1}{2} \sigma_y \alpha$$

then

$$\gamma = \gamma_m \left(1 + \frac{9a^2\beta^2 K_m^2 A_p}{\eta^3 \Pi \sigma_y^2} \sum \frac{i}{(i^2+j^2)^{3/2}}\right) \qquad 7.21$$

From Fig. (7.4) we also have that the volume of a "cell" of the composite is η^3 and the volume of the particle contained within this cell is $\frac{4}{3} \Pi a^3$. The volume fraction, V_f, of the filler is therefore given by:

$$V_f = \frac{\text{Volume of particle}}{\text{Volume of cell}}$$

$$= \frac{4\ \pi a^3}{3\ \eta^3} \qquad [7.22]$$

and hence:

$$\eta = \left(\frac{4\ \pi}{3\ V_f}\right)^{\frac{1}{3}} a \qquad [7.23]$$

Combining equations [7.21] and [7.23] to eliminate, η, we have:

$$\gamma_{\text{composite}} \simeq \gamma_m \left(\frac{1 + 0.7 \beta^2 K_m^2 A_p}{\sigma_y^2} \cdot \frac{V_f}{a} \sum \frac{i}{(i^2 + j^2)^{3/2}} \right) \qquad [7.24]$$

Equation 7.24 therefore predicts that the fracture energy of the composite is proportional to the volume fraction of the filler. This is observed in practice, as Fig. (4.3) reveals for a CT200/HT901 matrix containing ballotini of 100 μm in diameter. Equation [7.24] also predicts that the fracture energies of our epoxy resin/ballotini composites are inversely proportional to the particle size; this is to some extent observed in practice for in various cases an apparent increase in fracture energy occurs when particles smaller than about 50 μm are used.

To evaluate equation [7.24] for a range of particle sizes and volume fractions we require a knowledge of the values of the orientation constant, A_p, the coefficient, β, which depends upon the elastic moduli of the filler and the matrix, and we also need to sum the term:

$$\frac{i}{(i^2 + i^2)^{3/2}}$$

over an appropriate range.

Clearly, for spherical particles, we may set A_p equal to unity, this will not however be the case for lamellaror other shapes of particles where A_p will be expected to have a value of less than unity. The coefficient, β, is somewhat more difficult to determine: however, EDMONDS and BEEVERS (1968) have carried out a detailed photoelastic analysis of the stress distribution around circular inclusions (of a similar modulus to glass) in a cured CT200 matrix and have obtained a value for the stress at the interface of the particle of 2.5 times the uniaxially applied stress, σ_a. We have previously assumed that the interfacial stress is $3\beta\ \sigma_a$ and hence β will be approximately equal to 0.85. To evaluate the summation

$$\sum \frac{i}{(i^2 + i^2)^{3/2}}$$

we will have to make some further approximations but as stated previously we are attempting to show that our simple model predicts the types and magnitudes of the change that may be expected when a filler is added to an epoxy resin matrix. In deriving equation [7.24] we have assumed that our composite material may be represented (in two dimensions) by a square array of circular particles but of course in practice the composite will not be ordered in this manner and the particles will be randomly dispersed. However, let us still retain the square network and assume that to the first approximation we may consider that the tip of the crack is situated at the centre of the unit square of particles. If this is the situation then we may determine the region over which our summation must be evaluated.

Now since the stress at the matrix/particle interface is given by $\sigma = 3\beta$, (local macroscopic stress) and we have assumed that secondary deformation will occur when the local stress exceeds the flow stress of the matrix then we have from equation [7.7] that additional plastic zones will be produced at those particles where

$$r_{ij} \leq \frac{3 K_m^2 \beta}{2\pi \sigma_y^2} \qquad [7.25]$$

If we substitute typical values for K_m, β, and σ_y (which we will take as that value of flow stress at an arbitrary period of 135s, which is approximately equal to the mean time between successive jumps in a specimen fractured at the standard cross head speed) then plastic deformation will occur when $r_{ij} \leq 70\ \mu m$.

Let us now consider the following composites:-

CT200 plus a 0.3 and 0.1 volume fraction of 100 μm ballotini

CT200 plus a 0.1 volume fraction of 200 μm, and 25 μm ballotini.

The mean interparticle spacings for the above composites may be calculated from equation [7.23], these are presented in Table (7.1).

Table (7.1) indicates that to a reasonable approximation we need only consider the pair of particles immediately ahead of the crack tip since we already have that r_{ij} must be less than 70 μm and hence

$$\frac{i}{(i^2 + j^2)^{3/2}} = 2.85$$

TABLE (7.1)

The Mean Interparticle Spacings of Some Composites

Material	Mean Interparticle Spacing/ μm
CT200 plus a 0.3 volume fraction of 100 μm ballotini	120
CT200 plus a 0.1 volume fraction of 100 μm ballotini	175
CT200 plus a 0.1 volume fraction of 200 μm ballotini	300
CT200 plus a 0.1 volume fraction of 25 μm ballotini	45

Equation [7.24] now reduces to:

$$\gamma_{composite} \propto \gamma_m \left[1 + \frac{2\beta^2 K_m^2 A_p}{\sigma_y^2} \simeq \frac{V_f}{a}\right] \qquad [7.26]$$

If we now substitute typical values into equation [7.26] then we may predict from our model a fracture energy of CT200/ballotini composites.

This has been done and the two sets of data are presented in Figs. (7.8) and (7.9). It may be seen from these figures that the "fit" with the experimental data is extremely good. However, during the derivation of the final expression we have necessarily made a number of quite severe approximations and the excellent "fit" must be considered as being somewhat fortuitous. Nevertheless, the model does correctly predict the types and magnitude of the effects that may be expected when a particulate filler is added to an epoxy resin matrix.

One of the more important approximations that have been made is that we

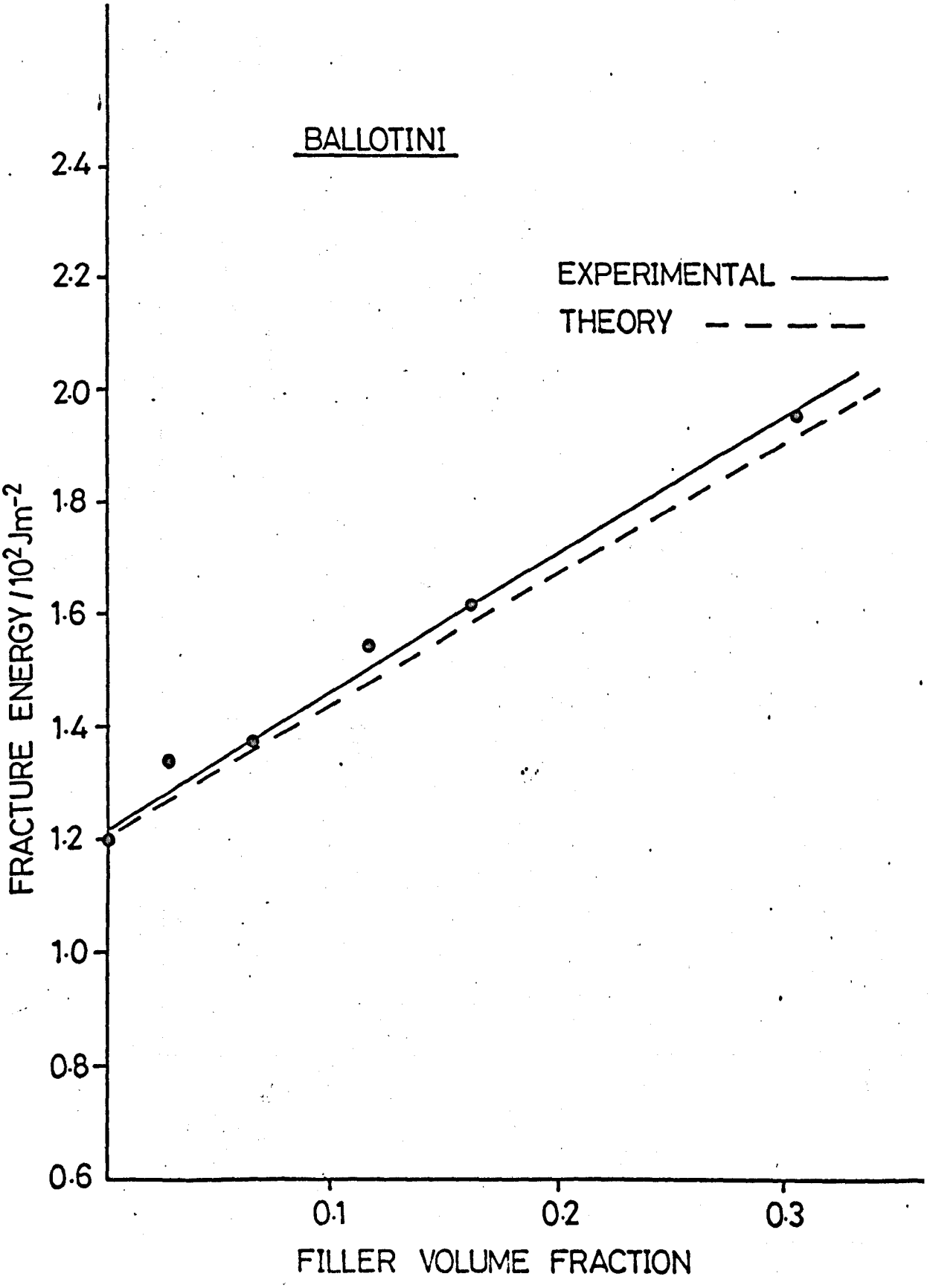

Fig. (7.8) The predicted and experimental fracture energies as a function of filler volume fraction.

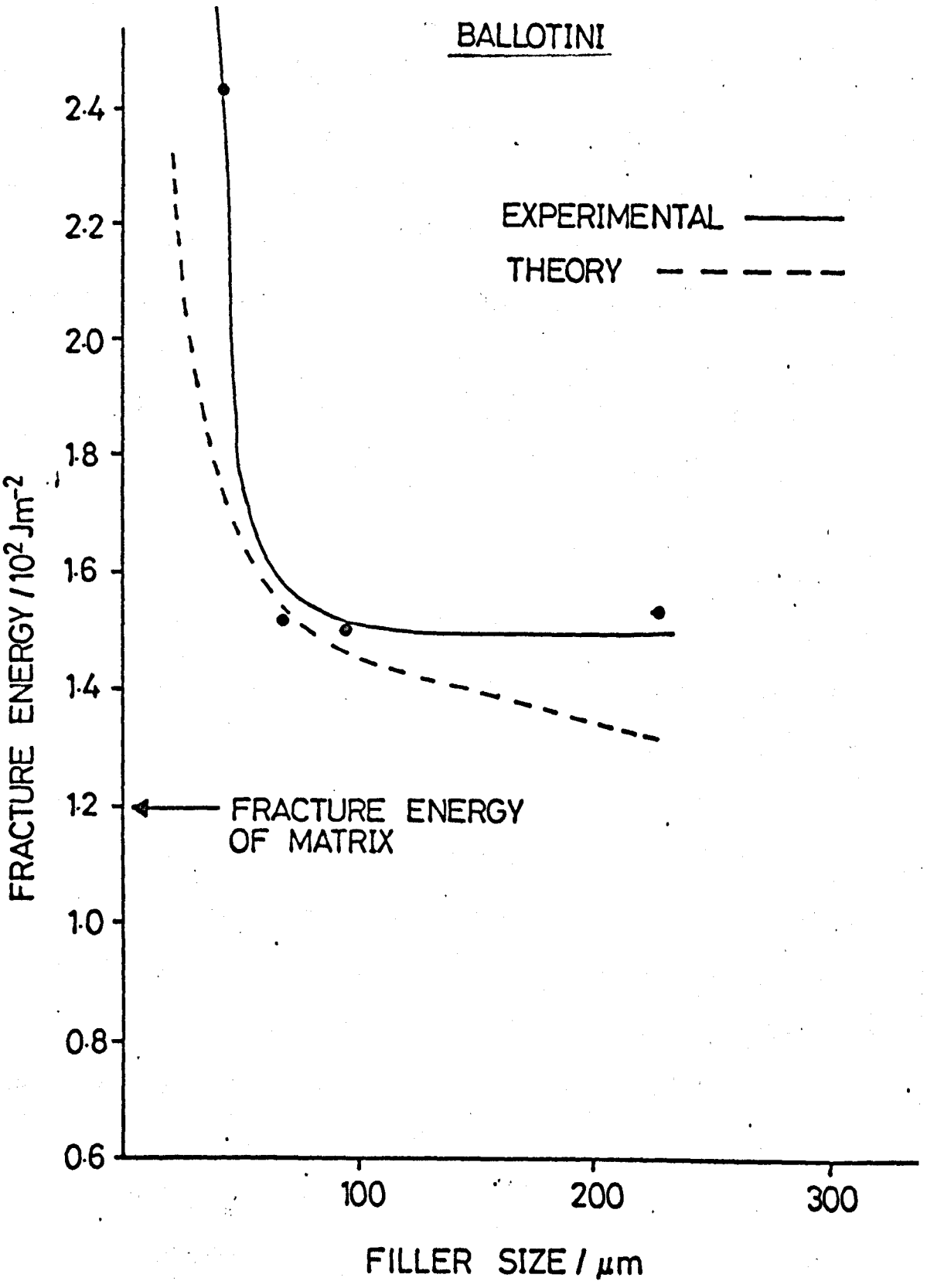

Fig. (7.9) The predicted and experimental fracture energies as a function of filler size

postulated that there was no overlap of the stress raising zones which are associated with the individual particles. This assumption is valid only at very low volume fractions; even at a volume fraction of 0.1, the interparticle spacing of spherical particles is only of the order of 1.5 times their diameter and hence overlap may be expected to occur. However, as the volume fraction of filler is increased and the mean interparticle spacing decreases the zone lengths will at first increase (because of the stress field overlap) above that allowed in the model but further decreases in the particle spacing will be expected to cause "saturation" because the length of the zone may not be greater than

$$\frac{\eta}{2} - a$$

Throughout the derivation of the simple expression for the fracture energy of a composite from our basic hypothesis, we have considered that the filler particles are acted upon only by a uniaxial tensile stress; this is not the case in practice since they are situated in the biaxial stress field associated with the principal crack. The likely error involved in making this assumption is difficult to estimate simply but it seems a priori unlikely that our expression which neglects the presence of the second principal stress would be in error by more than a factor of two. In any case we are concerned here simply with showing that the mechanism proposed is adequate to explain the observed order of magnitude of changes in fracture energy. It is considered that the agreement between the predictions of our still rather crude calculations and the observed experimental results suggests that the basic hypothesis provides a useful physical basis from which to describe the fracture of particulate filled epoxy resin composite materials.

From the foregoing discussion it is apparent that the composites with the higher fracture energies will be those where many secondary cracks or much additional plastic deformation accompanies the propagation of a primary crack. The composites with the higher fracture energies will therefore be

those containing particles which are potent stress-raisers and hence will be materials in which crack nucleation is relatively easy.

We have already postulated that the major factor determining the Charpy impact energy of our composites, and matrices, is the amount of strain energy that must be supplied to the system in order to initiate the fracture. It is, therefore, apparent that for our range of materials we shall expect those with the higher fracture energies to have the lower impact energies and also the lower strength. Both the above features are observed in practice.

7.4. Recommendations for Further Work

The experimental programme described in this thesis was intended primarily as a broad survey of the effects on crack propagation behaviour of adding a particulate filler to an epoxy resin matrix. All the fillers used have Young's moduli larger than the matrices and it would now be useful to examine the effects of adding a filler of lower modulus (for example, elastomeric particles) to ascertain whether our model could be extended to this situation. Talc may however have provided a filler type with a low effective modulus because of the low cohesion within the particles and the very low flow stress which lead us to suggest that individual filler particles would act as penny-shaped cracks.

Limitations on filler volume fraction were imposed by the specimen preparation technique and hence methods should be investigated to enable composites to be produced containing high filler loadings without seriously modifying the physical properties of the matrix.

Little is known about the plastic flow mechanism in the epoxy resin family of materials. During the course of this work craze-like defects were identified around a

crack tip. The study of these crazes may well lead to a better understanding of the processes involved during plastic deformation. Until very recently the epoxy resins have been thought to be devoid of any structure; we have however been successful in these laboratories in revealing an internal structure by two very different etching techniques. The demonstration of the existence of a structure may now present us with the possibility of being able to modify and observe the structure in relation to various physical properties which hopefully will lead to a better understanding of the behaviour of our matrix materials.

During the course of the development of our simple, quantitative model we made a number of rather severe approximations concerning the stress distribution and shape and size of the plastic zones around filler particles. Application of the recently developed "finite element" technique which may be used to determine the stress distribution in arbitary shaped solids should enable much more accurate estimates of the fracture energies of the composites to be made using the same physical hypothesis as proposed here. The finite element technique employs a system of integrated computer programs designed to perform the general stress analysis of arbitrary. two, or if sufficient computer capacity is available, three dimensional structures. The "structure" may be subjected to pressures, point loads, body forces, rotational forces, and temperature distributions. In addition, various parts of the structure may be allocated displacements, material properties may be temperature dependent and vary throughout the structure. This technique therefore appears to present us with the possibility of performing a complete stress analysis of a typical cracked composite material.

The basic postulate of our model is that the critical length of the local crack tip plastic zone is the same in the unfilled matrix as it is in all the composites. The

verification of this postulate does however appear to be difficult.. Two possible methods are: by determining the strain in the material adjacent to the crack tip by, for example, a moiré fringe method. It should then be possible to measure the length of the zone since a discontinuity in the strain will occur at its edge. Or alternatively by using an interferometric technique to examine the surface profile of the region close to the crack tip. Very simple experiments have shown that the formation of a plastically deformed region at the crack tip is accompanied by a "sinking" in the surface of the material. It is recommended that these techniques are persued since this assumption is a central feature of our model.

7.5. Final Summary

The original aim of this work was to examine the effect on the crack propagation behaviour in a composite of adding a range of particulate fillers to three commercial epoxy resin matrices. However, because of the paucity of information on the mechanical properties of the matrices a quite extensive experimental programme was undertaken to provide information that could be used in conjunction with the results obtained for the composite materials. As a consequence the main body of the data is concerned with just one matrix; CT200/HT901.

Nevertheless simple phenomenological models have been presented which in a general qualitative way have been able to account for the main features of the observations. It was suggested that crack jumping occurs in the epoxy resins, and possibly other materials, because the critical crack tip plastic zone size (or extension) at which local rupture occurs is lower when the strain rate in the material just ahead of the crack is high. Hence two fracture energies will be exhibited despite the fact that the flow stress of the material may fall with time if the variations in flow stress

can be more than compensated for by changes in the plastic zone size (or extension). Regions close to a crack tip, on fracture surfaces, and on the tensile surfaces of simple cantilever beams have been identified in our epoxy resins which closely resemble the crazes that are often found in stressed, glassy, thermoplastic polymers such as PMMA, polystyrene and polycarbonate. A simple phenomenological model has also been developed which explains some of the behavioural features that are observed when particulate fillers are added to our matrix.

However, a number of features still remain to be explained, for example, why does the addition of quite small quantities of filler remove the dependence of fracture energy on effective extension rate, or what is the nature of the structure of the epoxy resins? Although, many of our conclusions must be regarded as tentative the initial concept of a broad survey has proved useful if only to provide some new working hypothesis which can be tested in further detail at a later date.

REFERENCES

A.S.T.M., 1964, Spec.Tech.Pub.No. 381, (A.S.T.M. Philadelphia)

BENBOW, J.J. and ROESLER, F.C., 1957, Proc.Phys.Soc., B.70, 201

BERRY, J.P., 1961, J.Poly.Sci., 50, 107 and 313

BREARLEY, W., Private communication

BROUTMAN, L.J. and McGARRY, F.J., 1965, J.Appl.Poly.Sci., 9 589

CLARKE, F.J.P., TATTERSALL, H.G. and TAPPIN, G., 1966, Proc.Brit.Ceram. Soc., No. 6, 163

COATES, E., 1971, Private communication

EDMONDS, D.V. and BEEVERS, C.J., 1968, J. Mat.Sci. 3, 477

GILLIS, P.P. and GILMAN, J.J., 1964, J.Appl.Phys., 35, 647

GILMAN, J.J., 1960, J. Appl. Phys. 31, 2208

GRIFFITH, A.A., 1920, Phil.Trans.Roy.Soc., A 221, 163

GRIFFITHS, R, 1968, M.Sc. Thesis, University of Keele

GUERNSEY, R. and GILMAN, J.J., Proc.Intern.Conf. on Fracture, Swampscott, Mass, U.S.A. (Wiley, New York)

GUNASEKERA, S.P., 1970, M.Sc. Thesis, University of Keele

HAWARD, R.N., 1972, Amorphous Materials, Douglas and Ellis (Ed) (Wiley, New York) p.513

HILL, R., 1950, The Mathematical Theory of Plasticity (Oxford: Clarendon Press)

HULL, D., 1970, J.Mat.Sci., 5, 357

INGLIS, C.E., 1913, Trans.Inst.Naval Architects, 55, 219

IRWIN, G.R., 1948, Trans.Amer.Soc. Metals, 40, 147

IRWIN, G.R., 1958, Fracture, Hanbuch de Physik, Vol.VI, (Springer, Berlin)

KAMBOUR, R.P., 1965, J.Polym.Sci., A, 3, 1713

KAMBOUR, R.P. and HOLIK, A.S., 1969, J.Polym.Sci., A-2, 7, 1393

LANGE, F.F., 1970, Phil.Mag. 22, 179, 983

LINGER, K.R. and HOLLOWAY, D.G., 1968, Phil.Mag., 18 156, 1269

MARSH, D.M., 1964, Proc.Roy.Soc., A 279, 420

OBREIMOV, J.W., 1930, Proc.Roy.Soc. A, 127, 290

OROWAN, E., 1948-49, Rep.Prog.Phys. 12 185

SELSING, J., 1961, J.Amer.Ceram.Soc. 44, 419

SRAWLEY, J.E. and GROSS, B., 1967, Mater.Res.Stds. 7 155

SVENSSON, N.L., 1960, Proc.Phys.Soc., 77, 876

TABOR, D, 1951, The Hardness of Metals, (Oxford: Clarendon Press)

TAYLOR, E.W., 1949, Nature, (Lond.) 163, 323

1950, J.Soc.Glass.Tech., 34, 69

WAMBATCH, A.D., 1970, D.Sc. Thesis Washington University

WEIDERHORN, S.M., 1969, J.Amer.Ceram.Soc., 50, 407

WESTWOOD, A.R.C. and HITCH, T.T., 1963, J.Appl.Phys., 34 3085

WEYL, D., 1959, Ber.deut.Keram.Ges., 36, 319

WILLIAMS, J.G., 1965, Appl.Mat.Res. April, p.104